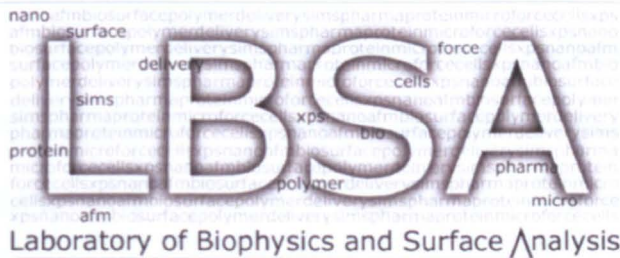


School of Pharmacy



**The University of
Nottingham**

UNITED KINGDOM • CHINA • MALAYSIA



Development of Nanoscale Screening Technology for the Detection and Quantification of Aggregation in Protein Therapeutics

Mudasir Ahmad Lone [BSc; ADCA; MRes]

Thesis submitted to

**The University of Nottingham for the Degree of
Doctor of Philosophy**

March 2013

Abstract

The use of proteins as therapeutics is one of the fastest growing sectors of the pharmaceutical industry, particularly monoclonal antibodies. However, a significant challenge in the development of such protein-based medicines is to counter aggregation of the proteins in solution (as these drugs are typically administered by injection). In solution form, aggregation of the normally monomeric protein ingredient affects therapeutic efficiency and reduces shelf life. Moreover, the rapid formation of aggregates in patients during the administration of therapeutic proteins can lead to immunological reactions which could be fatal. Hence, the long term storage of proteins in solution is discouraged. Lyophilization (vacuum drying) is considered to be an effective route for ensuring longer shelf life and better stability of protein therapeutics. However, aggregation can still occur, because the driving forces for aggregation (covalent as well as non-covalent interactions such as hydrogen bonds, van der Waals forces and hydrophobic interactions) are influenced by lyophilization induced changes in the pH, temperature, exposure to interfaces, and dehydration stress. Lyoprotectants such as sugars can counter the undesirable consequences of lyophilization depending upon their nature and potential. Several mechanisms have been proposed for the role of the lyoprotectants. The comprehensive investigation into the inherent nature and influence of lyoprotectants on a protein therapeutic during lyophilization is hence important. In this project an attempt has been made to develop a novel nanoscale screening methodology for the detection,

quantification, characterization and prevention of protein aggregation. Initially, ferritin and then a polyclonal IgG (antiglucose-6-phosphate dehydrogenase antibody) antibody have been used as model proteins for these studies. The effect of lyophilization on the level of aggregation of IgG was studied and compared to reports in the literature. IgG was exposed to seven cycles of lyophilization, where each cycle of lyophilization was followed by reconstitution and characterization. IgG was also lyophilized with different excipients (sucrose and mannitol, alone and in combination) in different molar ratios. In the liquid state, the formulations were characterized on the basis of particle size and antigen binding activity, whereas in the dry powdered form, the formulations were characterized by studying morphology, thermal stability, and secondary structural alterations in order to establish a relationship amongst the indicated properties. Atomic force microscopy (AFM), dynamic light scattering (DLS) and single particle tracking (Nanosight) were used to study particle size. The identification of different components at the nanoscale and general morphology were screened by AFM and scanning electron microscopy (SEM). Subsequently, the thermal properties and structural alterations respectively were analysed by differential scanning calorimetry (DSC) and infra read spectroscopy (ATR-FTIR) spectroscopy. The antigen binding activity was investigated by performing an indirect ELISA assay on the lyophilized formulations.

Lyophilization of ferritin and IgG caused a significant decrease in the proportion of monomeric species was confirmed by AFM, DLS and Nanosight. Dimeric,

lower-multimeric and larger aggregates existed in variable proportions for both ferritin and IgG. Powdered lyophilized ferritin formulations showed aggregation, increased crystallinity (concomitant decrease in amorphicity), porosity and flakiness which in case of IgG increased with repeated lyophilization. A consistent increase in the extent of aggregation (unfolding of Fabs and Fc) was detected by DSC and an increase in the β – sheet structure coupled with structural re-arrangement within the components by ATR-FTIR. The presence of sucrose in IgG formulations resulted in reduced aggregation and enhanced porosity. The inclusion of Mannitol promoted crystallinity, decreased porosity when used alone, however, improved the efficiency of sucrose in combined formulations. The nature of crystals formed by mannitol during lyophilization was shown by SEM and confirmed by AFM. The data obtained from DLS, NTA, AFM, DSC, ATR, and SEM was consistent with by ELISA results which indicated a significant fall in IgG activity upon repeated lyophilization, and improvement in the activity when IgG was formulated with sucrose, which significantly enhanced in combination with mannitol. The benchmark provided by this work would serve as a precursor for developing a novel screening standard for optimizing and improving the therapeutic efficiency of other proteins besides furnishing a detailed account of the disparity in correlating the data from multiple novel techniques. The findings of our work can be directly translated to biotech and biopharm industries for the enhancement of protein based therapeutics.

Acknowledgements

I am enormously indebted to my highly generous, kind and incredible supervisors: Pro-vice Chancellor, Professor Saul Tendler, Director Nottingham Nanoscience and Nanotechnology Center, Professor Clive Roberts and Associate Professor Dr. Stephanie Allen, for their precious supervision, backing and compassion. I wish to express my deepest appreciation and profound regards from the core of my conscience towards all of my mentors.

I would like to thank Associate Professor Snow Stonolik for DLS training, Professor Xinyong Chen for training me on several AFMs and my colleague Andrea Gonsalves for input on Nanosight. Thanks from the bottom of my heart to Lord Jenny for BSA and especially to Dr. Alan for Tween 20, TMB/OPD substrates. I would also like to express my gratitude to Professor David Pritchard for allowing me to use his Dynex plate reader. Special thanks to Dr. Jonathan Burley for his support with Polarization microscope and DSC instruments, Dr. Jagdish and Dr. Andy Meagrey for their input on DSC. I would not like to forget mentioning Professor Phil Williams who several times guided me in the data processing during Masters as well as during my PhD. Million dollar thanks to dear, wonderful, kind and always helpful Gail Atkinson. Cheers to everyone in the LBSA and thanks to all other folks in other labs within the BSB, for their assistance and cooperation during my Ph.D studies.

I would also like to express my sincere gratitude towards some of the following special people in my life: Latief Ahmad Teli, Ejaz Salaam, Raja, Wahid Wani, Ehsaan Ramzan, Hanan Barlahas, Majid Bashir, Faizan-Usman, Dr. Dimitra, Dr. Dimitri, Dr. Driton, Dr. David Piggot, Dr. Irfan Quadir, Dr. Igor, Dr. Arshad Latif, Dr. Dimitri, Dr. Uncle Nazeer, Dr. Darren Albutt, Dr. Asher, Dr. Millind, Dr. Dimitra, Dr. Felicity Heath, Dr. Victoria Sedmann, Dr. Toby, Dr. Emilia and Dr. Mathieu. Distinctive thanks to Dr. Farjina Khanum for her support and compassion in the preliminary stages. I also owe a lot of this achievement to Safoora Teli, who in a robust mode of generosity taught me how to deliver goods (such as PhD) under extreme intricate circumstances in life, besides metamorphosising my simple conscience about the principles of honesty, sincerity, truthfulness and faithfulness into a highly novel and refined one.

I acknowledge the unlimited help from The Almighty God, who kept me unnerved despite plenty of bottlenecks that held me on the back foot during my entire Ph.D. I would also like to pay huge thanks to Mrs. Saleema Wani for her care and love. Finally, I have no precise and enough words, that would enable me to thank my dear ultimate love and greatest mother Mrs. Misrah Bano, for her unconditional support, tolerance and abundant sacrifices through out her life for me. Without my mother, I could have achieved nothing in my life. I salute my lovely mother for her mighty contribution. Lastly abundant respectful regards and regards for my ever eternal mentor Respected Gulzar Sahib and Respected Soan Sahib for their pure, meaningless, most useful compassion and humility.

M. A. Lone The Plan of Thesis

Chapter 1 Introduction to therapeutic protein aggregation

**Chapter 2 Materials and methods for the preparation of samples;
and novel techniques employed.**

**Chapter 3 Nanoscale characterisation of the effect of lyophilization
on the propensity of ferritin aggregation**

**Chapter 4 Nanoscale characterisation of the effect of successive
lyophilization on the aggregation of IgG (Polyclonal).**

**Chapter 5 Characterization of the effect of sugar excipients on the
aggregation of IgG (Polyclonal) during multiple cycles
of lyophilization.**

**Chapter 6 The effect of sucrose and mannitol on the structure and
morphology traits of IgG (Polyclonal) during successive
lyophilization.**

**Chapter 7 An examination into the effect on the antigenic-binding
activity of IgG on its own and with excipients during the
successive cycles of lyophilization**

Chapter 8 Summary and potential for further investigations.

Abstract	i
Acknowledgements	iv
The thesis plan	vi
Table of contents	vii
List of figures	xix
List of tables	xxiv
List of abbreviations and symbols	xxvi

Chapter 1 Introduction to aggregation of therapeutic proteins

1.1	Biopharmaceuticals	1
1.2	Aggregation in proteins	5
1.2.1	Mechanisms of aggregation	9
1.2.2	Kinetics of aggregation	18
1.2.3	Significance of aggregation in protein therapeutics	19
1.2.4	Factors influencing protein aggregation	23
1.2.4.1	Influence of solution pH	23
1.2.4.2	Effect of salt	26

1.2.4.3	Effect of temperature	26
1.3	Lyophilization process	27
1.3.1	Primary drying	28
1.3.2	Secondary drying	30
1.4	Effect of the lyophilization on IgG and other proteins	31
1.5	AFM for mapping IgG aggregation	37
1.6	Protein therapeutics	40
1.7	Immunoglobulins (Antibodies)	40
1.7.1	Basic structure of IgG	41
1.7.2	Proteolytic cleavage of IgG	44
1.7.3	Structure of variable region	46
1.7.4	Isoelectric point of IgG	46
1.7.5	Crystallographic structure of IgG	47
1.7.6	Extinction coefficient of IgG	47
1.8	Conventional particle size characterization techniques	48
1.8.1	Analytical ultra-centrifugation	49
1.8.2	Size exclusion chromatography	51
1.9	Aims and objectives	54

Chapter 2 Materials; methods for the preparation of samples; and novel techniques employed for characterization

2	Introducton	58
---	-------------	----

2.1	Materials	58
2.2	Preparation of protein stock solution	60
2.2.1	Ferritin stock solution	60
2.2.2	IgG stock solution	60
2.3	Concentration determination	62
2.4	Storage of liquid protein solutions	63
2.5	Lyophilizer and lyophilization of samples	63
2.5.1	Lyophilization of ferritin samples	64
2.5.2	Lyophilization of IgG samples	65
2.6	Techniques employed for the investigation	67
2.6.1	Atomic force microscopy	67
2.6.1.1	Strength and weakness of measuring particle size with AFM	72
2.6.1.2	AFM imaging modes	74
2.6.1.3	AFM probe-sample interaction forces	76
2.6.1.4	Scanning probe image processor	78
2.6.2	Scanning electron microscopy	80
2.6.3	Dynamic light scattering	83
2.6.3.1	DLS data production	87
2.6.3.2	DLS measurements	91
2.6.4	Nanosight/Nanoparticle tracking analysis	92
2.6.4.1	NTA data production	95
2.6.4.2	NTA measurements	96
2.6.5	Differential scanning calorimetry	97

2.6.5.1	DSC measurements	103
2.6.6	Fourier-transform Infra-red spectroscopy	104
2.6.6.1	FT-IR modes of analysis	106
2.6.6.2	FT-IR measurements	112
2.7	T-test for statistical analysis	113

Chapter 3 Nanoscale characterization of the effect of lyophilization on the propensity of ferritin aggregation

3.1	Introduction	116
3.1.1	Ferritin and its structure	118
3.1.2	AFM studies of ferritin	121
3.2	Aims and objectives	122
3.3	Materials	122
3.4	Sample preparation methodology	123
3.4.1	Preparation of ferritin solution	123
3.4.2	Lyophilization of ferritin	123
3.4.3	Preparation of samples for AFM analysis	124
3.4.4	Preparation of samples for SEM analysis	125
3.5	Methods of analysis	125
3.5.1	Atomic force microscopy	125
3.5.1.1	AFM data analysis	126
3.5.2	Scanning electron microscopy	126

3.6	Results and Discussion	126
3.6.1	Imaging of ferritin samples in air	126
3.6.2	Imaging of ferritin samples in liquid	127
3.6.3	Particle size analysis	128
3.6.4	Morphological studies of ferritin powders	139
3.7	Conclusions	140

Chapter 4 Nanoscale characterization of the effect of successive lyophilization on the aggregation of IgG (Polyclonal)

4.1	Introduction	141
4.2	Aims and objectives	143
4.3	Materials	144
4.4	Sample preparation of methodology	144
4.4.1	Preparation of IgG solution	144
4.4.2	Lyophilization of IgG	145
4.4.3	Formulations of IgG	145
4.4.3.1	Samples from liquid IgG formulations	145
4.4.3.1.1	Liquid samples for AFM particle size analysis	145
4.4.3.1.2	Liquid samples for light scattering analysis	146
4.4.3.2	Samples from powdered IgG formulations	146
4.5	Methods of analysis	147
4.5.1	Atomic force microscopy	147

4.5.1.1	Analysis of AFM images	147
4.5.2	Light scattering	148
4.5.2.1	Dynamic light scattering	148
4.5.2.2	Nanoparticle tracking analysis	148
4.5.3	Scanning electron microscopy	149
4.5.4	Thermal stability analysis in the solid state	149
4.5.5	Secondary structural stability analysis in the solid state	149
4.6	Results and Discussion	150
4.6.1	Imaging of liquid IgG samples	150
4.6.2	AFM particle size analysis	154
4.6.3	Size measurements with DLS	163
4.6.4	Nanosight measurements	165
4.6.5	Morphology of the lyophilized powders of IgG	172
4.6.5.1	Characterization with AFM imaging	172
4.6.5.2	Characterization with SEM imaging	176
4.6.6	Thermal stability	178
4.6.6.1	Effect on the melting of IgG	178
4.6.7	Effect of lyophilization on the secondary structure of IgG	181
4.7	Conclusions	191

Chapter 5 Characterization of the effect of sucrose and mannitol on the aggregation of (Polyclonal) IgG during multiple cycles of lyophilization

5.1	Introduction	192
5.1.1	Excipients and their chemical structure	194
5.2	Aims and objectives	196
5.3	Materials	197
5.4	Sample preparation methodology	197
5.4.1	Reconstitution of lyophilized protein (IgG) powder	197
5.4.2	Lyophilization of reconstituted IgG	197
5.4.3	Preparation of IgG formulations	197
5.4.3.1	Liquid formulations	198
5.4.3.2	Powdered formulations	199
5.5	Methods of analysis	199
5.5.1	Dynamic light scattering	199
5.5.2	Atomic force microscopy	200
5.5.3	Differential scanning calorimetry	200
5.5.4	ATR-FTIR spectrometry	201
5.6	Results and discussion	201
5.6.1	Size measurements	201
5.6.1.1	Individual effect of sucrose and mannitol	201
5.6.1.2	Collective influence of sucrose and mannitol	203
5.6.2	AFM analysis of the lyophilized formulations (powders)	205
5.6.2.1	Controls for lyophilized sucrose and mannitol	205
5.6.2.2	IgG lyophilized with sucrose (powder)	209
5.6.2.3	IgG lyophilized with mannitol (powder)	211

5.6.2.4	IgG formulated with sucrose and mannitol in combination	213
5.6.3	Examination of thermal stability behaviour	217
5.6.3.1	Excipients and their thermal behaviour	217
5.6.3.2	Impact of sucrose and mannitol when used separately	222
5.6.3.3	Impact of sucrose and mannitol in combination	224
5.7	Conclusions	228

Chapter 6 The effect of sucrose and mannitol on the structure and morphology of IgG during successive lyophilization

6.1	Introduction	229
6.2	Aims and objectives	230
6.3	Materials	231
6.4	Sample preparation methodology	231
6.4.1	Preparation of IgG formulations	231
6.4.2	Powdered formulations	231
6.5	Methods of analysis	232
6.5.1	ATR-FTIR inspection	232
6.5.2	Scanning electron microscopic examination	232
6.6	Results and Discussion	232
6.6.1	Effect of sugars on secondary structure of powdered IgG	232
6.6.1.1	Sugar controls for Infra-red ATR-analysis	232
6.6.1.2	Secondary structure with sucrose and mannitol	234

6.6.2	Morphological examination	243
6.6.2.1	SEM controls for sucrose and mannitol	243
6.6.2.2	Comparative behaviour with sucrose and mannitol	245
6.6.2.3	Influence of sucrose and mannitol in combination	249
6.7	Conclusions	251

Chapter 7 An examination into the effect of multiple lyophilizations on the antigenic-binding activity of IgG on its own and with sugar excipients

7.1	Introduction	253
7.1.1	Mechanisms of an action of therapeutic antibodies	257
7.1.2	Overview of methods for studying antibody-antigen binding	260
7.1.3	ELISA, its principle and formats	262
7.2	Aims and objectives	264
7.3	Materials	264
7.4	Sample preparation methodology	264
7.4.1	Lyophilization of IgG alone and with sugars	264
7.4.2	Preparation of primary antibody solution	265
7.4.3	Preparation of secondary antibody solution	265
7.4.4	Preparation of antigenic solution	265
7.4.5	Preparation of buffer solutions	265
7.4.6	Preparation of required ELISA plate	266

7.5	Absorbance measurements	273
7.6	Results and Discussion	274
7.6.1	Antigen binding propensity of multiple times lyophilized IgG	274
7.6.2	Activity response of IgG lyophilized separately with sugars	276
7.6.3	Effect of the sugars in combination on IgG activity response	278
7.7	Discussion	281
7.8	Conclusions	283

Chapter 8 Summary; potential for further investigations

8.1	Outline of the investigations conducted in this study	284
8.1.1	Nanoscale characterization of the effect of lyophilization on ferritin and IgG	286
8.1.1.1	Characterization with AFM only	286
8.1.2	Multiple times lyophilized IgG without excipients	287
8.1.2.1	Characterization with DLS, AFM, DSC, SEM and ATR-IR	287
8.1.3	IgG lyophilized with excipients	288
8.1.3.1	Characterization with DLS, AFM and DSC	288
8.1.3.2	Characterization with SEM and ATR-IR	289
8.1.4	Antigen-binding activity of IgG	290
8.1.4.1	Antigen-binding activity of lyophilized IgG (on its own)	291
8.1.4.2	Activity of IgG with sugar excipients	291
8.1.5	Impact of this research work	293

Appendix 1

A.1.1	List of all materials used.	295
-------	-----------------------------	-----

Appendix 2

A.2.1	List of novel techniques employed	297
-------	-----------------------------------	-----

Appendix 3 AFM measurements of ferritin aggregates

A.3.1	Aggregation profile of ferritin in air (Cycle 0)	298
A.3.2	Aggregation profile of ferritin in liquid (Cycle 0)	299
A.3.3	Aggregation profile of ferritin in liquid (Cycle 1)	300

Appendix 4

A.4.1	AFM aggregation profile of IgG at 0.75 $\mu\text{g/ml}$ (Cycle 0)	301
A.4.2	AFM aggregation profile of IgG at 0.75 $\mu\text{g/ml}$ (Cycle 1)	302
A.4.3	AFM aggregation profile of IgG at 1 $\mu\text{g/ml}$ (Cycle 0)	303
A.4.4	AFM aggregation profile of IgG at 1 $\mu\text{g/ml}$ (Cycle 1)	304
A.4.5	NTA aggregation profile of IgG at 0.25 mg/ml (Cycle 0 – 7)	305
A.4.6	DLS characterization of IgG at 0.5 mg/ml (Cycle 0 – 7)	306
A.4.7	SEM characterization of of IgG (Cycle 0)	307
A.4.8	3D AFM scans of IgG (1 $\mu\text{g/ml}$) in 0.01 M PBS (Cycle 0)	308
A.4.9	3D AFM scans of IgG (1 $\mu\text{g/ml}$) in 0.01 M PBS (Cycle 1)	309
A.4.10	3D AFM scans of lyophilized IgG powders (Cycle 1 – 6)	310
A.4.11	SEM images of lyophilized IgG powders (Cycle 1 and 6)	311
A.4.12	Overlaid ATR spectra of IgG powders (Cycle 1 – 7; Raw)	312

A.4.13	ATR spectra of (1 – 7) times lyophilized IgG (Normalized)	313
A.4.14	Effect of cycles (1 – 7) on β – sheet main component in IgG	314
A.4.15	Aggregation behaviour of (0 and 7) cycled IgG over time	315

Appendix 5 Lyophilization of IgG with sugars

A.5.1	No aggregation in sugars (size detected down to 1 nm)	316
A.5.2	AFM images (topography and phase) of IgG with sugars	317

Appendix 6 Secondary structure of IgG with sugars

A.6.1	Influence of sugars on different β – sheet concentrations (I)	318
A.4.5	Influence of sugars on different β – sheet concentrations (II)	319

References		320
-------------------	--	------------

List of Figures

Chapter 1

Figure 1.1	Standard simplified model for protein aggregation.	10
Figure 1.2	Schematic of the most probable protein folding mechanism.	12
Figure 1.3	The multiple stages of protein aggregation.	14
Figure 1.4	3D and molecular secondary structure of a protein.	17
Figure 1.5	Steps involved in the formation of bityrosine.	22
Figure 1.6	Lyophilization (Phase diagram).	28
Figure 1.7	TM AFM images of antibody morphologies.	37
Figure 1.8	Tertiary structure of IgG molecule.	42
Figure 1.9	Schematics of ultracentrifugation technique.	49
Figure 1.10	Schematic of a size-exclusion chromatography column.	52

Chapter 2

Figure 2.1	UV absorption of IgG concentrations recorded at 280 nm.	62
Figure 2.2	Edwards's lyophilizer; type Modulyo K4.	64
Figure 2.3	Overview of the procedure of the lyophilization of IgG.	66
Figure 2.4	Schematic overview of the working of an AFM instrument.	68
Figure 2.5	Schematic of AFM probe-sample interaction forces.	71
Figure 2.6	Schematic of the grain analysis performed by SPIP	79

Figure 2.7	Schematic overview of the working of an SEM instrument.	81
Figure 2.8	Schematic diagram of dynamic light scattering instrument.	84
Figure 2.9	Imaginary particles with variable hydrodynamic diameter.	88
Figure 2.10	DLS intensity, volume and number distributions.	90
Figure 2.11	Labelled overview of the Nanosight instrument (LM 10).	93
Figure 2.12	Optical flat of Nanosight during laser illumination.	94
Figure 2.13	Typical example of a NTA sample report.	96
Figure 2.14	DSC instrument and underlying schematic of a DSC cell.	99
Figure 2.15	Graphical representation of heat flown through DSC cells.	102
Figure 2.16	DSC transitions under the influence of applied heat.	103
Figure 2.17	Schematic of working of an FT-IR spectrometer.	105
Figure 2.18	Splitting of polychromatic IR- IR-beam in FT-IR.	107
Figure 2.19	Typical KBr die and Liquid cells used in FT-IR analysis.	109
Figure 2.20	ATR crystal produces an evanescent effect because of TIR.	110

Chapter 3

Figure 3.1	Simplified structure of a ferritin molecule	119
Figure 3.2	Structure of ferritin iron core in Alzheimer's.	121
Figure 3.3	TM AFM scans of ferritin (Cycles 0 and 1) in air.	127
Figure 3.4	TM AFM scans of ferritin (Cycles 0 and 1) in liquid.	128
Figure 3.5	Relative particle size distribution of ferritin in liquid.	130
Figure 3.6	Relative particle size distribution of ferritin in liquid.	131

Figure 3.7	SEM images of lyophilized (cycles 0 and 1) ferritin.	139
------------	--	-----

Chapter 4

Figure 4.1	TM AFM scan of lyophilized of IgG (1 μ g/ml) in 3D.	151
Figure 4.2	TM AFM scans of (cycles 0 and 1) of IgG.	152
Figure 4.3	Particle size distribution of IgG (cycle 0 – 1) in liquid.	155
Figure 4.4	Typical DLS intensity distribution of IgG (cycle 0).	162
Figure 4.5	DSC profiles of multiple times lyophilized IgG.	163
Figure 4.6	DLS characterization of IgG lyophilized (0 – 7) alone.	165
Figure 4.7	NTA profile acquired of IgG (cycle 0).	166
Figure 4.8	NTA aggregation profiles of IgG lyophilized (0 – 7).	169
Figure 4.9	AFM images of 1, and 7 times lyophilized IgG powders.	174
Figure 4.10	AFM analysis of 1, 2, 3 times lyophilized IgG powders.	175
Figure 4.11	SEM images of lyophilized IgG powders.	177
Figure 4.12	DSC heating profiles of lyophilized IgG powders.	179
Figure 4.13	Spectroscopic examinations of lyophilized IgG powders.	182
Figure 4.14	Amide I/II ratios in multiple times lyophilized IgG.	184
Figure 4.15	Curve fitted amide band I in lyophilized IgG.	185

Chapter 5

Figure 5.1	Influence of sucrose and mannitol on IgG alone.	202
Figure 5.2	Influence of sucrose and mannitol on IgG in combination.	204
Figure 5.3	Control AFM images of lyophilized mannitol and sucrose.	208

Figure 5.4	AFM images of powders of IgG lyophilized with sucrose.	210
Figure 5.5	AFM images of powders of IgG lyophilized with mannitol.	212
Figure 5.6	AFM images of IgG with sucrose and mannitol separately.	214
Figure 5.7	AFM images of IgG with sucrose and mannitol together.	216
Figure 5.8	Overlaid standard DSC heating profiles of sucrose.	218
Figure 5.9	Overlaid standard DSC heating profiles of mannitol.	219
Figure 5.10	Part of the DSC profile: (Red trace; Figure 5.8) of sucrose.	220
Figure 5.11	DSC profiles of IgG with sucrose and mannitol separately.	222
Figure 5.12	DSC profiles of IgG with sucrose and mannitol together.	225

Chapter 6

Figure 6.1	IR-ATR spectra for sugar controls.	233
Figure 6.2	ATR spectra of IgG lyophilized with sugar excipients.	235
Figure 6.3	Amide I/II ratio in IgG formulated with sugar excipients.	237
Figure 6.4	Controls for SEM: lyophilized sucrose and mannitol.	244
Figure 6.5	SEM analysis of IgG lyophilized with sucrose.	246
Figure 6.6	SEM analysis of IgG lyophilized with mannitol.	247
Figure 6.7	SEM data of IgG with sucrose and mannitol together.	250

Chapter 7

Figure 7.1	Reported mechanisms of antibody action.	258
Figure 7.2	Schematic of formats of ELISA assay.	263
Figure 7.3	Chronology of steps involved in an indirect ELISA assay.	266

Figure 7.4	Plate layout for an indirect ELISA testing of samples (I - II).	270
Figure 7.4	Plate layout for an indirect ELISA testing of samples (III-IV).	271
Figure 7.4	Plate layout for an indirect ELISA testing of samples (V).	272
Figure 7.5	ELISA testing of multiple times lyophilized IgG.	275
Figure 7.6	ELISA of IgG lyophilized with sucrose and mannitol.	277
Figure 7.7	ELISA of IgG lyophilized in sucrose and mannitol together.	279

Chapter 8

Figure 8.1	Overview of the experiments performed in this project.	285
------------	--	-----

List of Tables

Chapter 1

Table 1.1	Morphologies of IgG and their dimensions by AFM.	38
Table 1.2	Average heights of IgG domains measured.	39
Table 1.3	Average separations between IgG domains.	40
Table 1.4	Average p (I) values reported for various IgGs.	47
Table 1.5	Comparative out-look on conventional techniques.	48

Chapter 2

Table 2.1	Distribution of IgG stock solution into various aliquots.	61
Table 2.2	Sample T-test report of ferritin particles (~ 4 – 12 nm).	115

Chapter 3

Table 3.1	Preparation of ferritin samples for AFM analysis.	124
Table 3.2	Percentage increase in ferritin (lyo) aggregates in air.	134
Table 3.3	Percentage increase in ferritin (lyo) aggregates in liquid.	135

Chapter 4

Table 4.1	IgG samples for AFM particle size analysis.	146
Table 4.2	Dynamics in the proportion of IgG aggregates in liquid.	159
Table 4.3	Tg and melting points of multiple times lyophilized IgG.	180
Table 4.4	The structural analysis of components in the amide band	188

I in multiple times lyophilized IgG.

Chapter 5

Table 5.1	Chemical structures presented above are of the excipients.	196
Table 5.2	Liquid formulations of IgG lyophilized with excipients.	198
Table 5.3	Lyophilized powders of IgG with excipients.	199
Table 5.4	Melting points and Tg of control excipients.	221
Table 5.5	Tg and melting points of IgG lyophilized with excipients.	227

Chapter 6

Table 6.1	Effect of excipients on components within amide band I.	240
-----------	---	-----

Chapter 7

Table 7.1	Monoclonal antibodies in line for clinical approval.	255
Table 7.2	List of therapeutic antibodies already approved.	256

Chapter 8

Table 8.1	Overview of the experiments performed in this project.	269
-----------	--	-----

List of symbols and abbreviations

A-6-PDH	Antiglucose – 6 – phosphate dehydrogenase
AUC	Analytical ultra – centrifugation
ATR	Attenuated total reflectance
API	Active pharmaceutical ingredient
AFM	Atomic force microscopy
BSE	Back scattered electrons
η	Coefficient of viscosity
CDRs	Complimentarity determining regions
CCD	Charge coupled device
Cp	Heat capacity
CM	Confocal microscopy
DMA	Differential mobility analysis
DSC	Differential scanning calorimetry
DLS	Dynamic light scattering
DCE	Disease combating efficiency
DH ₂ O	Deionised H ₂ O
DBSE	Diffacted back scattered electrons
Dq ²	Decay rate
dT/dt	Heating rate (°C/minute)
dH/dt	Rate of change of heat flow (J/min)

ΔH	Change in enthalpy
Δx	Deflection produced in cantilever
D	Diffusion coefficient
ELISA	Enzyme linked immunosorbant assay
EDS	Electron detection system
E_{adh}	Energy of adhesion
FFF	Field flow fractionation
F	Force
FT-IR	Fourier-transform infra-red
HRP	Horse radish peroxidase
G-6-PDH	Glucose – 6 – phosphate dehydrogenase
IgG	Immunoglobulin G
I	Intensity
I (t)	Light intensity with time
K_B	Boltzmann constant
K	Spring constant
λ	Wave length
mABs	Monoclonal antibodies
MCL	Multiple cycles of lyophilization
MEC	Molar extinction co – efficient
MAC	Membrane attack complex
M	Refractive index

NTA	Nanoparticle tracking analysis
N/m	Newton per meter
OPD	O – Phenylenediamine dihydrochloride
PM	Polarization microscopy
PCS	Photon correlation spectroscopy
PCR	Photon count rate
Q	Heat flow
q	Wave vector
QELS	Quasi elastic light scattering
R_h	Hydrodynamic radius
R	Gas constant
r	Sphere radius
R_E	Resistance of thermo – electric disc
SE	Secondary electrons
SEC	Size exclusion chromatography
SPIP	Scanning probe imaging processor
SPM	Scanning probe microscope
SEM	Scanning electron microscopy
SD	Standard deviation
TMB	Tetramethyl benzidine
TIR	Total internal reflection
TNF	Tumour necrosis factor

TNFR	Tumour necrosis factor receptor
TCR	Tumour cell receptor
TM	Tapping mode
T_m	Melting transition midpoint
T_h	Threshold
UV	Ultra violet
G – CSF	Granulocyte colony-stimulating factor
MCSF	Macrophage colony-stimulating factor
IFN	Interferon

Chapter 1

Introduction to aggregation in protein therapeutics

1.1 Biopharmaceuticals

Pharmaceutical products form the backbone of modern medicinal therapy [1, 2, 3]. The majority of pharmaceuticals remain low molecular mass organic substances, and are manufactured by direct chemical synthesis. Direct chemical synthesis is now employed even for the manufacture of drugs (such as aspirin) which were originally obtained from natural sources. The term 'biopharmaceutical' refers to products of a biological origin or from biotechnological endeavour. This includes vaccines, enzymes, hematopoietic growth factors [such as granulocyte colony-stimulating factor (G – CSF), macrophage colony-stimulating factor (M – CSF), erythropoietin (EPO) – which stimulates red blood cell formation], interferons [such as interferon alfa – 2a and interferon alfa – 2b (IFN – α 2a, IFN – α 2b)] and interleukins [such as recombinant human interleukin-1 β] which regulate immune response, monoclonal antibodies, hormones, antibiotics and plant metabolites [such as angiotensin – I – converting enzyme obtained from tabacco/tomato treats hypertension]. The advent of recombinant proteins and monoclonal antibodies in the 1980s, and their

subsequent use in therapeutics and vaccines have profited humans globally. The US Food and Drug Administration (FDA) have permitted 30 antibody based drugs until 2011 [4] and presently 418 protein based drugs are under developmental process [5]. The first biopharmaceutical product to come on the market was recombinant human insulin, produced in *Escherichia coli*. This product (trade name Humulin) was granted a marketing licence by the Food and Drug Administration (FDA) in 1982 [3]. The significance and urgency of developing proteins based drugs stems from their natural origin, direct extraction from biological source, considerably better bioavailability and lesser side effects compared to synthetic drugs and more astonishingly biopharmaceutical companies are developing such 73 medicines and vaccines, which are concentrated on enhancement of treatment regimes, more effective therapies and encouraging novel deterrent answers for AIDS and patients affected with cancer [5, 6]. The development of such biopharmaceuticals is anticipated to become increasingly important and is generally agreed to be urgently required in the 21st century for the prevention and treatment of diseases such as different forms of cancer, hepatitis, multiple sclerosis, strokes, diabetes, Parkinson's and Alzheimer's [7].

While highly effective as therapeutics, proteins are challenging to formulate as stable preparations. Proteins are intricate molecules possessed of abundant reactive chemical moieties and a subtle three-dimensional structure organized

into primary, secondary, tertiary and quaternary structural components [6]. This intricacy renders proteins with significant and new stability problems compared to traditional small molecular weight drugs. Hence protein based drugs can be exposed to several physicochemical changes during purification, formulation, handling and storage [7]. A slight alteration in protein structure can have a significant impact on protein activity and/or can therefore cause immunogenicity [8]. Therefore, the challenge of stabilizing proteins in the course of processing, formulation, storage and handling is growing. Another important aspect is protein instability, reduced bioavailability if administered via non-invasive routes due to the larger size and highly hydrophilic propensity of the protein molecules. Therefore, predominantly protein therapeutic compels parenteral administration. The protein formulation in the solution state is usually a favoured mode due to the avoidance of issues associated with change in tertiary structure, degradation and difficulties in adsorption across mucosal membranes, which in turn improves therapeutic efficacy and bioavailability. However, the development of stable protein formulations in the solution state is challenging because denaturation and aggregation can be induced by several influences to which protein in solution state is sensitive, such as agitation, freezing, heating and exposure to interfaces [9-12]. Furthermore, protein molecules can undergo chemical alterations (hydrolysis and deamidation facilitated by water) in the suspension state. Dried suspension formulations in a solid form have been used effectively to improve physico-chemical stability and long term storage of protein based drugs. One such widely employed and preferred method of drying is lyophilization [13, 14].

However, despite drying by using the effective method of lyophilization, aggregation can still occur and therefore, currently one of the major challenges for pharmaceutical companies is to prevent aggregation in bio-pharmaceutical products, particularly those based on proteins/peptides, such as IgG antibodies and Insulin [15, 11]. Protein based bio-pharmaceutical products when exposed to conditions different from their native environment can result in physical and chemical changes in protein structure as stated earlier, which can trigger aggregation or precipitation during drug formulation processes. As a consequence both drug dosage and biological activity of a therapeutic protein product can be adversely affected. The most concerning problem is that aggregates can trigger a severe immune response, which could even prove to be fatal [16]. Moreover, there is often a need for very high concentrations to achieve an effective and potential therapeutic dose, and hence this increases issues related to aggregation [16]. A related problem is the need to increase the shelf life of bio-pharmaceutical formulations, because increased shelf life provides the liberty to store the drugs for longer time while keeping their therapeutic efficiency intact. This in turn prevents the loss of millions of pounds each year caused by the limited shelf life of bio-pharmaceuticals [17]. Therefore, an effective formulation strategy/technique which would enable us to overcome the problem of aggregation in bio-pharmaceutical formulations for the preservation of their chemical and physical stability would be a welcome in the bio-pharmaceutical industry.

1.2 Aggregation in proteins

Aggregation of proteins is an important phenomenon and can have both positive as well as negative consequences. Most naturally occurring protein aggregation is productive, because it governs normal functioning of many biological processes. For example: fibrillation reaction of (G – actin – globular) \rightarrow (F-actin-fibrillar)_n, regulates the normal shape and mobility of cells in humans [18,19]. Neurodegenerative diseases such as Alzheimer's [20], Huntington's [21], and Parkinson's [22], the amyloidoses, and prion diseases are hypothesized to be the negative consequences of aggregation in β – amyloid, polyglutamine and α – synuclein respectively [23].

Aggregation involves nonspecific assemblage, association or polymerisation of two or more proteins/-polypeptides (either denatured or not) [24, 25]. Aggregation can be described as the formation of larger assemblies from completely or partially folded proteins/polypeptides.

The aggregation is considered to be normal when the starting reactant (monomer) is in its native form (natural). However, in cases of abnormal aggregation, there is a concern whether the starting reactant (monomer) begins in its native form, or in denatured state (more active). It is generally believed that the association of proteins in a non-native state is responsible for their abnormal aggregation. The driving force for the aggregation emanates from the interactions between inappropriately solvent exposed hydrophobic surfaces that are normal to the

protein's interior. Hydrophobic surfaces which are highly exposed upon denaturation act as sticky spots and interact with whatever they can during forces of interaction. In an aggregated protein solution, since an individual protein molecule can exist either in native (folded), partially folded or unfolded form, therefore, the nature of the constituents of different types of aggregates becomes highly unpredictable. Moreover, there is a general consensus that different species of aggregates produced in protein solution may exist in dynamic equilibrium with each other, which could be influenced by number of factors such as pH, ionic strength, buffer composition, surfactant concentration, besides thermal/mechanical stress, lyophilization, thawing, quenching, and exposure to interfaces or denaturing chemicals [13, 24]. It has been reported that any protein has a tendency to form aggregates when exposed to a suitable external environment both *in vivo* and *in vitro* and can be broadly categorized into an ordered [amyloid fibrils] and disordered aggregates [26, 27]. Amyloid fibrils are predominantly composed of highly organized β – sheet structures stabilized by hydrogen bonds. Each amyloid fibril is around 10 nm in diameter and composed of 2 – 6 cross β – structured proto – fibrils with β – sheets running perpendicular to the fibril [26, 27]. Although the aggregation depends on the characteristics of the amino acid sequence, the inter-peptide chain interactions may also cause conformational changes which would make it difficult to predict aggregation. *In vivo* examples of disordered aggregates (inclusion bodies) are those formed due to re-aggregation during renaturation of insoluble non-ordered protein. On the other hand, the *in vitro* disordered counterparts are those produced in the course

of the refolding of denatured (unfolded protein). These are usually produced at much larger concentrations of protein. These are classified as folding aggregates and are produced in near native environments when concentration exceeds a critical level. The natively folded proteins may aggregate in a way different from those folded non-natively. It has been reported that the former precipitate at an isoelectric point of protein. Since at an isoelectric point, there occurs no net charge on the surface of protein, pH of the solution reaches to equilibrium at the hydrophobic surface of the protein with considerable decrease in the formation of dipoles, van der Waals, or hydrogen bonds by water molecules on the protein's exterior. Therefore, water molecules diffuse away, thereby decreasing the volume occupied by the water molecules at the protein surface. In this fashion, protein-protein interactions become predominant and let protein to fall and precipitate. The precipitates of native protein show instant solubility in buffer environment identical to native. The reason is due to the induction of salt into the protein-solvent system (salting in); salt ions interact with the hydrophilic residues stationed on the protein's exterior surface. Consequently, the number of water molecules required to interact with hydrophilic amino-acid residues on the external surface of protein reduces whereas the amount of free water molecules for protein solvation increases. However, in contrast, the influence of increased salt concentration causes several water molecules to get attracted by salt ions which in effect decreases the proportion of water molecules available to interact with the charged part (hydrophilic) of the protein. Hence, protein solvation decreases, which consequently imparts greater strength to inter-protein

interactions than protein-water interactions. Eventually, the protein molecules precipitate by forming hydrophobic interactions and interactions between oppositely charged patches on the proteins's external surface (salting out). However the precise concentration instigating precipitation differs from protein to protein, thereby consenting separation of different proteins at different points. The dissociation of insoluble aggregates (non-natively folded and disordered) aggregates in contrast, occurs only in presence of high concentrations of denaturant or detergent [26, 27]. It is also believed that proteins with several short amino-acid sequences containing hydrophobic residues show an inclination towards β – sheet formation and likely demonstrate a greater tendency to form aggregates and/or amyloid fibrils [26, 27]. In contrast, the surrounding polar amino-acid sequences are considered responsible for improving the protein solubility. This is because solvation is favoured with increase in the number of hydrophilic amino acid residues on the protein's exterior surface and is expedited by electrostatic interactions between charged (positive or negative) hydrophilic amino acid residues and δ – positive or δ – negative dipoles induced in water [26, 27].

Despite various attempts in the last couple of decades to explain aggregation and its potential effects, some of the fundamental questions associated with aggregation are not yet fully understood. For an example: What is the nature of the species (starting reactants and intermediates) responsible for aggregation? What is the most detailed mechanism that could be accountable to explain

aggregation and the core kinetics involved in such a process? What would be the morphological and chemical structure of aggregates? What sort of specific intermolecular associations govern aggregation of a particular type of protein? Why some protein forms are ordered (amyloid) and sometimes disordered such as inclusion bodies, folding and amorphous aggregates? How do environmental factors affect aggregation and why are different proteins affected differently? Finally, how can we develop such methodologies that would enable us prevent, minimise and overcome aggregation fully? The following text will describe known mechanisms of protein aggregation.

1.2.1 Mechanisms of Aggregation

Several mechanisms have been proposed to protein aggregation such as by Goldberg *et al.* for the enzyme tryptophanase [28], King *et al* on the tailspike protein endorhamnosidase [29] and Wetzel *et al* on mammalian amyloid [30, 31]. According to Goldberg and his colleagues, aggregation proceeds via the formation of an intermediate and that under reasonable denaturant (denatured protein) concentration that aggregated, the addition of other folded proteins did not disturb the quantity of aggregated tryptophanase. This view that partially folded intermediates might be responsible for aggregation has been also describes molecular interactions between hydrophobic surfaces of subunits in an advocated by the descriptions given by King *et al* and Wetzel *et al*. Moreover, intermediates the aggregation of several proteins [32, 201].

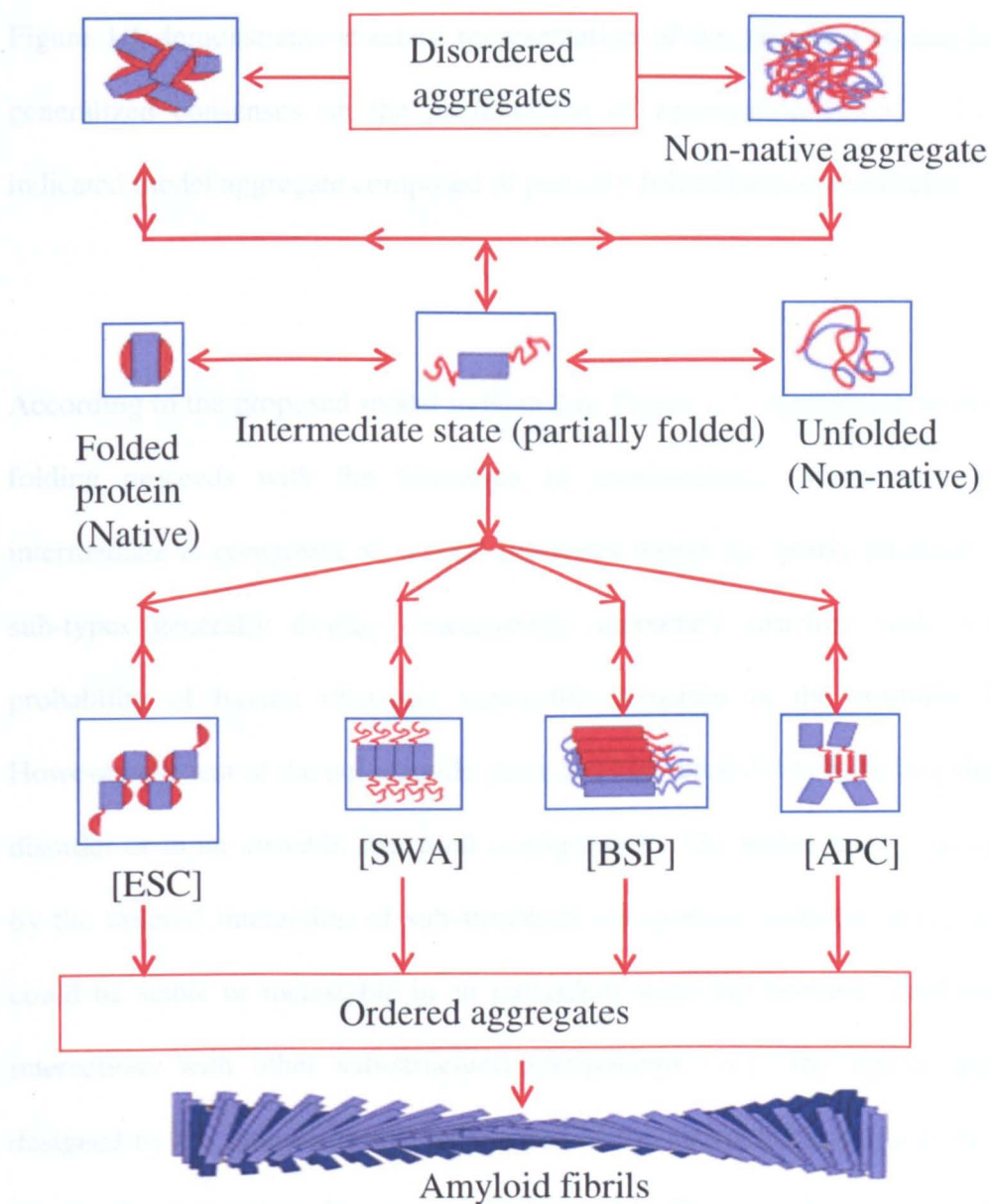
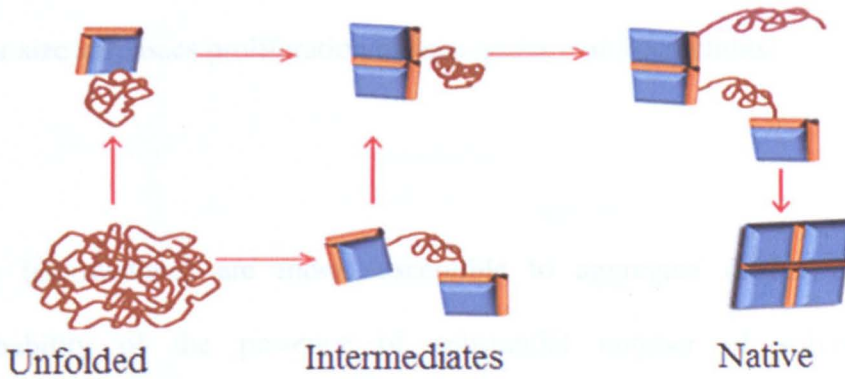


Figure 1.1 The standard model that gives a simplified account for protein aggregation. The partially unfolded intermediate could be produced either from a native or unfolded protein and has tremendous susceptibility to aggregate. The formation of ordered amorphous aggregates is governed by specific mechanisms such as an exchange of structural components [ESC]; sideways association [SWA]; β – sheet piling [BSP]; association of individual protein chains [APC]. Non-specific self-association of both and non-natively folded protein leads to the formation of disordered aggregates [29].

Figure 1.1 demonstrates standard representation of the proposed model having generalized consensus on the phenomenon of aggregation [29-31, 32]. The indicated model aggregate composed of partially folded protein molecules.

According to the proposed model indicated in Figure 1.1, aggregation or protein folding proceeds with the formation of intermediates, where each given intermediate is composed of several sub-types which are nearly identical. The sub-types generally display characteristic secondary structure with a high probability of having relatively native-like structure in the common core. However, the rest of the polypeptide chain has high probability to be in a state of disorder or in an unstable structural configuration. The native state is designed by the ordered interaction of sub-structural components (sub-domains), which could be stable or metastable in an individual state, but become stabilized by interactions with other sub-structural components [26]. The native state is designed by the intra-molecular interaction of the hydrophobic surfaces of sub-structural components Figure 1.2 [section A]. The specificity of such an interaction is influenced by several factors such as geometric shape and length of the hydrophobic area besides the attendance of other sub-structural components. Such specific interaction of the hydrophobic surfaces in an intermolecular fashion results in aggregation Figure 1.2 [section B]. This demonstrates that the commencement of aggregation involves interactions between the specific surface portions of the sub-structural components of two

A. Pathway that leads to formation of normal ensembling of sub-structural components



B. Pathway that leads to aggregation due to abnormal

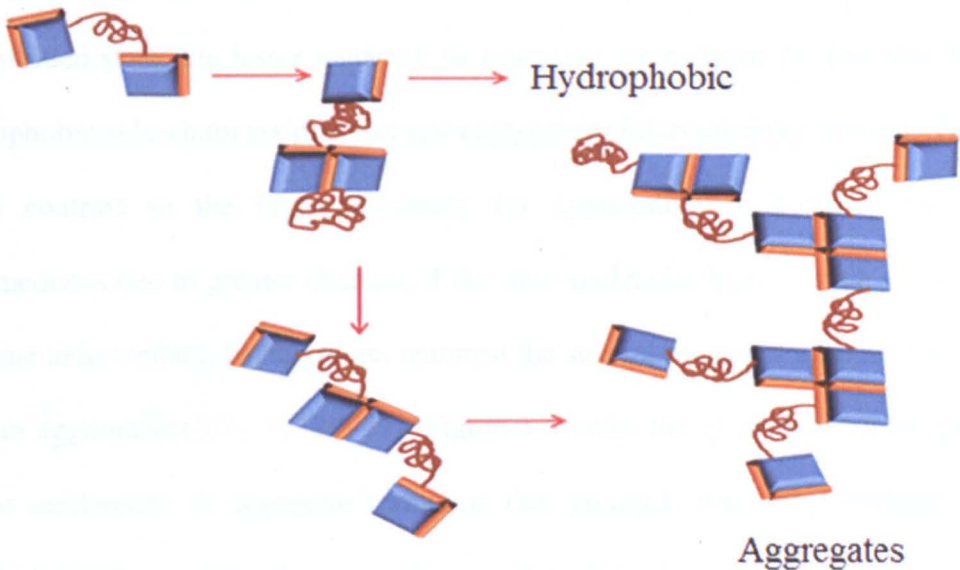


Figure 1.2 Schematic of the most probable folding mechanism of the sub-structural components of a given protein. [A] Represents normal folding pathway and is a consequence of intra-molecular whereas [B] leads to an aggregation and is a result of intermolecular interaction of hydrophobic surfaces (shown by orange faces) stationed on the sub-structural components. The folding, both in the native state and structures involved in aggregation start off from the partially folded intermediate. All the intermediates involved would be composed of conjoint sub-structural components [26].

molecules. To begin with, the aggregates formed are either dimers, trimers, tetramers and other lower multimeric forms would be soluble, but in due course their size surpasses proliferation of inter-molecular interactions.

The intermediates are more susceptible to aggregate further due to high probability of the presence of substantial number of solvent exposed hydrophobic surfaces. The unfolded native state results from the intra-molecular interaction of the hydrophobic faces of sub-structural components. Therefore, in an unfolded state, the lesser tendency to aggregate stems from the fact that the hydrophobic side-chain residues are not exposed for intermolecular contact. This is in contrast to the high propensity for aggregation in partially folded intermediates due to greater chances of the inter-molecular hydrophobic surfaces to come in to contact. Furthermore, amongst the several proposed mechanisms of protein aggregation [26, 28, 29, 32]. Figure 1.3 gives the most detailed account of the mechanism of aggregate formation that proceeds with the formation of amyloid fibrils in case of native (non-denatured) and non-native (denatured) starting reactants (monomers) [33]. Amyloid fibrils are predominantly composed of highly organized β – sheet structures stabilized by hydrogen bonds [Figure 1.4]. Each amyloid fibril is around 10 nm in diameter and composed of 2 – 6 cross β – structured proto – fibrils with β – sheets running perpendicular to the fibril. Although the aggregation depends on the characteristics of the amino acid sequence, the inter-peptide chain interactions may also cause conformational un-

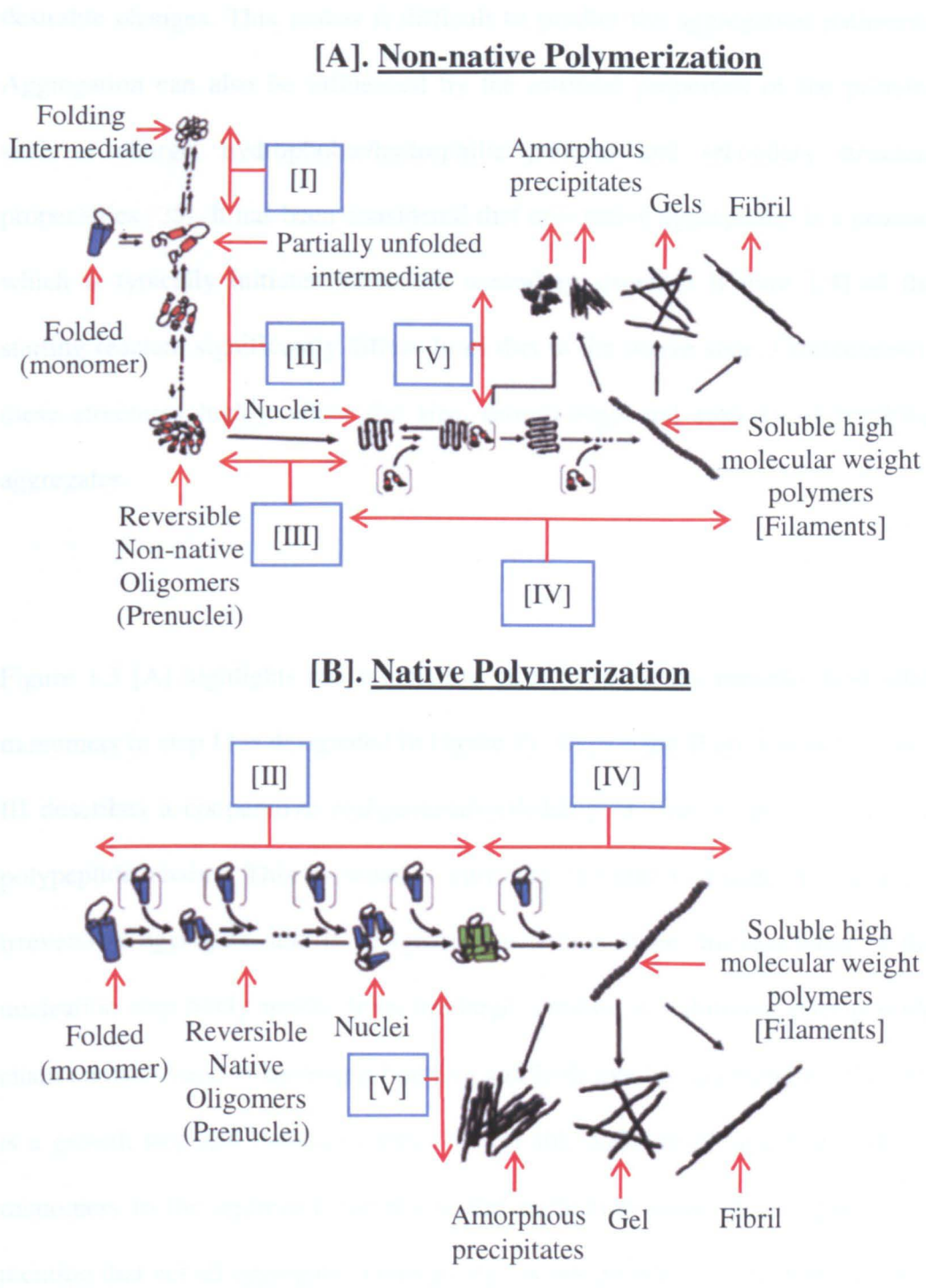


Figure 1.3 [A] and [B] respectively highlight the multiple stages of aggregation in non-native and native aggregation respectively. There seems to be a consensus that protein aggregation occurs via a mechanism that involves nucleation both in the case of native and non-native polymerisation (from [25])

desirable changes. This makes it difficult to predict the aggregation pathways. Aggregation can also be influenced by the intrinsic properties of the proteins such as charge, hydrophobic/hydrophilic patterns and secondary structure propensities [25]. It has been considered that non-native aggregation is a process which is typically initiated when the secondary structure [Figure 1.4] of the starting reactant significantly differs from that in the native state. Consequently, these structures highly affect the size, morphology and toxicity of resulting aggregates.

Figure 1.3 [A] highlights the association steps between the partially misfolded monomers in step I (as designated in Figure 3). Steps I and II are reversible. Step III describes a cooperative realignment/misfolding of two or more non-native polypeptide chains. This is what is currently thought to create the smallest irreversible aggregate, and is designated nucleation stage. Irreversibility of the nucleation step likely results from the large number of stabilizing inter-peptide chain contacts such as hydrogen bonding and hydrophobic interactions. Step IV is a growth step and involves further irreversible addition of single or multiple monomers to the aggregate formed in the nucleation stage. It is important to mention that not all aggregates undergo significant growth after nucleation. Most studies have confirmed that the polymers/filaments observed in stage IV are generally linear and are predominantly composed of β – sheet structures. However, this does not necessarily apply for all polymers. Step V shows that

sometimes condensation takes place where aggregates associate with each other by means of cross linking to form gels, or form fibrils by way of bundling or lateral association and even separate out as precipitates. The native state that yields proper function is considered to be a low energy stable conformation of a protein. An inter-chain contact with other parts of that protein or with other protein moieties produces energetically more favourable conformation than the native state of that protein, which consequently result in aggregation. Figure 1.3 [B] describes a native protein aggregation pathway which doesn't account for the conformational changes in step I.

The model shown in Figure 1.3 is considered to be more reasonable for natively folded proteins/polypeptides. The nucleation (III) and polymerisation (IV) steps are implicitly irreversible, and will occur if stage V is omitted. It has been observed that in some cases the reversible nature of step II corresponds to the predominant formation of β – sheet structures [Figure 1.4] [25].

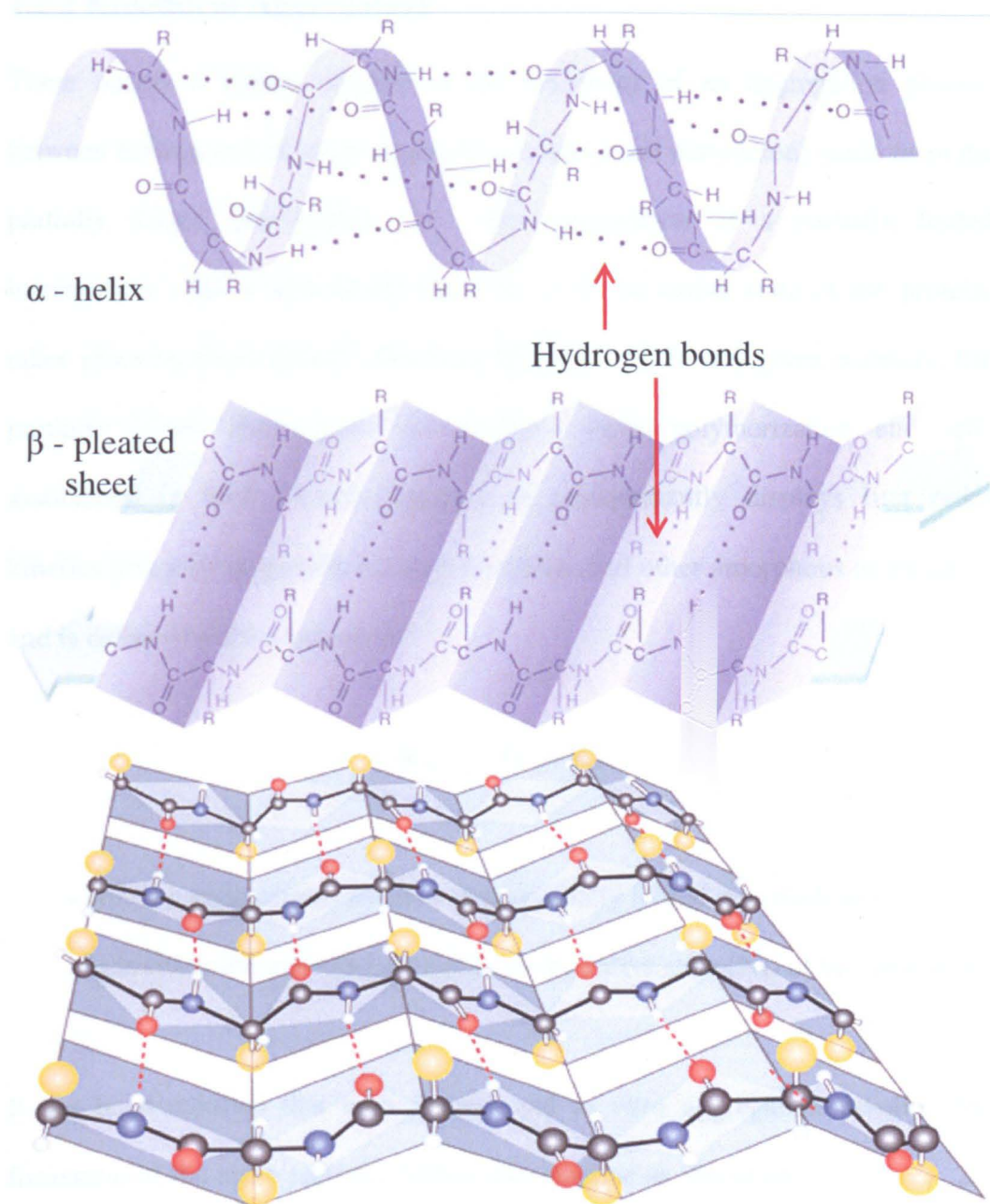
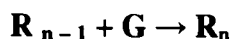


Figure 1.4 Three dimensional representation of the molecular secondary structure of a protein [Top panel] [34]; The bottom panel is ball and stick model representation of β – pleated sheet structure of an amyloid fibril which is formed as a result of an inter-chain hydrogen bonding (---) protein chains. The side chains run up and down the sheet and alter in the arrangement of aminoacids alongside the chain [35].

1.2.2 Kinetics of Aggregation

There occurs a kinetic struggle at the beginning of an aggregation process between folding and all other aggregates (ordered and disordered) made from the partially folded intermediate [36]. The aggregation of a partially folded intermediate, that is structurally different from the native state of the protein, takes place by three parallel directions [Figure 1.1]. In any given pathway, the partially folded intermediate can undergo chain polymerization and self-association or both. Protein aggregation predominantly displays first order kinetics [even in the growth of amyloid fibrils, and other amorphous aggregates] and is defined by the expression:



- **R** is the aggregation sensitive state (partially folded intermediate)
- **G** is either the unfolded state (U_f), or the native state (N_s) of the monomer.

It has been reported that both *in vivo* and *in vitro* aggregation involves the formation of the same partially folded intermediate as precursor [25, 26, 27, 29, 30, 31 and 32]. The extent of formation of partially folded intermediates in itself and the rate of the aggregation depends upon the nature of the protein amino acid sequence and as such is influenced by several environmental (solution) factors such the pH, temperature, ionic strength, the concentration of the protein and the occurrence of other solutes. The disparity in the stability of the native state to the

partially folded intermediate stems from the influences of the ingredients that constitute the solution environment. For instance, protein concentration has a substantial impact on the degree and rate of intermolecular interaction. The nature of the precursor that starts aggregation is intricate and affects the equilibrium between the native state and the partially folded intermediate. The equilibrium of the partially folded intermediate with native state always makes the partially folded intermediate precursor for aggregation [25, 26, 29]. The instability of the native state increases the amount of a partially folded intermediate and aggregation will be amplified. Longer lifetime of partially folded intermediates ensures enhanced inter-molecular interaction and therefore, favours aggregation.

1.2.3 Significance of aggregation in protein based therapeutics

The control and understanding of the abnormal aggregation is highly significant to biotech and pharmaceutical industries for keeping protein based drugs in a non-aggregated state in order to ensure their safety, efficacy and a longer shelf life. Otherwise, aggregation not only reduces the drug efficacy and shelf life, but can also lead to toxicity and evoke an immunological reaction [37]. From a pharmaceutical perspective, it is generally believed that protein based formulations usually experience aggregation during the early or final stages of developmental process, where they are most often difficult to detect [38]. The aggregates formed in protein based formulations show a high degree of

variability in their size, solubility, morphology and the nature of interactions which hold them together [39]. On the basis of their solubility, aggregates are broadly classified as:

A. Soluble aggregates

These are invisible particles to the naked eye and it is difficult to separate them from the protein formulation.

B. Insoluble aggregates

These are easily detectable, visible to the human eye and can be removed by filtering. The insoluble aggregates may be considered pathological in nature. This must not be confused with insolubility of the native state due to protein concentrations above the solubility limit (precipitating out). It must be realized that in many such cases of pathological aggregation the starting oligomer formed may be comprised of soluble aggregates, but become insoluble when they exceed a certain size.

Both soluble and insoluble aggregates create problems in the development of a protein based biopharmaceutical. Consumption of such a formulation can stimulate immunogenic response which can prove fatal. Aggregation of insoluble

aggregates in general is considered irreversible under native-like environments. [25 – 27]. However, it does not mean that aggregation cannot be reversed. For example *in vivo* reversal of aggregated amyloids has been reported [25 – 30]. Several studies have shown that an addition of protein fragment could inhibit aggregation by disrupting specific interactions and that enhanced hydrophobicity of the interface of sub – structural components could amplify the drive for an aggregation. This has been best evidenced by the investigations conducted by Brems *et al.*, [40] on bovine growth hormone (BGH). On the basis of the nature of interactions between the monomers, aggregation is of two types:

a. Irreversible aggregation

This type of aggregation can occur due to covalent bond formation between multiple monomers of a given protein/polypeptide or due to simple protein-protein interactions. Disulphide bond formation of free thiols is one of the most common pathways for the formation of covalent aggregates. Formation of bityrosine crosslinks due to the enzymatic oxidation of tyrosine residues is often believed to promote covalent aggregation in proteins. It has been proposed that in the presence of peroxidase and hydrogenperoxide at basic pH results in tyrosine is oxidized to form a tyrosyl radical cation which upon loss of proton forms neutral a radical [Figure 1.5]. Therefore, the formation of bityrosine is materialized by the oxidative phenolic coupling of two tyrosyl radicals followed by tautomerization [8, 12, 13, 14, 15, 41, 42].

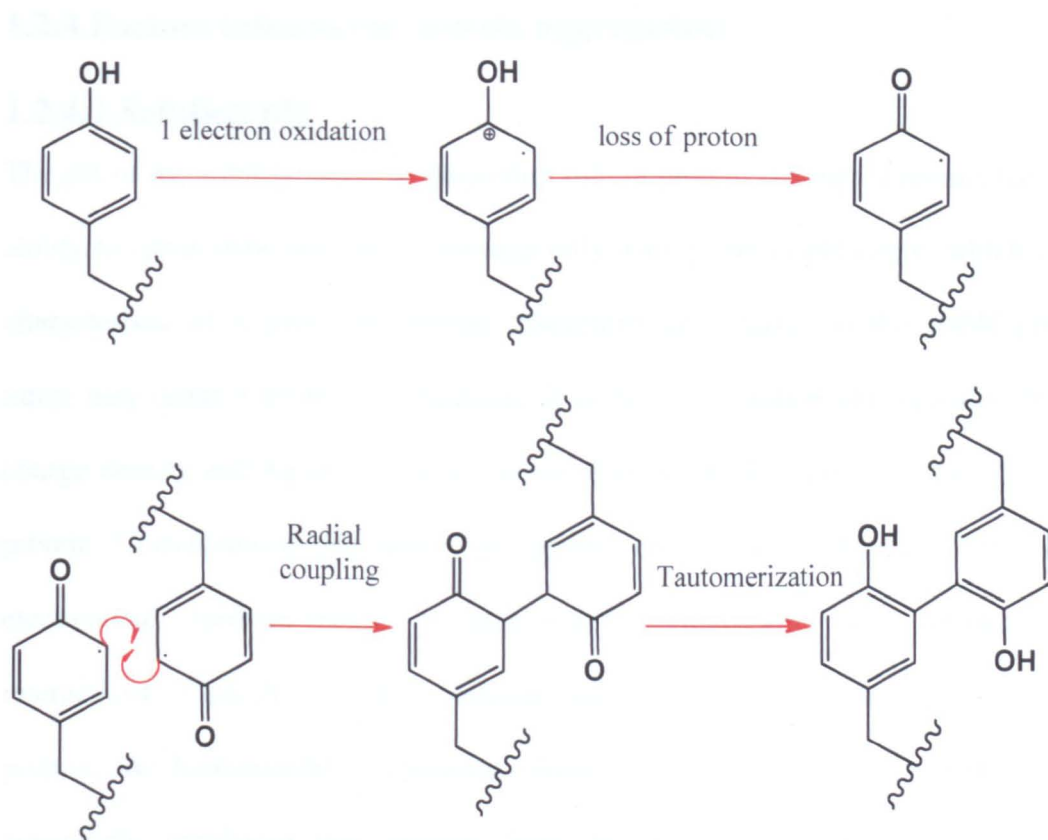


Figure 1.5 Representation of the sequence of steps involved in the formation of bityrosine: oxidative phenolic coupling of two tyrosyl radicals coupling is succeeded by tautomerization [42, 280].

b. Reversible aggregation

This kind of aggregation takes place due to the weaker interactions such as hydrogen bonding, dipole-dipole and van der Waals interactions between the reacting monomers. However, the reversibility of these protein aggregates could be influenced by the alteration in pH, salt concentration and concentration of protein itself (explained in section 1.2.4) [13, 14, 15, 41].

1.2.4 Factors influencing protein aggregation

1.2.4.1 Solution pH

The pH of the solution plays an important role in protein stability. Proteins have ability to retain their stability in solution only over a certain pH range, which is characteristic of a particular protein. Therefore, any change in the stable pH range may cause a protein to aggregate. It is because solution pH regulates the charge density and nature of charge (positive or negative) on the surface of the protein. Consequently, this affects the protein conformation and the nature of electrostatic (protein-protein; protein-water; protein-ion, and ion-water) interactions. Typically, at pH far distant from the isoelectric point (pI) of the protein, the fundamental electrostatic interactions that destabilize protein are nonspecific repulsions that emanate from the charged groups of hydrophilic amino acid residues on the external surface of a highly charged protein. In addition, any increase in the acidity or basicity of the solution builds up the number of charged groups on the surface of protein. Therefore, there occurs an increase in the charge repulsions within the protein which disrupts the folded protein conformation. The pH induced protein unfolding is facilitated due to an increase in the charge density on the folded protein (native) in order to attain a conformation of lower electrostatic free energy. Furthermore, specific charge interactions by way of ion pairing can also affect protein conformation [24, 31, 43]. Other than the change in conformation; in case of proteins with anisotropic charge distribution on the protein surface, the charges on protein molecules also give rise to the attractive forces between neighbouring protein molecules stem

from dipole interactions which are formed as a result of electrostatic interactions between an acidic amino acid residue of one protein and basic amino acid residue of other. Such protein-protein interactions are highly attractive and result in energetically favourable aggregation. However, the dominance of attractive forces is opposed by the formation of repulsive electrostatic interaction forces between protein molecules; and also favours protein dissolution. The repulsive electrostatic forces are formed as a consequence of the movement of oppositely charged ions (present in buffer solution) towards charged amino acid residues situated on the surface of protein.

1.2.4.2 Effect of salt

The effect of the presence of an electrolyte (salt) on protein in solution is an intricate process to understand. It is because ions in solution can destabilize the physical structure by altering protein conformation; interfere with solubility (e.g., salting-in and salting-out) and influence the tendency of the proteins to form non-native aggregates. The ions released from salt in a solution bind to proteins by interacting with unpaired charged side chains (hydrophilic amino acid residues) on the protein surface. The cross-linking of the hydrophilic amino-acid residues via multivalent ions stabilizes the native state of protein. However, in case of non-native state of protein, the salt ions initiate the destabilization of the protein by binding to peptide bonds which carry dipole moment which arises from partial positive charge on the amino group and partial negative charge on

the carbonyl oxygen. The electrostatic interactions (attraction and repulsion) between the charged species both within the protein and between protein molecules are regulated by electrolyte (salt) in the solution. The conformational stability is influenced by intra-molecular electrostatic interactions. On the other hand, solubility equilibrium and the rate of aggregate formation are governed by inter-protein electrostatic interactions. The ion-induced dipoles in water molecules at low concentration of salt shields surface charge, which reduces electrostatic (both intra and inter-protein) interactions by improving solvation. However, at high concentration of salt, in addition to charge-shielding effects, supplementary ions of the salt guard protein surface with multi-ion charges, which trigger decrease in thermodynamic stability of the native conformation besides rendering proteins lower degree of solubility in solution. The reason is layer of salt ions forms firm background on the surface of protein; all hydrophilic amino-acid residues on the protein's external surface become unavailable for interaction with water molecules [24, 31, 43].

Therefore, available salt ions interact with water molecules, which increase the proportion of water molecules to solvate salt ions. Consequently, decrease in amount of free water molecules results in inter-protein interactions (between oppositely charged patches on the external surface of two proteins and hydrophobic interactions). The precise concentration causing in precipitation differs from protein to protein, consenting separation of different proteins at

different points. The resultant effect of salt on protein stability in solution is therefore multidimensional, as there are multiple ways by which salt ions interact with protein molecules which affect electrostatic interactions (intra – protein; inter – protein, protein – water; water – ion; ion – protein, ion – ion).

1.2.4.3 Effect of temperature

The biological function/s of protein is determined by its specific globular conformation which is thermodynamically stable and least energetic with free energy of the order of 5 – 20 kcal/mole. The free energy obligatory for the formation of the folded conformer is expedited by energy drawn from inter-peptide interactions, hydrophobic interactions, hydrogen bonding, van der Waals forces and electrostatic forces (charge repulsion or ion pairing). However, the conformational entropy acts as a contradictory force to protein folding. With an increase in temperature, the thermal kinetic energy for activated protein molecules increases, therefore, the conformational entropy of the protein observes an increase in the degrees of freedom both on molecular level (translational, rotational, and vibrational degrees of freedom) as well as on the level of chain configuration. The change in temperature, pH, or salt concentration of the protein-solvent system can create alterations in the protein's native conformation, which in turn can initiate unfolding and destabilization of the structure of the protein. Generally, proteins experience thermal denaturation at temperatures slightly above their stability temperature. However, the

denaturation lead aggregation can initiate at temperatures well beneath the equilibrium melting temperature of the protein, which advocates for the aggregates that are not made from completely unfolded molecules but from partially unfolded protein species. The aggregation kinetics is strongly influenced by temperature and rate of aggregation increases exponentially with temperature [24, 31, 43].

1.3 Lyophilization process

General methods of drying of bio-pharmaceutical products (such as antibodies, proteins/peptides, hormones etc) always cause loss in their activity or some other damage, because such products are very delicate and heat sensitive. Therefore, an improved and more complex form of drying called lyophilization (freeze drying), is now widely employed, because it significantly minimises the extent of damage caused by general drying [12, 13, 14, 43]. Figure 1.6 shows a schematic phase diagram of lyophilization process. The process of removal of solvent directly from solution while in the frozen state is called lyophilization. However, this process can promote the inactivation of some proteins. However, this process can promote the inactivation of some proteins. Therefore, specific cryo – protectants in the form of carbohydrates (such as glucose and sucrose), proteins (such as albumin; and amino acids such as lysine, arginine or glutamic acid) are added to the specific product in order to minimise

such inactivation. Some alcohols and polyols have also been used as cryo-protectants [12, 44].

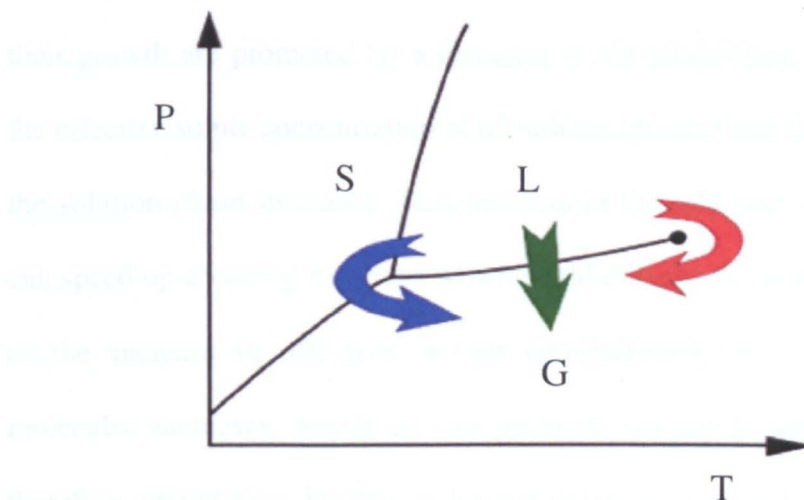


Figure 1.6 Lyophilization: (blue arrow) brings the system around the triple point, in order to avoid the direction liquid – gas transition observed in case of general drying (green arrow).

Lyophilization involves in two stages primary and secondary drying. The detailed description of the indicated stages is given in the following text.

1.3.1 Primary drying

This is initiated by placing the material in a freeze – drying flask and rotating the flask in a bath, called a shell freezer, which is cooled by mechanical refrigeration, dry ice, methanol or liquid nitrogen. In this step, it is important to

cool the material below its triple point, i.e; the lowest temperature at which the solid and liquid phases of the material can coexist. This ensures that sublimation rather than melting will occur during secondary stage of drying. Usually, the freezing temperatures are between $-50\text{ }^{\circ}\text{C}$ and $-80\text{ }^{\circ}\text{C}$. Ice crystal formation and their growth are promoted by a decrease in the temperature, as a consequence, the effective solute concentration of all solutes (protein and excipients) present in the solution phase increases. This increase in the effective solute concentration can speed up chemical reactions which could damage the protein. Moreover, due to the increase in effective protein concentration, the intimacy of protein molecules increases, which in turn promotes protein-protein interactions, and therefore aggregation. Further, reduction in temperature causes crystallization of solutes, and they are effectively removed from solution. Crystallization of individual buffer constituents at different temperatures, may lead to change in pH values of the remaining solution, due to which aggregation can be induced [1, 11, 13]. As the temperature is further lowered, the viscosity of unfrozen solution increases dramatically until molecular mobility effectively ceases. This unfrozen solution will contain protein as well as the excipients, and at most 50% water. As molecular mobility effectively ceases, chemical reactivity also ceases. The consistency of this 'solution' is that of a glass, and the temperature at which this is attained is called glass transition temperature (T_g). For most protein solutions, T_g values reside between $-40\text{ }^{\circ}\text{C}$ and $-60\text{ }^{\circ}\text{C}$. The primary objective of the initial stages of lyophilization usually is to decrease product temperature below the T_g as quickly as possible [1, 11, 13, 45].

1.3.2 Secondary drying

The second step in the lyophilization process involves the application of a vacuum to the system usually at temperatures slightly in excess of 0 °C. This results in the sublimation of the crystalline water, leaving behind a powdered material. The removal of water from any bio-pharmaceutical product yields a powdered product, usually displaying low water content of the order of 3 % [11]. Lyophilization gives the opportunity to avoid denaturation caused by heating the product, by maintaining it frozen throughout drying. This is the most obvious advantage over liquid – phase drying. Moreover, liquid – phase drying triggers an undesirable shrinkage and concentration of active constituents which causes damages protein as well as a movement of these constituents to the surface of evaporation, where they form a dense, impermeable skin that inhibits drying, and later, rehydration. Lyophilization ensures greater reduction in the chemical biological-mediated inactivation of the biopharmaceutical and an improved shelf life of the product. Therefore, lyophilization is often considered to be a valuable tool for preserving many bio-pharmaceutical products [45]. Advantages of freeze drying are the minimum damage and loss of activity in proteins. Rapid and completeness of rehydration, leaves product porous and friable, and effectively cleans products. The main disadvantage of this technique is its high capital cost. It also usually takes long time, for example 24 hours per cycle. So far several studies have investigated the impact of lyophilization on the level of aggregation in other proteins and IgG [15, 43 – 60]. A brief introduction of these studies is given in the following sections:

1.4 Effect of the lyophilization on IgG and other proteins

As mentioned earlier in the section 1.1, protein based formulations show an inherent propensity to form aggregates in solution, therefore, pharmaceutical industries often use dry powdered preparations for increased stability and shelf life. For this purpose, one of the most widely employed methods of drying is freeze drying (lyophilization). Mostly lyophilization of protein based formulations is accompanied by some level of structure collapse which may or may not be associated with activity loss. Several studies have investigated the impact of lyophilization on proteins such as β – galactosidase, catalase [57], and lactate dehydrogenase (LDH) [15, 58]. Studies have shown that β – galactosidase (150 kDa monomer) loses most of its activity after lyophilization in the absence of lyoprotectants. This loss in activity has been assigned to partial unfolding followed by the formation of insoluble aggregates after lyophilization. Other proteins such as catalase retain 40 % activity after freezing, while after lyophilization only 13 % activity had been reported [15, 56, 58]. Some others have reported that catalase retains 80 % of its initial activity after freeze thawing, but only 30 % after lyophilization [15]. The partial dissociation of catalase into monomers and dimers during lyophilization has been found to be the likely reason of inactivity [15, 56, 58]. The loss in the activity of the lactate dehydrogenase has been seen to be concentration dependent and increase in its activity at higher concentrations after lyophilization had been found significantly greater than after freezing [15, 58]. However, the addition of a lyoprotectant has been shown to prevent inactivation of most of the studied proteins during and

after lyophilization [15, 57, 58]. It has also been observed that the recovery of the activity in all proteins follows the same pattern after lyophilization and appears to be concentration dependent [46, 59, 60, 61]. Similarly other proteins such as glutamate (GDH) in 20 mM potassium phosphate buffer have been found to retain 65 % of their activity after lyophilization [62]. Although, the recovery of protein activity varies with the nature of protein, the higher recovery had been reported at higher concentration. However, in the context of IgG, due to the availability of the limited literature published on its aggregation response to freeze drying, variation in the immunoglobulin concentration, buffer composition, added salts and specific freezing and drying (lyophilization) conditions makes the formulation of general conclusions regarding the relative impact of these variables on aggregate formation uncertain. Investigations of the effect of multiple cycles of lyophilization by different researchers have observed that IgG has a strong propensity to form insoluble aggregates (42 %) when dissolved in 0.05 M PBS and 0.5 N NaCl at neutral pH (42 %) [46, 47].

Size exclusion chromatography (SEC) studies have shown that the multiple cycles of lyophilization of L6 mouse – human monoclonal IgG₁ antibody (dissolved in 0.5 M PBS and 0.5 N NaCl), promotes the formation of stable dimers (2.5 – 16 %) at the expense of monomers [48]. Studies have shown the formation of IgG dimers increases with buffer concentration during lyophilization. Moreover, the effect of concentration in the range of 1 – 10

mg/mL was reported not to have significant impact on the level of aggregation [49]. The decrease in monomers coupled with an increase in the formation of insoluble aggregates of IgG (at 1 mg/mL in 0.01 M PBS containing 0.22 N NaCl) after lyophilization and reconstitution, following both fast and slow cooling has also been reported [49]. Moreover, the addition of NaCl to a highly concentrated solution of IgG (50 mg/ml) results in the dissolution of larger aggregates into homogenous solution with particle size under 10 nm [41]. Rapid cooling of IgG dissolved in 0.05 M phosphate buffer and 0.5 N NaCl at pH 7 during lyophilization has been reported to change the the average particle size of IgG from 400 nm (for slow cooling) to 1 μ m. The reason for the difference in average particle size has not been explained [48]. It has also been reported that rapid cooling consistently results in higher levels of aggregates protein in a buffer containing 0.01 M PBS at pH = 7.1 with 0.22 N NaCl [49]. These studies suggested that rapid cooling could be detrimental to protein integrity.

It has also been reported that the level of insoluble aggregate formation is directly related to the freezing rate over the range of 0.5 $^{\circ}$ C to 50 $^{\circ}$ C/min when human growth hormone was subjected to cooling after lyophilization [61]. Moreover, the biological activity of the proteins is lost because of freezing, due to partial unfolding or complete denaturation of proteins after adsorption to the ice surface, which results in aggregate formation upon reconstitution [50]. Scanning electron microscopy (SEM) studies showed that annealing after fast

freezing reduces the percentage of aggregates in the reconstituted solids from 32 % to about 12 % [49]. These studies have also confirmed that denaturation of proteins becomes irreversible after lyophilization.

The effect of concentration on the level of aggregation in solutions of IgG after lyophilization has also been studied. It has been reported that the aggregate level formed in human IgG after multiple cycles of lyophilization decreased with increasing IgG concentration until, at 50 mg/ml IgG, no aggregation took place [47, 61]. An increase in the protein concentration on the level of aggregation was also studied in other antibody formulations, for example an increase in the concentration of interleukin-1 receptor antagonist from 1 to 100 mg/ml, diminished the level of aggregates from 50 % to 0.01 % [51]. The, cause of this decrease, however, was not explained. Although, from these studies, it is clear that an increase in the protein concentration reduced aggregation, some studies have also shown a 20 fold increase in concentration results in a 50% increase in the aggregation of IgG [52]. It has been also observed that higher protein concentration inhibits crystallization of buffer salts. This is due to an increase in intermolecular protein interactions at higher concentration; as a consequence, protein crystallizes, and occupies water (30 – 70 %) and/or buffer in its big cavities which are formed as a result of inter-protein interaction between two or more than monomers [52, 61]. Most of the water remains disordered within the crystal). Moreover, it has also been reported that the quantity of aggregates in

IgG formulations decreased significantly with a concentration increase from 4 mg/ml – 8 mg/ml [18, 53]. However, it has been also reported that pH changes during freezing do not appear to be a likely explanation for the concentration effect.

Studies of the impact of buffer composition on the level of aggregation in IgG formulations have revealed that at constant buffer concentration, potassium salts (at 0.01 M) consistently result in a significantly lower level of aggregates relative to sodium phosphate (at 0.01 M). However, adding either NaCl (0.22 N) or KCl (0.22 N) results in increased aggregation compared to buffer alone. In addition; relative to buffer alone, the NaCl resulted in more aggregation than KCl at the same concentration (0.22 N) [49]. The reduced aggregation with KCl has been correlated to significantly lesser surface area of lyophilized solids from solutions compared to that of NaCl. The other reason behind increased stabilizing effect of KCl has been attributed to higher stability of KCl glass which potentially increases the stability of proteins during the freezing stage of lyophilization [49].

Surfactants are commonly used in formulations to prevent protein adsorption to surfaces and to minimise interfacial denaturation by preferentially adsorbing to hydrophobic surfaces and to hydrophobic regions of proteins. The use of surfactant, either in the reconstitution medium or in the formulation has been found to significantly decrease, but not eliminate aggregation. For example the

incorporation of polysorbate in the reconstituted solution of interleukin-1 receptor antagonist reduced the aggregate level by about 27 % [51].

The detection and quantification of IgG aggregates following lyophilization, for example using SEC (1 mg/mL of IgG in 0.01 M potassium phosphate buffer containing 0.22 N NaCl) [49] and DLS (1 mg/ml IgG in 100 mM phosphate pH 7.2) [63] has confirmed the presence of monomeric and dimeric IgG species. This has been proved by comparing their hydrodynamic radii with calculated sizes of IgG (subunits or whole molecules) from the protein data bank [49]. DLS studies have shown that the hydrodynamic radius of IgG monomer ranges from 5 nm – 6 nm and that of a dimer (9.75 nm – 11.38 nm) [49], whereas differential mobility analysis (DMA*) studies have shown particles 8 nm - 9 nm in size are monomers and particles 10nm-11.6nm in size as dimers [52]. Moreover, DMA studies have also confirmed that the lengths of Fab and Fc, subunits as 8.9 nm and 7.7nm respectively. The width of each subunit confirmed by DMA studies is 4nm [52]. The average size for Y shaped IgG molecule from protein data bank is 7.3 nm (1/2 molecule), 9.3 nm (monomer; single molecule), 11.7 nm (dimer; 2 molecules), 13.3 nm (trimer; 3 molecules), 14.4 (tetramer; 4 molecules), 15.2 (pentamer; 5 molecules), 15.9 (hexamer; 6 molecules). This size range has also been reported and complimented in the previous studies on IgG aggregation [52].

*[*DMA is a method for measuring low-order soluble protein aggregates in solution. Protein solutions are electrosprayed and different aerosolized populations are separated according to their electrophoretic mobility using a differential mobility analyzer. Particles in the size range of 3nm-250nm can be separated].*

1.5 AFM for mapping IgG aggregation

In this thesis, novel technique AFM was employed for the characterization of IgG aggregation. Therefore, it became essential to shed some light on the relevant studies of IgG previously performed with AFM. It was the study of antibody/antigen interaction by AFM for example by Allen *et al* [64] and many others [65, 66] which stimulated the interest of imaging of bio-molecules and their aggregation state.

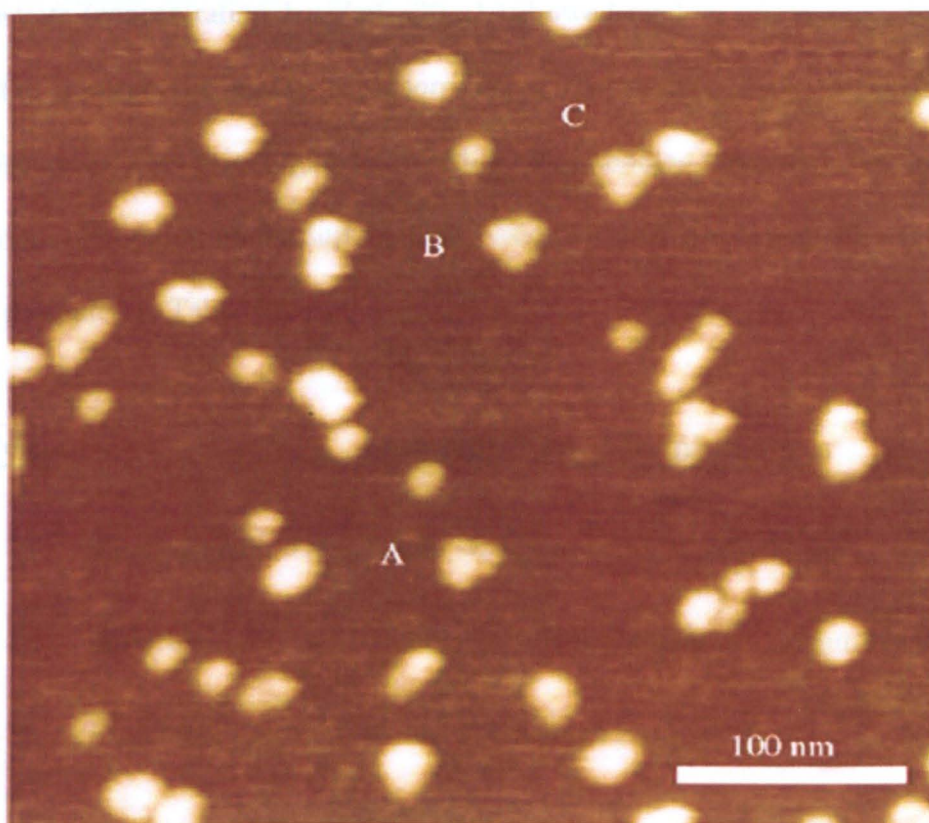


Figure 1.7 A tapping mode image (obtained in the attractive interaction regime) of several antibodies having four distinct morphologies according to the orientation of domains with respect to the substrate surface [67].

High resolution imaging of antibodies with AFM in air and fluid is a challenge. However the tapping mode imaging in air has revealed the sub-molecular details of isolated IgG antibodies on flat surfaces such as mica [66]. It has been shown that by controlling the forces between tip and sample, sub molecular resolution of IgG can be obtained [66]. Tapping mode AFM images (obtained in the attractive interaction regime) of IgG antibodies incubated onto mica surfaces have confirmed that their three dimensional structure resembles a Y – shaped conformation [66]. The observed AFM images of an IgG sample dried onto mica substrate (concentration 1 $\mu\text{g/mL}$, 20 μL) showed random orientations, because of the non-specific nature of adsorption of the antibodies on the surface of substrate as shown in Figure 1.7. Although antibodies were observed to have random orientation on the surface, four basic morphologies which were reported are presented in Table 1.1

Type	Description of Morphology
1	Single domain with a lateral size (longest axis) of $\sim 18\text{ nm}$
2	Molecules with two roughly equivalent domains of $\sim 10\text{ nm}$ across
3	Antibodies with two domains, one large ($\sim 11\text{ nm}$)
4	Some molecules with three roughly equivalent domains of $\sim 8\text{ nm}$ across

Table 1.1 Different morphologies of IgG domains and their dimensions reported in AFM studies [66, 67].

Features with morphology type four had an overall morphology that resembles the characteristic Y-shaped conformation of the IgG antibody molecule. However, it has been reported, that even though these four classes of orientation were dominant, variations in orientation from one molecule to the next were still apparent. The features A, B, and C in Figure 1.7 were reported to be three IgG molecules with flat orientation, where three 50 kDa subunits (2 F_{ab} and F_c) were resolved. Two of these molecules (A and B) consist of one subunit which was significantly higher than the other showing that they have subtle differences in orientation. These studies also revealed that the height of individual antibody subunits and subunit separation varied from one molecule to another. The difference in the orientation of subunits with respect to the substrate surface and with respect to each other was proposed to be the most probable reason for the variation in size. There is only a small variability from molecule to molecule due to flexibility in the hinge region connecting Fab with the Fc domain. Table 1.2 and Table 1.3 respectively present the confirmed average heights of Fab and Fc subunits and the average separation between subunits with a measured error of 0.1 nm studies [66 - 69].

<u>Domains</u>	<u>Average Heights</u>
Fab ₁	1.56 nm
Fab ₂	1.36 nm
Fc	1.40 nm
Inter-subunit distance between two 25 kDa IgG sub – units	3.30 nm

Table 1.2 Average heights of IgG domains measured by AFM [66, 67, 68].

<u>Domains</u>	<u>Average Separation</u>
Fab₁ and Fab₂	7.30 nm
Fab₁ and Fc	6.80 nm
Fc	7.70 nm

Table 1.3 Average separations between IgG domains measured by AFM [67].

1.3.1 Basic structure of Immunoglobulin G

This AFM based study therefore confirmed that mean separation between IgG subunits was around 7.56 nm which is comparable with X – ray crystallography measurements [67]. The possible reasons for small difference between AFM and X – ray data were attributed to the fact that the AFM measurements are made as 2D projection and the X – ray as 3D [66].

1.6 Protein Therapeutics

Insulin, Blood Factors (VIII, IX, VII, Protein C, Antithrombin), Erythropoietin, Interferons, Enzymes, Bovine Pancreatic Trypsin Inhibitor (Aprotinin/BPTI), Growth Hormones (Nutropin, Nutropin Depot and Protropin). Please visit chapter 7 for more details.

1.7 Immunoglobulins (Antibodies)

Immunoglobulins are glycoprotein molecules produced by plasma cells in response to an immunogen (antigen), and which function as antibodies. The

immunoglobulins derive their name from the binding, which makes them they migrate with globular proteins when an antibody containing serum is placed in an electrical field. Five classes of immunoglobulins have been characterised: IgM, IgG, IgA, IgD and IgE. Human IgG can be subdivided into IgG₁, IgG₂, IgG₃, IgG₄. Murine IgG can be subdivided into IgG₁, IgG_{2a}, IgG_{2b}, and IgG₃ [1, 3, 63].

1.7.1 Basic structure of Immunoglobulin G

Immunoglobulins of all classes display a similar basic four-chain structure consisting of two identical light (L) chains and two heavy (H) chains. All IgGs are monomers. The subclasses differ in the number of disulphide bonds and length of the hinge region. IgGs are one class of immunoglobulins of about 150 kDa in mass and consist of three subunits (two Fab and one Fc). Figure 1.8 shows a schematic representation of an (IgG) molecule and the description of its different parts are as under:

(i) Heavy (Blue) and Light chains (Green)

The heavy chains are almost twice the length and mass of light chains, being about 50 kDa, while the light chains are 25 kDa. Both chains fold locally into characteristic β – sandwich domains, with three strands on one side and four on the other. This motif is known as the immunoglobulin fold. The light chain has two of these domains and the heavy chain has four (i.e; 12 in total, each being

about 12.5 kDa). There are four folds or domains in each of the 50 kDa subunits. In the Fab subunits, the folds from the light and the heavy chains crossover each other to form two smaller subunits each of about 25 kDa mass. However, in the Fc subunit, only one of these subunits is formed by crossover of two immuno -

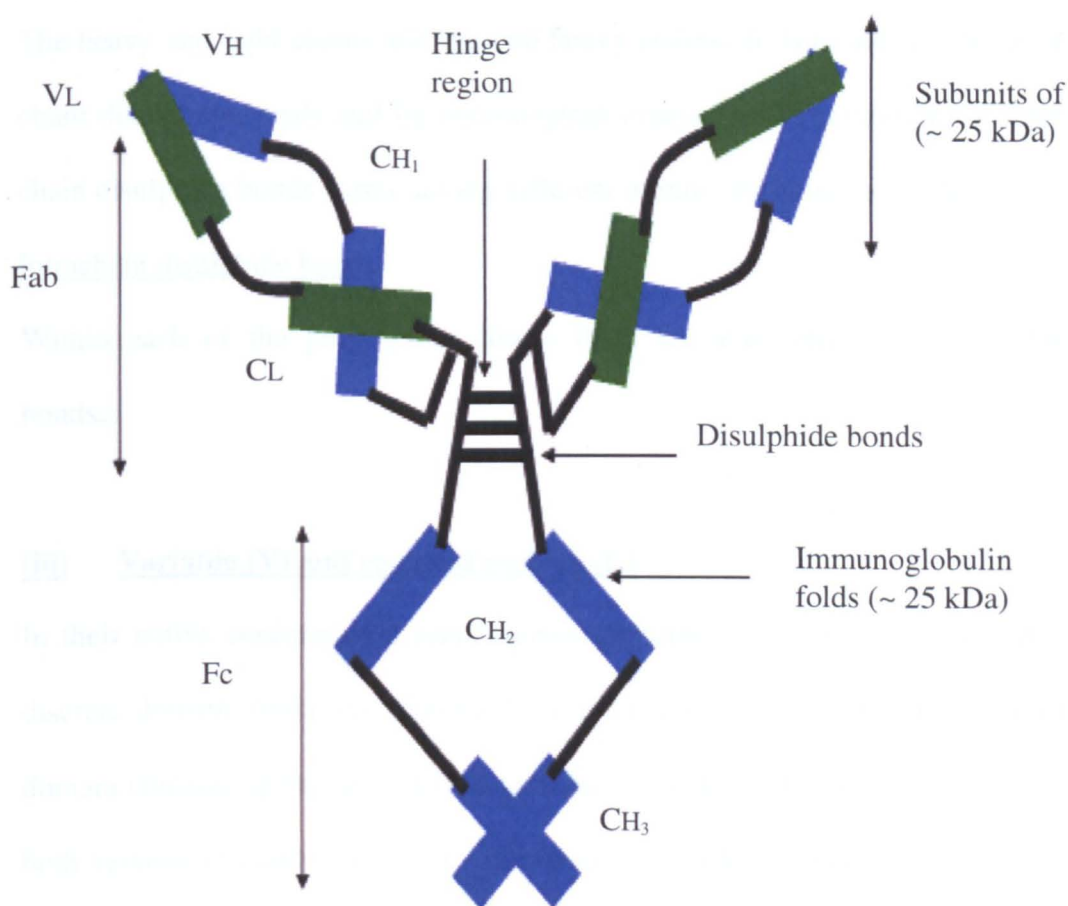


Figure 1.8 The tertiary structure of IgG molecule. Each rectangle represents a **12.5 kDa fold of an immunoglobulin**. Blue and green rectangles respectively represent heavy and light polypeptide chains. Solid black lines indicate di-sulphide linkages between light and heavy chains. The overlapped folds form domains each ~ 25 kDa in molecular mass (Adapted from [67]).

immunoglobulin domains of the heavy chain, while the two nearest to the hinge region remain separated. The overall structure is held together by disulphide linkages and non – covalent interactions [67, 70].

(ii) Disulphide bonds

Interchain disulphide bonds

The heavy and light chains and the two heavy chains are held together by inter-chain disulphide bonds and by non-covalent interactions. The number of inter-chain disulphide bonds varies among different immunoglobulin molecules.

Intrachain disulphide bonds

Within each of the polypeptide chains there are also intra-chain disulphide bonds.

(iii) Variable (V) and constant regions (C)

In their native conformation each immunoglobulin is seen to be composed of discrete domain structures, stabilised by intra-chain disulphide linkages. Each domain contains approximately 110 aminoacid residues. H and L chains contain both variable (V) and constant (C) domains. V_L and V_H contain 110 amino-acid residues each, but C_L (110 aminoacids) and C_H (330 – 440 aminoacids) differ in the number of aminoacid residues. The variable regions house the actual antigen binding site of the antibody. Variable regions of antibodies displaying different (antigen binding) specificities differ in amino acid sequence. Constant regions (within any one antibody class/subclass) do not. Light chains contain one

variable (V_L) and one constant (C_L) domain. Heavy chains contain one variable (V_H) and three constant (C_{H1} , C_{H2} and C_{H3}) domains.

(iv) Hinge region

This is the region at which the arms of the antibody molecule form the classic Y shape. The flexible hinge (H) region (in fact heavy chains display a short sequence joining C_{H1} and C_{H2} , which contains several proline residues). The flexibility of an antibody molecule results from this region.

(v) Oligosaccharides

As mentioned earlier immunoglobulins are glycoproteins. Carbohydrates are attached to the C_{H2} domain in most immunoglobulins via an N – linked glycosidic bond. However, in some cases carbohydrates may also be attached at other positions. Elimination of the carbohydrate moiety has no influence upon antigen binding; however, it does disturb several antibody effector roles and modifies its serum half – life [67, 71].

1.7.2 Proteolytic cleavage of IgG

Immunoglobulin molecules on treatment with proteolytic enzymes (such as papain) cleave at their hinge regions, yielding two separate antigen binding F(ab), and one constant (Fc) fragments. Each F(ab) fragment contains the light chain and the V_H and C_{H1} domains of the heavy chain. However,

immunoglobulin incubation with other proteases (e.g; pepsin) results in antibody fragmentation immediately below the hinge region. This leaves intact two inter-chain disulphide linkages towards the C – terminus of the hinge region. This holds the two antigen binding fragments together. The products of this fragmentation are denoted $F(ab')^2$ and Fc.

(i) F(ab) fragments

The F(ab) fragments are termed because they contain the antigen binding sites of the antibody. Each F(ab) fragment is monovalent, and hence the IgG is divalent. The antigen binding site of the antibody is created by both the V_H and V_L . An antibody is able to bind a particular antigenic determinant because it has a particular combination of V_H and V_L . Different combinations of V_H and V_L result in antibodies and can bind different antigenic determinants. The F(ab) subunits are identical in sequence to each other, giving symmetry to the molecule.

(ii) Fc fragment

Digestion with papain also produces a fragment that contains the remainder of the two heavy chains C_{H2} and C_{H3} domain. This fragment was called Fc because it was easily crystallized. The effector functions are mediated by this part of the immunoglobulin molecule. Different functions are mediated by the different domains in this fragment.

(iii) $F(ab')^2$

$F(ab')^2$ because of its bivalent nature retains the ability to precipitate antigen in *vitro*. The F_c region of the molecule is digested into small peptides by pepsin. The $F(ab')^2$ can bind an antigen, but it does not mediate the effector roles of the whole antibodies [67, 71].

1.7.3 Structure of the variable region

The variability of the amino-acid sequence in the variable domains of the antibody is responsible for generating the antigen binding sites. The comparisons of the amino – acid sequences of the variable regions of the immunoglobulin show that most of the variability resides in three regions called hyper-variable regions or the complementarity determining regions (CDRs). CDR's are found in both the H and the L chains [70].

1.7.4 The iso – electric point (pI) of IgG

Monoclonal antibodies such as IgG have no unique isoelectric point. The antibodies have variable regions which contain charged residues. It has been reported IgG molecules have an isoelectric point varying from 4.35 to 9.95 between pH 7 and 9.95, and are most basic isotype of the immunoglobulin [72, 73]. The average pI values of different types of IgG with standard deviations are presented in Table 1.4.

<u>Type</u>	<u>Average (pI)</u>	<u>SD</u>
IgG ₁	7 – 9.5	0.4
IgG ₂	7 – 9.5	0.6
IgG ₃	8 – 9.0	0.8
IgG ₄	5.5 – 6.0	0.8

Table 1.4 Average p(I) values reported for various IgGs

1.7.5 Crystallographic structure of IgG

X-ray crystallographic studies have confirmed the three dimensional structure of human IgG, with average distances of almost 6.6 nm between Fc – F(ab)₁, Fc – F(ab)₂ = 9.2 nm, F(ab)₁ – F(ab)₂ = 7.5 nm. Moreover, the resolution of the x- ray derived structures is around 2.7 Å [74].

1.7.6 Extinction co-efficient of IgG

It has been shown that most mammalian antibodies (IgGs) have protein extinction coefficients in the range of 12 – 15. For a typical IgG with a molecular weight = 150 kDa, this value corresponds to a molar extinction coefficient (ε) equal to 210,000 M⁻¹ cm⁻¹ [75, 76].

1.8 Conventional particle size characterization techniques

The characterization of protein aggregates has been investigated by using conventional analytical techniques such as analytical ultracentrifugation (AUC) [77], field flow fractionation (FFF) [78], size exclusion chromatography (SEC) [79, 80], static and dynamic light scattering (SLS and DLS) [81]. Each of these techniques has certain merits and problems which are described in Table 1.5. To a lesser extent atomic force microscopy (AFM) been employed to characterise aggregates in protein based bio-pharmaceutical formulations such as IgG [67, 82, 83, 84].

<u>Method</u>	<u>Merits</u>	<u>Demerits</u>
AUC	Quantifiable, potential for measuring aggregate distributions in formulation buffer, no matrix interactions	Slow (~ day) obtaining aggregate size distributions requires fitting of the sedimentation profiles
SEC	Widely used in biotech industry, Fast (< 1 h)	Interactions with matrix can alter the aggregate distributions, complicate quantitation and sizing, mobile phase usually different from formulation buffer
DLS	Fast (< 1 h), high sensitivity for large aggregate distributions in formulation buffer, no matrix interactions	Difficult to resolve small aggregates, from monomer obtaining size distribution requires fitting of correlation, highly concentrated solution leads to loss of scattering intensity

Table 1.5 Comparative out-look of conventional techniques.

A brief introduction of AUC and SEC is given in the following section

1.8.1 Analytical ultra-centrifugation (AUC)

AUC was developed by Svedberg in the 1920's, and is used for the characterisation of purified proteins in dilute solutions and has played a significant role in understanding of the colloidal systems, especially macromolecular systems [85]. AUC consists of the application of a centrifugal force with the simultaneous real-time observation of the resulting redistribution of the macromolecule. AUC uses a conventional ultracentrifuge equipped with an optical system for the observation of the protein redistribution in real time during the centrifugation. Analytical rotors take in 10 – 400 μ L of sample between windows that are optically transparent and perpendicular to the plane of rotation. The optical detection system is synchronised with the rotor revolution, such that data are acquired only when the sample is in the path of the light as shown in Figure 1.9.

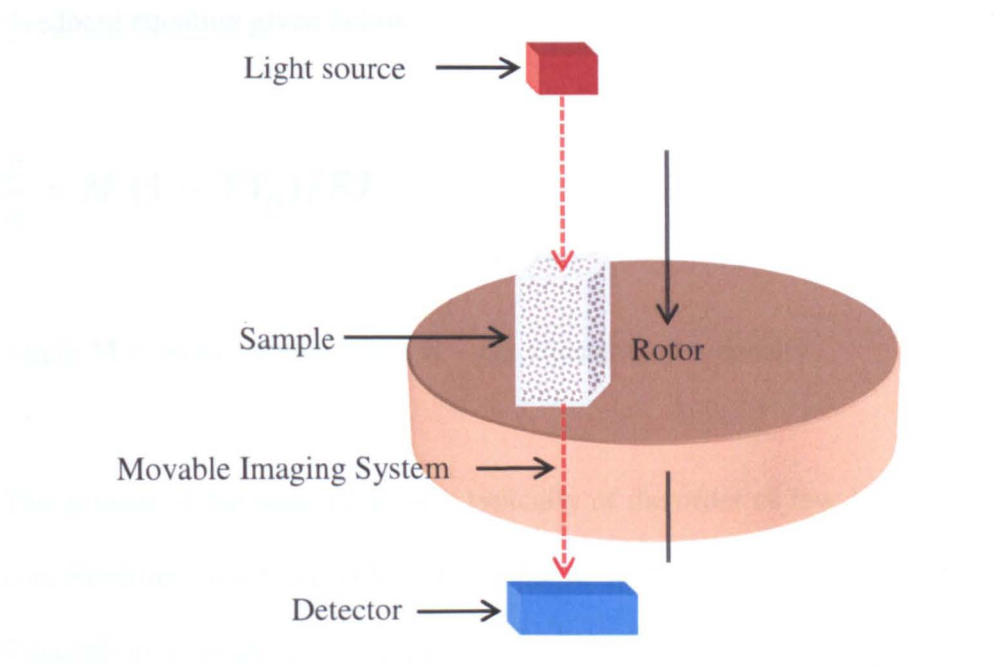


Figure 1.9 Schematics of a typical analytical ultracentrifugation technique [85].

The optical detection system usually dual beam UV spectrophotometer equipped with a mono-chromator and a highly sensitive interferometer records the refractive index gradients. For the study of protein interactions, proteins complexes which sediment faster in solution, are transported through the solution, as a consequence of this reversibly formed complexes that dissociate can readily re-associate during the experiment [63, 86]. Thus, permitting hydrodynamic and thermodynamic characterisation of even the weak and transient interactions. AUC of non-interacting proteins can reveal the gross shape, molar mass and the heterogeneity of the sample. The heterogeneity of the sample includes even the detection of traces of oligomers and aggregates, which can be of interest for pharmaceutical, biotechnological and bio-sensor applications. The sedimentation process is governed by three factors: the gravitational force, the buoyancy and the hydrodynamic friction. These three forces help us in deriving Svedberg equation given below:

$$\frac{S}{D} = M (1 - VV_{\rho})/RT \quad 1.2$$

where **M** is molar protein mass, **R** – gas constant, **ρ** – density.

The amount of the material used is typically of the order of few 100 μ g. Typical concentrations used are 0.5 – 1 mg/ml at a detection wavelength 280 nm. Concentration gradients are established during centrifugation, a 10 – 1000 fold increase in concentration is observed in a single cell. Interacting components

may have size ranging from peptides to very large macro-protein complexes. In general, affinities in the range of $10^4 - 10^8 \text{ M}^{-1}$ can be determined and kinetic dissociation rate constants of the order of $\sim 10^{-5} - 10^{-2}$ can be distinguished [17, 87].

1.8.2 Size exclusion chromatography (SEC)

SEC is also called gel filtration chromatography and is widely used for the characterisation and purification of biological polymers such as proteins, carbohydrates, and nucleic acids in solution based on their size (hydrodynamic volume) [86, 88]. High- performance SEC is a simple method for molecular mass estimation and is therefore widely employed for the characterisation of biopolymers [89]. In this technique, an apparatus called a size exclusion column consists of a hollow tube packed with minute beads designed to have pores of variable size (Figure 1.10).

This technique uses beads (porous particles) to separate molecules of different sizes, and determines their molecular weights and molecular weight distributions. Molecules that are smaller than the pore size can enter the beads and therefore, have a longer path and longer transit time than larger molecules/aggregates that cannot enter beads. Particles larger than the pore size cannot enter the pores and elute together as the first peak in the chromatogram. This condition is called total exclusion. Molecules that can enter pores will have an average retention time in

beads that depends on the molecular size and shape. Different molecules therefore, have different total transit/retention times through the size exclusion column. This portion of a chromatogram constitutes the selective permeation region. Molecules that are smaller than pore size can enter all pores, and have the longest residence time on the column and elute together as the last peak in the chromatogram. This last peak in the chromatogram determines the total permeation limit.

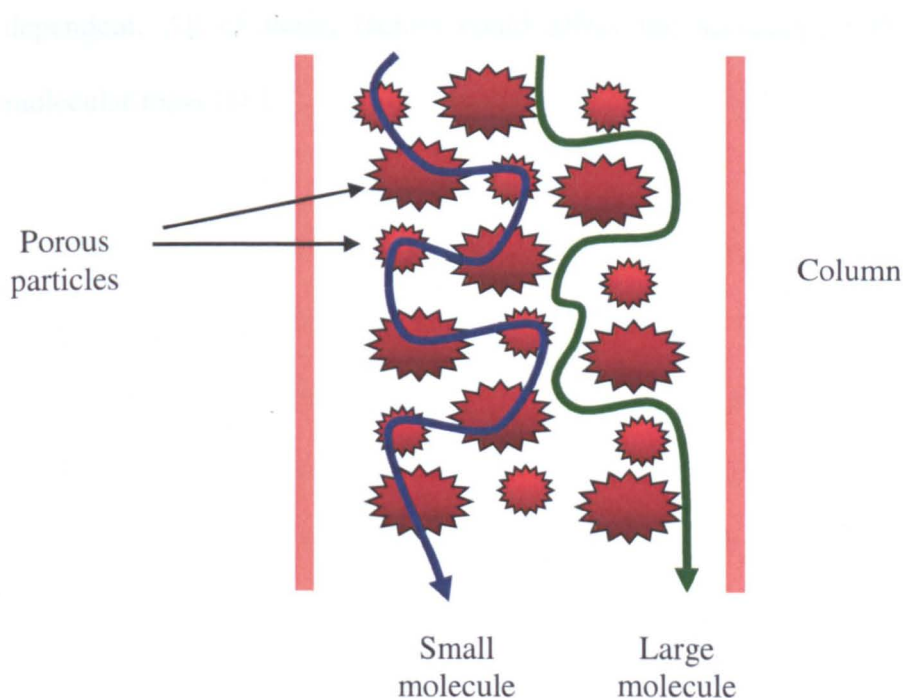


Figure 1.10 Schematic of a size – exclusion chromatography column.

One of the limitations of this technique is that it does not measure mass or hydrodynamic volume of particles in solution, because it is not able to determine how much space a particular molecule takes up when it is in solution. Use of this

technique, however, derives from an exact relationship between hydrodynamic radius and molecular mass which could be employed for all polymers. This method also suffers from a few restrictions that prevent correct estimation of molecular mass. Retention difference is caused by different diffusivities of the proteins into pores, besides electrostatic interaction and hydrophobic interaction with the matrix, which may give rise to aberrant retention. In addition, SEC may influence aggregate composition, since aggregation is highly concentration dependent. All of these, factors could affect the accuracy of the calculated molecular mass [88].

1.9 Aims and Objectives

As described in the introduction, in liquid state biopharmaceuticals, the complete/partial loss in activity and a reduced shelf life are the potential consequences of protein aggregation. Loss in protein activity is possibly induced due to the subtle or massive changes in the protein environment such as changes in pH, temperature, and ionic strength. Therefore, there is a growing demand to find an effective formulation strategy which would enable us to better predict or overcome the problem of aggregation.

Presently, in order to avoid the potential consequences of aggregation in solution, pharmaceutical companies often prepare powdered (dry) preparations, and lyophilization is one of the most widely employed methods for this purpose. Although, lyophilization is considered to be a viable option for the manufacture of dry protein formulations, it is still not the best option for completely stopping aggregation, because formation of insoluble aggregates and loss of monomers has been reported in many protein solutions, reconstituted from their respective lyophilized powders. The detection limit for some of the conventionally used techniques for aggregate detection lies within the micrometer range and therefore, they can fail to detect much finer structures such as fragments, and monomers etc. So far the effect of lyophilization in minimising aggregation in biopharmaceutical formulations including IgG, using conventional techniques has been found to be dependent on the nature of protein itself and the precise

lyophilization conditions employed. Very little work has been done to investigate the effect of multiple cycles on proteins such as IgG using novel techniques such as AFM, whose detection limits are much more penetrative (can detect ~ 1 nm) and can therefore, account for much interested species such as fragments and monomers in more detail.

The main aim of this study was to explore the effects of the process of lyophilization on the fundamental characteristics required of any protein (such as IgG) from therapeutic considerations. Our idea was to test the inherent ability of IgG to resist aggregation (due to change/s in its native state), when exposed to multiple cycles of lyophilization. Both conventional and novel analytical methods were employed to map the effects of the lyophilization process, number of cycles of lyophilization, sugar-protein concentration, temperature and humidity (in absence and presence of lyoprotectants) on therapeutically significant parameters of IgG such as particle size, secondary structure, thermal stability, morphology, porosity/flakiness and antigen binding activity. Size analysis was performed using both conventional and new particle characterisation techniques (DLS), such as Nanosight (single particle tracking based upon light scattering) [90] and AFM. Results from Nanosight, DLS and AFM experiments were useful for comparative analysis. Scanning electron microscopy (SEM) [91] and AFM were employed for morphological studies; ATR-Infrared spectroscopy [92] and differential scanning calorimetry (DSC) [93] were used for the investigation of

secondary structure and thermal stability respectively. The activity determination was carried with enzyme linked immunosorbant assay (ELISA) [94]. Therefore, an attempt was made to identify critical formulation and processing variables affecting aggregation of IgG during multiple cycles of lyophilization. The parameters examined were, the effect of IgG concentration, the number of cycles of lyophilization, particle size, secondary structure, thermal stability, morphology, antigen binding activity, and effect of lyoprotectants (sucrose and mannitol) alone and in combination. Preliminary studies focused on the particle size characterization of ferritin and pure polyclonal IgG molecules.

The new hypothesis is presented to explain the significance of nanoscale investigation and other major factors that need to be optimized for the therapeutic stability and efficiency of protein based biopharmaceuticals such as IgG during lyophilization. It has been proposed that upon exposure to multiple cycles of lyophilization, an IgG antibody forms a range of aggregates of variable size, both in absence and presence of lyoprotectants. The propensity of IgG molecules to aggregate is associated with decrease in the proportion of monomers and growth of crystalline material besides decline in the porosity/flakiness, alterations in the secondary structure, reduced binding activity, and dip in the thermal unfolding resistance. The formation of different crystalline structures at nanoscale reveals a strong connection between aggregation and alterations in the secondary structure. IgG lyophilized with

sucrose (when used separately) and in combination (with mannitol), prove beneficial in maintaining the required therapeutic characteristics of an IgG antibody during multiple cycles of lyophilization. This hypothesis is based upon the size measurement results of the aggregates determined by complimentary techniques. Moreover, the proposed hypothesis finds more strength from the other analyses such as as the study of morphology, spectroscopic, thermal stability and binding activity of the lyophilized formulations of IgG.

Chapter 2

Materials and methods for sample preparation; Conventional and unconventional techniques employed for characterization

2 Materials and Methods

This chapter summarises the methods and materials used in the preparation and lyophilization of protein formulations and their characterization using a range of analytical techniques.

2.1 Materials

The batch numbers of all the materials which were used in this work are listed in Appendix 1. All proteins used in this study were supplied as lyophilized powders: - Ferritin (horse spleen ferritin in 0.15 M NaCl), IgG (anti – glucose – 6 – phosphate dehydrogenase (G – 6 – PDH) antibody produced in rabbit (IgG

fraction of antiserum in 0.01 M PBS); and (glucose-6-phosphate dehydrogenase from baker's yeast (*S. cerevisiae*). The reconstitution of lyophilized protein powders was performed in filtered water to desired stock concentrations. D – sucrose (99 %); D – mannitol (98 %); D – sorbitol (98 %) were obtained from Sigma Aldrich. Secondary antibody (HRP – linked anti – Rabbit IgG) was supplied by Bioscience UK Ltd. D - (+) – trehalose dehydrate (99.5 %) was obtained from Fluka. The phosphate buffered saline (PBS) tablets; bovine serum albumin (BSA) ELISA block; TWEEN 20 washing solution; 6. 3, 3', 5, 5'-tetramethylbenzidine (TMB) liquid substrate system were all supplied by Sigma Aldrich.

Two types of silicon nitride AFM cantilevers used, termed – 'DNP-S' and 'SNL', were both obtained from Nanoprobes (BrukerNano) CA. Phosphorous doped Si (RTESPA) cantilevers with nominal spring constant of 20 – 80 N/m were used for AFM imaging of lyophilized powders. All cantilevers were rinsed with deionised water and dried in a stream of nitrogen prior to imaging. Mica (G 250 – 1, 3"x 1") was obtained from Agar Scientific. Sterile 0.2 µm Ministart filters from Anachem were employed for the filtration of deionised water and PBS solution. Nitrile gloves were worn at all times in order to avoid contamination. Double sided adhesive tape was used to stick clean mica to magnetic sample stubs, their surfaces following cleaving to expose a fresh surface were then incubated with a 10 – 20 µl of sample solution prior to imaging with AFM in

liquid. Polypropylene plates (Immuno 96 MicroWell™) were obtained from Sigma for the determination of activity with ELISA experiments. Specimen supports for SEM (12.5 mm aluminum pin stubs; Agar Scientific, cat. no. G301) covered with black carbon discs were gold coated for imaging with SEM; TA hermetic lids and pans for DSC experiments and clean glass slides were used in ATR-FTIR experiments.

2.2 Preparation of protein stock solution

2.2.1 Ferritin stock solution

10 µl aliquots of ferritin solution (50 mg/ml in 0.15 M NaCl) were diluted with filtered deionised water to a concentration of 0.1 ng/ml. This was stored in five 1 ml aliquots in a refrigerator to be used for the preparation of samples for conducting AFM imaging experiments.

2.2.2 IgG stock solution

For the preparation of the IgG stock solution, 200 ml of 0.01 M PBS solution was prepared by dissolving one PBS tablet in deionised water. The 0.01M PBS solution was then filtered through sterile 0.2 µm filters from Anachem. The lyophilized powder of IgG (G – 6 – PDH) antibody was first reconstituted in 2 ml of filtered deionised water to give 2 ml in PBS as per manufacturer's instructions. This resulted in approximately 2 ml solution of IgG with a

concentration of 90 mg/ml in PBS. This was followed by diluting the 2 ml solution of IgG (concentration 90 mg/ml) to a concentration of 2 mg/ml by adding 88 ml of filtered 0.01 M PBS by applying the equation:

$$C_1V_1 = C_2V_2 \tag{2.1}$$

This process resulted in 90 ml of 2 mg/ml solution of IgG, which was then subsequently stored in a number of aliquots. The details of volumetric breakdown into aliquots are given in Table 2.1

<u>Serial No.</u>	<u>Number of aliquots</u>	<u>Volume in each aliquot</u>	<u>Total volume</u>
1.	50	1 ml	50 ml
2.	51	0.5 ml	25.5 ml
3.	50	0.2 ml	10 ml
4.	50	0.1 ml	4 ml
5.	50	0.01 ml	0.5 ml

Table 2.1 The breakdown of IgG protein solution obtained after reconstitution into different volume aliquots.

2.3 Concentration determination

The protein concentration of IgG solution was determined by UV absorption at 280 nm using a molar extinction co – efficient (MEC) of 210,000 M⁻¹ cm⁻¹. This value of MEC is typical for an IgG with molecular weight equivalent to 150000 Daltons. UV absorption was performed at 0.5 mg/ml, 0.6 mg/ml, 0.7 mg/ml, 0.8 mg/ml, 1 mg/ml, 1.5 mg/ml and 2 mg/ml using UV photo spectrometer. UV absorbance plot of the indicated concentrations is shown in Figure 2.1.

2.5 Lyophilizer and lyophilization of samples

A typical lyophilizer (Lyophilizer 2000, Lyophilizer and Associates, Inc.)

Figure 2.1 shows the UV absorbance plot for a range of concentrations of IgG.

The UV absorbance plot for a range of concentrations of IgG is shown in Figure 2.1.

The UV absorbance plot for a range of concentrations of IgG is shown in Figure 2.1.

The UV absorbance plot for a range of concentrations of IgG is shown in Figure 2.1.

The UV absorbance plot for a range of concentrations of IgG is shown in Figure 2.1.

The UV absorbance plot for a range of concentrations of IgG is shown in Figure 2.1.

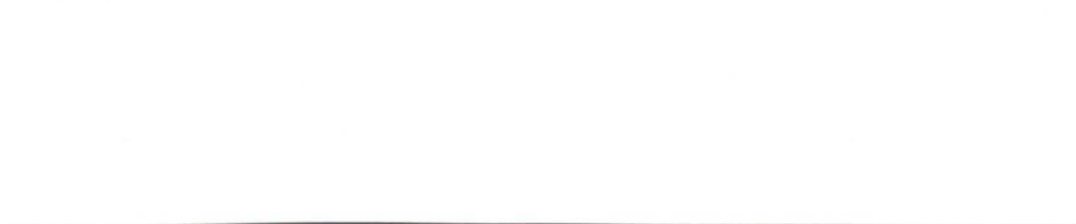
The UV absorbance plot for a range of concentrations of IgG is shown in Figure 2.1.

The UV absorbance plot for a range of concentrations of IgG is shown in Figure 2.1.

The UV absorbance plot for a range of concentrations of IgG is shown in Figure 2.1.

The UV absorbance plot for a range of concentrations of IgG is shown in Figure 2.1.

Figure 2.1 UV absorption plot for a range of concentrations of IgG, which were recorded at 280 nm.



2.4 Storage of liquid protein solutions

The long term storage of liquid IgG protein stock solutions filled in various aliquots was ensured by freezing at -4°C . However, the lyophilized powdered formulations of IgG (in glass vials) were stored in a desiccator at room temperature in order to make sure that the formulations were moisture free.

2.5 Lyophilizer and lyophilization of samples

A typical Modulyo Lyophilizer [S.W. Jennings and Company Ltd, Scientech House, East Bridgford, Nottingham, UK] with Edwards Pump (Crawley, West Sussex, UK) as shown in Figure 2.2, was employed for the lyophilization process. Lyophilization was accomplished in two steps as is typical. In the first step, the freezing of all the protein formulations was performed in liquid nitrogen (for 1 – 2 minutes, freezing temperature ~ -50 to -80°C). In the second step, the application of a vacuum to the frozen protein formulations at a temperature slightly in excess of 0°C was applied. This resulted in the sublimation of the crystalline water, leaving behind a powdered protein material. The removal of water from a biopharmaceutical product yields a powdered product, usually displaying low water content on the order of 3 %. This temperature was held for 8 – 12 hours at a pressure of 60 mT.



Figure 2.2 Image of an Edwards's lyophilizer, type Modulyo K4 equipped with vacuum chamber. Technical specifications: 220 V, 50 Hz. Temperature range – 50 °C up to ambient.

2.5.1 Lyophilization of ferritin samples

Two (0.5 ml and 1 ml) aliquots of ferritin solution (0.1 ng/ml in 0.15 M NaCl) were separately poured into two clean glass vials with the help of pipette and then the vials covered with parafilm. The vials were first frozen in liquid nitrogen for a couple of minutes. The parafilm covering the mouth of glass vials was perforated with a clean needle so that all the moisture would be removed during lyophilization (vacuum drying). The pre-lyophilized ferritin samples were

then mounted in the lyophiliser, and left to dry at a suction pressure of 0.1 mbar at a temperature of 25 °C for 8 – 12 hours. This resulted in the formation of powdered ferritin which was then reconstituted in filtered deionised water prior to AFM imaging.

2.5.2 Lyophilization of IgG samples

Seven aliquots of IgG solution were stored in a freezer (0.5 ml each, concentration 2 mg/ml each) were allowed to defrost for 10 – 15 minutes before use. From aliquots, the solutions were poured into clean glass vials with the help of a pipette. The vials were then covered with parafilm. The vials were then frozen in liquid nitrogen as above, and subjected to the lyophilization process as described in section 2.5.1. However, in the case of IgG, after the end of the first cycle, one sample was taken out and stored in a fridge as shown in Figure 2.3. The remaining six samples were reconstituted in filtered water and then again subjected to the lyophilization process as above. After the end of the second cycle, another sample was taken out and stored in a fridge. The remaining five samples which had been lyophilised twice were reconstituted in 0.5 ml of filtered water again as in the step 2. The same procedure (take one out after each cycle, reconstitute rest in filtered water and lyophilise rest) was adopted in steps 3, 4, 5, 6, and 7, so that after the end of each cycle of lyophilization process. In this way, as shown in Figure 2.3, seven samples of IgG exposed to 1, 2, 3, 4, 5, 6, and 7 cycles of lyophilization were prepared.

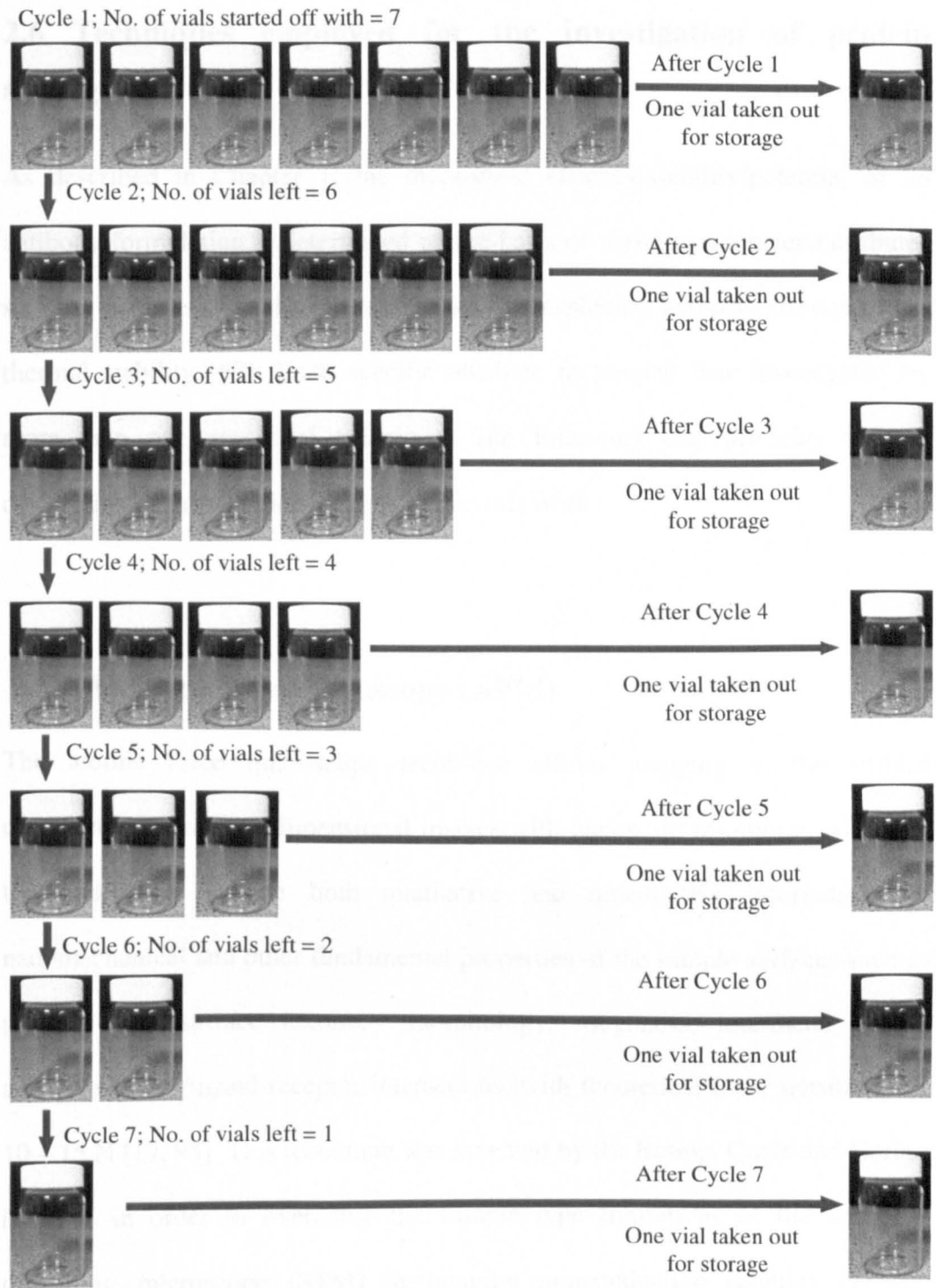


Figure 2.3 Schematic overview of the methodology adopted during the multiple cycles (seven) of lyophilization of IgG. After the end of each cycle one sample is taken out for storage and rest are reconstituted and exposed to next cycle and so on.

2.6 Techniques employed for the investigation of protein aggregation

As described in Chapter 1, the therapeutic efficacy/viability/potential of an antibody formulation is determined on the basis of various parameters/attributes such as particle size, shape, morphology, amorphicity, activity, structural and thermal stability [67]. Each specific attribute mentioned was investigated by more than one analytical technique. The following text provides a basic description of the techniques employed in this work.

2.6.1 Atomic Force Microscopy (AFM)

The atomic force microscopy technique allows mapping of the surface characteristics in three dimensional images with nanoscale resolution. AFM has the ability to provide both qualitative and quantitative information on nanomechanical and other fundamental properties of the sample surfaces such as particle size, surface texture, morphology, roughness, interfacial forces, adhesive forces/ligand-receptor interactions, with theoretical force sensitivity of 10 – 15 N [17, 95]. This technique was invented by the Binnig, Quate and Gerber in 1986 in order to overcome the sample type limitations of the scanning tunnelling microscope (STM) in imaging nonconductive samples [17,96]. However, the possibility of modifying the surface, manipulating individual molecules, and single molecule force measurement has made AFM an ideal tool for biological applications [97]. One important advantage of this technique is the

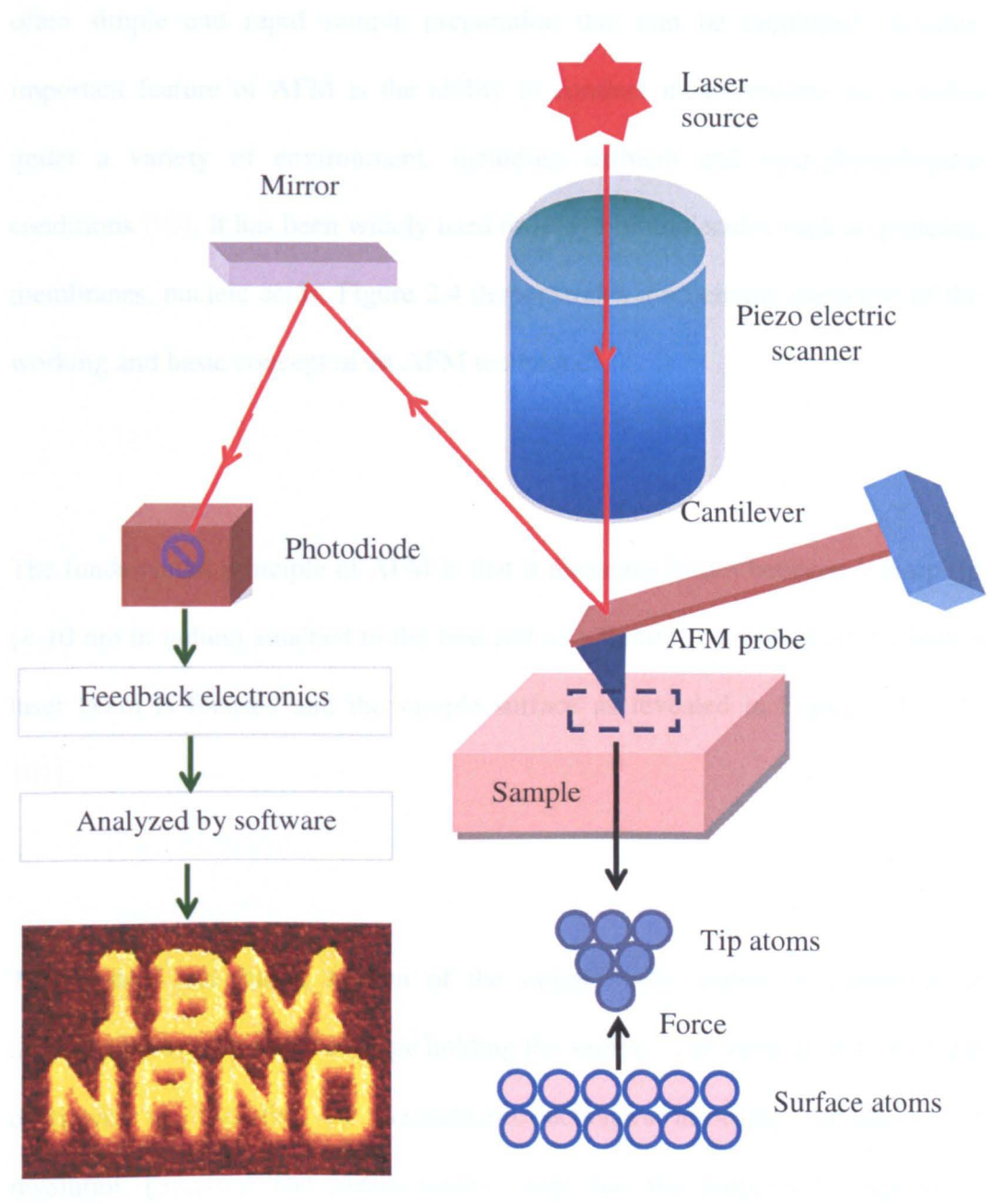


Figure 2.4 Schematic overview of the working of an AFM instrument showing a beam bounce reflection method of detection using a laser and an appropriately positioned sensitive photo detector. Interactions between the atoms of the AFM tip and sample surface produces deflections in the cantilever and are monitored by a detector (using feedback electronics) to generate the map of the surface characteristics in the form of images. **IBM NANO** is a typical AFM image showing oxide lines of about 20 nm wide silicon dioxide pattern on a silicon wafer [98].

often simple and rapid sample preparation that can be employed. Another important feature of AFM is the ability to conduct measurements on samples under a variety of environment, including ambient and near-physiological conditions [99]. It has been widely used to image biomolecules such as proteins, membranes, nucleic acids. Figure 2.4 demonstrates a schematic overview of the working and basic concept of an AFM technique.

The fundamental principle of AFM is that it measures forces between a sharp tip (< 10 nm in radius) attached to the free end of a flexible cantilever onto which a laser beam is focused and the sample surface as revealed in Figure 2.4 [100, 101].

The vertical and lateral motion of the sample with respect to cantilever is achieved by a piezo-ceramic stage holding the sample. The vertical motion of the cantilever is controlled by piezoelectric actuators affording sub-nanometer resolution [97,102]. The piezo-ceramic stage has the property to expand or contract in the presence of voltage gradient. By rastering the tip in the $x - y$ direction over the surface of a sample, forces (attractive or repulsive) resulting from the interactions between the tip and the surface cause bending (positive or negative) of the cantilever can be monitored. This bending is typically detected by the deflection (Δx) produced in the laser reflected from the back of cantilever

and is directly proportional to the force (F) acting on the tip in accordance with the Hooke's Law:-

$$F = -k\Delta x \quad 2.2$$

where k is spring constant of the cantilever,

Δx is the deflection produced in the cantilever.

If the spring constant of the cantilever (typically $\sim 0.1 - 1$ N/m) is less than surface the cantilever bends and the deflection is monitored. Finally, the deflection produced in the laser is collected by a photodiode for image generation [103]. The deflection produced in the laser as a consequence of cantilever bending as demonstrated in Figure 2.5 which shows a force-distance profile of an interaction between AFM probe and sample surface in greater detail. The AFM probe sample interaction curve demonstrates an approach cycle and a retract cycle [104]. The approach cycle (O^*CA) initiates at the free level region (O^*) where no deflection is produced in the signal, as no forces act on the probe because probe is at a detachment from the surface. This stage is manifested by green line (O^*C) of the curve, in Figure 2.5.

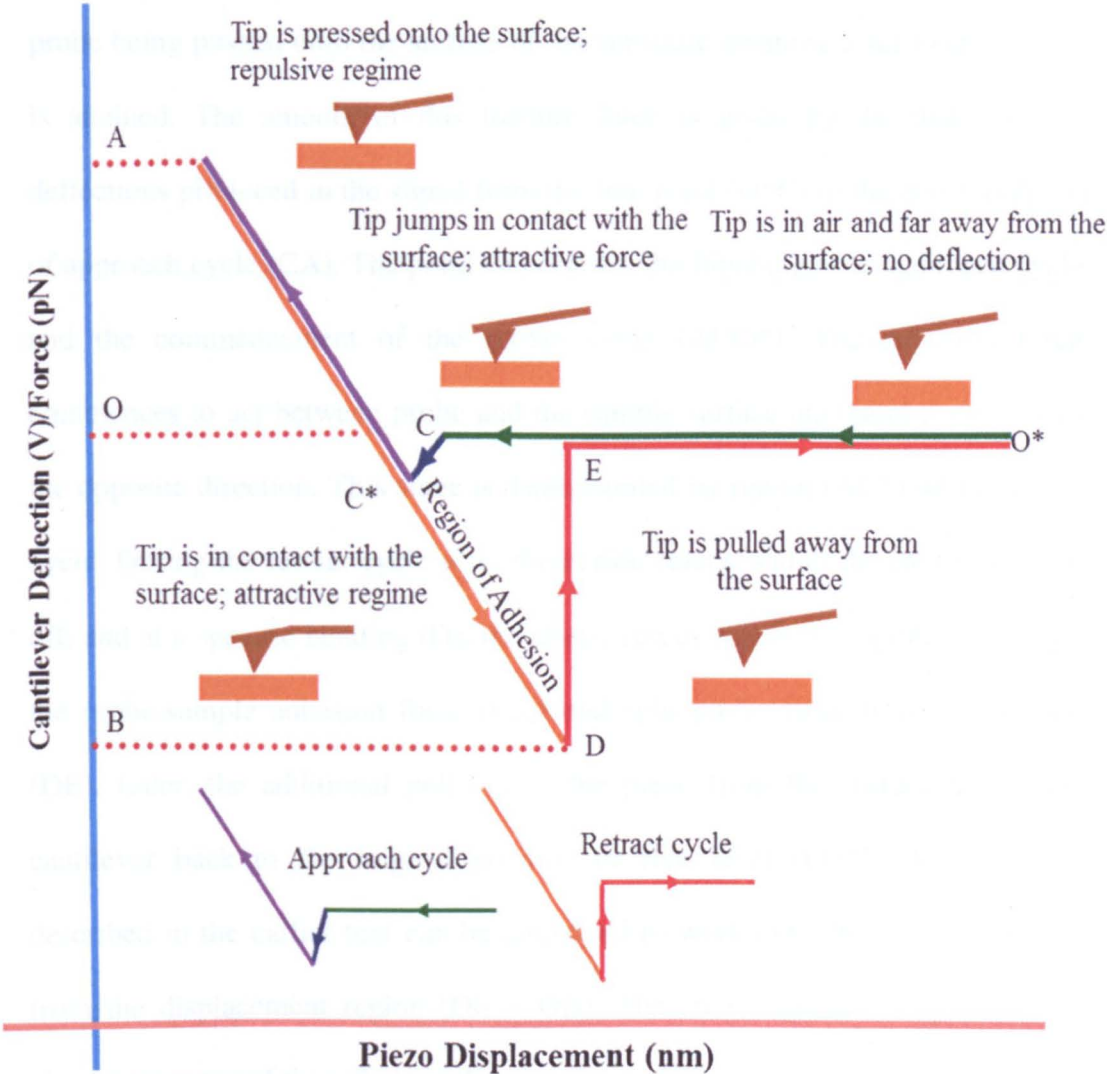


Figure 2.5 Schematic of force as a function of AFM probe-sample interaction.

2.6.1.1 Approach and retract cycles

The short dip (blue) in the same curve corresponds to an attractive jump to contact the surface. As the probe approaches the surface, the attractive forces begin to operate on the probe and just at a particular distance; the strength of attractive forces conquer the stiffness of the cantilever and the probe hops (C) in contact with surface. The purple line (CA) of the curve communicates to the

probe being pushed onto the surface of the substrate awaiting a set loading force is attained. The amount of this loading force is given by the difference in deflections produced in the signal from the free level (O^*C) to the contact region of approach cycle (CA). The point (A) denotes the finishing of an approach cycle and the commencement of the retract cycle (ADO^*). The adhesion force commences to act between probe and the sample surface and bend cantilever in the opposite direction. This stage is demonstrated by region (AC^*) of the retract cycle. During the retract cycle way, the elastic forces within the cantilever kick off, and at a specific bending (D), the elastic forces within the cantilever surpass the probe-sample adhesion force (F_{adh}) and split probe away from the surface (DE). Later, the additional pull out of the piezo from the surface brings the cantilever back to the original position or free level (EO^*). Hooke's Law described in the earlier text can be employed to work out adhesion force (F_{adh}) from the displacement region ($DE = OB$). The area under the loop (CC^*DE) gives the energy of the adhesion (E_{adh}).

2.6.1.1 Strength and weakness of measuring particle size with AFM

Strengths:

(a) AFM can characterize size of the particles in a wide variety of environments including an ambient and near physiological conditions. (b) Single molecules/individual particles and groups of particles can be resolved with AFM. Physical properties for each particle within a set of particles can be examined to

generate a statistical distribution for the entire set of particles. (c) The diameter of the particle in the $x - y$ plane determines the particle diameter with SEM. However, with AFM over other techniques such as SEM, is the maximum height of the particle that defines particle size and is independent of tip diameter, because the laser beam/probe quality does not influence particle height measurement. Moreover, with AFM, size information for individual particles can be measured in terms of (length, width, height and volume). (d) AFM has the ability to characterize particle size in height from 1 nm to 5 μm and in two dimensions can scan up to 80 μm x 80 μm . (e) The statistical significance of the data generated from ensemble particle size characterization techniques, has always been a point of concern. However, in case of AFM, it is easy to achieve superior statistical significance by combining data from several scans to acquire information on the larger population of particles. (f) AFM image analysis and data processing permits to measure statistics on groups of particles. Mass distribution can be worked out with information of the density of material.

Weakness and limits of resolution:

(a) AFM takes more time in scanning a sample surface compared to SEM. (b) The particle size characterization with AFM is predominantly limited by probe geometry. Generally, AFM instruments enjoy horizontal (X-Y) resolution of around 1 nm. However, the diameter of tip employed for scanning limits the horizontal resolution (X-Y - axis). On the other hand, the vertical resolution (less

than 0.1 nm) along Z – axis is limited by the vibration environment of the instrument (such as noise associated with floor, thermal noise etc).

2.6.1.2 AFM imaging modes

AFM operates in three basic data acquisition modes:

(i) *Contact mode (static)*

In this mode, the AFM tip is allowed to continuously contact the surface and hence the tip-sample interaction is dominated by short range repulsive forces. This mode provides the highest possible resolution but can be difficult to use on soft samples which can deform under the load applied by the AFM probe or may be damaged by the lateral forces generated during scanning. This mode is typically operated in a constant force setting whereby the cantilever deflection is maintained at a constant value by adjusting the height of the sample in response to any changes in the measured force [97, 105].

(ii) *Non-contact mode*

Non-contact mode minimizes tip-sample interaction, as the tip-sample separation of (0.5 – 2 nm) ensures a reduced interaction of the tip and sample within the longer range attractive force region [67, 105, 106]. The attractive forces from the sample are substantially weaker than the forces used by contact mode. Considering the fact that very small forces (attractive Van der Waals forces) are

acting between the tip and sample surface, a small oscillation is given to the tip in order to ensure the detection of these small forces for the collection of images. This mode involves the use of a silicon probe having a high spring constant of the order of 20 – 100 N/m, so that it does not stick to the sample surface at lower amplitudes. The limitation of non-contact mode is that it produces images with lower spatial resolution due to reduced force gradient that is being sampled. In addition because of contaminant layers in ambient environments can interfere with the oscillation it typically requires operation in ultra-high vacuum for better resolution [97,105].

(iii) *Dynamic mode (Tapping mode)*

Dynamic AFM mode, also known as tapping mode (TM) AFM, was developed to improve lateral resolution and minimise sample distortion or damage, because it eliminates a large part of the permanent shearing forces experienced in contact mode [44, 45]. In tapping mode AFM (an amplitude modulation technique) the tip intermittently contacts the surface in a normal direction and the tip sample separation varies between approximately 0.1 – 10 nm [67, 97,105, 106]. The contact time depends on the mechanical properties of the sample and the set point used in imaging. The cantilever oscillates close to its resonant (natural) frequency and the feedback loop maintains constant pre-set amplitude of oscillation (or frequency, or phase), so that tip-sample interaction is maintained during scanning.

2.6.1.3 AFM probe-sample interaction forces

AFM has two distinct force interaction regimes, attractive and repulsive as shown in Figure 2.5. In the attractive regime a net attractive force dominates the amplitude of oscillation, while in the repulsive interaction regime a net repulsive force controls the cantilever dynamics. The long-range attractive [(electrostatic and capillary forces (due to the water layer often present in an ambient environment)] and short-range repulsive forces (*van der Waals forces*) control the cantilever motion in repulsive and attractive interaction regimes respectively [67,97, 104]. The former dominates AFM tip scans at large distances (non-contact mode) from the sample surface whereas latter operates when tip is in contact with the surface (contact mode). The forces acting between the sample and the tip cause a change in the amplitude of oscillation, as a consequence produce change in resonant frequency and phase of the cantilever [97, 100, 106]. The change in the amplitude of oscillation is used as a feedback signal and vertical adjustments of the piezoscanner are recorded to measure topographic (height) variations of the sample. The phase change of the cantilever maps different components of the sample which exhibit different adhesive, viscoelastic and mechanical properties. TM AFM enables simultaneously mapping of topography, phase contrast and hence an element of compositional analysis [67, 68, 97, 107].

The liquid AFM topography imaging experiments reported in this thesis were performed using Nanoscope IIIa MultiMode II (BrukerNano) using DNP-S' and 'SNL' silicon nitride cantilevers in contact mode. However, AFM imaging (topography and phase) of multiple times lyophilized powdered samples of IgG (IgG on its own and in combination with excipients) was performed using Nanoscope IIIa MultiMode, e-Nanoscope with a humidity controller (BrukerNano) and Dimension 3000 (BrukerNano) using RTESPA cantilevers in tapping mode (TM) AFM. A scan rate of 1 Hz over a $1\ \mu\text{m} \times 1\ \mu\text{m}$ scan size and an amplitude set point of one volt were typically used. **Set point** is quantity of the force applied by the tip on to the sample surface. This force is constantly maintained by feedback electronics and could be either a certain deflection of the cantilever (in contact mode) or a certain amount an oscillation of the cantilever (in tapping mode), which regulates the force with which the tip taps on the sample surface. Set point is the characteristic of the nature of the AFM tip. These measurements were conducted at room temperature. Using the same scanning parameters, the images were also recorded at a range of different humidity (10 %, 20 %, 40 %, and 60 %) to investigate the impact of moisture on protein aggregation. For each sample, more than 50 images (topography and phase) were taken using three different types of probes described in the materials section. The imaging data were analyzed using scanning probe image processor (SPIP)TM V4.

2.6.1.4 Scanning probe image processor

Scanning probe image processor (SPIP)TM V4 contains many generic analytical and visualization tools that can be applied on various types of images and curve data. SPIP is provided with a grain analysis tool. The grain analysis menu is used for the detection and quantification of grains or other regions for which boundaries can be defined, based on height or slope conditions. Grain analysis was used for the measurement of the size of aggregates and individual protein molecules. Grains are the islands left when the image landscape is flooded to a threshold level. The threshold is a limit chosen (or horizontal line), to impose a binary condition, so that only a part of the signal above the threshold is considered a segment or grain while the rest is omitted. Therefore, the parts under the threshold level can be regarded as grains to be detected. The grain analysis module is able to detect grains/segments and calculate a large number of properties for individual segments in the image. Statistics for the whole set of segment properties (such as width, volume, length area etc) are calculated and results can be directed to the screen and files. The grain analysis module also performs automated detection and reporting to text files besides creating HTML reports containing combined numerical and graphical results. A graphic explanation of grain analysis is given in Figure 2.6. SPIP generates area, length, width and volume histograms of all the individual particles produced from each image. In order to study trends based on more data points, all the values of length, area, width and volume of all individual nano-particles collected from SPIP generated text files of more than 50 images for each of zero cycled and one

time lyophilized ferritin (at 0.1 ng/ml) and IgG (at 1μg/ml, 0.75 μg/ml) were compiled together in an excel file.

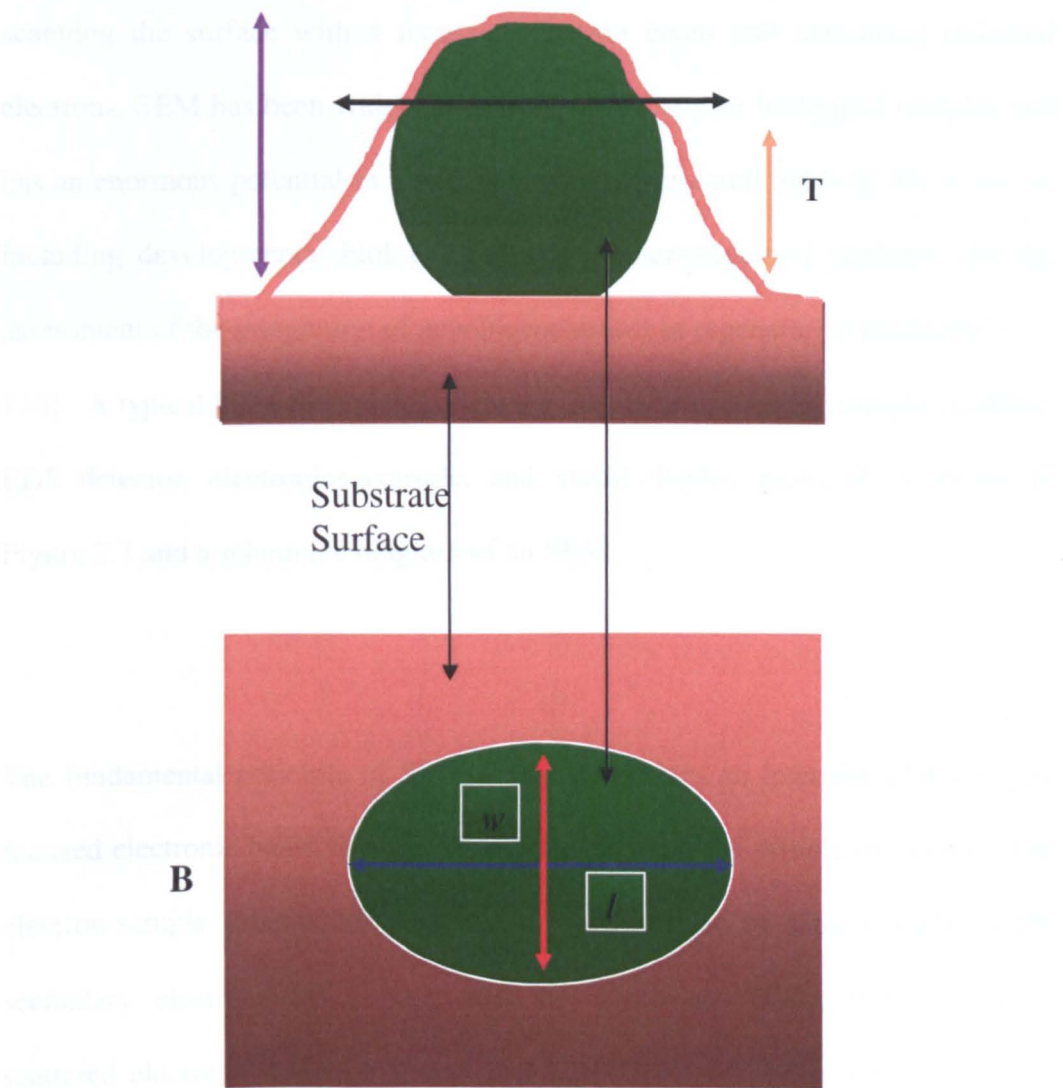


Figure 2.6 Schematic of the grain analysis performed by SPIP software on a particle immobilized on the surface of substrate. [A] Shows the side view of the particle and gives a measure of the height from the surface; represented by purple arrow (h). Threshold (T_h) value shown by orange arrow is used for generating area, length, width and volume histograms. [B] Shows the top view: Blue and red arrows represent the width and length of the particle respectively.

2.6.2 Scanning electron microscopy (SEM)

SEM enables high resolution visualization in terms of morphology, topography, chemical composition in solid materials [108]. SEM analyses a surface by scanning the surface with a focussed electron beam and measuring reflected electrons. SEM has been widely employed to investigate biological samples and has an enormous potential in a wide spectrum of research fields in life sciences, including developmental biology, pathology, microstructural anatomy and the assessment of the integration of new bioconstructs in regenerative medicine [109, 110]. A typical SEM instrument, showing the electron column, sample chamber, EDS detector, electronics console, and visual display monitors is shown in Figure 2.7 and a schematic diagram of an SEM.

The fundamental principle of SEM is that it involves an interaction of a highly focused electronic beam of large kinetic energy with the sample of interest. The electron-sample interaction generates a wide variety of signals such as the secondary electrons (SE), back scattered electrons (BSE), diffracted back scattered electrons (DBSE), X-rays and heat [109,111]. Images obtained from each signal provide specific information about the sample. For example; images from the secondary electrons (SE) typically provide morphological and topographical data, whereas back scattered electrons (BSE) illustrate rapid phase contrast in multiple phase samples [112].

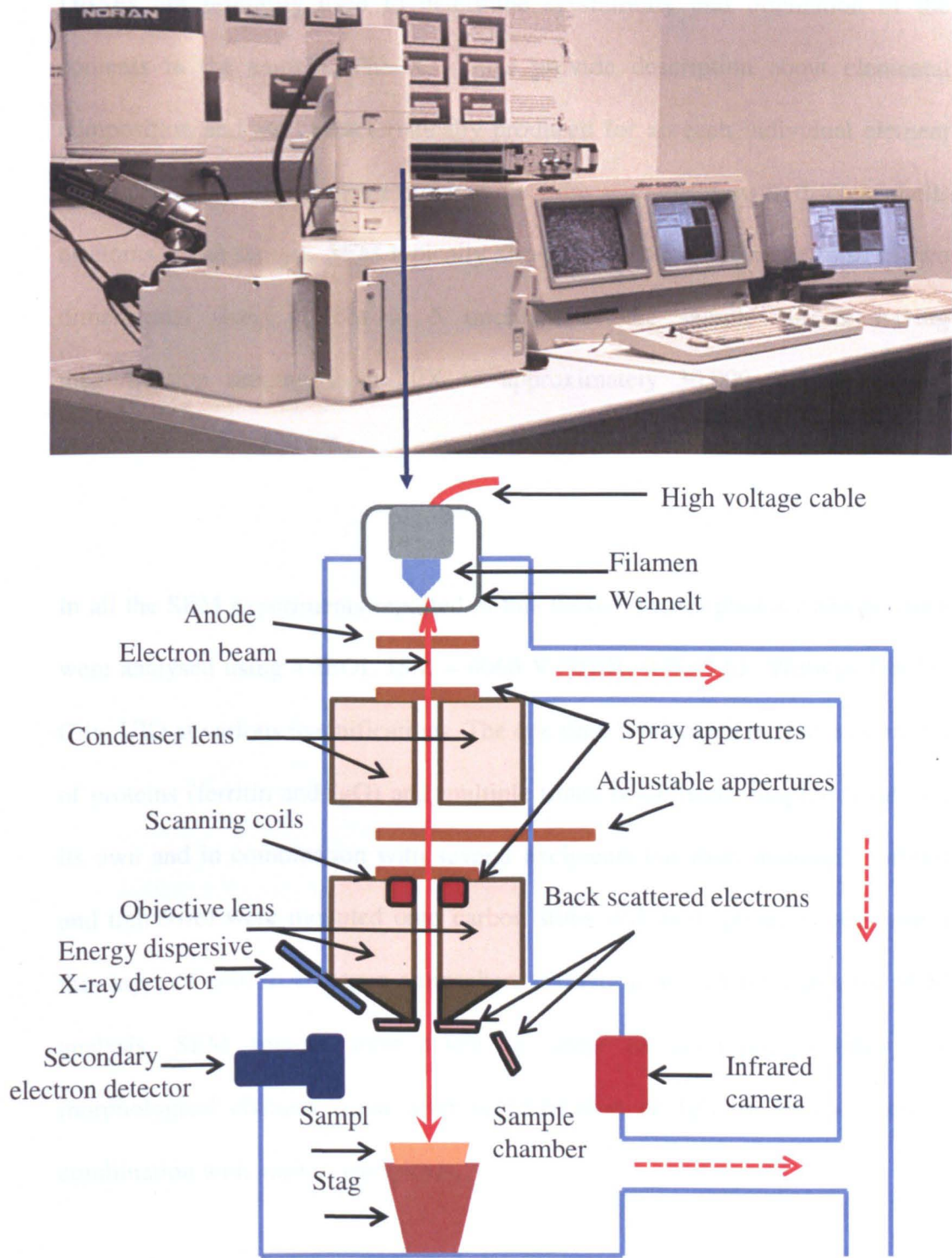


Figure 2.7 Schematic overview of the working of an SEM instrument.

DBSEs are primarily used to determine crystallinity and orientation of the contents in the sample. The X – rays provide description about elemental composition and are characteristically produced for an each individual element by an inelastic collision of the incident electrons with electrons in discrete shells of atoms in the sample. SEM typically allows data collection in the form of two dimensional scans (1 cm to 5 microns) of the sample surface having magnification ranging from 20X to approximately 30,000 X, with spatial resolution of 10 – 100 nm.

In all the SEM experiments reported in this thesis, the morphology and porosity were analysed using a JEOL JSM – 6060 V (JEOL (UK) Ltd., Welwyn Garden City, UK) at various magnifications. The one time lyophilized powdered samples of proteins (ferritin and IgG) and multiple times lyophilized samples of IgG on its own and in combination with several excipients (sucrose, mannitol, sorbitol and trehalose) were mounted onto carbon stubs and then sputter coated with a thin layer of gold in an argon atmosphere (50 Pa) at 30 mA for 2 min for SEM analysis. SEM images were taken in order to determine whether any morphological changes occur after lyophilization of IgG on its own and in combination with various excipients.

2.6.3 Dynamic light scattering

Dynamic light scattering (DLS) is a rapid, non-invasive and a well-established technique widely employed for the sizing of nanoparticles of different materials (proteins, polymers, micelles, carbohydrates, colloidal dispersions, emulsions, microemulsions) in suspension. The technique is also known as photon correlation spectroscopy (PCS) and quasi elastic light scattering (QELS). DLS is typically used to measure hydrodynamic sizes, polydispersities (distribution of size) and the presence of aggregates in protein samples [81, 113, 114]. DLS can measure size of particles lower down to 1 nm [114, 115].

The basic principle behind this technique is that it measures the variation in light scattered by the solute particles in a suspension within very short time periods (one tenth of a millisecond/microsecond) at a fixed scattering angle, typically 90° and correlates the data to produce a diffusion coefficient (D).

In a typical DLS as shown schematically in DLS Figure 2.8, a laser beam from a laser diode is allowed to illuminate a solution in which particles are undergoing Brownian motion. The light is scattered in different directions, and the intensity of the scattered light fluctuates at a rate which is dependent upon the size of particles. The fluctuations result in a time varying signal which is monitored by a high sensitivity detector. It is essential that enough light is scattered to achieve

where η is the refractive index of the buffer.

2.1.1.1. The measurement of the wave vector

The measurement of the wave vector

Equation 2.1 is caused by the diffusion of

provides correlation function as follows:

$$G(t) = \int_{-\infty}^{\infty} \dots$$

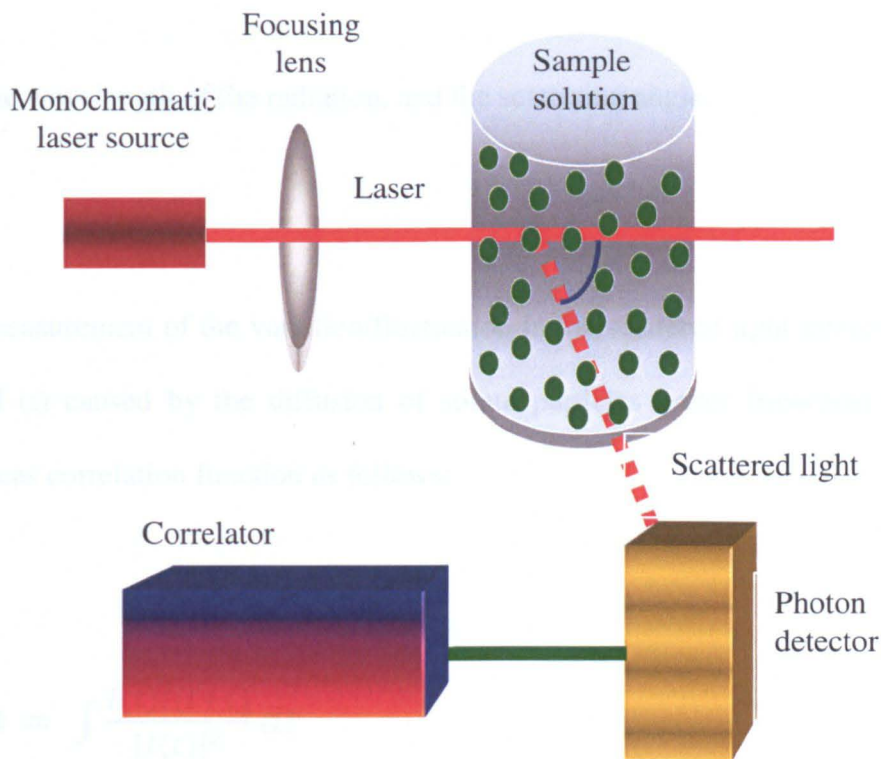


Figure 2.8 Schematic diagram of a conventional, 90° dynamic light scattering instrument.

Under ideal conditions, the correlation function is given by

Equation 2.2 shows the correlation function is given by

Equation 2.3

sufficient statistical accuracy of the correlation function. The wave vector determines the length scale over which molecular motions (Brownian motions) are detected and it is given by the equation

where θ is the angle between the incident and scattered light.

$$q = 2\pi\eta \sin\left(\frac{\theta}{2}\right) \lambda \tag{2.3}$$

where η is the refractive index

where η is the refractive index of the buffer,

λ is the wavelength of the radiation, and the scattering angle.

The measurement of the variation/fluctuation in the scattered light intensity with time $I(t)$ caused by the diffusion of solute particles under Brownian motion produces correlation function as follows:

$$G(\tau) = \int \frac{I(t)I(t+\tau)}{[I(t)]^2} dt \quad 2.4$$

Under ideal conditions (for a monodisperse suspension), analysis of the time dependence of the intensity fluctuation, one would expect single exponential decay as follows:

$$G(\tau) = 1 + \beta \exp(-Dq^2\tau) \quad 2.5$$

where τ is delay time, Dq^2 is the decay rate,

D is diffusion coefficient and the fitting parameter $\beta \sim$ ratio of coherent signal to incoherent noise.

The diffusion co-efficient, defines the Brownian motion of solute particles in the suspension, and therefore, can be used to calculate the hydrodynamic radius of the particles in solution using Stokes – Einstein equation as follows:

$$D = \frac{K_B T}{6\pi\eta R_h} \quad 2.6$$

where K_B is Boltzmann constant, T is absolute temperature, η is viscosity of the solvent, D is diffusion co-efficient and R_h is the hydrodynamic radius [39].

The hydrodynamic diameter measured in DLS is a value that refers to how a particle diffuses within a fluid. The diameter that is obtained by this technique is the hydrodynamic diameter of a sphere that has the same translational diffusion coefficient as the particle. The translational diffusion coefficient depends on the number of factors such as the size of the particle core, its surface structure, concentration and the type of ions in the solution. Ionic strength of the medium also highly influences the diffusion speed by changing the thickness of electrical double layer around the particle. The change in the thickness of dissolved particle alters its diffusion speed which in turn affects the determined hydrodynamic diameter. The hydrodynamic diameter of any particle in a solution of low ionic strength would hence be apparently larger than its true diameter due

to the formation an extra layer of ions which surround the particle. The reverse would be the case in case of high conductivity medium. An altered surface structure of polymer particles due to changes in the ionic strength or due the change in molecular conformations of the polymer would also affect its motion and hence, can affect the measurement of the size by several nm. In addition the change in the shape of the particles may not affect the diffusion speed. For example in case of a rod shaped particle, only a change in its length will affect its diffusivity in solution which will affect the size measured, however, the diffusivity would hardly be affected due to any change in its diameter. That is why, in the case of proteins, only conformational changes which are generally dependent on the nature of the dispersing medium, can affect the diffusion speed are detected by DLS [116].

2.6.3.1 DLS data production

The raw data from a DLS experiment is an intensity distribution related to particle size. However, the intensity distribution can be misleading, in that a small amount of aggregation or the presence of larger particles can dominate the distribution and in this way can mask the presence of smaller aggregates and/or monomers. Therefore, using the concept of Mie theory [117], DLS software automatically processes an intensity distribution into mass, number and volume distributions and are best for describing the relative proportion of multiple components in the same sample based on their mass, number or volume. The

number, mass, volume distributions respectively give the relative total number, mass and volume of particles in the solution. The disparity stuck between intensity, volume (mass) and number distributions can be understood by taking into account, a total of 12 spherical particles of four different diameters to DLS as shown in Figure 2.9.

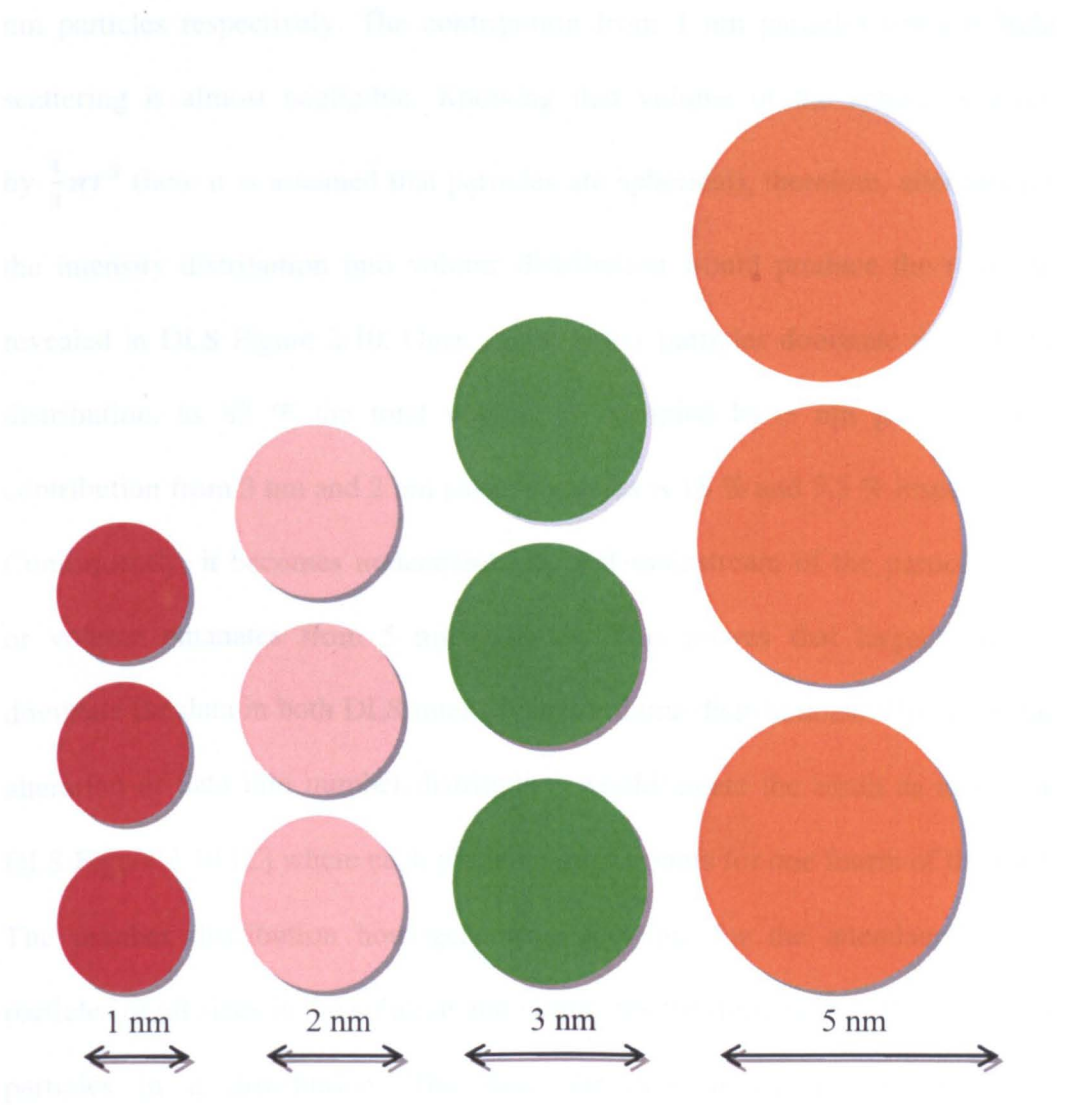


Figure 2.9 Twelve spherical particles in total with variable hydrodynamic diameter: 3x1 nm, 3x 2 nm, 3x3 nm and 3x5 nm particles.

The intensity of light scattering is directly proportional to 6th power of radius of the particle, $I \propto r^6$) has been stated [116, 118]. Therefore, intensity distribution of these particles would generate a result as shown in DLS Figure 2.10. The intensity of the light scattered predominantly corresponds to the 5 nm particles (95 %), whereas only 4.5 % and 0.38 % light scattered accounts for 3 nm, and 2 nm particles respectively. The contribution from 1 nm particles towards light scattering is almost negligible. Knowing that volume of the sphere is given by $\frac{4}{3}\pi r^3$ (here it is assumed that particles are spherical), therefore, alteration of the intensity distribution into volume distribution would produce the result as revealed in DLS Figure 2.10. Once again, larger particles dominate the volume distribution, as 85 % the total volume is occupied by 5 nm particles. The contribution from 3 nm and 2 nm particle species is 18 % and 5.5 % respectively. Consequently, it becomes understandable, that mainstream of the particle mass or volume emanates from 5 nm particles. This proves that larger particles dominate the data in both DLS intensity and volume distributions. However, the alteration of data into number distribution would create the result as shown in DLS Figure 2.10 [C] where each particle size accounts for one fourth of the total. The number distribution homogeneously accounts for the attendance of all particles of all sizes in the solution and eliminates the dominating effect of larger particles in a distribution. The data alteration is highly important and recommended when there are multiple modes and peaks. However, alteration is useless, if intensity distribution is a fairly single smooth peak.

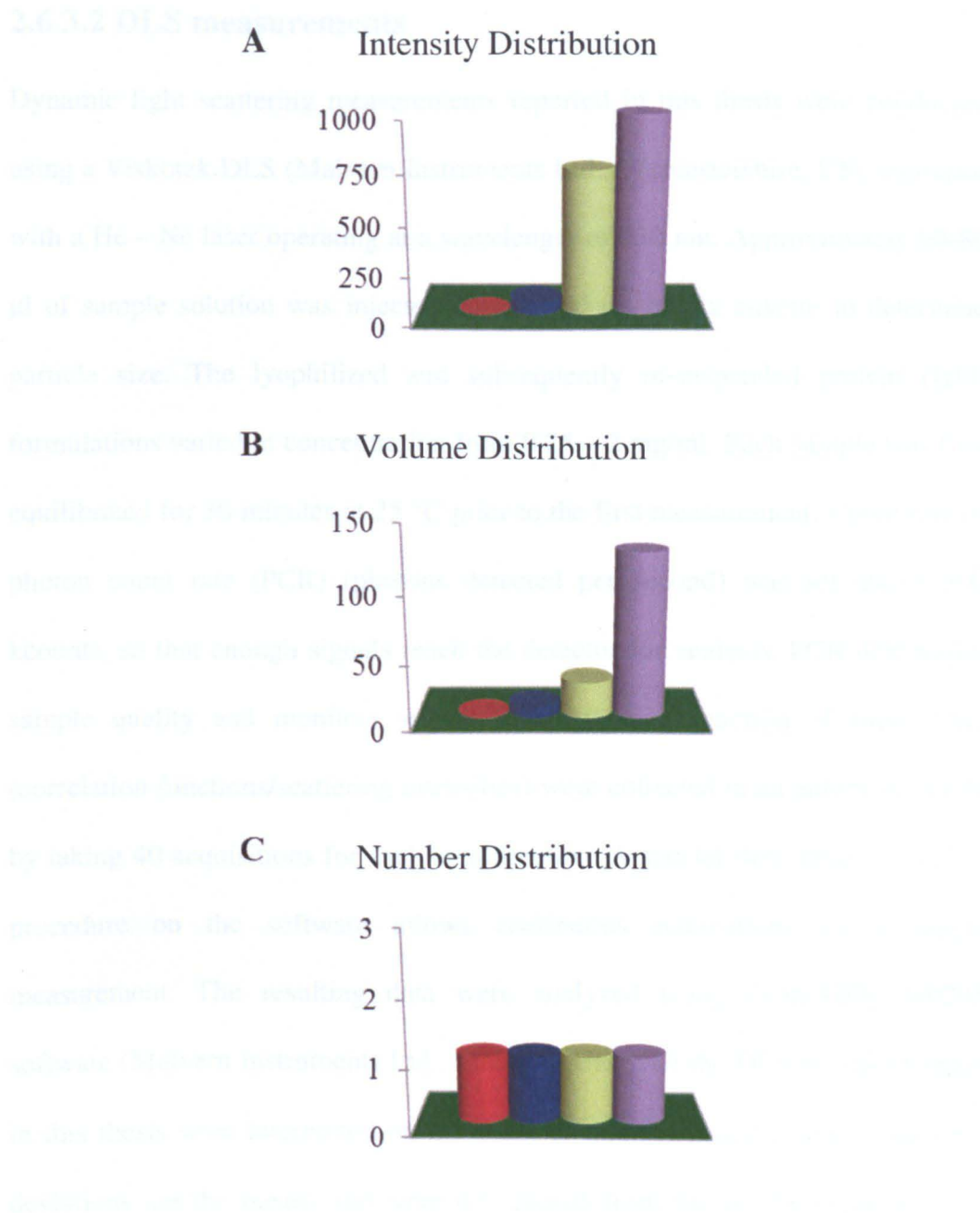


Figure 2.10 [A], [B], and [C] respectively represent a typical intensity, volume and number distributions: of a total of twelve particles of four different sizes: - **1 nm** (red bars), **2 nm** (blue bars), **3 nm** (green bars), and **5 nm** (purple bars) in a hypothetical nanoparticle solution. Number distribution unequivocally demonstrates the presence of particles of all sizes. This is contrast to intensity and volume distributions, where particles larger in size dominate the distribution. Hence, the attendance of smaller species remains masked.

2.6.3.2 DLS measurements

Dynamic light scattering measurements reported in this thesis were conducted using a Viskotek DLS (Malvern Instruments Ltd., Worcestershire, UK) equipped with a He – Ne laser operating at a wavelength of 630 nm. Approximately 60-80 μ L of sample solution was injected into the 80 μ L quartz cuvette to determine particle size. The lyophilized and subsequently re-suspended protein (IgG) formulations varied in concentration from 0.25 – 2 mg/ml. Each sample was first equilibrated for 30 minutes at 25 °C prior to the first measurement. Count rate or photon count rate (PCR) (photons detected per second) was set above 300 kcounts, so that enough signals reach the detector for analysis. PCR determines sample quality and monitors sample stability as a function of time. Data (correlation functions/scattering intensities) were collected in an automatic mode by taking 40 acquisitions for each measurement. A special flow mode operating procedure on the software allows continuous acquisitions for a single measurement. The resulting data were analyzed using OmniSIZE 300295 software (Malvern Instruments Ltd., Malvern, UK). All the DLS results reported in this thesis were interpreted on the basis of number distributions. Standard deviations are the means and were determined from the results obtained from repeated measurements.

2.6.4 Nanosight/Nanoparticle tracking analysis (NTA)

In comparison to DLS, Nanoparticle tracking analysis is a relatively newer system for characterization of particles and generally measures particle size from 30 – 1000 nm, with the lower recognition limit down to 10 nm being reliant upon the refractive index of the nanoparticle material [119, 120]. NTA enables direct/real time visualization, detection, counting, and measurement of concentration. Like DLS, the particle size is determined from the fluctuations in scattered light intensity due to the Brownian motion of the particles [119, 120, 121]. However, unlike DLS, NTA technique compensates the masking effect of larger particles, because in this technique, laser light scattering microscopy is conjoined with a charge-coupled device (CCD) camera, which facilitates the visualization and recording of motion of individual nanoparticles in solution. Figure 2.11 shows the basic set-up. NTA enables size characterization of both monodisperse and polydisperse samples with fine peak resolution. Regardless of having potential advantages over DLS, NTA is known to have several limitations such as NTA measurements are time consuming and essentially require a skilled operator for software adjustments. In addition, the shear caused to the sample during administration into the cell and the stress experienced by sample (when comes in contact with glass, stainless steel, and O – ring of the chamber) is more aggressive than DLS operation [120].

The fundamental principle of this technique is that it allows the tracking of the Brownian motion of individual nanoparticles in solution. A finely focused laser beam (640 nm) is passed through a prism edged optical flat refracts at the interface between the flat and the thin layer of suspension placed above it. The refracted laser beam produces an illumination region across the thin liquid film in which nanoparticles can be visualized, with the help of magnification microscope objective, as shown in Figure 2.12. A CCD camera is used to capture a video field of view of approximately 100 μm x 80 μm .

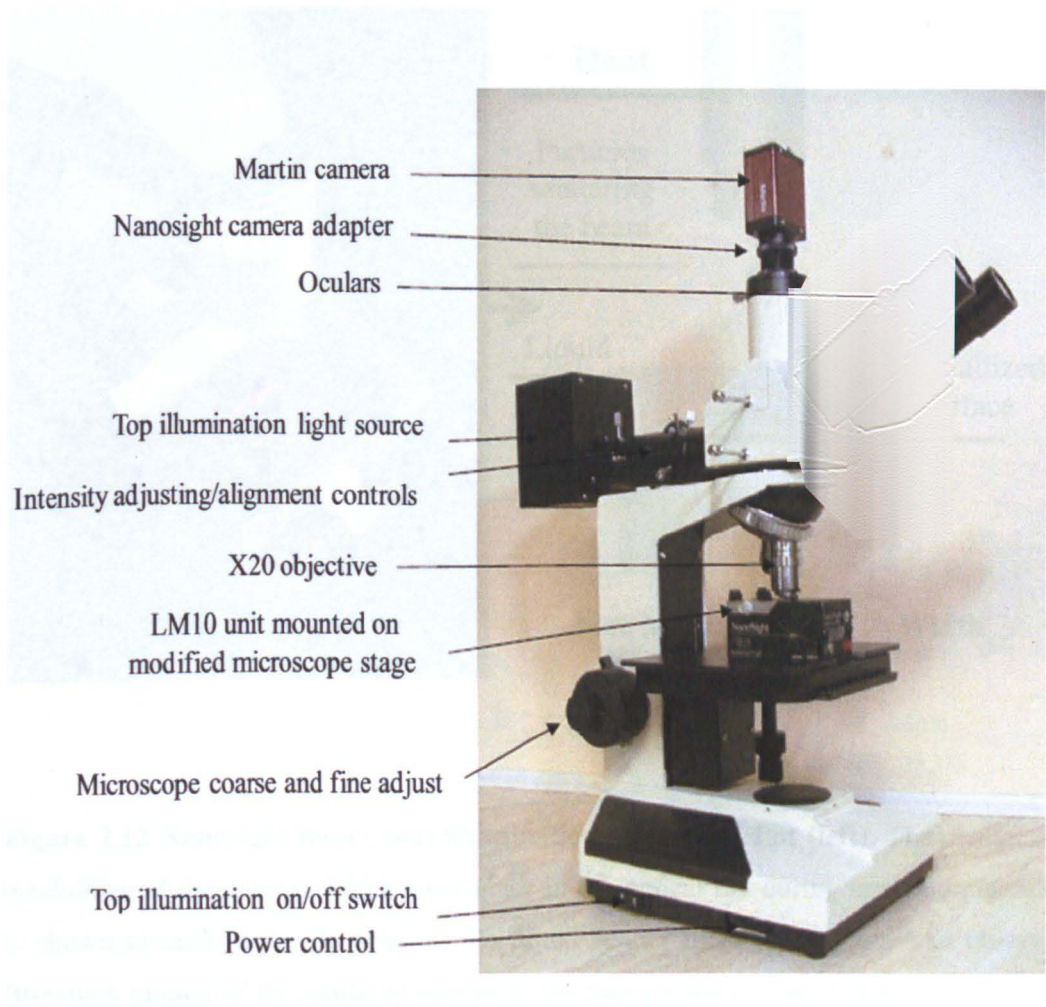


Figure 2.11 Schematic and labelled overview of the Nanosight instrument (LM 10).

In NTA the Brownian motion of the particles in a suspension is analysed by a video. A video of the movement of each particle is analysed on a frame-by-frame basis and the particle's size is established from an analysis of the average speed of movement. The NTA, inbuilt software is then proficient to spot and follow individual nanoparticles moving under Brownian motion. The individual positional changes are tracked in two dimensions, and the average distance each

2.6.4.1 NTA data production

Figure 2.12 demonstrates an example of data produced by NTA.

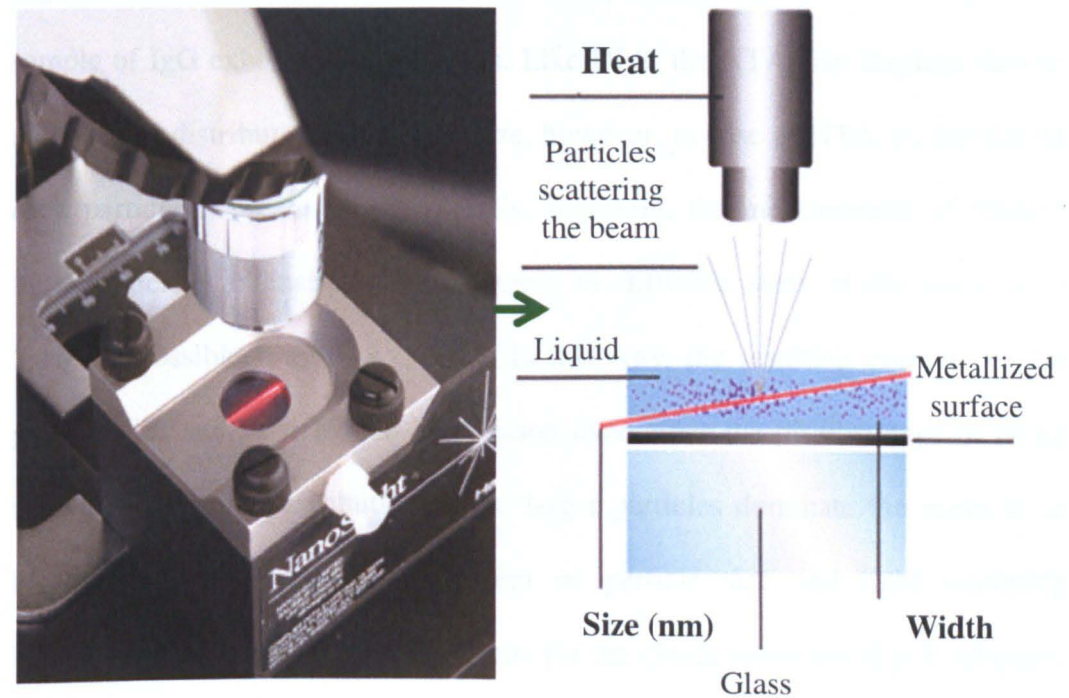


Figure 2.12 Nanosight laser (red) illuminations in optical flat (left). The analytical breakdown of the process which takes place in the optical flat during laser illumination is shown towards right. Particles in the liquid scatter the light and one can observe Brownian motion of the scattered nanoparticles through microscope fitted on the top of the optical flat (Figure from Nanosight Ltd).

particle moves in x and y directions in the image are automatically calculated from which particle diffusion coefficient is determined. Subsequently, this diffusion coefficient related to the motion to a particle diameter according Stokes-Einstein equation as described earlier in DLS section.

2.6.4.1 NTA data production

Figure 2.13 demonstrates an example of data produced by NTA for a lyophilized sample of IgG exhibiting aggregation. Like DLS, the NTA also displays data as an intensity distribution of particle size, however, in case of NTA, as the size of each particle is measured individually; therefore, the measurement of relative light scattering intensity by populations of different sizes at the same time becomes possible (Figure 2.13 [C]). In this way, the resulting estimate of the particle size and particle size distribution overcomes the disadvantage of being an intensity biased distribution where larger particles dominate the mean as in DLS. The simultaneous measurement of particle size and light scattering intensity makes NTA an ideal technique for the characterization of poly-disperse samples Figure 2.13. Furthermore, NTA also enables measurement of concentration directly from the particle size distribution in the form of a direct number/frequency distribution, Figure 2.13 [B]. The emergence of various peaks up to 100 nm is an indicative of a sample with diverse populations of smaller aggregates (Figure 2.13 [B]). It is important to have sufficient number of particles to be analysed within an acceptable time period (e.g; < 60 seconds for

the production of statistically meaning and reproducible particle size distribution). This is typically ensured when a given sample at least contains between 10^7 and 10^9 particles/ml.

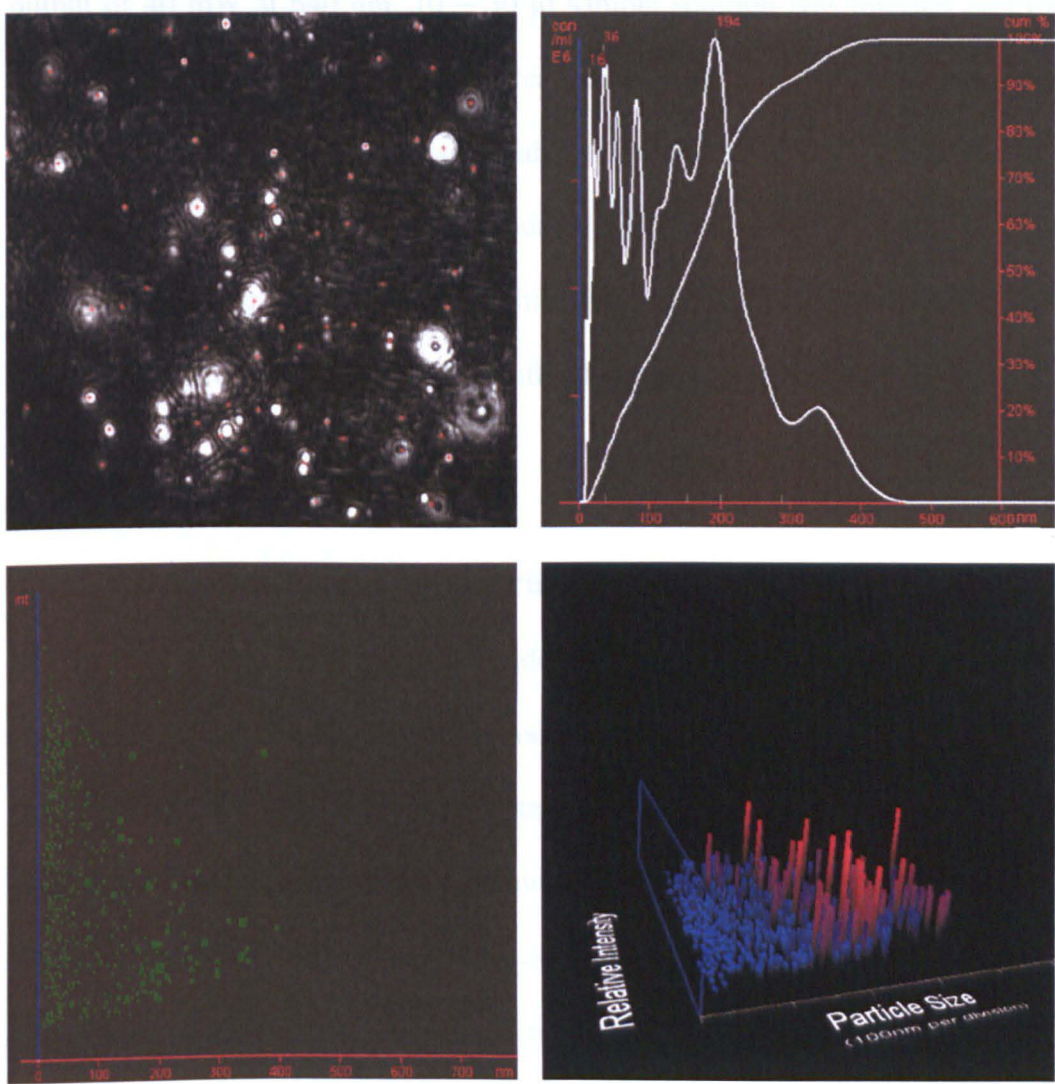


Figure 2.13 Typical example of a sample report produced by nanoparticle tracking analysis (NTA) software for one time lyophilized solution (0.25 mg/ml) of an IgG exhibiting aggregation. [A]: video frame images of nanoparticle tracks, the white dot like structures represent scatters of the IgG nanoparticles particles under Brownian motion, [B]: shows particle size distribution profile, [C]: plot of particle size against relative intensity, [D]: 3D plot of particle size against relative intensity.

2.6.4.2 NTA measurements

Particles sizes and size distributions reported in this thesis were measured using a NanoSight LM10 (NanoSight Ltd., Amesbury Wiltshire, UK) enabled with laser output of 40 mW at 640 nm. 10 – 30 μ l sample solution was injected into the sample chamber using a syringe. At least three measurements were performed following each injection. The image analysis (tracking of individual particles and their size measurement) was carried out by using the Nanosight software. The displayed frequency size distribution histograms by software were output to a spreadsheet for comparative analysis with DLS results.

2.6.5 Differential scanning calorimetry (DSC)

DSC is a thermal analysis technique widely employed for investigating the phase behaviour (thermal transitions) which occur within samples under the influence of a regulated increase or decrease in temperature [122]. The basic principle of DSC is that it determines the temperature and heat flow in and out of sample which is associated with material transitions (melting points, glass transition temperature, crystallinity, polymorphism, and decomposition) of polymers in solid, liquid or in mixed phases (e.g; suspensions) as a function of time and temperature. These measurements provide quantitative and qualitative information about the physical and chemical changes that involve endothermic or exothermic processes. Distinctively, in case of proteins; DSC measures the enthalpy (ΔH) of unfolding due to heat denaturation. Under the influence of

applied heat, equilibrium between the native (folded) conformation and its denatured (unfolded) state is sustained. The higher the thermal transition midpoint (T_m), when 50 % of the protein molecules are unfolded, the more stable the molecule. DSC is also used to determine the change in heat capacity (ΔC_p) of denaturation. Heat capacity changes associated with protein unfolding are primarily due to changes in the hydration of side chains that were buried in the native state, but become solvent exposed in the denatured state. By studying the thermal transitions occurring within the material, information is acquired on the nature of the polymer in the context of thermal strength [122].

A typical DSC instrument as shown in Figure 2.14 measures heat into or out of sample relative to a reference with a linear temperature ramp. The sample material is enclosed in a pan and empty reference pan are placed on a thermoelectric disk surrounded by a furnace. The furnace which is subjected to a linear heating rate, allows the heat to be transferred to the sample pan and reference pan through thermoelectric disk, in order to raise the temperature of both pans identically over time. The difference in the specific heat capacity (C_p) of the sample and the reference pan is measured by the area of thermocouples, and the consequent heat flow is measured by the area of thermocouples, and the consequent heat flow is determined by the following equation:-

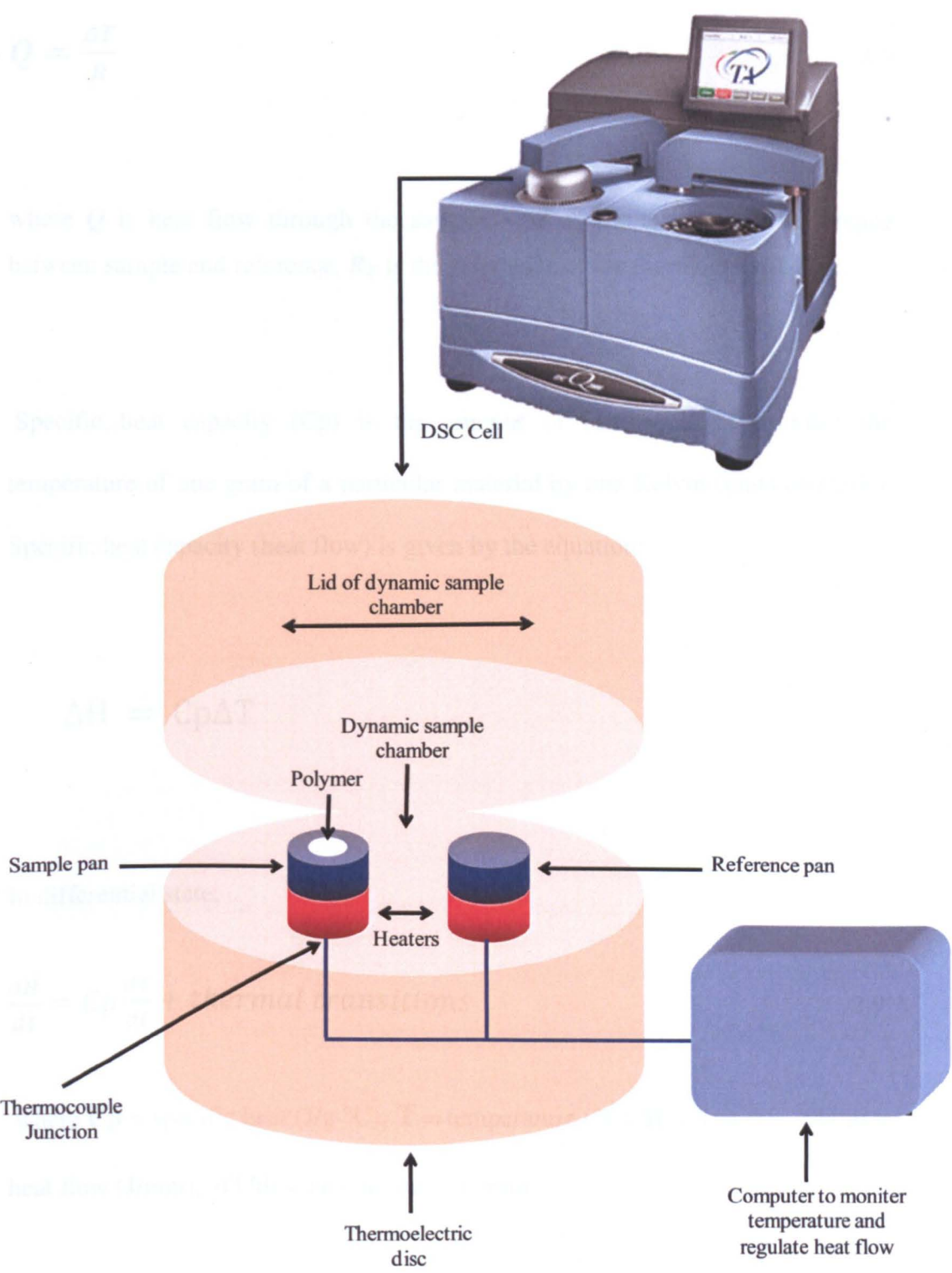


Figure 2.14 DSC instrument on top (blue) and underlying schematic of a typical DSC cell.

$$Q = \frac{\Delta T}{R} \quad 2.7$$

where Q is heat flow through the sample, ΔT is the temperature difference between sample and reference, R_E is the resistance of the thermoelectric disk.

Specific heat capacity (C_p) is the amount of heat required to raise the temperature of one gram of a particular material by one Kelvin (units of J/g K). Specific heat capacity (heat flow) is given by the equation:

$$\Delta H = C_p \Delta T \quad 2.8$$

In differential state;

$$\frac{dH}{dt} = C_p \frac{dT}{dt} + \text{thermal transitions} \quad 2.9$$

where C_p = specific heat (J/g °C), T = temperature (°C), H = heat (J), dH/dt = heat flow (J/min), dT/dt = heating rate (°C/min).

Owing to the difference in the specific heat capacities of the pan loaded with the sample and the reference pan, the amount of heat required to ensure the

temperature of the sample is the same to that of the reference is the amount of excess heat absorbed (endothermic transition) or released (exothermic transition) by the molecules in the sample. Figure 2.15 provides a brief description of how this excess heat changes as a function of temperature.

DSC has the capability to elucidate various underlying factors that affect the folding and stability of polymeric biomolecules. These include van der Waals, hydrophobic, and electrostatic interactions, hydrogen bonds, hydration of the exposed residues, conformational entropy, and the physical environment (such as pH, buffer, and excipients). The difference in the specific heat capacity (C_p) emanate from changes in the alignment and strength of the above indicated bonds/interactions responsible for stabilizing protein structure. DSC is highly sensitive technique able to pick up structural change produced in the molecule, because changes in the conformation affect the position, sharpness, and shape of thermal transition(s). Figure 2.16 shows a typical DSC trace revealing glass transition, crystallization, cross linking and melting events, polymer can undergo when subjected to heat. The sudden downward shift observed in the DSC trace is indicative of a polymer having undergone a glass transition (T_g). At T_g more heat flows through the polymer and indicates an increase in the heat capacity (C_p). The T_g is characteristic of polymers and its larger value is indicative of increased thermal stability.

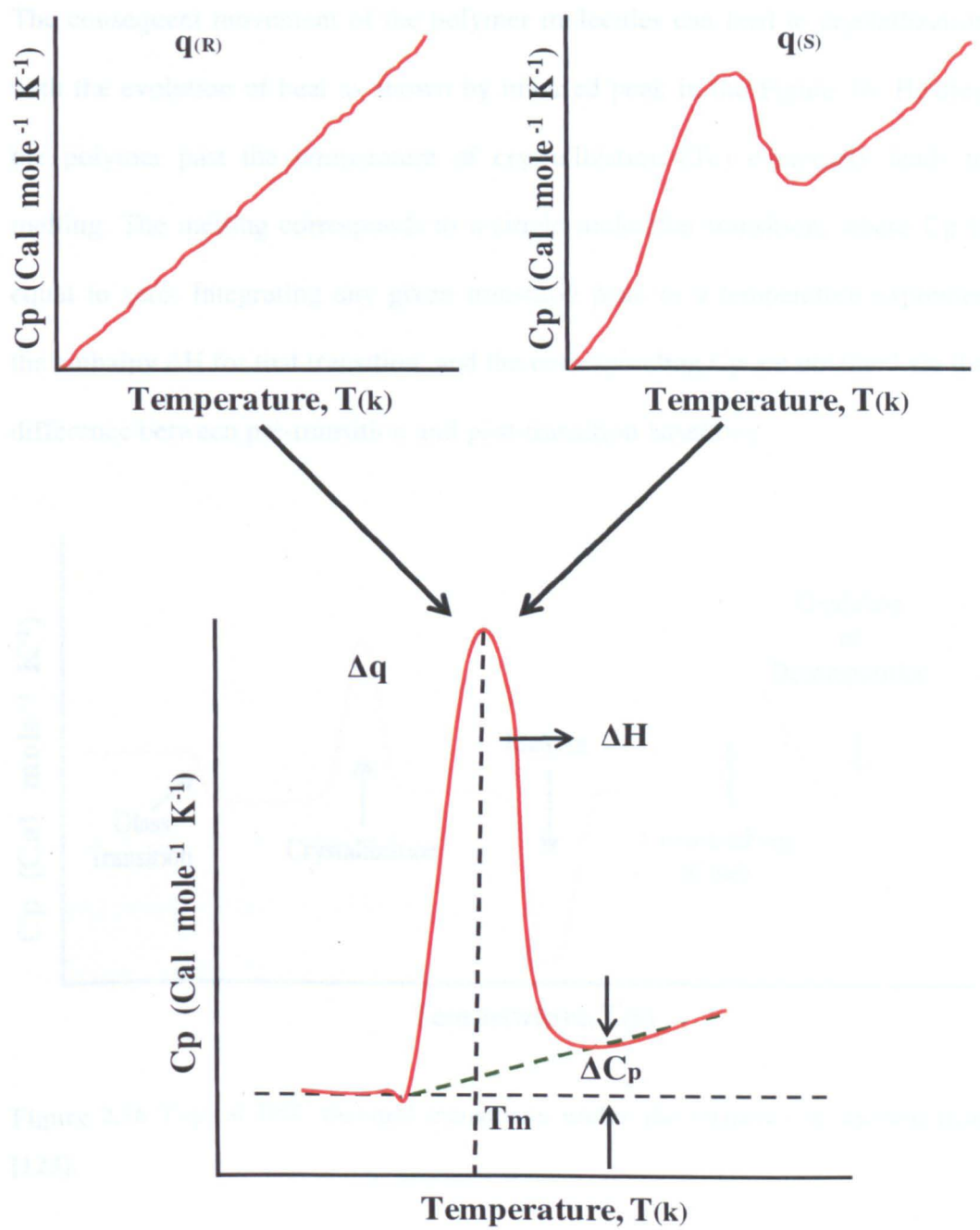


Figure 2.15 Graphical representation of heat flown through a reference cell (q_s) and a sample cell (q_s). The amount of excess heat absorbed by the sample cell is equivalent to the heat absorbed by the molecules in the sample. The subtraction of the DSC scans (sample – reference) shows how this excess heat changes (Δq) as a function of temperature; ΔH -corresponds to change in enthalpy, ΔC_p represents change in the heat capacity (C_p), T_m – Melting point [122].

The consequent movement of the polymer molecules can lead to crystallization with the evolution of heat as shown by inverted peak in the Figure 16. Heating the polymer past the temperature of crystallization (T_c) eventually leads to melting. The melting corresponds to a single molecular transition, where C_p is equal to zero. Integrating any given transition peak to a temperature expresses the enthalpy ΔH for that transition, and the corresponding C_p are obtained via the difference between pre-transition and post-transition baselines.

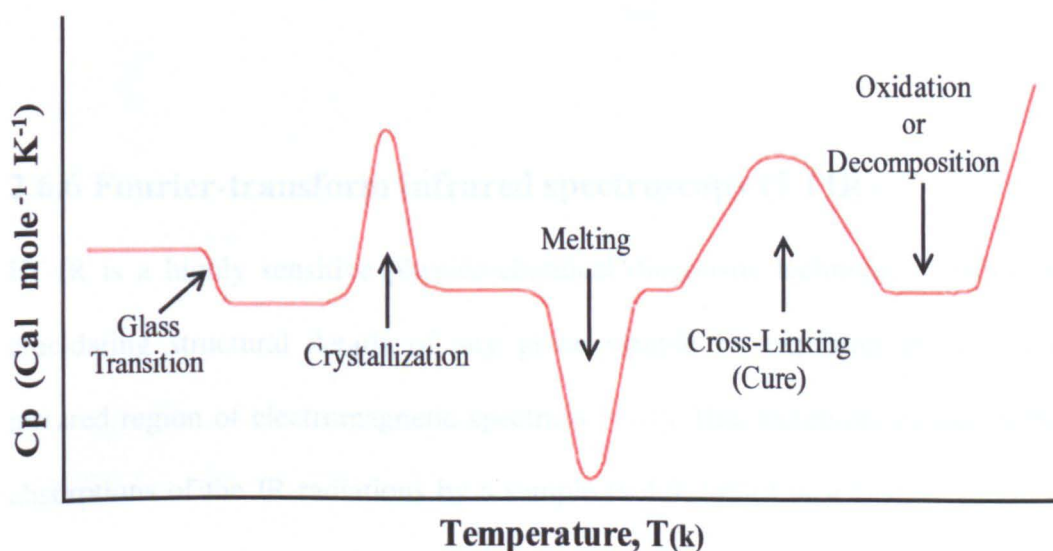


Figure 2.16 Typical DSC thermal transitions under the influence of applied heat [123].

2.6.5.1 DSC Measurements

DSC experiments reported in this thesis were carried out using a Q – 2000, differential scanning calorimeter (TA Instruments Ltd, Fleming Centre, Manor, Crawley, West Sussex, UK) with a constant $10\text{ }^{\circ}\text{C min}^{-1}$ heating rate,

from 0 °C to 200 °C in a dry nitrogen atmosphere. Dry powdered samples (2 – 5 mg) were analyzed in crimped hermetically sealed aluminium pans. Samples were heated from 0 °C – 200 °C at a scan rate of 10 °C/min. The thermograms obtained for the DSC results were analysed using TA universal analysis-NT software. The melting point of the IgG antibody lyophilized multiple times on its own and the T_g /melting point of the sugar-containing antibody formulations were obtained as the midpoint of the corresponding transition by integrating the slope of the DSC curve.

2.6.6 Fourier-transform infrared spectroscopy (FTIR)

FT-IR is a highly sensitive physico-chemical diagnostic technique, capable of elucidating structural details of any given sample by exposing them in the infrared region of electromagnetic spectrum [124]. This technique measures the absorptions of the IR-radiations by a sample (solid, liquid or a gas), to produce an IR spectrum that can be used to identify functional groups and molecular structure of the sample. A particular molecular entity exhibiting a unique chemical structure when subjected to FT-IR spectroscopic examination, the characteristic FT-IR spectrum displayed corresponds to the structural fingerprint of the examined molecule. Therefore, any shift in the native structure of the interested molecule will be observed in the FT-IR spectrum. In this way, alteration from the original structure observed in the FT-IR spectrum of the exposed molecule discloses structural/molecular deformation/discrepancies that

have occurred under given conditions. The biomolecular species such as proteins, lipids, carbohydrates and vitamins etc have been widely and successfully characterized by FT-IR [125, 126, 127, 128].

Figure 2.17

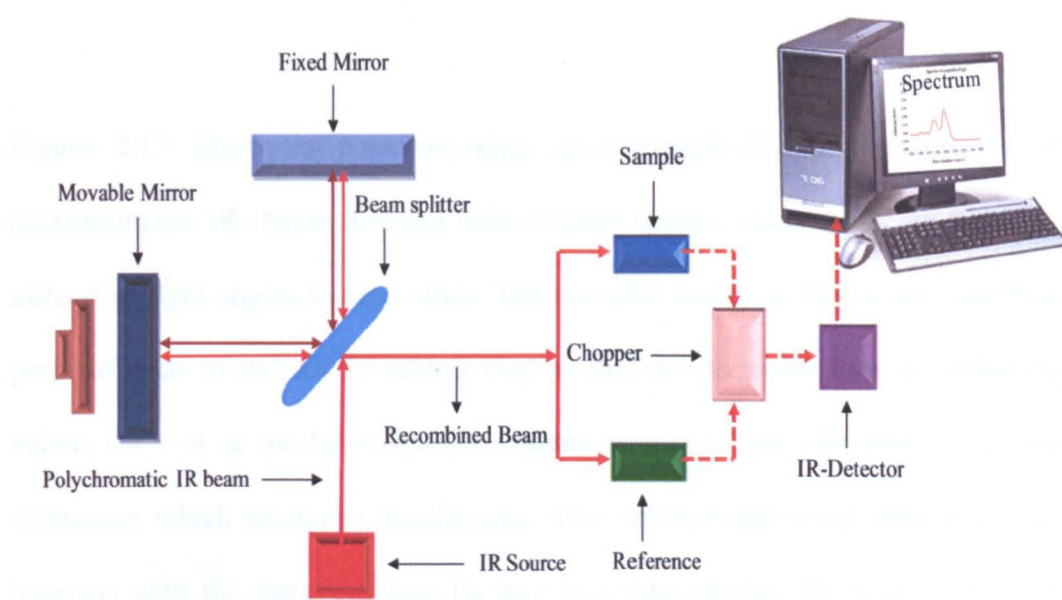



Figure 2.17 Basic set up of the process of working of an FT-IR spectrometer. A polychromatic IR beam splits at the beam splitter. Recombined polychromatic IR-beam hits the sample/and reference on its way to detector for the generation of an infrared spectrum of the sample under observation with the help of software installed on the computer.

FT-IR spectroscopic technique exercises the phenomenon of interference and Fourier transformation for its swiftness and sensitivity. Unlike conventional spectroscopy, FT-IR spectroscopy irradiates the sample of interest with all wavelengths simultaneously in the infrared region of electromagnetic spectrum and the quantity of light absorbed by the sample is determined by tailoring

different frequencies in the reflected beam. This process is repeated numerous times. Finally, all the data collected is processed by an inbuilt software programme in the computer to calculate the amount of absorption at each wavelength.



Figure 2.17 illustrates basic working of a typical FT-IR spectrometer. A polychromatic IR- beam directed onto a beam splitter sends the beam onto two mirrors at right angles to each other. The movable mirror as moves in a direction perpendicular to its axis in such a way so that the recombination of reflecting beams (\longleftrightarrow) at the beam splitter () results in the introduction of path difference which produces interference. This recombined wave (output signal) interacts with the sample before its way to a detector for the production of an interferogram (sum of the sine waves of all frequencies present). Fourier transformation of the interferogram produces the resultant spectrum. The polychromatic nature of the IR- beam makes it non- attenuated and therefore the signal to noise ratio of the resultant spectrum is very much high, which is necessary for improving the quality of spectrum to be obtained.

2.6.6.1 FT-IR modes of analysis

FT-IR spectroscopy can be performed in three modes depending on the property of sample:

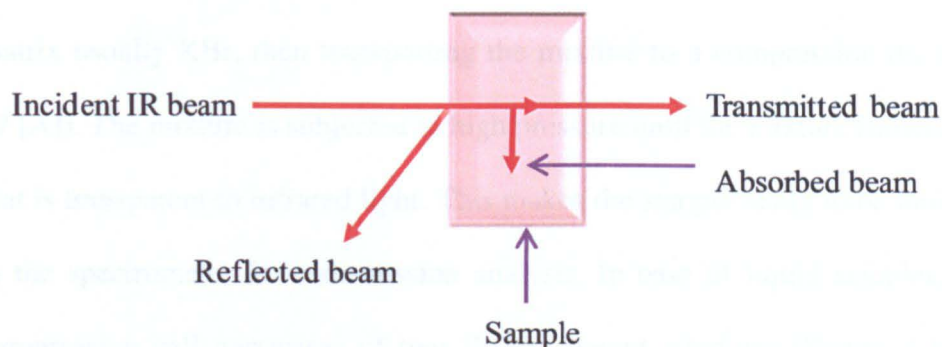


Figure 2.18 Transmitted, absorbed and reflected portions of an incident polychromatic IR-beam after hitting the sample. The measurement/detection of a specific portion determines the mode of FT-IR analysis.

(iv) *Transmission mode*

In this mode of operation, the recombined IR beam passes through the sample and the amount of infra-red energy that gets transmitted is measured (Figure 2.18). Both solid and liquid samples can be examined in this mode of analysis. The intensity of the IR-spectrum is determined by the sample thickness and should be typically in the range of tens of few microns ($0.1 - 15 \mu\text{m}$) [129]. The micron thickness is ensured by introducing a small quantity of sample onto a diamond window of a micro compression cell to flatten and thin. Solid samples are usually compressed in a pellet and one of the most commonly employed methods for the examination of solid samples in the transmission mode is pressing in a pellet (alkali halide such as such as NaCl, KBr or CaF_2). This

involves grinding of the solid material to a fine powder and dispersing it in a matrix usually KBr, then transporting the mixture to a compression die (Figure 19 [A]). The mixture is subjected to high pressure until the mixture forms a pellet that is transparent to infrared light. This makes the sample ready to be introduced in the spectrometer for transmission analysis. In case of liquid samples, micro compression cell comprises of two IR-transparent windows (Figure 2.19 [B]). The film thickness considered necessary and path length for quantitative analysis is ensured by introducing a spacer usually made of Teflon or Lead [129].

(v) ***Reflectance mode***

It involves reflecting the light off the sample and detects the infra-red energy that is reflected from the sample. The infra-red radiation reflected off from the surface can be either specular (directly reflected from surface without any absorption by sample) or diffuse (where IR-energy penetrates into sample surface a short depth and bounces back after reflecting internal portions of the sample). The specular reflection is non-invasive and does not require any sample preparation. However, a small quantity of sample (in case of hard polymers) that clings to the surface of silicon carbide disc is needed during diffuse reflection.

The spectra in general are collected from the sample under reflectance mode with clean gold surface as background.

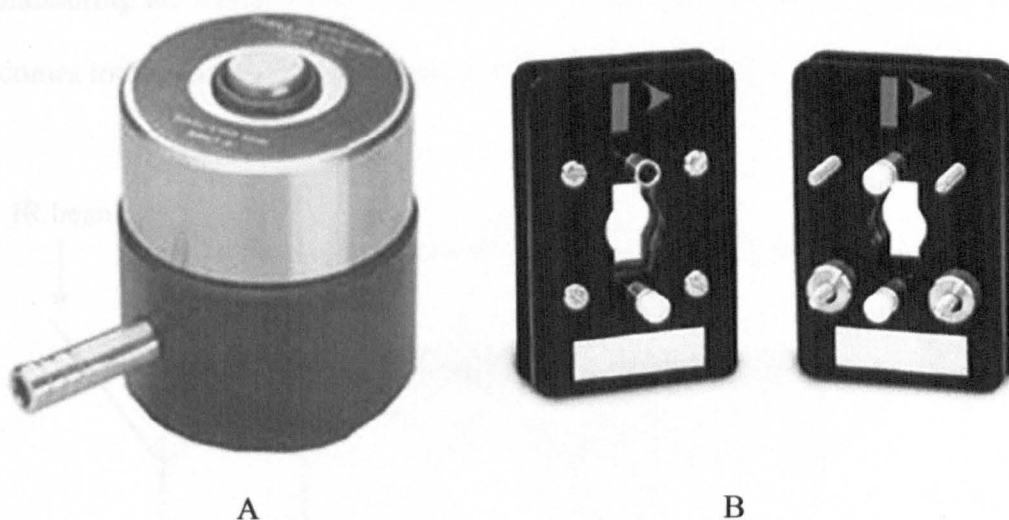


Figure 2.19 [A] KBr die for IR analysis: This set includes evacuable die body, base, plunger, two 13 mm polished steel pellets, O-ring vacuum seals, and knock-out ring for sample disc extraction. **[B] Liquid cells:** Each cell has precise path length which is standardized by making use of the interference blueprint produced by an empty cell in the IR-beam. These cells utilize a spacer which is merged with the window material.

The specular reflection is non-invasive and does not require any sample preparation. However, a small quantity of sample (in case of hard polymers) that clings to the surface of silicon carbide disc is needed during diffuse reflection. The spectra in general are collected from the sample under reflectance mode with clean gold surface as background.

(vi) Attenuated total reflection mode

This mode is highly recommended when samples are strongly absorbing. Attenuated total reflection mode (a type of reflection mode) operates by

measuring the changes that occur in a totally internally reflected, infra-red beam comes into contact with the sample as shown in Figure 2.20.

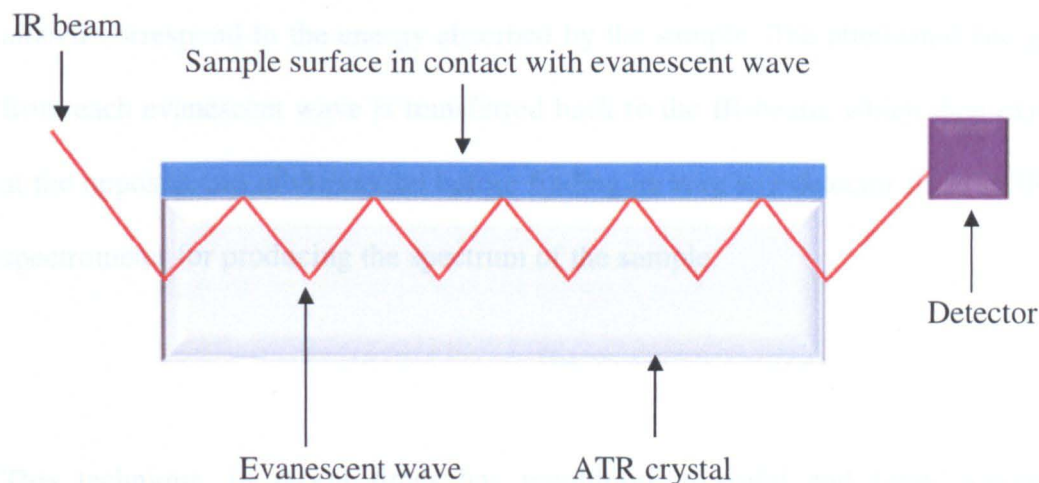


Figure 2.20 IR – beam observes the phenomenon of total internal reflection within the ATR crystal, hence produces an evanescent effect. A thin sample is mounted on to the vertical face of the crystal with upper surface exposed.

An IR beam is directed onto an optically dense crystal with a high refractive index at a certain angle of incidence experiences the phenomenon of total internal reflection inside the crystal. Multiple internal reflections (usually between 5 and 10) occur, however their number within the crystal depends on the angle of incidence, length and thickness of the crystal. The consequence of total internal reflection produces an evanescent wave (a bubble of infrared immobilized on the surface) that extends beyond the surface of the crystal into the sample held in contact with the crystal. This evanescent wave protrudes only

a few microns ($0.5 - 5 \mu\text{m}$) beyond the sample surface and into the sample. This penetration demands a better contact between the sample and the crystal surface. Regions of the IR-spectrum where evanescent wave would be attenuated or altered correspond to the energy absorbed by the sample. The attenuated energy from each evanescent wave is transferred back to the IR-beam, which then exits at the opposite end of the crystal before finding its way to a detector fixed in IR-spectrometer for producing the spectrum of the sample.

This technique, in recent times has revolutionised solid and liquid sample analyses by IR-spectroscopy, because it conveniently prevails over the most imperative challenges of IR-spectroscopy which are the sample preparation and the spectral reproducibility [130]. This is for the reason that ATR works by way of an evanescent effect which ensures least possible damage to the sample compared to that when the sample is irradiated by a non-attenuated IR beam. However, the two important requirements for the success of this technique are: tight contact between crystal and sample, and significantly higher refractive index of the crystal than the sample. This is due to the fact, that for the phenomenon of total internal reflection to occur, the refractive index of the ATR crystal should be significantly greater than that of the sample; otherwise the incident IR-beam will be transmitted in the crystal. Typically refractive index values of ATR crystals lies in between 2.38 and 4.00 at 2000 cm^{-1} with an effective penetration depth of almost $1 \mu\text{m}$ [129]. Zinc Selenide (ZnSe),

Germanium (Ge) and diamond are by far the generally employed materials which are used as ATR crystals. While expensive, diamond is by far the best ATR crystal material, because of its robustness and durability.

2.6.6.2 FT-IR measurements

FT-IR experiments described in this thesis were performed using a Nicolet FT-IR-spectrometer using diamond crystal. The recorded spectra were obtained for the determination of changes in the secondary structure of IgG lyophilized on its own as well in combination with different excipients. Sample powder (2 – 3 mg) was placed on a clean glass slide and then mounted on the sample stage. The spectra for each sample were recorded from 4000 cm^{-1} to 650 cm^{-1} in ATR mode at room temperature. Each measurement was an average of 200 scans, at a scan speed of 0.15 cm^{-1} and the resolution of 2 cm^{-1} . The optical bench was purged with dry nitrogen to avoid interference from water vapour infrared absorption. Each spectrum was background corrected for the glass slide. The amide I ($1720\text{ cm}^{-1} - 1600\text{ cm}^{-1}$) and amide II ($1575\text{ cm}^{-1} - 1480\text{ cm}^{-1}$) regions were used to analyze changes in the secondary structure of protein [129, 130].

2.7 T – test for statistical analysis

T-test involves statistical inspection of two mean values of data produced from two samples in order to determine whether or not the difference between two means reflects a true change. Generally, t–test is employed when the variances of two normal distributions are not known. The test statistic in the t-test is known as the t-statistic or (t value) and is given by the formula given below:

$$t_{Stat} = \frac{\bar{X}_1 - \bar{X}_2}{\sqrt{\frac{s_1^2}{N_1} + \frac{s_2^2}{N_2}}} \quad 2.10$$

where:

\bar{X}_1 and S_1^2 denote the mean and standard deviation of the data set from sample 1

\bar{X}_2 and S_2^2 represent the mean and standard deviation of data set from sample 2

N_1 and N_2 signify number of data entries in the sample 1 and 2 respectively.

The t – test takes into an account the following important factors:

- (i) t – Statistic is the calculated t value using the formula given above.
- (ii) t – Critical: is a cut-off value to which the value of the test statistic is compared in order to decide whether or not the null hypothesis is rejected. The t-critical is governed by level of alpha and whether the test is one-tailed or two-tailed.

- (iii) Degrees of freedom (df): correspond to the number (N) of values that are there in the data and are given by $N - 1$ for one-sample and paired-samples t-tests.
- (iv) Significance level alpha (α): is a threshold value which represents an acceptable probability in a statistical test. The value of α could range from any where between 0 – 1. However, the frequently used values for alpha are 0.01, 0.05, and 0.1. Mostly the standard for alpha is 0.05.
- (v) P-value: represents the probability of the existence of the result obtained alone in comparison with the recognized distribution of conceivable findings, even if the null hypothesis is right and no true difference exists between two samples.

The t-test results are deemed statistically significant by two ways: one is when t-statistic value exceeds t-critical value and the other is when the P - value does not exceed the chosen significance level of alpha. The statistical significance of data reported in this thesis was determined using t – test using an excel spread sheet. Table 2.2 shows an example of one such analysis in cycle 0 and cycle 1 times lyophilized ferritin particles (~ 4 – 12 nm in width). The t-statistic (~ 12) is larger than t-critical (1.86) and P- value is much smaller than the significance level at threshold ($\alpha = 0.05$). This suggests the significant difference in the proportion of the measured particles in the two indicated samples of ferritin.

Width	Cycle 0	Cycle 1
Size Range 4.0-12 (nm)	Number of Particles	Number of Particles
Measurement 1	70	53
Measurement 2	69	51
Measurement 3	74	48
Measurement 4	76	55
Measurement 5	72	50

t-Test: Two-Sample Assuming Unequal Variances		
	Variable 1	Variable 2
Mean	72.2	51.4
Variance	8.2	7.3
Observations	5	5
Hypothesized Mean Difference	0	
df	8	
t Stat	11.813606	
P(T<=t) one-tail	0.000001	
t Critical one-tail	1.859548	
P(T<=t) two-tail	0.000002	
t Critical two-tail	2.306004	

Table 2.2 T-test report of the number of ferritin (~ 4 – 12 nm in width) particles in cycle 0 and cycle 1 times lyophilized ferritin performed on excel spreadsheet.

Chapter 3

Nanoscale characterization of the effect of lyophilization on the propensity of ferritin aggregation

3.1 Introduction

This chapter describes the effect of the lyophilization on the aggregation of ferritin. In the preliminary studies, ferritin was employed as a study material. The idea of the utilization of ferritin was endorsed for various reasons such as its relatively lower cost; availability of significant studies reported in literature; adsorbs easily on the hydrophilic surfaces, making it easy and quick to prepare samples; its high stability and its attributes for easy characterisation makes it convenient for studying protein adsorption onto solid substrates [131-133]. The other fundamental objective of this study was also to get myself familiarized with AFM technique in order to gain experience of imaging proteins in air and liquid while using not much expensive proteins. As described in the Chapter 1, in liquid state biopharmaceuticals, the complete/partial loss in activity and a reduced shelf life are the potential consequences of protein aggregation. Loss in protein activity is possibly induced due to the subtle or massive changes in the protein environment such as changes in pH, temperature, and ionic strength. Therefore,

there is a growing demand to find out an effective formulation strategy which would enable us to better predict or overcome the problem of aggregation. Presently, in order to avoid the potential consequences of aggregation in solution, pharmaceutical companies often prepare powdered (dry) preparations, and lyophilization is one of the most widely employed methods for this purpose. Although, lyophilization is considered to be a viable option for the manufacture of dry protein formulations, it is still not the best option for completely stopping aggregation, because formation of insoluble aggregates (described in chapter 1) and loss of monomers has been reported in many protein solutions which were reconstituted from their respective lyophilized powders. The detection limit for some of the conventionally used techniques (such as SEC, AUC) for aggregate detection lies within the micrometer range and therefore, they can fail to detect much finer structures such as fragments, and monomers etc. So far the effect of lyophilization in minimising aggregation in biopharmaceutical formulations such as antibodies, using conventional techniques has been found to be dependent on the nature of protein itself and the optimum lyophilization conditions employed. Very little work has been done to investigate the effect of lyophilization on proteins using unconventional techniques such as AFM, which has relatively much higher resolution (can detect ~ 1 nm) and can therefore, easily account for much interested species such as fragments and monomers in more detail. The identification of critical formulation is determined by the optimization of processing variables such as effect of concentration, lyophilization, pH change, sugar lyoprotectants, buffer concentration, counter

ion (Na^+ versus K^+ phosphate), added salts, cooling rate, residual moisture level, and presence of a surfactant [134, 135]. However, the parameters examined in these preliminary studies were the effect of protein concentration and the number of cycles of lyophilization. AFM studies were focused on evaluating the effect of lyophilization on the aggregation of ferritin molecules on the basis of their size and morphology. A brief introduction of ferritin, its structure, and the AFM studies conducted on ferritin is described in the following sections:-

3.1.1 Ferritin; its tertiary and quaternary structure

Ferritin can be described as a nano-particle and consists of an organic protein coat (apoferritin) surrounding an 8 nm sized cavity, that can be fully or partially occupied by a hydrated iron (III) oxide known as mineral ferrihydrite $[\text{FeO}(\text{OH})]_8$ $[\text{FeO}(\text{H}_2\text{PO}_4)]$ as shown in Figure 3.1 [A]. The iron oxide core inside the sphere can store up to 4,500 iron atoms which are stored as nanoparticles inside the ferritin [137, 138]. The apo-ferritin shell offers great possibilities for incorporating diverse functionalities. It prevents metallic core agglomeration and causes the particles to be water soluble. Ferritin is water soluble and an iron storage intracellular protein with a molecular weight of 450 kDa [136, 137].

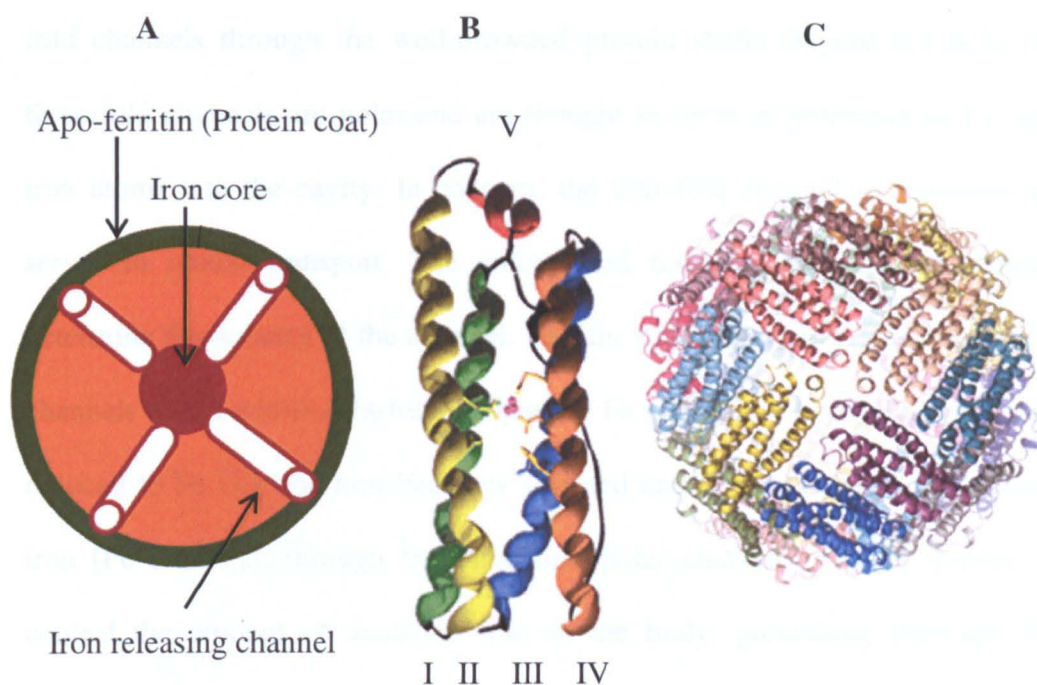


Figure 3.1 Structure of ferritin: [A] **Simplified structure of a ferritin molecule:** - A typical cross section structure of ferritin molecule with an iron core surrounded by an organic protein coat (apo-ferritin), Iron releasing channels are extending out from the core. [B] **Diagram of ferritin subunit:** - α – helices and ferroxidase centre side chains: helix I (green); helix II (light green); helix III (blue); helix IV (orange) and short helix V (red). Pink dots in the middle represent Iron atom positions [C] **Tertiary crystal structure:** - of *Pseudonitzschia multiseries* ferritin [138, 145, 279].

Ferritin consists of 24 polypeptide subunits, which self-assemble to form a hollow and roughly spherical protein shell with octahedral symmetry [137, 138]. Inner and outer shell diameters are ~ 8 nm and ~ 12 nm respectively. Each subunit is composed of four α -helical strands (I, II, III, IV) with a short fifth helix (small stretch V) toward top at the C – terminus (see Figure 3.1 [B]). Interactions amongst subunits result in the construction of three-fold and four-

fold channels through the well-crowded protein shells (Figure 3.1 [C]). The three-fold channels are polar and are thought to serve as pathways to transport iron atoms into the cavity. In contrast, the four-fold channel is non-polar and serves in proton transport. The amino acid residues that line the channels determine the polarity of the channel. Ferritin stores iron and releases it through channels in a controlled fashion. When the Fe (III) in the crystalline mineral is reduced to Fe (II), the iron becomes solvated and ferritin releases the solvated iron $[\text{Fe}(\text{H}_2\text{O})_6]$, through the three fold polar channels. Hence, ferritin can control the amount of available iron in the body, preventing disorders like anaemia and iron over load. The three dimensional structure of ferritin is hence crucial to its function within the body [137, 138]. Ferritin is not readily required for cellular activity. The storage of iron when present in excess prevents from its auto-toxicity. Otherwise when free leads to the formation of oxygen free radicals ($\text{OH}\cdot$) by catalysing the reaction between hydrogen peroxide and Fe (II). The production of such free radicals could strongly damage tissues and are found to be the main reason for the neurodegenerative diseases such as Alzheimer's. It has been reported that in Alzheimer's, the configuration of ferritin iron core alters significantly from that in normal state [137,139, 140]. The nature of the core which is predominantly ferrihydrite; Fe (III) oxide in physiological state, gets transformed partially into other ferric-ferrous oxides such as magnetite in a pathological state (Figure 3.2). It is the aggregation of ferritin that produces change in the normal oxidation state of iron within the ferritin core and which leads to abnormal functioning of the protein. Therefore, from the biomedical

point of view, it would be also useful to examine if there is any difference in the above stated aggregation behaviour of ferritin after lyophilization under near physiological conditions.

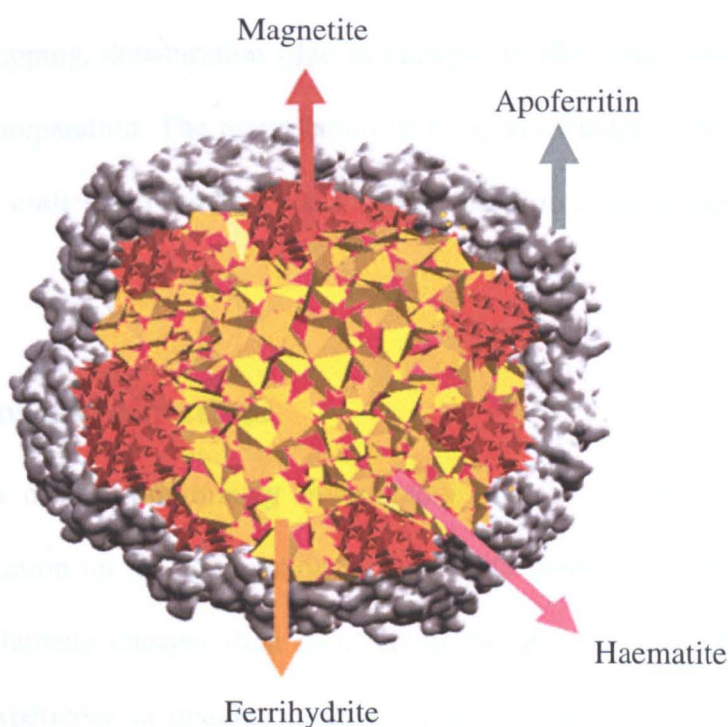


Figure 3.2 Schematic of state of iron core structure of Ferritin in Alzheimer's:- The presence of magnetite and hematite indicate dysfunction in the physiological state of ferritin because the different phases do not coexist within the same core in the normal configuration [140, 141].

3.1.2 AFM studies of ferritin

AFM studies have shown that it can form an ordered monolayer in a hexagonal manner on flat surfaces such as mica [136, 137, 138, 142]. The ordered monolayers of ferritin molecules had been imaged with high reproducibility.

AFM measurements have also confirmed that size of the individual ferritin nanoparticles ranges from 7 nm – 20 nm, which is close to its crystallographic size (8 – 12 nm) [137, 142, 143, 144]. The increase in size during AFM imaging has been attributed to several factors, such as distortion of sample by the tip during tapping, denaturation (due to changes in pH, ionic strength etc) during sample preparation. The assimilation of basic knowledge of model protein and its AFM studies was fundamental for me to perform imaging experiments.

3.2 Aims and objectives

The aim of this preliminary investigation was to characterise the effect of lyophilization on the aggregation ferritin. With plenty of literature available and being relatively cheaper than IgG, ferritin became an ideal choice to gain an initial experience in imaging proteins in air and liquid. Therefore, the plan of characterizing ferritin with SEM and AFM in particular in these investigations was to provide foundation for examining the behaviour of medically and therapeutically significant IgG antibody in the subsequent chapters that are reported in this thesis.

3.3 Materials

Horse spleen ferritin (50 mg/ml solution in 0.15 M NaCl), phosphate buffered saline (PBS) tablets, Mica (G250 - 1, 3"x 1"), Deionised water of 18 M Ω cm

resistivity was used for the preparation of ferritin samples, and as a medium for conducting measurements with AFM. Sterile 0.2 μm Ministart filters for filtration of deionized water. Silicon nitride AFM cantilevers (termed –‘DNP-S’ and ‘SNL’), from Nanoprobes (Veeco) CA. SEM (12.5 mm aluminum pin stubs. The batch numbers of all the indicated materials are listed in the Appendix 1.

3.4 Sample preparation methodology

3.4.1 Preparation of ferritin solution

10 μl of ferritin solution (50 mg/ml) was diluted in filtered deionised water to a concentration of 0.1 ng/ml. This was stored in five 1ml aliquots in a refrigerator to be used for the preparation of samples for conducting AFM imaging experiments.

3.4.2 Lyophilization of ferritin

A Modulyo Lyophilizer [S.W. Jennings and Company Ltd, Sciencetech House, East Bridgford, Nottingham, UK] with Edwards Pump (Crawley, West Sussex, UK) was employed for the lyophilization process. Two (0.5 ml and 1 ml) aliquots of ferritin solution with concentration of 0.1 ng/ml were separately poured into two clean glass vials with the help of pipette and then the vials covered with parafilm. The vials were first pre-freezed in liquid nitrogen

for a couple of minutes. The parafilm covering mouth of glass vials was made perforated with a clean needle so that all the moisture would be sucked during freeze drying (vacuum drying). The pre-freezed ferritin samples were then mounted in the freeze drier, and left to dry at a suction pressure of 0.1 mbar at a temperature of 25 °C for 8 hours. This resulted in the formation of powdered ferritin which was then reconstituted in deionised water prior to AFM imaging.

3.4.3 Preparation of ferritin samples for AFM analysis

Three types of samples with the same protein concentration were prepared, and are presented in Table 3.1

<u>Sample</u>	<u>Preparation scheme</u>
1.	20 µl of zero cycled ferritin, (concentration 0.1 ng/ml), was deposited onto a clean mica surface supported by a round steel disc, and allowed to dry for half an hour; this sample was imaged with AFM in air
2.	20 µl of zero cycled ferritin, (concentration 0.1 ng/ml), was deposited onto a clean mica surface supported by a round steel disc, and allowed to dry for half an hour; and then directly imaged with AFM in liquid (deionised water)
3.	20 µl of lyophilized ferritin (concentration 0.1 ng/ml), was deposited onto a clean mica surface supported by a round steel disc, and allowed to dry for half an hour; and then directly imaged with AFM in liquid (deionised water)

Table 3.1 Scheme of the preparation of ferritin samples for AFM analysis

3.4.4 Preparation of ferritin samples for SEM analysis

Powdered (1 μg) ferritin from manufacturer and 1 $\mu\text{g/ml}$ solution of ferritin was lyophilized to its powdered form for SEM analysis

3.5 Methods of analysis

3.5.1 Atomic force microscopy

Ferritin samples (1, 2 and 3) were imaged with Multimode AFM with Nanoscope V controller (Digital Instruments, Veeco, Santa Barbara, CA, USA) equipped with an E – scannerTM (approximately 14 μm X – Y scan range). Mechanical noise was minimised by placing the apparatus on an air table. “DNP” silicon nitride (Si_3N_4) cantilevers with a nominal spring constants of 0.1 N/m, were used at room temperature. Ferritin (mounted on double sided tape) was imaged in air as well as in deionised water. For imaging in liquid, deionised water was injected into a fluid cell around the sample in ferritin. This was done in order to avoid the aggregation of protein, which may be induced during of the sample prior to imaging. The images were obtained by scanning the sample surface in a tapping mode while keeping the oscillation amplitude constant. Tapping mode allows high resolution images of adsorbed molecules and avoids unfavourable tip sample interactions. The images were recorded at a scan rate of 2 kHz (512 x 512 pixels).

3.5.1.1 AFM data analysis

Scanning probe image processor (SPIP)TM V4 was employed for the processing (grain analysis) of AFM images as described in section 2.6.1.2. Threshold level of 3.1 nm was fitted to the plane. The values of length, area, width and volume of all individual nano-particles were respectively compiled together in an excel file in order to determine mean size. For each sample indicated, data collected from SPIP generated text files is from more than 50 images.

3.5.2 Scanning electron microscopy

The effect of lyophilization on the particle morphology and porosity was examined using a JEOL JSM-6060LV (JEOL (UK) Ltd., Welwyn Garden City, and UK) at various magnifications. The powdered samples of ferritin (lyophilized and non-lyophilized) were mounted onto carbon stub and gold coated at 30 mA for 2 min in an argon atmosphere prior to SEM analysis. SEM analysis was conducted under high vacuum at a voltage 10 – 12 kV. Scan sizes were variable (1 – 5 μm).

3.6 Results and discussion

3.6.1 Imaging of ferritin samples in air

AFM has been widely employed for studying the adsorption of ferritin onto various surfaces [136 – 147]. TM mode AFM analysis of both (zero and once

freeze dried) ferritin samples in air confirmed that deposits of ferritin of variable sizes were randomly distributed onto the hydrophilic surface of mica as shown in Figure 3.3. Generally, it was observed from more than 20 AFM scans that the arrangement of the deposits of the ferritin molecules was denser in the case of non-lyophilized ferritin sample than in lyophilized sample.

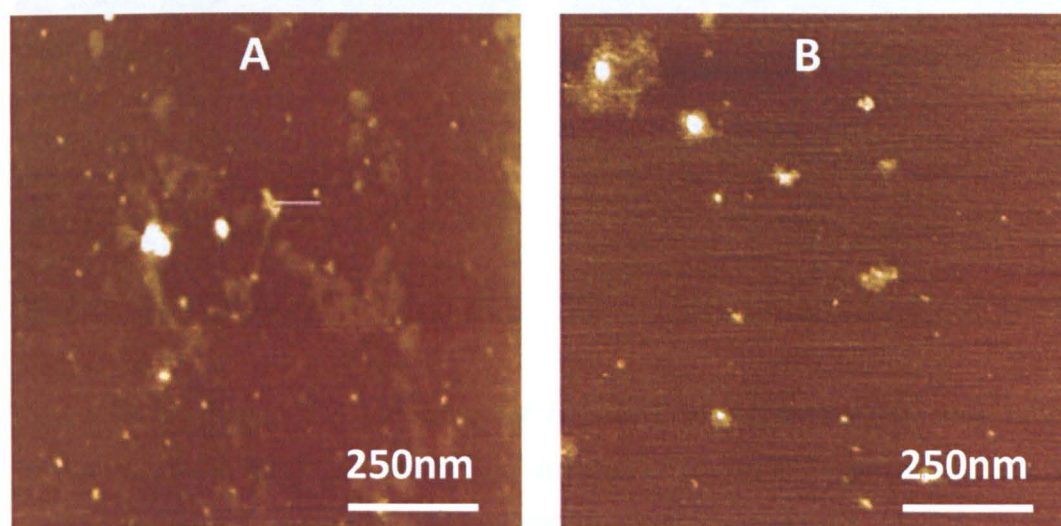


Figure 3.3 one micron TM AFM scans of: [A] Non-lyophilized and [B] Lyophilized ferritin samples in air. Z – scales were different: 9.8 nm for non – lyophilized and 6 nm for lyophilized ferritin sample. Concentration of both samples was 0.1 ng/ml.

3.6.2 Imaging of ferritin samples in liquid

TM AFM imaging of ferritin samples (both non-lyophilized and lyophilized) in liquid produced scans (Figure 3.4) containing fewer deposits of randomly ordered ferritin molecules. The hydrophilic nature of the substrate surface can result in unstable attachment of the molecules, which may lead to random and

less packed adsorption of ferritin onto the surface of substrate [136, 142 – 147].

Like in air, aggregates were detected both before and after lyophilization.

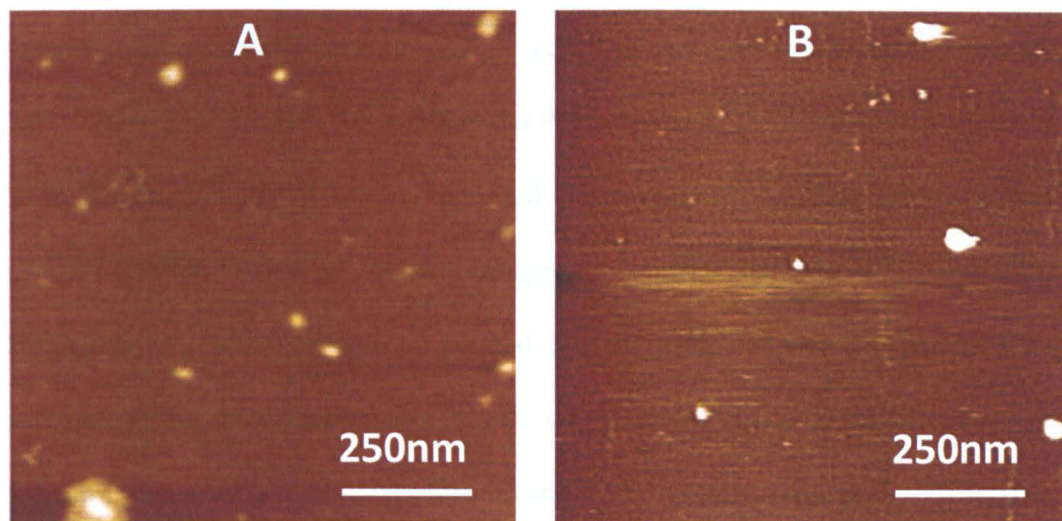


Figure 3.4 one micron TM AFM scans of: [A] Non – lyophilized and [B] Lyophilized ferritin samples in liquid. Z – scales were different: 7 nm for non – lyophilized and 5 nm for lyophilized ferritin sample. Concentration of both samples was 0.1 ng/ml.

3.6.3 Particle size analysis

The grain analysis of all individual TM AFM scans of ferritin (non-lyophilized and lyophilized) samples in air/liquid using SPIP software made it easy to scrutinize particle size. For each sample, numbers of particles measured per image were around ~ 50 – 100. Almost 2500 particles were examined after combining the data from 30 representative images. The particle size was demonstrated on the basis of area, length, width and volume of a particle. Histograms presented in Figures (3.5 and 3.6) represent normalized data

generated after SPIP testing. Normalisation of data was performed by dividing the number of particles of a particular size range by the total number particles in population. For an example, if we want to normalise a series data: 2, 5, 7, 9; then the proportion of each data set will be equal to that set divided by the sum of $2+5+7+9 = 23$, i.e; $2/23$, $5/23$, $7/23$, and $9/23$ represent the normalised values of 2, 5, 7, and 9 respectively in the total population of 23. The normalisation process enabled to find out the percentage proportion of features before and after lyophilization, which were then plotted in histograms. Figure 3.5 provides an account of the comparative analysis of size distribution of all the deposits of ferritin molecules in non – lyophilized and once lyophilized samples of ferritin when imaged in air. Figure 3.6 studies the same effect when imaging was performed in liquid.

Size analysis in air (Figure 3.5) and in liquid (Figure 3.6) suggested the formation of a range of aggregates which were binned into various groups as follows: $(20 - 30 \text{ nm}^2)$, $(30 - 200 \text{ nm}^2)$, $(200 - 300 \text{ nm}^2)$, $(500 - 1000 \text{ nm}^2)$ and those $(> 1000 \text{ nm}^2)$ on the basis of area (Figures 3.5 and 3.6 [A]); $(8 - 12 \text{ nm})$, $(13 - 25 \text{ nm})$, $(25 - 40 \text{ nm})$, $(40 - 100 \text{ nm})$ and those $(> 100 \text{ nm})$ on the basis of length (Figures 3.5 and 3.6 [B]); $(4 - 12 \text{ nm})$, $(13 - 25 \text{ nm})$, $(25 - 40 \text{ nm})$, $(40 - 100 \text{ nm})$ on the basis of width (Figures 3.5 and 3.6 [C]); and $(4.5 - 12 \text{ nm}^3)$, $(12 - 100 \text{ nm}^3)$, $(100 - 500 \text{ nm}^3)$, $(500 - 1000 \text{ nm}^3)$, $(1000 - 2000 \text{ nm}^3)$ and those $(> 2000 \text{ nm}^3)$ on the basis of their volume (Figures 3.5 and 3.6 [D]).

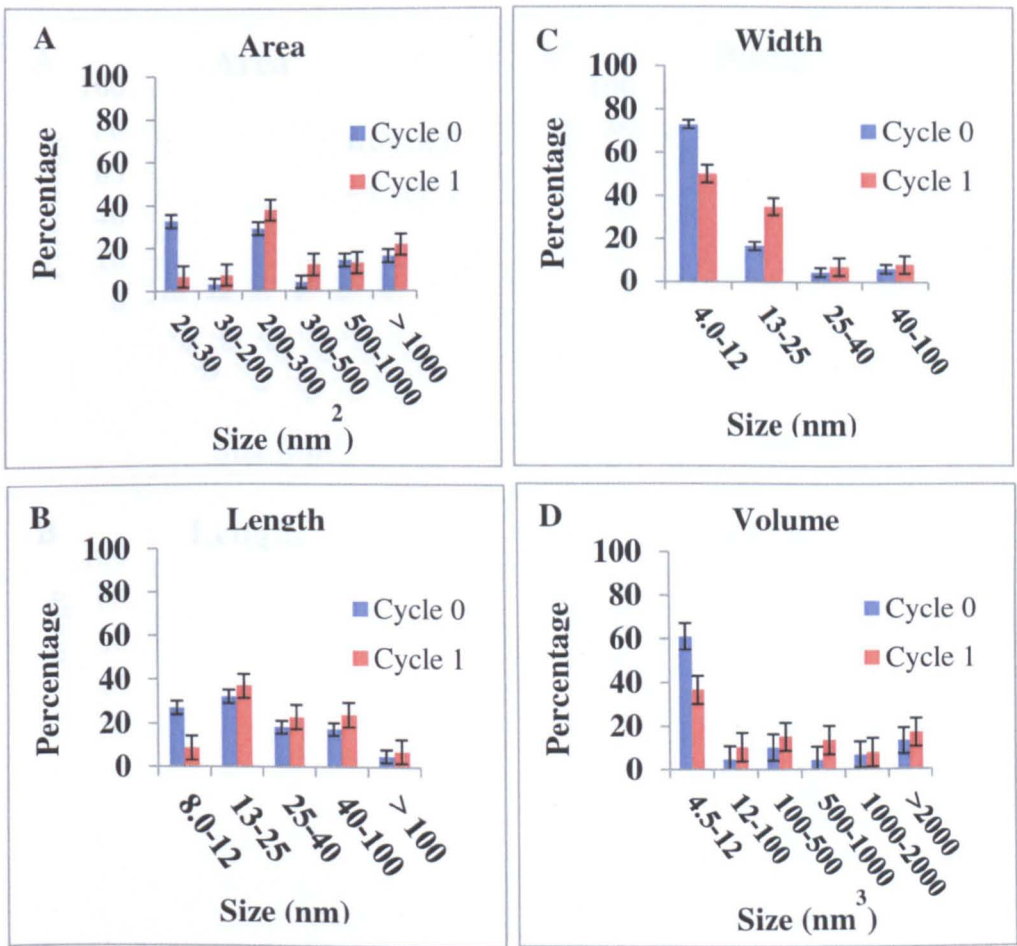


Figure 3.5 Effect of lyophilization on the relative particle size distribution in air: - [A], [B], [C], and [D] respectively show the comparison of the area, length, width and volume of ferritin nano-particles at a scan size of 1 μm before and after lyophilization in air. In each set, blue and red bars represent data obtained form 30 AFM scans (1 μm each) before and after lyophilization. Each error bar represents a standard deviation in the percentage of given set of particle size in several representative AFM scans which were recorded at different locations of the sample. Relatively larger standard deviations post lyophilization suggests non-homogeneous surface distribution of ferritin particles.

However, it is important to note that due to hydration in liquid, there occurs an increase in the size range of first group indicated in the area distribution (Figure 3.6 [A]) from (20 – 30 nm^2) to (40 – 62 nm^2). Both in air and liquid the presence

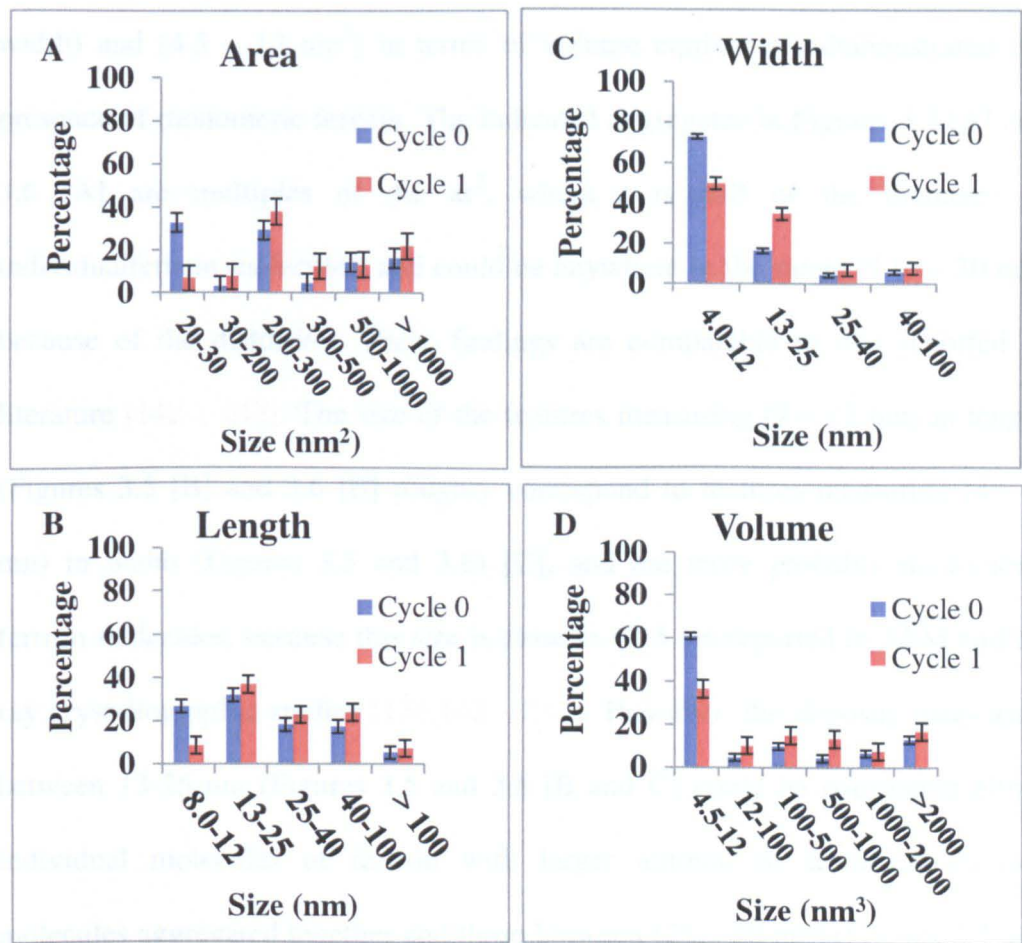


Figure 3.6 Effect of lyophilization on the relative particle size distribution in liquid:- [A], [B], [C], and [D] respectively show the comparison of the area, length, width and volume of ferritin deposits at a scan size of 1 μm before and after lyophilization in deionised water. In each set, blue and red bars represent data obtained from 30 AFM scans (1 μm each) before and after lyophilization. Standard deviation in the percentage of each set of particle size in many AFM images are highlighted by error bars.. The fairly lower standard deviations in liquid for sets of particle sizes after lyophilization advocate relatively homogeneous surface distribution of ferritin particles in liquid.

of smallest sized aggregates (20 – 30 nm^2) in air and (40 – 62 nm^2) in liquid on the basis of area), (8 – 12 nm on the basis of length), (4 – 12 nm on the basis of

width) and $(4.5 - 12 \text{ nm}^3)$ in terms of volume equivocally demonstrated the presence of monomeric ferritin. The indicated aggregates in Figures 3.5 [A] and 3.6 [A] are multiples of the πr^2 , where r is half of the diameter of individual ferritin molecules, and could be anywhere in the range of $(6 - 20 \text{ nm})$ because of the distortion. These findings are comparable to that reported in literature [142 – 147]. The size of the features measuring $(8 - 12 \text{ nm})$ in length (Figures 3.5 [B] and 3.6 [B] roughly correspond to features measuring $(4 - 8 \text{ nm})$ in width (Figures 3.5 and 3.6) [C], and are more probably monomeric ferritin molecules, because this size is close to 12.5 nm reported in AFM and X-ray crystallographic studies [136,142 – 147]. However, the deposits measuring between $13\text{-}25 \text{ nm}$ (Figures 3.5 and 3.6 [B and C] could be considered either individual molecules of ferritin with larger amount of distortion or two molecules aggregated together and those between $(25 - 40 \text{ nm})$ (Figures 3.5 and 3.6 [B and C] could be more than two aggregated together or distorted. The most likely cause of the distortion could be due to the flattening of the protein by the AFM tip while scanning the substrate surface [142 – 147].

The other probability could be due to the spreading of the protein on to the solid surface during immobilization step, consequently exceeding $x - y$ dimensions of the protein [136,142 – 147]. Moreover, most likely due to the stress induced during lyophilization. A stress results in the aggregation of protein by changing the conformation of the molecule has been reported [147, 148, 149]. In addition,

trapping of moisture between the AFM tip and the substrate surface might have induced inter and intra-molecular hydrogen bonding, resulting in conformational changes, which might have induced an aggregation [147, 148, 149].

There occurred a significant decrease in the proportion of monomeric (likely) ferritin deposits after lyophilization. T – test described in chapter 2 (section 2.7) was employed to check statistical significance of our results. In air: - on the basis of area (26 % in 20 – 30 nm²), on the basis of length (8.3 % in 8 – 12 nm), on the basis of width (23 % in 4 – 12 nm and on the basis of volume (25 % in 4.5 – 12 nm³) distributions presented in Figure 3.5. Similar trend was observed in liquid (Figure 3.6):- on the basis of area (36 % in 40 – 62 nm²), on the basis of length (18 % in 8 – 12 nm) and on the basis of width (22 % in 4 – 12 nm). In contrast in air, however, the proportion of (4.5 – 12 nm³) increased by 10 % after lyophilization (Figure 3.6 [D]). This could be explained due to the fact, that volume distribution takes height of the aggregate into account rather than radius, which could be reduced due to the flattening of the aggregate by intermittent tapping of AFM tip in air (enhanced). Both in air and in liquid, the proportion of aggregates other than the first indicated group presented in Figures 3.5 and 3.6 [A, B, C and D], showed a significant increase after lyophilization. T – test was used for significance check (see section 2.7 chapter 2). Table 3.2 (for air) and Table 3.3 (for liquid) summarize the percentage increase in the indicated group of aggregates after lyophilization on the basis of area, width, length and volume.

Table 3.2 Percentage increase in the proportion of ferritin aggregates after lyophilization in air	
AREA (nm ²)	
30 – 200	4.5 %
200 – 300	8.67 %
300 – 500	8.17 %
500 – 1000	1.15 %
➤ 10000	5.45 %
WIDTH (nm)	
13 – 25	18.5 %
25 – 40	2.5 %
40 – 100	2 %
LENGTH (nm) Table 3.2 (Continued)	
13 – 25	4.9 %
25 – 40	4.7 %
40 – 100	6.6 %
➤ 100	2.1 %
VOLUME (nm ³)	
12 – 100	5.6 %
100 – 500	5 %
500 – 1000	9.13 %
1000 – 2000	0.97 %
➤ 2000	3.77 %

Table 3.3 Percentage increase in the proportion of ferritin aggregates after lyophilization in liquid	
AREA (nm ²)	
60 – 200	– 2.6 %
200 – 300	20.7 %
300 – 500	4.65 %
500 – 1000	8.86 %
➤ 1000	3.59 %
WIDTH (nm)	
13 – 25	16 %
25 – 40	5.3 %
40 – 100	0.7 %
LENGTH (nm)	
13 – 25	15 %
25 – 40	10.2 %
40 – 100	3 %
➤ 100	3.5 %
VOLUME (nm ³)	
12 – 100	4 %
100 – 500	4.5 %
500 – 1000	3.9 %
1000 – 2000	0.9 %
➤ 2000	– 22.5 %

It is evident from the comparatively analysis of the data presented in Tables (3.2 and 3.3) that increase in the proportion of indicated groups of aggregates following lyophilization of ferritin in liquid is significantly more than in air. This is likely due to the extensive hydration of ferritin molecules in liquid [150]. The adsorption of a protein onto a solid surface is a complex process [151]. The changes in surface structure due to changes in the interior of the protein core and inter-molecular bonding could be the other reasons for larger size in liquid [151]. Moreover, the effect of protein shell on the shape of ferritin molecule can result in a high surface area to volume ratio [146, 152]. This has been also supported by the fact that the reconstitution of dry proteins in liquid can restructure core (i.e., disordered) relative to the particle's exterior [153]. Moreover, most likely due to the stress induced during lyophilization. A stress results in the aggregation of protein by changing the conformation of the molecule has been reported [148, 154]. In, addition, trapping of moisture between the AFM tip and the substrate surface might have induced inter and intra-molecular hydrogen bonding, resulting in conformational changes, which might have induced an aggregation [149, 155]. This is probably due to fairly low salt concentration in the trapped moisture, the attractive electrostatic interactions between an acidic amino acid residue of one protein and basic amino acid residue of other, both within the molecule and between adjacent protein molecules would dominate the repulsive interaction interaction forces.

The measurement of the size of the ferritin deposits in terms of area, length width and volume histograms are consistent with each other in terms of overall trend. However, the measurement in terms of width as shown in Figures 3.5 [C], 3.6 [C] shows 4-12 nm features, a size range which is more closer to the size of individual ferritin molecules reported in AFM and X – ray crystallographic studies [142, 144, 145, 147]. The width could be most likely considered diameter of the particle. Both in air and in liquid, the proportion of features measuring 4 – 12 nm (on the basis of width), demonstrated a similar, but significant decrease (23 %) after lyophilization Figures 3.5 [C] and 3.6 [C]). However, the proportion of features measuring 8-12 nm (on the basis of length) suggested more decrease in the liquid by about 10 % after lyophilization. This could be due to excessive hydration, which might have led to an increase in the size. The other likely cause of the more increase in y dimensions of the protein, probably caused by the distortion of molecule during TM AFM. This increase in size is also supported by literature [67, 142, 146, 156, 157]. The distributions in Figure 3.5 [A], [B], [C] and [D] complement each other and show similar trends displayed in Figure 3.6 [A], [B], [C] and [D] to explain the impact of lyophilization on the level of aggregation. However, from the Figure 3.6 [D], the increase in the proportion of $(5 - 12 \text{ nm}^3)$ aggregates after lyophilization and decrease in the proportion of aggregates $(> 2000 \text{ nm}^3)$ appears doesn't appear to correspond to area distributions in Figures 3.6 [A]. This could be due to the reason of the distortion of the single proteins caused during the tapping mode AFM [67, 142, and 157]. Moreover, the larger proportion of smaller aggregates

both in air is likely due to the drying forces in air which set individual molecules apart and even breaks protein in to subunits. In liquid, the other likely reason is repulsion caused by the hydrophilic surface of mica, because isoelectric point (pI) of ferritin native is 7.3 [65]. Therefore, it would be appropriate to omit volume distributions, and draft conclusions on the basis of data given in area, width, and length distributions. To be more precise, the width or length distributions serve the best purpose to explain the effect of lyophilization on aggregation, because the size of the ferritin deposits equivalent corresponding to the size of individual ferritin molecules (monomers) or dimers was best illustrated by width or length distributions.

Over all, the SPIP analysis of AFM scans indicated that lyophilization caused a reasonable decrease in the proportion of monomeric and smaller aggregates both in air and liquid. However, in liquid the reduction in their proportion was relatively more. The particles observed diameter of the ferritin molecules was found identical as well as larger than that reported in literature [136, 142 – 147, 158, 159]. This finding compliments to that reported in AFM studies of lysozyme, where the observed diameter was found about five times greater than that confirmed by X – ray crystallography [146]. Lyophilized samples in liquid, formed relatively lesser proportion of bigger aggregates ($> 2000 \text{ nm}^3$).

3.6.4 Morphological studies of ferritin powders

The morphology of the non-lyophilized and lyophilized ferritin deposits is illustrated by the SEM scans in Figure 3.7 Ferritin appears to be more porous prior to lyophilization. The larger agglomerates come into sight in both samples. Sharp crystalline surfaces also become visible and this effect predominates after lyophilization.

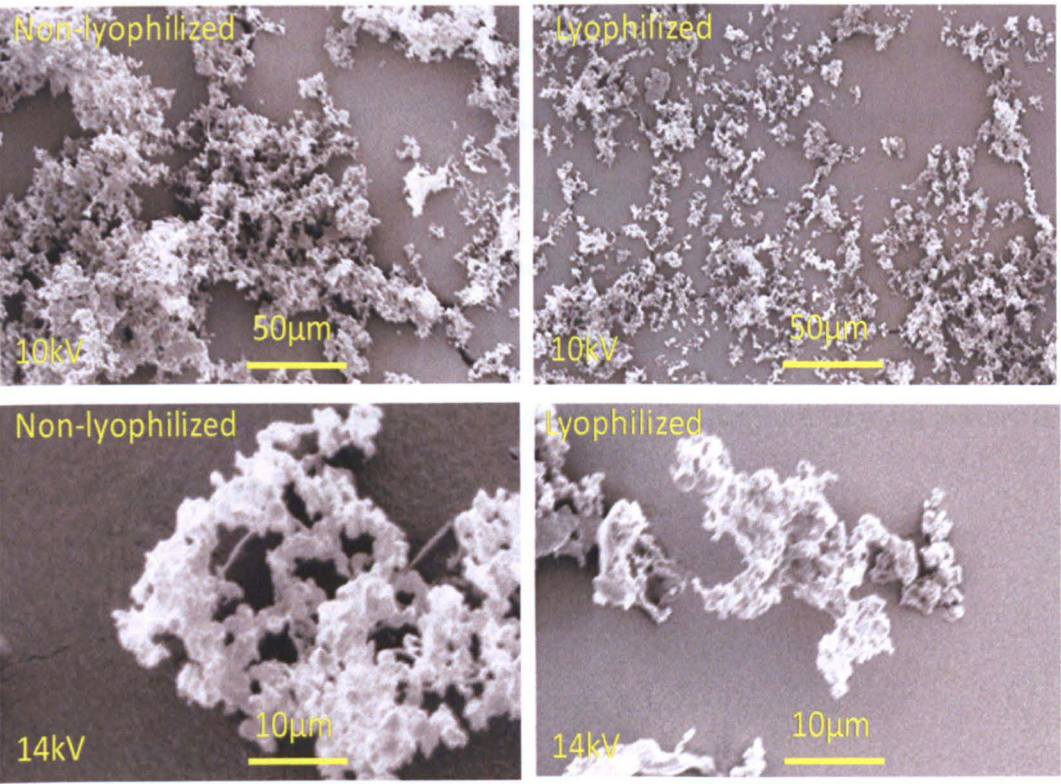


Figure 3.7 SEM images of non-lyophilized and one time lyophilied ferrtin. Top two (50 micron) obtained at low maginification; bottom two (10 micron) collected at high magnification.

3.7 Conclusions

AFM images of both non – lyophilized and lyophilized ferritin confirmed that deposits of ferritin molecules are randomly arranged onto the hydrophilic surface of mica. In air, arrangement of the deposits of ferritin molecules onto mica surface was denser than in liquid. Lyophilization was found to reduce the proportion of monomeric ferritin significantly more when the experiments were performed in liquid. Contrary effect was observed in case of aggregates (other than monomeric) whose proportion was found to increase after lyophilization significantly. Approximately 50 % of the population of ferritin species (monomeric) were detected in the non-lyophilized samples, both in air and in liquid, which suggests an inherent tendency of ferritin to resist aggregation. Lyophilization, however, significantly reduced the proportion of such species both in air and liquid. Furthermore, the propensity of ferritin to remain porous is adversely affected by lyophilization.

Chapter 4

Nanoscale characterisation of the effect of multiple cycles of lyophilization on the aggregation of polyclonal IgG antibody without excipients

4.1 Introduction

This chapter describes the effect of multiple cycles of lyophilization on the aggregation of a polyclonal IgG (antiglucose-6-phosphate dehydrogenase) antibody without excipients. Antibodies and antibody based protein therapeutics currently represent a rapidly growing class of medicines. However, due their inherent tendency to aggregate especially in solution, protein inactivity may result [160]. The dry formulations are favoured to aqueous preparations as the water (nucleophile in hydrolysis reactions and a plasticizer) proliferates the molecular freedom of movement of reactive chemical moieties/groups. Therefore, making aqueous formulations of proteins therapeutics are inherently less stable than their corresponding dried form. This increased stability of dry formulations has captured the attention toward the development of drying methods, which has lead to the lyophilization, a popular and considered most effective process of water

removal. However, despite drying with lyophilization, undesirable changes still occur in the protein formulation, which destabilize protein. Consequently, the unstable proteins aggregate and result in the loss of monomers. This has been reported for various proteins which reconstituted again after being exposed to lyophilization [46, 51, 160, 161, 162, 163]. The extent of change from native state produced in the protein as a consequence of lyophilization or reconstitution following lyophilization depends on the nature of a protein based formulation as discussed in the introductory chapter [1, 13, 55, 163, 164]. The occurrence of aggregates in protein formulations is detrimental, because aggregation reduces the therapeutic effectiveness due to the loss of the active (usually monomeric) form of the protein. Furthermore, administration of such proteins based drugs to a patient can lead to immunological repercussions and can be fatal [165]. In this way, aggregate formation is a hindrance in the development and commercialization of therapeutic proteins [165]. Over the last few decades quantification and identification (type) of aggregates present in protein formulations has become increasingly important for drug development companies and regulatory agencies. Sub-visible aggregates (0.1 – 1 μm) represent the most threatening species amongst all aggregates, primarily due to difficulty in their detection by majority of the standard techniques presently employed for such an analysis and are potentially due to their ability to mimic highly immunogenic viruses and bacteria with respect to size [90, 166]. The presence of sub-visible and visible (1 – 50 μm) aggregates in protein formulations has made the characterization of protein aggregates a complex

phenomenon and therefore, justified the demand for the use of several analytical techniques to detect and quantify different aggregates that comes under their detection capability [77, 78, 79, 80, 81, 82, 161, 167]. In this chapter, an attempt has been made to detect and quantify such aggregates in an IgG antibody sample and to probe the ability of an IgG antibody to withstand such changes that could trigger aggregation. IgG was lyophilized multiple times (0 – 7) and the aggregation state of the antibody was investigated in the liquid state and in dry form. Several parameters were examined in these studies such as the particle size, the effect of protein concentration, thermal and structural stability, and morphological characteristics.

4.2 Aims and objectives

The main aim of this study was to examine the behaviour of a polyclonal IgG antibody in response to the effect of multiple cycles of lyophilization (MCL). The exposure of IgG to MCL was to probe the indigenous capability of IgG to resist aggregation. Probing the potential of IgG (without any dissolved lyoprotectant) to counter aggregation is part of the development of a novel standard screening method that would enable us to scrutinize the impact of MCL when IgG will be lyophilized with lyoprotectants for comparative analysis.

4.3 Materials

Lyophilized powder of anti-glucose-6-phosphate dehydrogenase (G-6-PDH) antibody produced in rabbit (IgG fraction of antiserum in 0.01 M PBS), phosphate buffered saline (PBS) tablets, Mica (G250-1, 3"x 1"). Deionised water of 18 M Ω cm resistivity was used for the preparation of 0.01 M PBS (pH 7.4) solution, which was filtered (0.2 μ m) and subsequently used for the reconstitution of lyophilized IgG, and as a medium for conducting size measurements of IgG aggregates. Sterile 0.2 μ m Ministart filters for filtration of deionized water. Silicon nitride AFM cantilevers (termed –‘DNP-S’ and ‘SNL’), from Nanoprobes (Veeco) CA for imaging in liquid. Silicon nitride AFM cantilevers (RTESPA, Nanoprobes (BrukerNano, Coventry, UK) were utilized for tapping mode AFM imaging of powdered formulations of lyophilized IgG in air. 12.5 mm aluminium pin stubs and black carbon discs from Agar Scientific were employed for conducting SEM imaging experiments. The batch numbers of all the indicated materials are listed in the Appendix 1.

4.4 Sample preparation methodology

4.4.1 Preparation of IgG solution

This has been already described in section 2.1.1.2 of Chapter 2.

4.4.2 Lyophilization of IgG

Lyophilization of IgG has been discussed in section 2.1.4.2 of Chapter 2.

4.4.3 Formulations of IgG

Samples of IgG (1.2 mM) exposed to multiple (1, 2, 3, 4, 5, 6, and 7) cycles of lyophilization were formulated in the form of liquids and dry powders.

4.4.3.1 Samples from liquid IgG formulations

The mode of sample preparation of IgG from liquid formulations was decided by the parameter (attribute) to be analyzed and the working methodology of an investigating appliance. Initial studies involved the preparation of IgG samples for particle size analysis with AFM. The high sensitivity of the employed instruments and the natural tendency of IgG to aggregate at high concentration led us to work with a minimum possible concentration of IgG.

4.4.3.1.1 Liquid samples for AFM particle size analysis

Two types of samples with two different concentrations were prepared. The scheme of sample preparation for probing the effect of lyophilization on particle size is presented in Table 4.1

<u>Sample</u>	<u>Preparation scheme</u>
1.	20 µl of zero cycled IgG, (concentrations: 0.75 µg/ml and 1 µg/ml) was deposited onto a clean mica surface supported by a round steel disc, and then directly imaged with AFM in 0.01 M PBS
2.	20 µl of lyophilized (one cycled) IgG, (concentrations: 0.75 µg/ml and 1 µg/ml) was deposited onto a clean mica surface supported by a round steel disc, and then directly imaged with AFM in 0.01 M PBS

Table 4.1 Scheme of the preparation of IgG samples for AFM particle size analysis

4.4.3.1.2 Liquid samples for light scattering experiments

Samples of IgG (1.2 mM) exposed to 1, 2, 3, 4, 5, 6, and 7 cycles of lyophilization were reconstituted in filtered deionised water and subjected to light scattering for particle size analysis. IgG was also analysed at three different concentrations: 0.125 mg/ml, 0.25 mg/ml, and 0.5 mg/ml of IgG in order to investigate the impact of concentration.

4.4.3.1.3 Samples from powdered IgG formulations

Powdered formulations of IgG (1.2 mM) exposed to (1 – 7) cycles of lyophilization were directly utilized for required examination such as AFM, SEM, DSC, and ATR-FTIR.

4.5 Methods of analysis

4.5.1 Atomic force microscopy

AFM tapping mode imaging was utilized for particle size analysis as well as to study the different components in the powdered lyophilized formulations of IgG. Taping mode (TM) AFM imaging in liquid for particle size analysis was performed using a Multimode AFM with a Nanoscope V controller (Bruker Nano) equipped with an E-scanner (approximately 14 μm X–Y scan range). IgG samples (1 and 2) described in section 4.4.3.1 were imaged with “DNP” silicon nitride (Si_3N_4) cantilevers at room temperature. IgG samples were imaged in liquid (0.01 M PBS) only and PBS was directly injected into the cell, followed by the injection of protein (IgG) in order to evade the aggregation of protein. Imaging (topography and phase) of dry powders was performed with a D – 3000 AFM and a Multimode II AFM (Bruker Nano) equipped with an E-scanner. RTESPA” silicon nitride (Si_3N_4) cantilevers were used for imaging of powdered samples at room temperature. The amplitude of oscillation was set constant during the image acquisition. The images were acquired at a scan speed of 2 kHz (512 x 512 pixels).

4.5.1.1 Analysis of AFM images

Grain analysis of the acquired AFM images obtained for IgG in liquid was carried out by making use of Scanning probe image processor (SPIP)TM V4 in the same way as described in the section 2.6.1.2 of Chapter 2.

4.5.2 Light scattering

4.5.2.1 Dynamic light scattering

The characterization of particle size was also conducted using a Viskotek DLS (Malvern Instruments Ltd, Worcestershire, UK) equipped with a 630 nm laser. Approximately 80 μ l of sample solution was injected into the cuvette to determine particle size. Each sample was first equilibrated for 30 minutes at 25 °C prior to the first measurement. Data collection was performed by taking 40 acquisitions for each measurement.

4.5.2.2 Nanosight Nanoparticle tracking analysis

NanoSight LM10 (NanoSight Ltd., Amesbury Wiltshire, UK), enabled with laser output of 40 mW at 640 nm was also introduced for particle size characterization. A syringe was employed to introduce 10 – 30 μ l of protein solution into the sample chamber until the liquid sample reached the tip of the nozzle. For each sample, a minimum of three measurements were recorded. All measurements were recorded at room temperature. Nanosight software enabled the image analysis (tracking of individual particles and their size measurement). The displayed frequency size distribution histograms by software were output to a spread sheet for comparative analysis with DLS results.

4.5.3 Scanning electron microscopy

The effect of lyophilization on the particle morphology and porosity was examined using a JEOL JSM-6060LV (JEOL (UK) Ltd., Welwyn Garden City, and UK) at various magnifications. The powdered samples of IgG (lyophilized and non-lyophilized) were mounted onto carbon stub and gold coated at 30 mA for 2 min in an argon atmosphere prior to SEM analysis. SEM analysis was conducted under high vacuum at a voltage 10 – 14 kV. Scan sizes were variable (1 – 50 μm).

4.5.4 Thermal stability analysis

A Q-2000, differential scanning calorimeter (TA Instruments Ltd, Fleming Centre, Manor, Crawley, West Sussex, UK) with purged nitrogen gas was used. Dry powdered samples (2-5mg) were analyzed in crimped hermetically sealed aluminium pans. Samples were heated from 0 °C – 200 °C at a scan rate of 10 °C/min. The melting points of the IgG antibody lyophilized multiple times on its own were obtained as the midpoint of the corresponding transition by integrating the slope of the DSC curve.

4.5.5 Structural stability analysis in the solid state

A Nicolet FT-IR-spectrometer was employed to record spectra for the determination of changes in the secondary structure of lyophilized IgG. Sample powder (2 – 3 mg) was placed on a clean glass slide and then mounted on the

sample stage. The spectra for each sample were recorded from 4000 to 650 cm^{-1} in ATR mode at room temperature. Each measurement was an average of 200 scans, at a scan speed of 0.15 sec^{-1} and a resolution of 2 cm^{-1} . The optical bench was purged with dry nitrogen to avoid interference from water vapour infrared absorption. Each spectrum was background corrected for the glass slide. The amide I (1720 – 1600 cm^{-1}) and amide II (1575 – 1480 cm^{-1}) regions were used to analyze changes in the secondary structure of protein [129].

4.6 Results and Discussion

A first step in this study involved particle size characterization of the effect of multiple cycles of lyophilization on the aggregation profile of IgG. The particle size characterization was performed with AFM, DLS and NTA. In the next set of experiments, AFM and SEM imaging of lyophilised powders of IgG was performed. Subsequently, the lyophilised powdered samples of IgG were subjected to DSC and ATR – FTIR analysis for mapping any changes in the thermal and structural stability.

4.6.1 Imaging of IgG samples in liquid

The comprehensive characterisation of IgG on solid/liquid interfaces is of considerable significance for antibody based applications in medicine and industry [168, 169, 170, 171]. However, an inability to control and eliminate

non-specific adsorption of IgG to solid interfaces creates a hindrance for their applications in the above mentioned fields [169, 170, 171]. The other reason is repulsion caused by the hydrophilic surface of mica. It has been also reported that as one moves away from isoelectric point ($pI \sim 6$) of IgG, the decrease in adsorption rate becomes evident at pH 8.0 than that at pH 4.0. The reason is an increase in the electrostatic repulsion between the charged antibody molecules within the adsorbed layer [72, 74, and 172]. Therefore, these imaging experiments (IgG in liquid) were performed with care to avoid surface induced aggregation. Surface induced aggregation was confirmed for an IgG sample which was prepared, when 20 μl of IgG [(1 $\mu\text{g/ml}$), once lyophilized] was incubated onto the surface of substrate for one minute and dried prior to liquid imaging Figure 4.1.

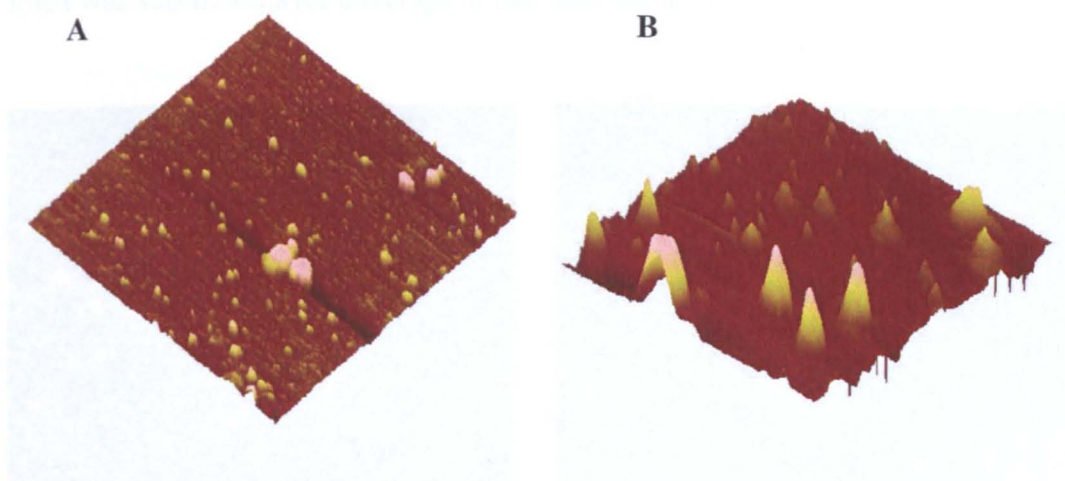


Figure 4.1 3D - TM AFM one micron scans of lyophilized (Cycle 1) sample of IgG (concentration 1 $\mu\text{g/ml}$): [A] Sample directly injected into the liquid cell; Z – scale 6.7 nm. [B] Sample incubated on mica in air for a minute; Z – scale is 16.7 nm. Slight exposure to an air pronounced the formation of much larger aggregates of IgG aggregation. The formation of monomeric and lower multi-meric forms were not detected.

On exposure to air, IgG significantly aggregates on a hydrophilic surface [173]. This is consistent with the observation here of large aggregates (Figure 4.1) formed due to a lateral reorganization of the adsorbed protein layer at the air - liquid interface [173, 174]. The pattern of the aggregate formation depends on the nature of protein and some properties of the adsorbed protein (such as the number of contact points with the surface) [173, 174]. In order to avoid the possible chances of surface or drying induced aggregation, IgG sample solution (in 0.01 M PBS) were directly injected into the liquid cell rather than allowing it to incubate onto the mica surface. Figure 4.2 represents tapping mode AFM images of zero-cycled and once lyophilized samples of IgG immobilized on hydrophilic mica surfaces in buffer (0.01 M PBS) after direct injection. In general, more than 40 images indicated that the arrangement of IgG molecules on mica was sub-monolayer coverage at this concentration.

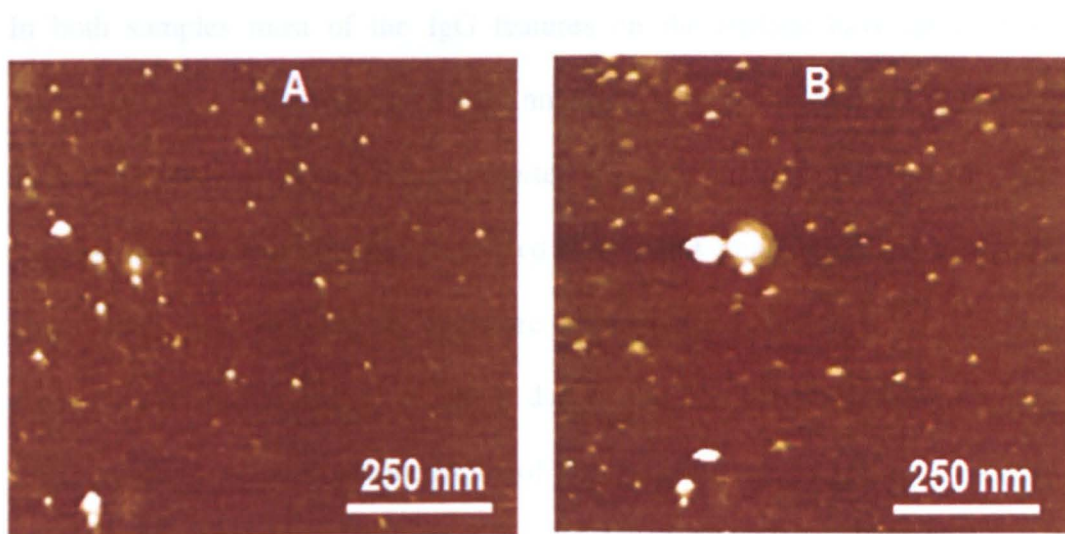


Figure 4.2 TM AFM scans of: [A] Non – lyophilized and [B] Lyophilized IgG molecules on the hydrophilic surface of mica. Z – scale for each scan is 6.7 nm. Concentration of both samples was 1 $\mu\text{g/ml}$.

AFM scans of zero and one time lyophilized IgG show a range of aggregates (up to 200 nm in diameter) and randomly immobilized IgG particles on the hydrophilic surface of mica is shown in Figure 4.2. The randomness and sparse distribution of IgG molecules is most likely due to the poor physisorption of IgG molecules to the hydrophilic mica surface as well as the concentration employed. Moreover, the adsorption of soft proteins (such as IgG) onto solid interfaces is governed by several factors, which makes it difficult for AFM to characterise the protein properly due to relatively uncontrolled and random orientation of the protein on a surface. For example when mica is used, electrostatic forces can develop and can play a significant role in protein adsorption [136, 171, 175].

In both samples most of the IgG features on the surface have an average dimensions (x – in the range of 8 – 12 nm and y – in the range of 18 – 25 nm). This is the very close to the size reported for monomeric IgG [67, 176]. The dimensions of monomeric IgG measured from AFM imaging data, are slightly larger than that reported in literature from other techniques [177]. This disagreement in size is mostly likely due to the compression of the tip that enhances the – x and – y dimensions of the imaged proteins and tip – sample convolution effects. The proportion of multimeric (60 nm) and larger aggregates with diameters (> 100 nm) increased after lyophilization.

4.6.2 AFM particle size analysis

The grain analysis of all the individual TM AFM scans of IgG nanoparticles (non-lyophilized and lyophilized) was performed as described in section 3.5.3. Both samples of IgG were scanned with AFM at a concentration of 1 $\mu\text{g/ml}$. The AFM scans obtained were subjected to SPIP analysis as described in section 3.1 and 3.2 to produce distributions as shown in Figure 4.3. Size analysis suggested the formation of a range of aggregates which were binned into several groups as follows: on the basis of area (Figure 4.3 [A], length (Figure 4.3 [B]: width (Figure 4.3 [C] and volume (Figure 4.3 [D]. The four parameters: - area, length, width and volume were set to ensure proper size characterization of IgG which is quite intricate because IgG molecules are highly susceptible to multiple surface attachment orientations due to their two dimensional and extremely flexible natures [178]. The aggregation profile of the detected grains produced in this way made it convenient to quantify the effect of lyophilization [Figure 4.3]. AFM was able to detect particle species of IgG with variable dimensions. The IgG features measuring (200 – 300 nm^2), (18 – 25 nm), (8 – 12 nm) and (12 – 100 nm^3) respectively on the basis of area, length, width and volume constituted the largest proportion of features both before and after cycle one of lyophilization. The indicated aggregates in Figure 4.3 [A] and [D] are multiples of the πr_1^2 , and $4/3\pi r_2^3$ respectively where r_1 is half of the diameter of IgG fragments, and could be anywhere in the range of (1 – 12 nm) because of the distortion and r_2 is the height of fragments from the surface and could be (1.3 – 1.5 nm). These findings are comparable to that reported in literature for IgG [9].

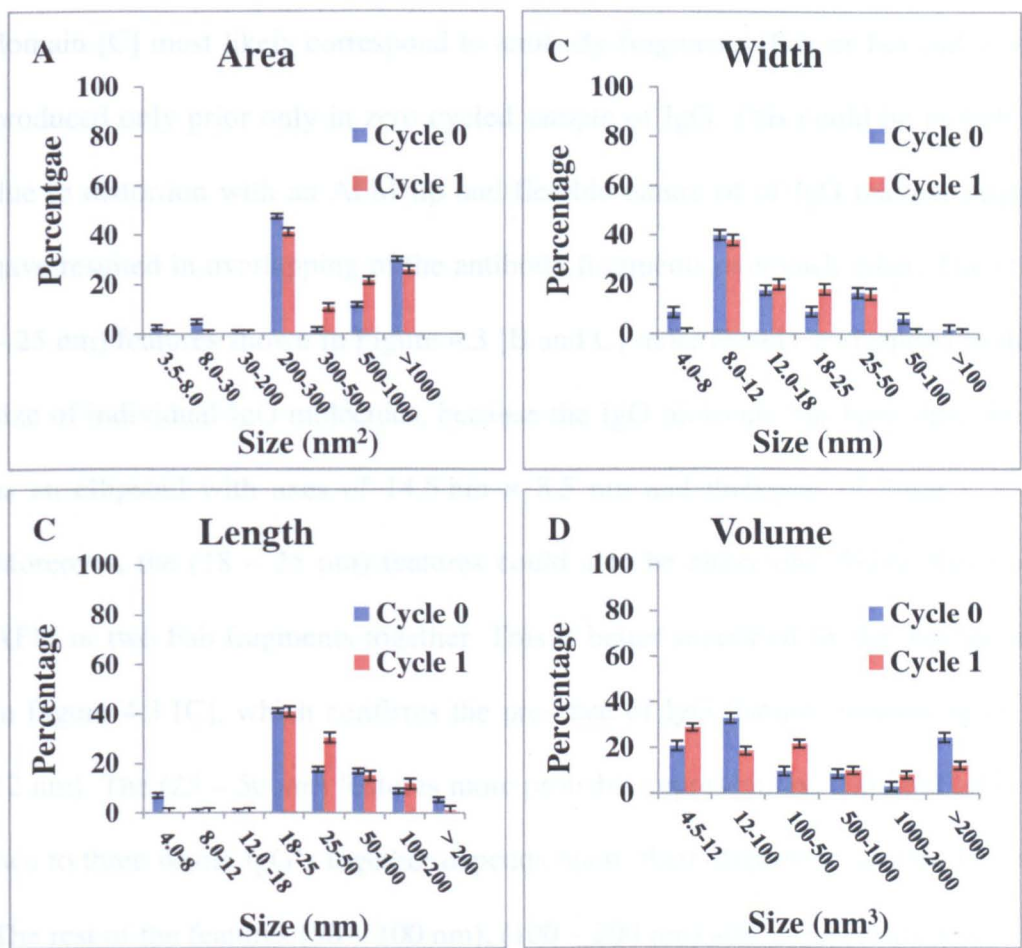


Figure 4.3 Relative particle size distribution of: IgG (cycle 1) in liquid at a concentration of 1 µg/ml. Blue and red bars respectively represent data before and after lyophilization. [A], [B], [C], and [D] respectively show the comparison of the AFM measurements of the areas, lengths, widths and volumes of IgG deposits in zero – cycled and once lyophilized IgG in 0.01 M PBS. In each set, blue and red bars represent data obtained from 40 AFM scans (1 µm each) before and after lyophilization, (a) and (b) respectively show standard deviations and an average size of adsorbed IgG features in each distribution before and after lyophilization.

In Figure 4.3 [C], the size of the features measuring (8 – 12 nm) in width, most probably represent whole IgG molecules with two roughly equivalent domains (~ 8 – 12 nm) across, whereas (13 – 18 nm) likely correspond to single IgG

domain [C] most likely correspond to antibody fragments (Fab or Fc) and were produced only prior only in zero cycled sample of IgG. This could be probably due to distortion with an AFM tip and flexible nature of of IgG thatthat might have resulted in overlapping of the antibody fragments over each other. The (18 – 25 nm) features shown in Figure 4.3 [B and C] more closely correspond to the size of individual IgG molecules, because the IgG molecule has been described as an ellipsoid with axes of 14.5 nm \times 8.5 nm and thickness of 4 nm [179]. Moreover, the (18 – 25 nm) features could also be either one whole distorted AFM or two Fab fragments together. This is better supported by the data given in Figure 4.3 [C], which confirms the presence of IgG features measuring (8 – 12 nm). The (25 – 50 nm) features more probably represent one distorted IgG or two to three whole IgG's together depends upon their alignment on the surface. The rest of the features (50 – 100 nm), (100 – 200 nm) and above) correspond to aggregates formed from larger numbers of IgG molecules. This is possibly due to the concentration of the applied IgG and the exposure time at the interface is long enough to decrease the probability of detecting individual IgGs. Moreover, it is also well-known that under such experimental conditions there is a high propensity for IgG to aggregate [180]. Another possible reason could be sweeping of the adsorbed or weakly bound proteins during imaging even in tapping mode, the AFM tip can move the proteins from their position and can promote aggregation [179]. All these findings are supported by other measurements reported in AFM and X-ray crystallographic studies [178, 179].

Table 4.2 gives a simplified and summarized account of percentage change produced in each indicated group of aggregates in Figure 4.3. Analysis of data in Table 4.2 is an indicative of a significant change produced in the aggregation profile as a consequence of lyophilization. This was confirmed by observing 6 % and 4.2 % decrease respectively in the proportion of the first (200 – 300 nm²) and second (> 1000 nm²) largest family of aggregates. However, the proportion of aggregates measuring (300 – 1000 nm²) increased 18 % after lyophilization, though their contribution towards total aggregate proportion was significantly much lesser than the first and second largest families. This has not been reported in earlier studies [180, 181].

Similarly length and width (Figure 4.3 [B and C]) distributions demonstrated almost an identical aggregation profile. The percentage decrease (7 – 9 %) produced in distorted Fab or Fc (4 – 8 nm) in lyophilized IgG was almost identically addressed by length and width (Figure 4.3 [B and C]) distributions. However, following lyophilization, an increase in the proportion of 8 – 12 nm) species [two Fabs together or whole IgG] by 2.5 % and (12 – 18 nm) particles [longest axis IgGs and one whole IgG or couple of IgG's together] by 9 % was better picked up by width distribution [for results see Table 4.2]. The increase (12.7 %) in propensity of IgG molecules to form lower multimeric forms (25 – 50 nm) for lyophilized IgG was confirmed by length distribution. The increase in the proportion of higher multimeric (50 – 100 nm) aggregates by almost 6.33

% (Figure 4.3 [B]) was also confirmed by width distribution (Figure 4.3 [C]) by 2 %. Despite some similarities or dissimilarities, the aggregation profile displayed in Figure 4.3 [A and D] confirmed the indicated group ($200 - 300 \text{ nm}^2$), ($12 - 100 \text{ nm}^3$) that represented the largest proportion of aggregates observed a significant decrease after lyophilization. In contrast, the increase in the proportion of other large indicated groups of aggregates was less significant (Figure 4.3 [A and D]). Moreover, the aggregation profile displayed in Figure 4.3 [B and C] confirmed significant decrease in the proportion of fragments, and increase in the proportion of likely monomeric and distorted IgGs (one, two or three together). This is likely caused either by drying stress or due to the distortion produced by intermittent tapping of the tip with the surface of the substrate or both [178]. The data are consistent with that reported in literature for IgG aggregate formation at the ice/freeze-concentrate interface [179]. The statistical significance was determined by utilizing t-test discussed in the section 4.7 of chapter 2.

Table 4.2 Percentage increase in the proportion of IgG aggregates after lyophilization (– means decrease)

AREA (nm²)	
3.5 – 8	2.8 %
8.0 – 30	5 %
30 – 200	0.6 %
200 – 300 (First largest family ~ 50%)	6.1 %
300 – 500	– 9 %
500 – 1000	– 9.8 %
➤ 1000 (2 nd largest family ~ 30%)	4.15 %
WIDTH (nm)	
4 – 8 (Distorted Fab or Fc)	8.7 %
8 – 12 (Two Fabs or whole IgGs)	2 %
12 – 18 (Longest axis IgGs)	– 2.5 %
18 – 25 (One deformed or two whole IgGs)	– 9 %
25 – 50 (Two deformed or three whole IgGs)	0.5 %
50 – 100 (Aggregates)	6.3 %
➤ 100	1.8 %
LENGTH (nm)	
4 – 8 (Deformed Fab or Fc)	7.09 %
8 – 12 (Two Fabs or whole IgGs)	0.61 %

12 – 18 (Longest axis IgGs)	0.61 %
18 – 25 (One deformed or two whole IgGs)	0.29 %
25 – 50 (Two deformed or three whole IgGs	– 12.7 %
50 – 100 (Large aggregates)	1.9 %
100 – 200 (Larger aggregates)	– 2.9 %
➤ 200 (Largest aggregates)	4.5 %
VOLUME (nm³)	
4.5 – 12	– 8.1 %
12 – 100	14.5 %
100 – 500	– 11.8 %
500 – 1000	– 1.5 %
1000 – 2000	– 5.1 %
➤ 2000	12.1 %

4.6.3 Size measurements with DLS

The multiple times lyophilized samples of IgG were separately subjected to DLS analysis for the determination of particle size (hydrodynamic diameter). Multiple measurements were recorded for each sample Figure 4.4 displays a typical DLS intensity distribution of lyophilized IgG sample (cycle 0 at 0.25 mg/ml) that was recorded at the mid-point of an experiment. The intensity distribution for each sample was obtained after compiling more than 40 readings together at 25 °C and measurements were performed in 0.01 M PBS. The DLS intensity distribution (Figure 4.4) is an indicative of a heterogeneous protein solution containing particles of different diameters. An increase in hydrodynamic radius or broadening of the distribution peak suggests an increase in protein aggregate size [70, 79, 89, 88, 182, 183]. The DLS data shown in Figure 4.4 [A] confirms the population of aggregates in the size range of (4 – 1700 nm). The peak measuring 5.7 nm corresponds roughly to the size of monomeric IgG, whereas 34.4 nm particles pertain to the existence of smaller aggregates formed during lyophilization. The highest intensity peak (146 nm) in the distribution represents the aggregates that scatter most of the incident light. The aggregates measuring above 1000 nm (for instance 1671 nm in Fig 4.4) were of lesser significance, due to their relatively lower and almost negligible proportion in the sample solution (details given in Chapter 2). DLS measurements of multiple times (0 – 7) lyophilized formulations of IgG were recorded at three different molar concentrations (0.125 mg/ml, 0.25 mg/ml and 0.5 mg/ml). It is important to mention that the DLS data is inter-convertible as shown in Figure 4.4 [B], which

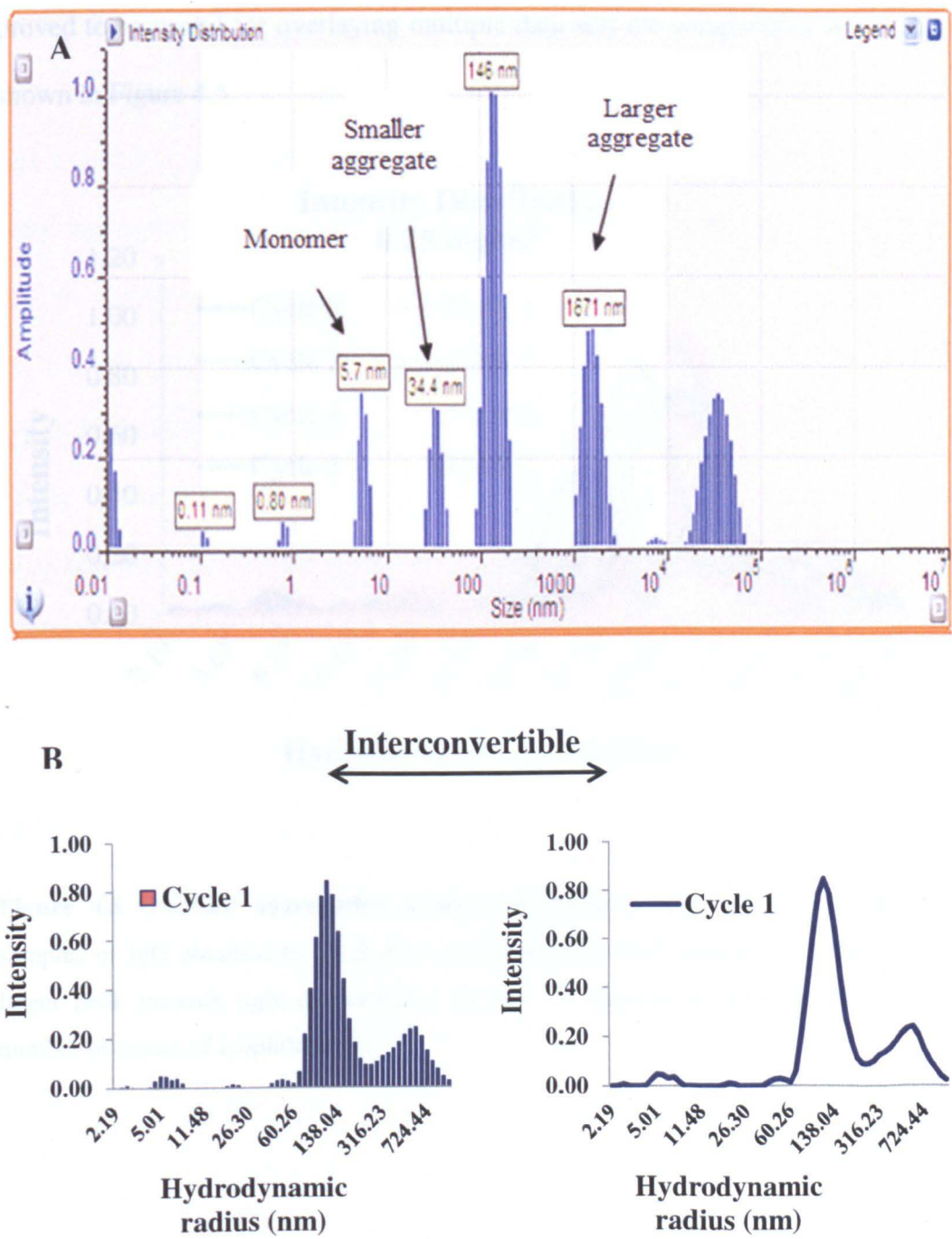


Figure 4.4 Typical DLS intensity distribution of IgG (0.25 mg/ml). [A] Cycle 0 and [B] Cycle 1: representing an example of data inter-conversion from bar to line chart. The intensity distribution was obtained after compiling more than 40 readings together at 25 °C and measurements were performed in 0.01 M PBS.

proved to be useful for overlaying multiple data sets for comparative analysis as shown in Figure 4.5.

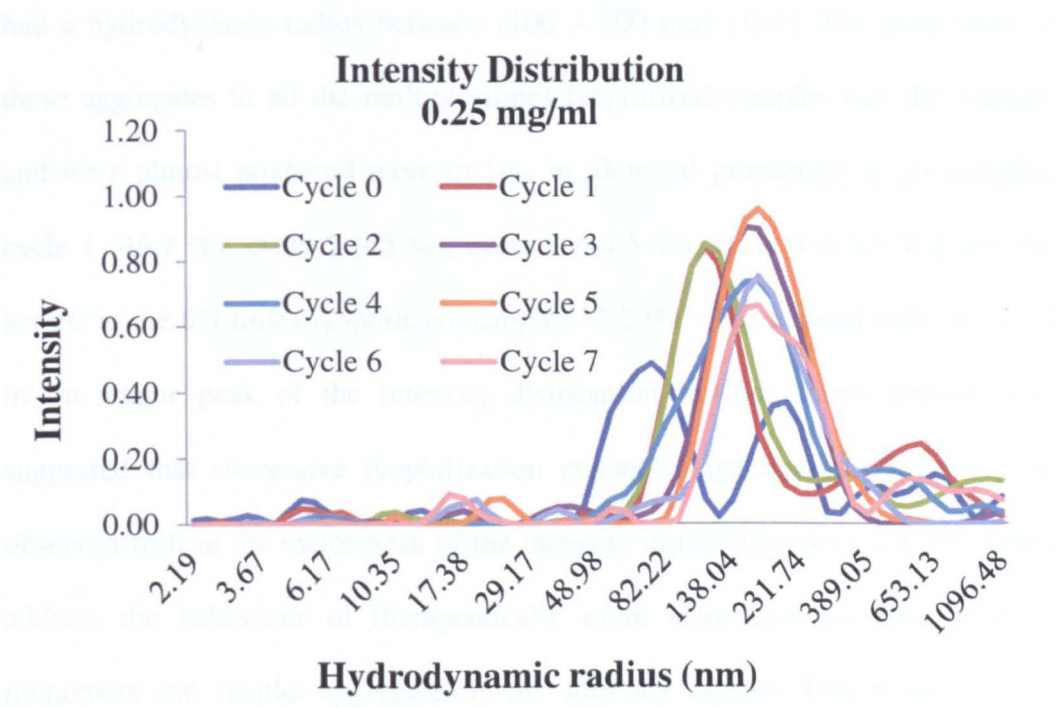


Figure 4.5 Overlaid aggregation profiles of: multiple times (0 – 7) lyophilized samples of IgG obtained by DLS at room temperature (0.25 mg/ml). The shift of the larger peak towards right demonstrates increase in aggregation with increase in the number of cycles of lyophilization.

The DLS aggregation profiles of all the multiple times (0 – 7) lyophilized formulations of IgG without excipients (Figure 4.5) demonstrated similar propensity toward aggregation and confirmed the formation of aggregates of variable sizes which were categorised into seven classes: (4 – 7 nm), (10 – 15

nm), (15 – 20 nm), (20 – 30 nm), (30 – 100 nm), (100 – 500 nm) and (500 – 1000 nm). Most of the aggregates detected by DLS in all lyophilized samples had a hydrodynamic radius between (100 – 200 nm) [184]. The proportion of these aggregates in all the multiple times lyophilized samples was the highest, and were almost produced more or less in identical proportion in all samples: cycle 1 (46.7 %), cycle 2 (45 %), cycle 3 (44.5 %), cycle 4 (43.4 %)] and the lowest in the 6/7 times lyophilized sample (32.2 %). The general shift observed in the major peak of the intensity distribution towards larger particle size suggested that successive lyophilization enhanced aggregation. However, the observed shift in the major peak of the intensity distribution does not effectively address the behaviour of therapeutically more significant particles such as monomers and smaller aggregates in the antibody sample. This is because the DLS intensity distribution is biased to larger particles (see section 2.8.1). Therefore, the number distributions presented in Figure 4.6 were taken into consideration. It was observed that there was a consistent decrease in the proportion of monomeric and other smaller sized IgG aggregates with multiple cycles of lyophilization which is consistent with AFM results. This indicated that the exposure to repeated cycles of lyophilization increases aggregation propensity and is likely due to the repeated stress caused to the protein during multiple cycles of lyophilization. Such stresses include for an example, an increase in the effective solute concentration that occurs during initial freezing of the protein solution and can lead to changes in the pH, and possible increases in the inter protein interaction during the sublimation phase in vacuum [54, 57, 185, 186].

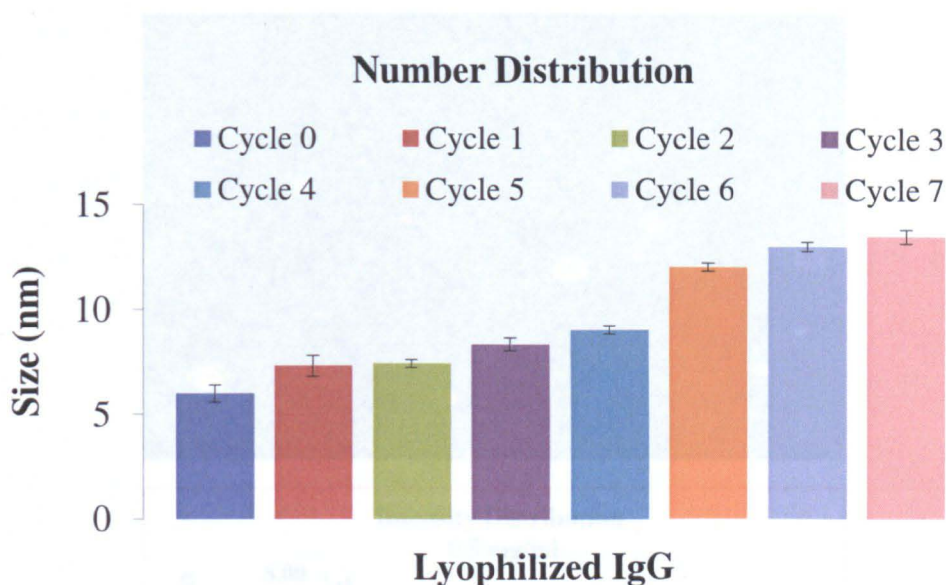


Figure 4.6 Influence of successive cycles of lyophilization: on the aggregation of IgG (1 mg/ml) without added excipients. The figure shows size analysis of the particles after successive lyophilization. The error bars represent average of the standard deviations of three sets of measurements recorded for each sample. Blue bar towards the extreme left corresponds to the size of IgG in non-lyophilized sample, whereas pink towards the extreme right shows the size of IgG features in seven times lyophilized sample of IgG.

4.6.4 Nanosight measurements of IgG

The multiple times (0 – 7) lyophilized formulations of IgG studied in DLS experiments were monitored in situ in the NanoSight sample chamber at room temperature. NTA enabled real time visualization of the multiple times (0 – 7) lyophilized formulations of IgG at two different molar concentrations (0.25 mg/ml and 0.5 mg/ml). A minimum of three measurements were recorded for each sample by NTA. All measurements were recorded for 50

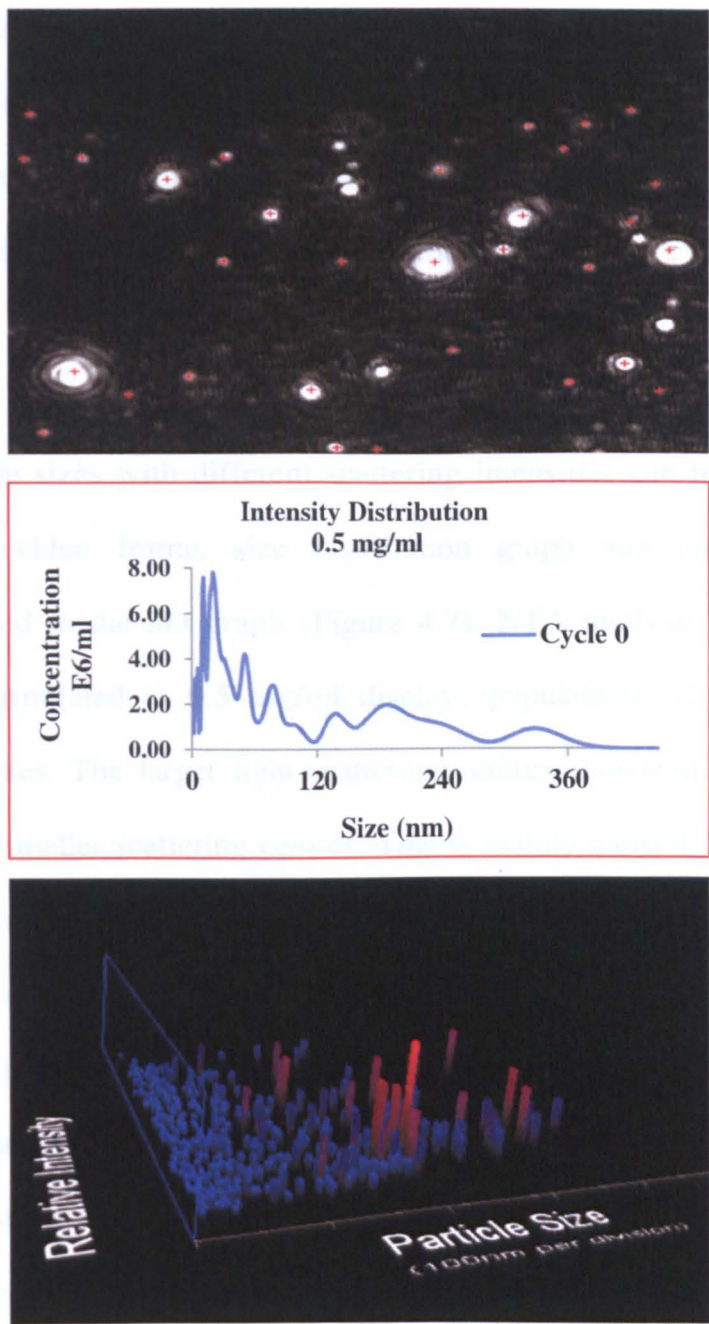


Figure 4.7 Size distribution of (10 – 400 nm) population acquired: from NTA measurements of non-lyophilized sample of IgG that was formulated in PBS at a molar concentration of 0.5 mg/ml (middle section) with the corresponding NTA video frame (top section) and 3D graph (intensity versus size (concentration); bottom section). Measurement was recorded at room temperature for zero-cycled sample of IgG at molar concentration of 0.5 mg/ml.

seconds with manual shutter and gain adjustments. The different particle species were captured by employing single shutter and gain mode operation. Figure 4.7 demonstrates a representative example of one such measurement recorded in non-lyophilized IgG (cycle 0) at room temperature.

The particle sizes with different scattering intensities can be observed in the NTA video frame, size distribution graph and can be visibly distinguished in the 3D graph (Figure 4.7). NTA analysis of IgG (zero cycled) formulated at 0.5 mg/ml displays populations of aggregates of different sizes. The larger light scattering centres shown in top panel are more than smaller scattering centres. This is mainly caused by a masking effect of the larger aggregates over the smaller ones. The smaller species that are close to monomers and lower multimeric forms travel so quickly that they frequently travel out of focus in the detection area before they can be tracked to be studied for the ultimate result. The disparity in scattering intensities displayed by the 3D graph confirms the attendance of different populations of similar sizes. The multiple peaks stationed at different positions between (10 – 400 nm) shown by the 2D graph are complemented by several distinct size populations (blue, purple and red) displayed in 3D graph. Therefore, the third dimension (scattering intensity) in NTA sheds light on the resolution of aggregate populations and also provides information about the nature of the aggregates. NTA

allowed precise sizing and a clear distinction of the several size populations for the entire multiple times lyophilized samples of IgG. With optimized settings, all populations of aggregates in the size range of (12 – 1000 nm) in the multiple times (0 – 7) lyophilized samples were detected and sized by NTA and are displayed in Figure 4.8. The NTA studied formulations of IgG showed aggregation profiles with multiple peaks which is indicative of the presence of multiple populations of aggregates of same size. The effect of successive lyophilization that was demonstrated by NTA aggregation profiles was compared with those produced by DLS. It was observed, that the Nanosight produced aggregation profiles (Figure 4.8) for all multiple times lyophilized formulations of IgG were similar to those of DLS with a main peak under and at around 200 nm. Both techniques show broadening of the distribution peak and therefore, suggested an increase in the hydrodynamic radii of the aggregates with multiple cycles of lyophilization.

The aggregate distribution obtained by NTA shows polydispersity and an overall increase in the concentration of the larger aggregates with successive lyophilization. However, the dissimilarity in the lower detection limits of the two techniques was obvious when characterizing the monomers. DLS was able to detect the monomeric IgG (~ 4 – 8 nm) due to the better lower detection limit compared to Nano sight. The monomeric IgG only detected by DLS with an average size in the range (~ 4 – 8 nm) is consistent

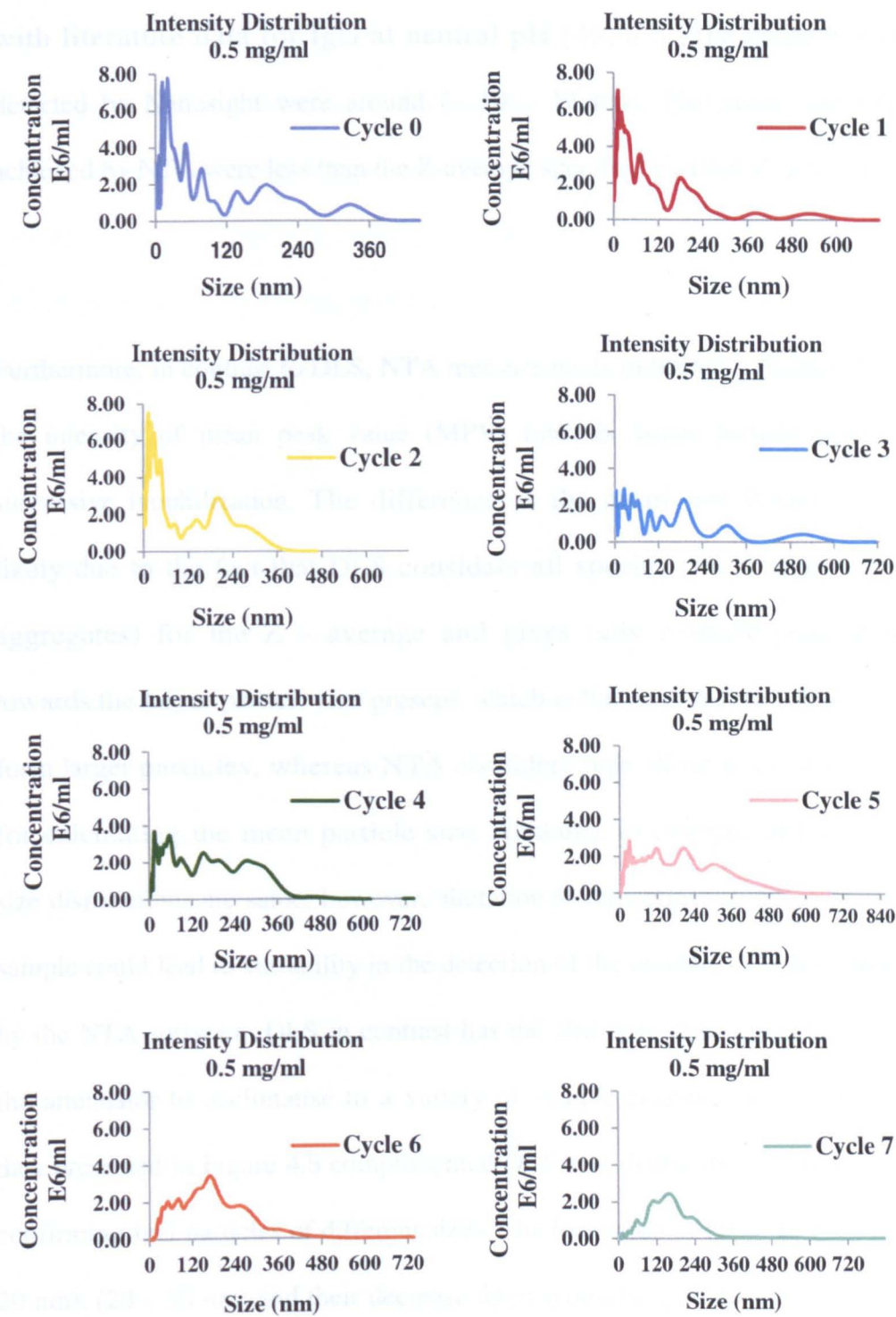


Figure 4.8 Aggregation profiles of: multiple times (0 – 7) lyophilized and reconstituted IgG formulations (0.25 mg/ml) obtained by NTA at room temperature.

with literature data for IgG at neutral pH [49, 63]. The smallest species detected by Nanosight were around ($\sim 10 - 12$ nm). The mean size values achieved by NTA were less than the Z-average specified by DLS (Figure 4).

Furthermore, in contrast to DLS, NTA measurements indicated a smaller shift in the intensity of mean peak value (MPV) towards larger particle size with successive lyophilization. The difference in the mean size values is most likely due to the fact that DLS considers all species (monomers and all aggregates) for the Z – average and gives only a single peak shifted towards the larger particle size present, which is linked to its predisposition to form larger particles, whereas NTA considers only those tracked particles for calculating the mean particle size. Although, in essence, all the particle size distributions are same; however, alteration in the optimization for the same sample could lead to variability in the detection of the number of larger particles by the NTA software. DLS in contrast has the ability to automatically regulate the attenuator to acclimatise to a variety of sample concentrations. The NTA data presented in Figure 4.8 complimented DLS size distribution (Figure 4.5) in confirming IgG particles of different sizes. The formation of (10 – 15 nm), (15 – 20 nm), (20 – 30 nm) and their decrease upon lyophilization displayed a pattern identical to that shown by DLS. The class of IgG aggregates in the size range of 100 – 200 nm represented the largest proportion of aggregates was shown by NTA. This finding and consistent increase in the formation of (500 – 1000 nm)

aggregates with multiple cycles of lyophilization was complimentary to DLS. However, in contrast to DLS, NTA showed relatively more decrease in the proportion all smaller aggregates (10 – 15 nm, 15 – 20 nm, 20 – 30 nm and 30 – 100 nm) towards the final cycles of lyophilization (6, 7). This is probably caused due to the IgG fragmentation (an effect of repeated stress) which Nanosight is not able to detect.

In case of DLS results for all the multiple times lyophilized formulations, the standard deviations of the aggregate sizes measuring between (100 – 1000 nm) are larger than the ones displayed for NTA results. This is associated to the fact that the DLS software has to fit the data of an autocorrelation curve of a sample that has populations with size differences smaller than the peak resolution limit of DLS. As a consequence, the single peak as calculated by the DLS software is susceptible to alterations in shape and position between successive measurements.

Over, all it appeared, that with multiple cycles of lyophilization, the proportion of larger aggregates (200 – 1000 nm) increased, whereas that of monomeric and lower multimeric forms decreased due to the obvious reasons of repeated stress that causes protein denaturation. The different analytical methods applied show

results in their respective measurement range [67, 114, 177, 178, 184, 187]. However, AFM size analysis detected much smaller and more diverse particle sizes than both DLS and NTA. AFM, DLS and NTA data can be compared and are complementary. Both AFM and DLS distribution of the IgG-samples confirmed that not only the particles within reported size are present, but a wide range of aggregates exist in IgG samples.

4.6.5 Morphology of the lyophilized powders of IgG

4.6.5.1 Characterization with AFM imaging

One and seven times lyophilized powders of IgG, prepared and reconstituted in filtered deionized water (without excipients) were studied by AFM (Figure 4.10). The topography data for the one and seven cycle sample (Figure 4.10 [A, C]) shows surfaces decorated with globular features. The phase data is particularly clear as the variation of tip interaction with the surface of the protein particles and provides the basis for the observed contrast [188]. The phase images of both one and seven times lyophilized samples show surfaces proposed to be primarily consisting of solidified salts with some smaller and larger globular features (Figure 4.10 [B, D]). The globular features associated with amorphous appearing regions represent aggregates of IgG. However, it is hard to say that the solidified salts are crystalline, because their edges are not straight. It is evident in the phase data that the smallest globular features are consistent in size with monomeric IgG (~11 – 15 nm) and were present in both samples

(Figure 4.10 [B, D]). This is close to the size of IgG molecules reported in AFM studies [67, 176, 187, 189]. However, the mean size of the agglomerates increased significantly with successive cycles of lyophilization [(cycle 1:- minimum ~ 31 nm, maximum ~ 245 nm, (Figure 4.10 [B]): (cycle 7:- minimum ~ 45 nm and maximum ~ 358 nm, Figure 4.10 [D]). This increase in the propensity of IgG to form larger aggregates with repeated lyophilization lie in agreement with DLS findings reported in this chapter as well as earlier reported [47, 49, 51, 61, 70].

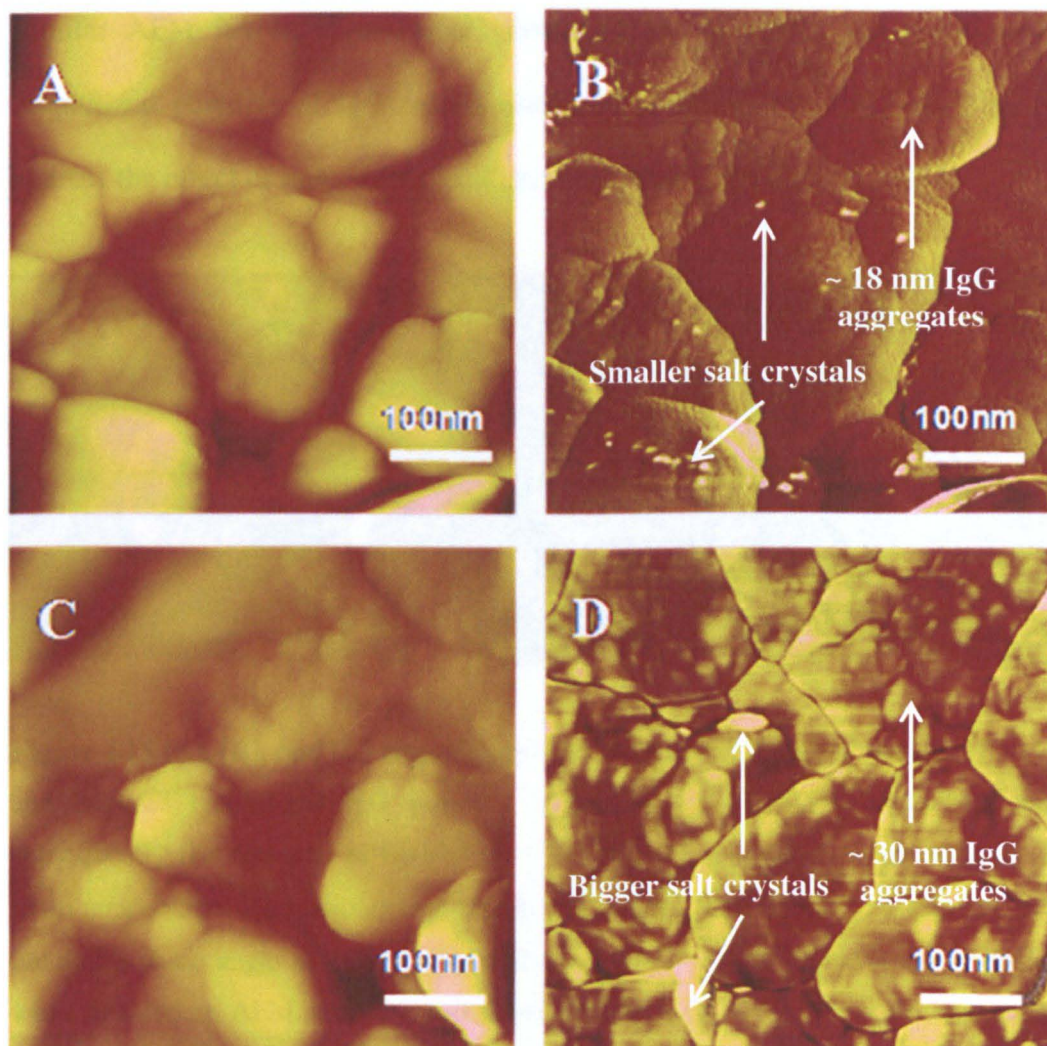


Figure 4.10 [A - C] and [B - D] respectively represent the AFM topography and phase images of: 1, and 7 times lyophilized IgG powders which were formulated and subsequently reconstituted in filtered deionized water. All the samples were imaged at room temperature under ambient conditions. Each scan is one micron. All images have height (Z – scale) of 100 nm and a phase angle of 160°. Concentration of the lyophilized protein was 2 mg/ml when in solution. AFM phase images [C and D] reveal both crystalline (white particulates) and amorphous (brown areas) like features. Globular features consistent with IgG in terms of size can also be observed. The size of the smaller globular features is similar to the size of monomeric IgG (~ 16 – 20 nm) reported in previous AFM studies (*Ultramicroscopy* 105:103 – 110). The larger globular features likely represent aggregates of IgG.

Similar AFM investigations were conducted for one, two and three times lyophilized powders of IgG reconstituted in PBS (0.01M PBS) in order to address the effect of induction of salt into the system upon reconstitution.

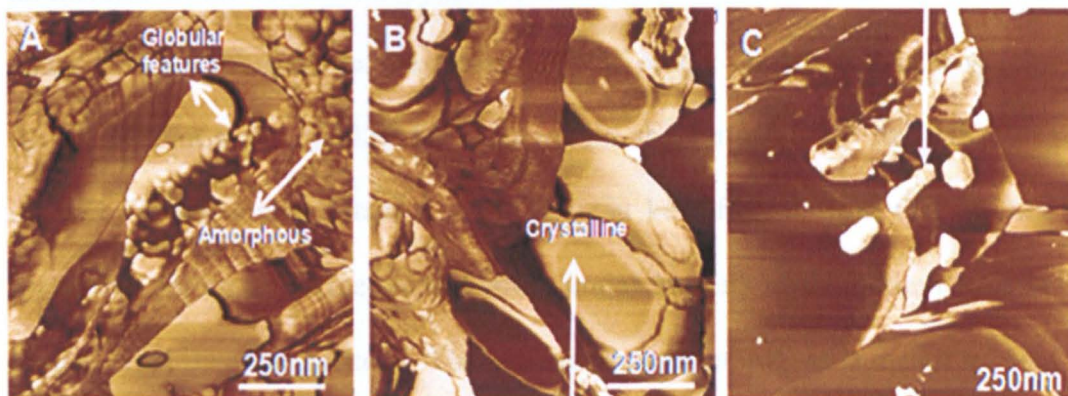


Figure 4.11 [A], [B], and [C] respectively represent the AFM phase images of: 1, 2, and 3 times lyophilized IgG powders without added excipients formulated and subsequently reconstituted in filtered 0.01 M PBS. All the samples were imaged at room temperature. Each scan is one micron. All images have height (Z – scale) of 100 nm and a phase angle of 160°. Concentration of the lyophilized protein was 2 mg/ml when in solution. AFM images reveal larger crystalline like structures when compared to amorphous features. Globular, protein like features mostly appear to be associated with amorphous regions. The dimensions of the globular features and the propensity of the formation of crystalline like structures increased due to repeated lyophilization.

AFM phase images of one, two, and three times lyophilized samples demonstrated the presence of significant crystalline areas, likely corresponding to the excess salt in the system (Figure 4.11). Furthermore, an increase in size of the revealed globular features (attributable to the IgG) observed was consistent with the increase in the proportion of crystalline material, which results in the

expulsion of solutes during lyophilization [190]. Hence compliments the DLS findings in that repeated stress caused to the antibody formulation during successive lyophilization enhances aggregation. This could be probably due to an increase in the content of crystalline material (salts) as revealed by AFM. In addition, the difference in the freezing point of the constituent salts species (0.138 M NaCl and 0.0027 M KCl) within the buffer (0.01 M PBS), and disparity in the ionized state of each salt can be different from that of their respective nonionized (free) states during initial freezing of the protein solution in the lyophilization process. The drastic change in pH as a result of this difference in freezing point could denature the protein being lyophilized and has been previously reported [13, 55, 191], and most probably enhances buffer salt crystallization in case of studied IgG formulations.

4.6.5.1 Characterization with SEM imaging

The morphology of the multiple times lyophilized deposits is illustrated by the SEM scans in Figure 4.12. IgG appears to be more porous and flaky prior to lyophilization. The more porous nature of the formulation is an indicator of potentially better solubility of the powder. The formation of aggregates clearly occurs after cycle 1 and the proportion of these aggregated areas became more apparent with increasing number of cycles of lyophilization. The growth of crystalline like areas becomes visible after cycle 1 and increases remarkably with successive lyophilization. Therefore, SEM micrographs demonstrated an

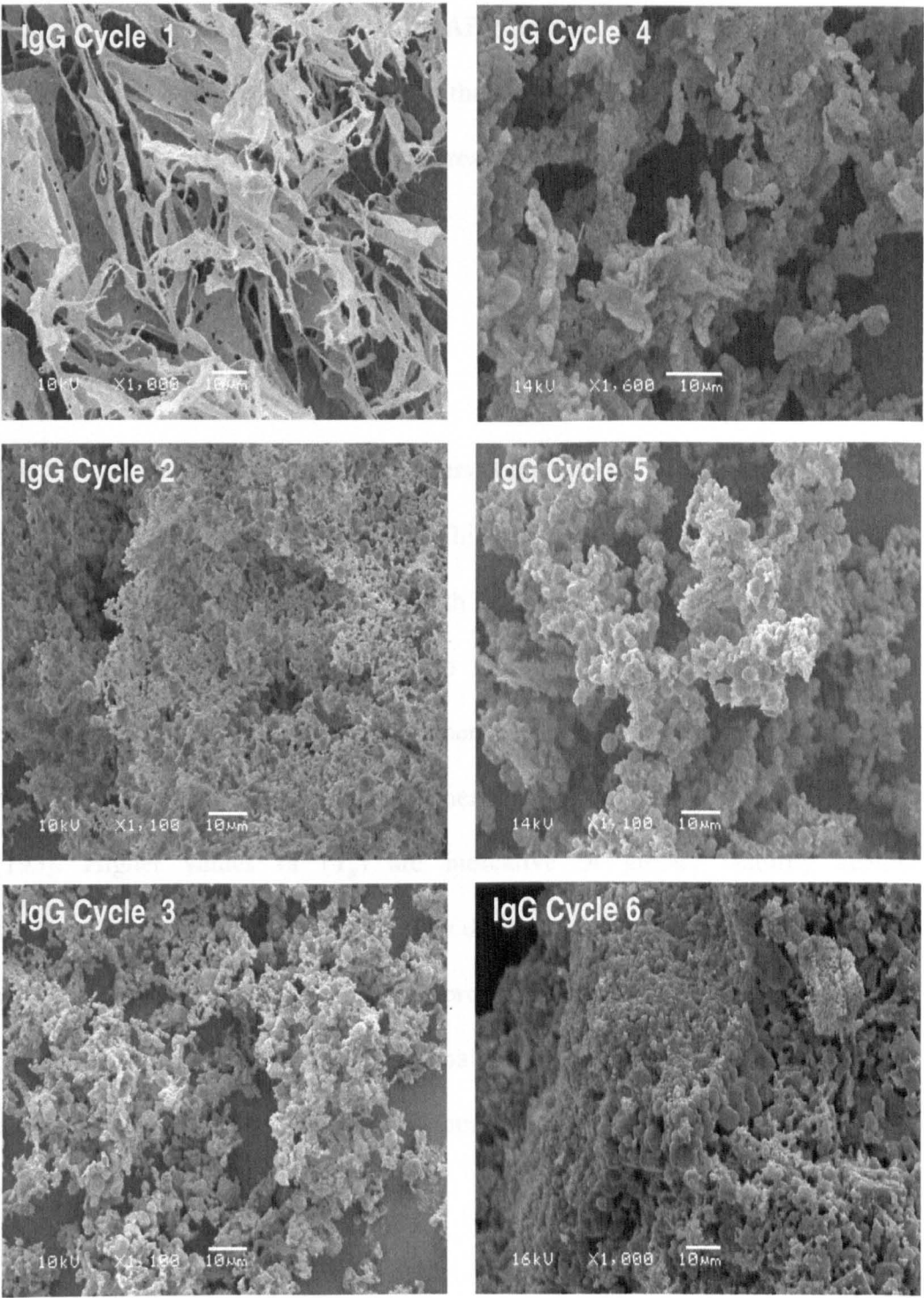


Figure 4.12 Labelled SEM observation of multiple times lyophilized (1 – 7) IgG: 10 micron scans obtained at magnification between 10 kV – 16 kV.

an effect similar to that displayed by AFM images, and strongly supports the DLS findings with this impression that the dissolved salts likely get crystallized during/after lyophilization due to the reasons discussed earlier in the section 4.6.5.1 (AFM results).

4.6.6 Thermal Stability

The thermal stability of organic polymers could also be influenced by the stress produced during lyophilization [192]. This is because stress initiated changes in the protein structure reduces the strength of bonds between the polymer chains, hence, making it more susceptible to melting or/thermal denaturation. For example: in the case of organic polymers (such as IgG antibody), secondary, non-covalent bonds between the polymer chains become weak above the (T_g) [193]. Higher values of (T_g) are indicative of greater stability against denaturation. This effect was studied by differential scanning calorimetry which gives a measure of the melting of the protein [194]. Therefore, in these follow up studies, the melting points were analyzed for IgG lyophilised on its own without added sugars in order to find out any relevance with results shown by AFM, DLS, NTA and SEM.

4.6.6.1 Effect of lyophilization on the melting of IgG

DSC thermogram of each time lyophilized IgG sample showed two transitions:

DSC thermogram of each time lyophilized IgG sample showed two transitions: one distinct and prominent transition peak proposed to be the denaturation temperature around $\sim 58.2\text{ }^{\circ}\text{C}$ with an enthalpy, $\Delta H = 0.26\text{ J/g}$ (Figure. 4.13). This is similar to that reported for IgG molecules ($\sim 61\text{ }^{\circ}\text{C}$) [195, 196].

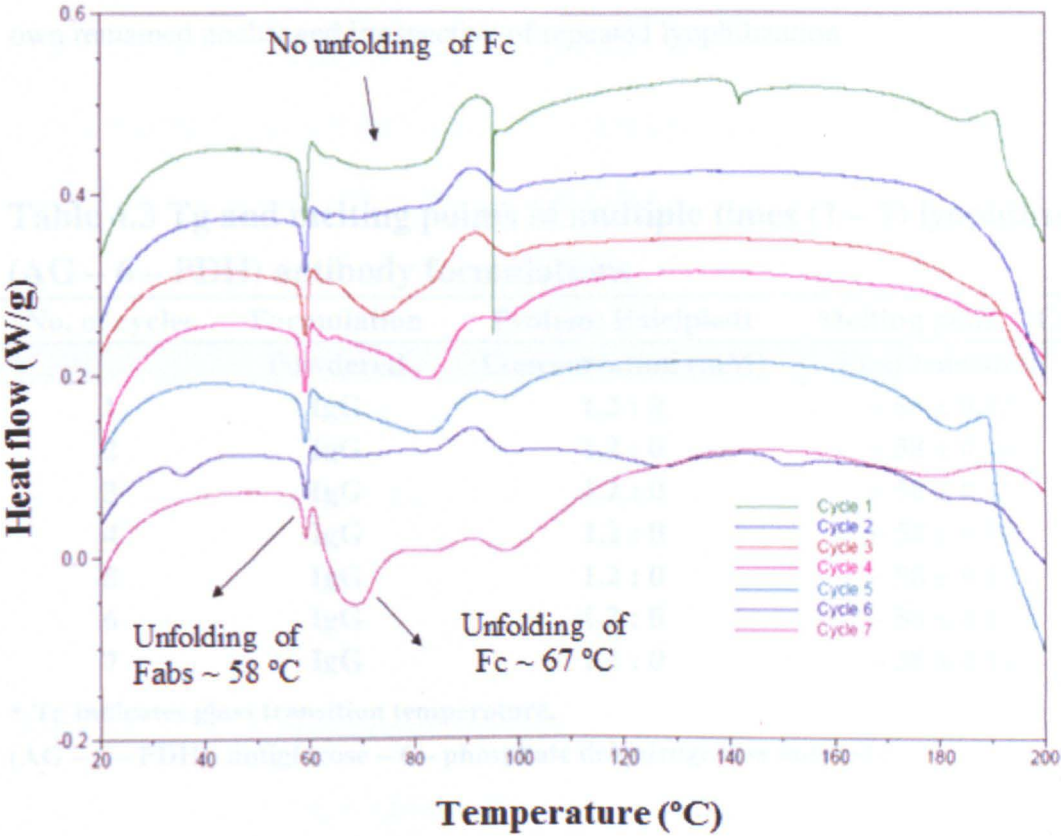


Figure 4.13 Overlaid standard DSC heating profiles of: one to seven times lyophilized IgG powders. The powdered formulations were heated up to $200\text{ }^{\circ}\text{C}$ at the rate of $10\text{ }^{\circ}\text{C}$ per minute. IgG denatures around $58\text{ }^{\circ}\text{C}$ irrespective of the number of cycles of lyophilization.

The first transition is believed to correspond to the unfolding of the two F(ab) domains in multi-domain IgG protein [195, 197]. The second transition

corresponds to the melting of the Fc domain and was found to decrease with repeated lyophilization (from ~ 85 °C to below ~ 67 °C) (Figure 4.13). Tg could not be measured in antibody samples prepared without excipients [198]. DSC thermograms of one to seven times lyophilized powders of IgG demonstrate that the melting temperature (T_m) or the temperature of denaturation of IgG lyophilized on its own remained unchanged irrespective of repeated lyophilization.

Table 4.3 Tg and melting points of multiple times (1 – 7) lyophilized (AG – 6 – PDH) antibody formulations

No. of cycles	Formulation	Protein: Excipient	Melting point (°C)
	Powdered	Concentration (mM)	First transition
1	IgG	1.2 : 0	~ 58 ± 0.15
2	IgG	1.2 : 0	~ 58 ± 0.16
3	IgG	1.2 : 0	~ 58 ± 0.15
4	IgG	1.2 : 0	~ 58 ± 0.12
5	IgG	1.2 : 0	~ 58 ± 0.13
6	IgG	1.2 : 0	~ 58 ± 0.18
7	IgG	1.2 : 0	~ 58 ± 0.11

* Tg indicates glass transition temperature,
(AG – 6 – PDH): antiglucose – 6 – phosphate dehydrogenase antibody

There was no significant change observed in the temperature at which first transition initiated (Table 4.3). This suggests the ability of IgG to resist the unfolding stresses induced during multiple cycles of lyophilization (Figure 4.13). However, the effect of successive cycles of lyophilization on the unfolding of IgG is not identical, as shown by nature of DSC traces. DSC traces show that the propensity of antibody to unfold appears to increase during

repeated lyophilization. This was further confirmed by observing shift in the melting point of Fc fragment from ~ 85 °C (Cycle 1) to ~ 67 °C (Cycle 7). Therefore, our results suggest that repeated stress caused due to lyophilization weakens the covalent structure of Fc fragment, therefore, making it more susceptible to unfolding. This may also arise from intrinsic structural elements of the Fc fragment which are more susceptible to stress than the F(ab) fragments (albeit that the Fc has a higher transition temperature and is therefore inherently more stable). It is also known that increased flexibility is induced to the hinge region due to repeated lyophilization [195,196]. During successive lyophilization the tendency of IgG (when lyophilized on its own) to unfold increases, therefore, makes IgG more prone to aggregation, and hence, supports the conclusions drawn from the DLS and AFM studies.

4.6.7 Effect of lyophilization on the secondary structure

The endothermic enthalpic change observed in DSC experiments is assigned to the unfolding of a part of the protein molecule. DSC does not give any detailed information on a molecular scale, about the change in the protein structure. Therefore, any possible damage caused to the secondary structure of an IgG antibody during multiple cycles of lyophilization IgG was investigated using FT-IR spectroscopy.

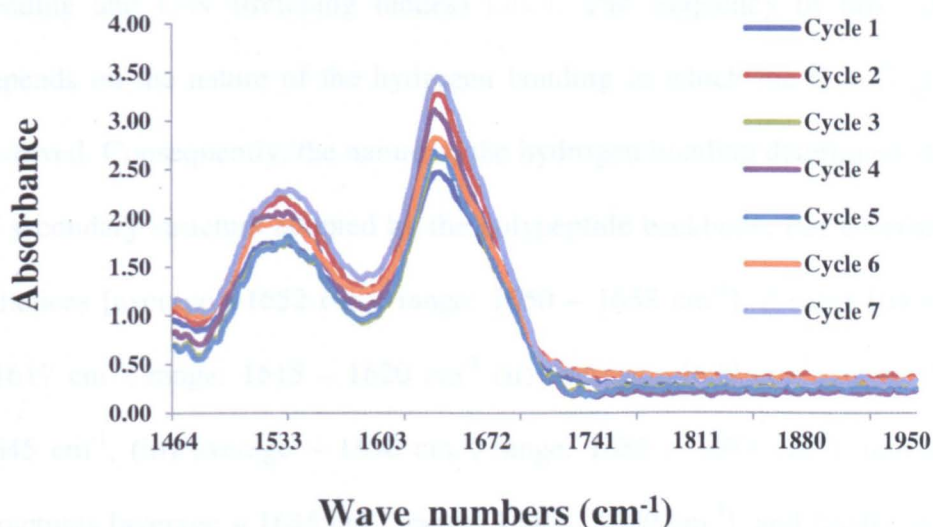


Figure 4.14 Overlaid, base line corrected and normalized FTIR – ATR spectra of: one to seven times lyophilized IgG deposited on the clean surface of a glass slide. Spectra were recorded between 1300 and 1800 cm^{-1} . The two main peaks towards right under each curve correspond to amide bands I and II.

The overlaid ATR spectra for the one to seven time lyophilized IgG powders (without added excipients) are shown in [Figure 4.14]. Typical amide I and amide II ATR absorbance spectra were observed for each sample. This identified that the removal of water through lyophilization had a negligible impact on the appearance of the amide bands I and II absorbance spectra. Typically, FT-IR spectrum of any structurally stable protein such as an IgG antibody show two main molecular absorption regions or amide bands (I and II) [199]. The amide I and II absorption regions emanate from two chemical groups of the peptide back bone. The amide I band primarily represents the $\text{C}=\text{O}$

stretching vibrations of the peptide bond groups (coupled to the in plane NH bending and C-N stretching modes) [200]. The frequency of this vibration depends on the nature of the hydrogen bonding in which the C = O group is involved. Consequently, the nature of the hydrogen bonding determines the type of secondary structure adopted by the polypeptide backbone. For an example: - α -helices [average $\sim 1652\text{ cm}^{-1}$, range: $1650 - 1658\text{ cm}^{-1}$], β -sheet [(i) average $\sim 1617\text{ cm}^{-1}$, range: $1615 - 1620\text{ cm}^{-1}$ (ii) average $\sim 1639\text{ cm}^{-1}$, range: $1628 - 1645\text{ cm}^{-1}$, (iii) average $\sim 1690\text{ cm}^{-1}$, range: $1686 - 1697\text{ cm}^{-1}$], non-ordered structures [average $\sim 1645\text{ cm}^{-1}$, range: $1640 - 1650\text{ cm}^{-1}$], and finally turns [(i) average $\sim 1670\text{ cm}^{-1}$, range: $1660 - 1667\text{ cm}^{-1}$, and $1676 - 1680\text{ cm}^{-1}$ [26, 31]. Molecular absorptions in the regions from ($1690 - 1638\text{ cm}^{-1}$) and ($1568 - 1517\text{ cm}^{-1}$) respectively correspond to amide bands I and II (Figure 4.14). Our results show amide I and II peaks centred at 1639 cm^{-1} and 1545 cm^{-1} which is an indicative of IgG powders rich in β - sheet content [201, 201]. The absorbance spectra in this region are used frequently for determining the secondary structure composition of various proteins, including IgG [199, 202, 203, 204, 205]. These values are close to those reported in literature ($1690 - 1600\text{ cm}^{-1}$) and ($1600 - 1480\text{ cm}^{-1}$) and appeared in all lyophilized samples of IgG [200, 201, 206]. This suggests maintenance of secondary structure during repeated lyophilization. Therefore, secondary structure of the IgG molecules within the lyophilized formulations can be described as native. However, in order to quantify the effect of successive cycles of lyophilization on the structure of IgG, ATR-spectrum obtained from each sample of IgG (data shown from 1 - 7), were normalized

(smoothed and base line corrected) and the ratio of the area of amide bands I and II were calculated. The ratio of areas under amide bands I/II determine the β – sheet character present in the protein. Our results demonstrated no significant change in the amide I/II ratio during multiple cycles of lyophilization (Figure 4.15 blue bars). Apparently, it seems, as if aggregation is not a consequence of changes in the secondary structure which could be detected by FT-IR. However, the small changes in the amide I/II ratio are attributed to differences in the secondary and possible tertiary structure.

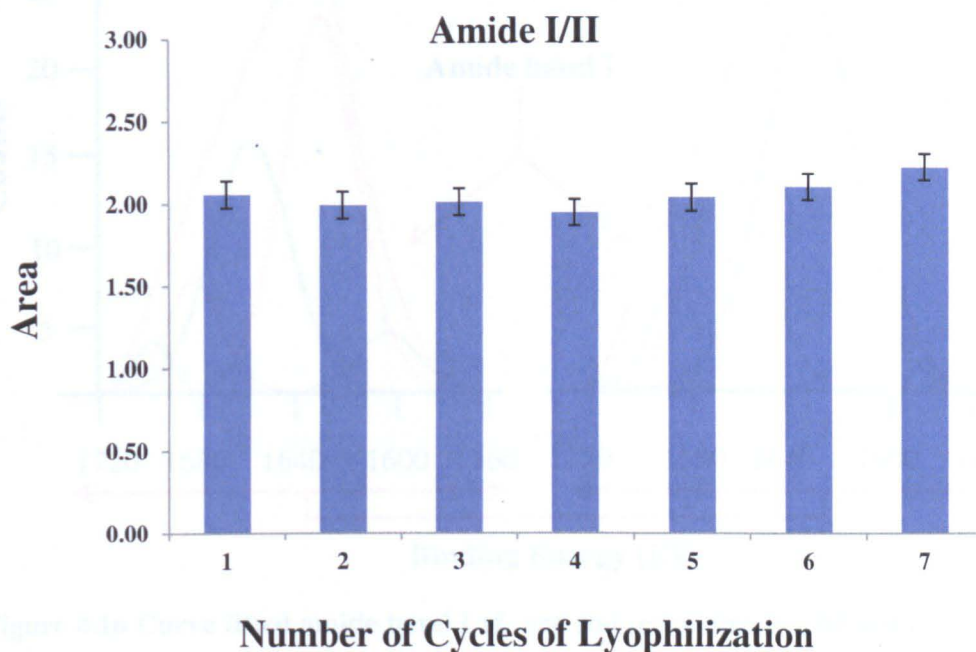


Figure 4.15 Ratio of areas under bands I and II in: one to seven times lyophilized IgG powders. The error bars represent standard deviations (SD ~ 0.08) recorded for three sets of measurements recorded for each sample. Successive lyophilization appears to have no significant impact on the amide I/II ratio.

The secondary structural changes are induced because of stress caused due to repeated lyophilization which consequently produce the deformation, bending stretching, and more importantly disruption of carbonyl – C = O, and -N-H bonds of the peptide backbone. Considering the fact that the sensitivity of the amide band II for the polypeptide is small and IgG largely consists of β -sheet structures (76 %) whereas α -helix content is relatively small (~ 9 %) has been previously reported [198, 200].

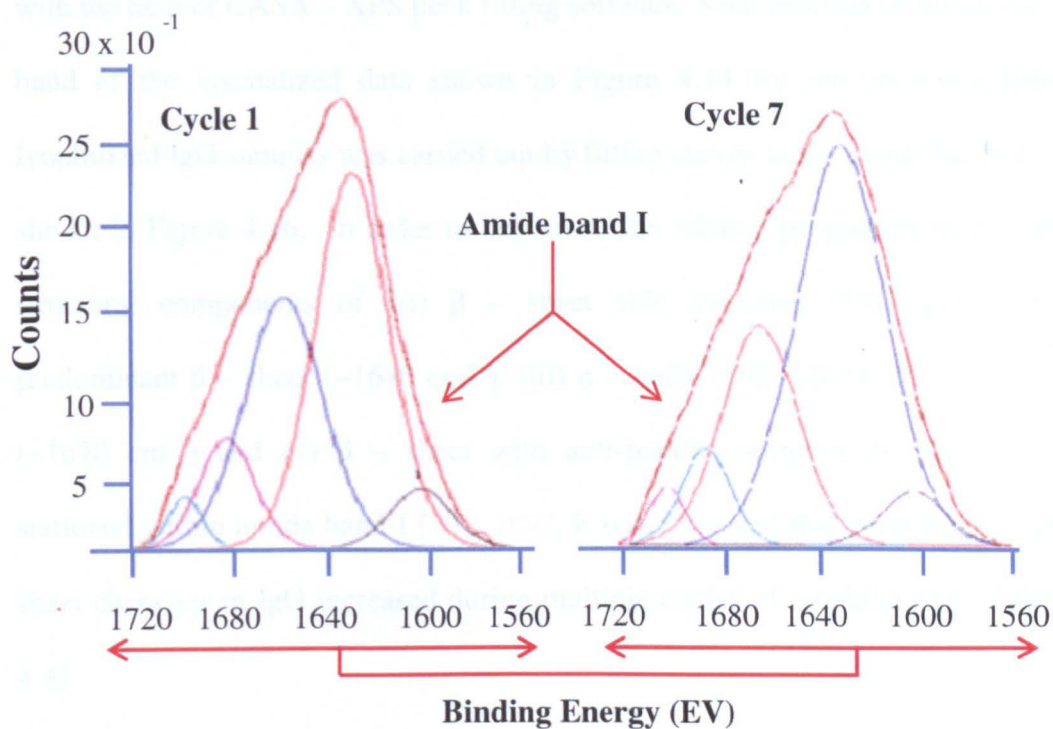


Figure 4.16 Curve fitted amide band I of: one and seven time lyophilized IgG on its own. Reconstitution was performed in filtered deionized water. Large peak corresponds to amide band I and predominantly represents β – sheet structure. Each band contains five fitted components: - (i) green (β – sheet with anti-parallel structure) (ii) pink (β – turns) and (iii) blue (α – helix), (iv) red (predominant β – sheet with parallel structure) and (v) black (amino-acid side chains). The short band next to band I represents amide band II, more likely shows changes arising from N-H bending vibration and also some contribution from C-N stretching [129, 207].

The interpretation of data was further carried out utilizing only amide band I by performing the structural analysis of different components stationed in amide band I during multiple cycles of lyophilization. It was observed that total area under the amide band I significantly increased in the 7th cycle. The structural analysis is complicated because the absorption bands of different structural components almost overlap in the amide I band. Therefore, it became vital to improve the processing of the spectral data. In our studies, this was achieved with the help of CASA – XPS peak fitting software. Such analysis of the amide I band of the normalized data shown in Figure 4.14 for one to seven time lyophilized IgG samples was carried out by fitting curves to the amide bands I as shown in Figure 4.16, in order to determine the relative proportion of various structural components of [(i) β – sheet side stretches (1617 cm^{-1}), (ii) predominant β – sheet ($\sim 1640\text{ cm}^{-1}$), (iii) α – helix (1652 cm^{-1}), (iv) β – turns ($\sim 1670\text{ cm}^{-1}$) and (v) β – sheet with anti-parallel structure ($\sim 1690\text{ cm}^{-1}$), stationed within amide band I [206, 207]. It was observed that percentage of β -sheet character in IgG increased during multiple cycles of lyophilization [Table 4.4].

On the other hand, α – helical content was observed to disappear after cycle one. The consistent increase in the β – sheet character coupled with complete absence of α – helical content is consistent with an increase in the probability of aggregation, by enhancing inter-protein interactions during solution phase and drying. Hence, aggregation gets initiated. The decrease in the α -helical content

upon lyophilization has been reported in other proteins (such as poly (L – lysine) [208], Insulinotropin [209], fibronectin [210], lysozyme [211], and chymotrypsin [212].

Table 4.4. Structural analysis of different structural components stationed in amide band I
Percentage concentration and area under occupied by each component

Amide band I	Component 1	Component 2	Component 3	Component 4	Component 5
(~1690-1600 cm ⁻¹)	β – sheet	β – sheet	α – helix	β – turns	β – sheet
	<i>Amino-acid Side chains</i>	<i>Main in the Middle Amide I</i>			<i>Anti-parallel structure</i>
Range	(~1615 -1620 cm ⁻¹)	(~1628 -1645 cm ⁻¹)	(~1650 -1658 cm ⁻¹)	(~1660 -1677 cm ⁻¹)	(~1686 -1697 cm ⁻¹)
Peak position	(~1617 cm ⁻¹)	(~1639 cm ⁻¹)	(~1652 cm ⁻¹)	(~1670 cm ⁻¹)	(~1690 cm ⁻¹)
Cycle 1 (%:area)	2 : 4.1	55.37 : 110.7	10.5 : 20.1	2.02 : 4	30.54 : 61.1
Cycle 2	4.1 : 2.03	52. : 90.07	0 : 0	15.35 : 24.4	27.7 : 44
Cycle 3	0 : 0	52.71 : 175.5	0 : 0	4.32 : 13.5	39.32 : 123.1
Cycle 4	0 : 0	52.70 : 127.4	0 : 0	33.8 : 81.8	13.54 : 32.7
Cycle 5	0 : 0	59.57 : 177.5	0 : 0	4.30 : 13.7	39.5 : 122.9
Cycle 6	0 : 0	46.95 : 69.1	0 : 0	51.34 : 75.6	1.71 : 2.5
Cycle7	0 : 0	38.75 : 73.40	0 : 0	61.25 : 109	0 : 0

However, in case of IgG studied, the complete absence of α -helical content associated with concomitant increase in β – sheet structure upon repeated lyophilization (Table 4.4) has not been previously reported. This is because in suspended state, water molecules which remain hydrogen bonded to the C = O moieties present in α – helical slices, when undergo dehydration during lyophilization only affects α – helical content and not β – sheet [213, 214]. Therefore, the one of the likely reason that could be asserted for observed increase in the β – sheet content upon dehydration during lyophilization is forced intermolecular cohesion between protein molecules with no competition from water molecules, and are considered energetically attractive, which otherwise in suspended state are entropically prohibitive (not favoured). Therefore, this structural rearrangement may also explain the exothermic aggregation peak (depth of the first transition peak: unfolding of Fabs). Fabs are heat sensitive [215]. The above described structural rearrangement quickens the thermal denaturation (unfolding) of Fabs. However, the proportion of completely or partially unfolded molecules within the aggregates depends on the intensity of structural rearrangement (proportion of β – sheet). The successive lyophilization induced greater structural rearrangement (β – sheet character). Consequently, the rate of aggregation would be correspondingly faster in the sample that has been exposed to more cycles of lyophilization. At a faster rate, IgG molecules that participate in aggregation had not enough time to unfold completely. Thus, it could be proposed that the proportion of partially unfolded molecules will be more in the samples having undergone maximum structural

arrangement, which obviously in our studies would be the sample exposed to more number of lyophilization cycles (cycle 7). Furthermore, Fc is more sensitive to lowering pH [215]. The lowering of pH caused by significant increase in the proportion crystalline material demonstrated by AFM (Figure 4.11) could well explain the increase in the unfolding (melting) propensity of Fc fragment during repeated lyophilization.

The secondary structural changes in the components of multiple times lyophilized IgG (Table 4.4) is an indicative of protein in the aggregated state, therefore, validates our DLS findings, where we observed an increase in the propensity of size IgG to form larger aggregates. This also lies in agreement with AFM results, where an increase in the size of aggregates and proportion of crystalline material was found during repeated lyophilization. Furthermore, an increase in the magnitude of unfolding peak (depth of the first transition peak) during successive lyophilization shown by DSC (Figure 4.13) complements the fact that secondary structural changes shown by ATR weakened the intra-protein bonded network, and therefore, reduced the thermal stability of IgG.

4.7 Conclusions

The present study provides a comprehensive analysis of the effect of repeated lyophilization on the aggregation, stability and protection of a polyclonal IgG antibody on its own. The tendency of IgG to aggregate increased during multiple cycles of lyophilization. IgG lyophilized on its own offers some resistance against aggregation, however, this resistance is not enough to withstand stresses during multiple cycles of lyophilization. The increase in the mean size of the globular features and their association with amorphous regions in the powdered formulations shown by AFM compliment the DLS, NTA and DSC findings respectively. The porosity of antibody formulation decreased whereas likely crystalline content increased with multiple lyophilizations was confirmed by SEM results. Moreover, the growth of crystalline material shown by SEM is complimented by AFM. The unfolding of IgG is probably a complex process. The significant increase in the β -sheet character (structural rearrangement) compliments DSC in proving that the propensity of unfolding of IgG increased. This research is pharmaceutically significant in that it provides insight into the underlying factors which govern aggregation phenomenon at nanoscale level. This work can be employed as a broad spectrum strategy to characterize aggregation in protein therapeutics.

Chapter 5

Nanoscale characterization of the effect of sucrose and mannitol on aggregation of polyclonal IgG during multiple cycles of lyophilization

5.1 Introduction

The propensity of IgG to withstand the alteration in its intrinsic state that is produced by lyophilization or reconstitution following lyophilization was investigated in the previous chapter. It was observed that the inclination of IgG to aggregate increased during multiple cycles of lyophilization. A possible reason for this is dehydration that can cause undesirable protein denaturation/aggregation which in turn could result in the loss of an activity upon rehydration [214, 216]. The effect of crystallization of the dissolved salts could be another possibility [216]. Several studies on the stabilization of proteins have indicated that additives like sucrose, trehalose, sorbitol etc can resist protein aggregation throughout lyophilization and storage in the dried form [9, 217,

218]. However, as discussed in the introductory chapter, there is disagreement over the mechanisms by which such additives stabilize proteins; with dehydration being most often cited [12, 25, 26, 27, 29, 30, 31, 32, 218]. This impression of guarding protein activity/stability during lyophilization and drying is endorsed by Timasheff's preferential exclusion mechanism [219], the glassy state hypothesis [220] and the water replacement hypothesis [221], although the use of sugar additives prone to crystallization during lyophilization should be avoided [13, 55]. The storage stability of a protein formulation has been reported to be a characteristic of its glass transition temperature (T_g), noting that it should be stored well below its (T_g) [223].

In the light of the above discussed criteria, we investigated the stability of a polyclonal IgG antibody by formulating the protein with sugar excipients such as sucrose and mannitol, individually and in combination during multiple cycles of lyophilization (up to 7). In these investigations, the choice of excipients was based on previous studies [10, 12, 200, 223]. The samples formulated were stored at $-4\text{ }^{\circ}\text{C}$ for up to several months, and their protein stabilities were compared. To characterize potential changes that occur during lyophilization dynamic light scattering (DLS) was used to study the size of the protein and any aggregates in solution and atomic force microscopy (AFM) to image the dried formulations at high resolution [68]. In addition, thermal analysis was carried out using differential scanning calorimetry [224] to study glass transition,

crystallization and melting events and FT-IR in attenuated total reflection (ATR) mode to determine changes in the secondary structure [225]. Taken together these complementary approaches were selected to provide physical and structural insights into the multiple times lyophilised formulations of IgG.

5.1.1 Excipients and their chemical structure

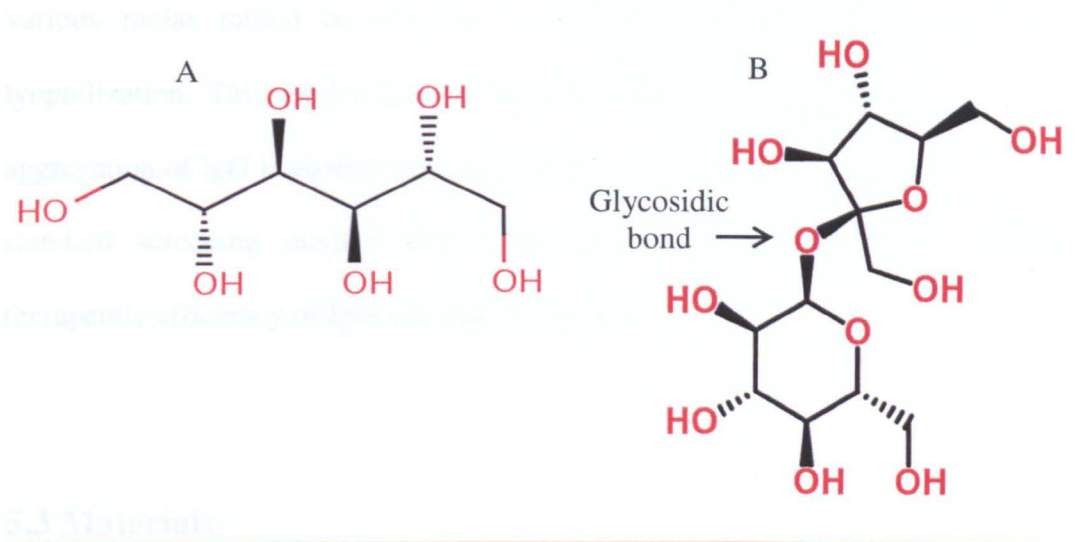
Sucrose and mannitol were the two excipients used in this study. The molecular formulae, molecular weight and chemical structure for the indicated excipients are presented in Table 5.1.

I. Mannitol

Mannitol is white, odourless, crystalline monosaccharide, usually used as an additive for matrix formation during lyophilization. Typically when introduced at concentrations up to 10 % w/v, mannitol becomes able to produce an amorphous matrix that can effectively support bio-pharmaceuticals (such as proteins) during lyophilization [13, 226, 227]. The amorphous structure produced during frozen state enables mannitol to prevent collapse of therapeutic protein while creating small canals for water sublimation during secondary drying of the lyophilization process. The other remarkable attribute of mannitol is its general inertness and instantaneous rehydration following lyophilization [13, 226, 227].

II. Sucrose

Sucrose (α - D - glucopyranosyl - (1 - 2) - β - D - fructofuranoside) is a white crystalline solid, a non-reducing disaccharide formed by a glycosidic linkage (bond) between carbon atom one of alpha D - glucose and the carbon atom two (β) form of D - fructose. The glycosidic bond formed is also referred to as an α - β ;1 - 2 bond, because there is an α - OH from the glucose bonding to a β - OH from the sucrose. As both of the hydrogen atoms removed during dehydration come from OH groups (α - 1 and β - 2) that were created during ring closure. The glycosidic linkage is established between the reducing ends of both glucose and fructose, and not between the reducing end of one and the non-reducing end of the other. Consequently, this results no free anomeric carbon atom available for the further establishment of bonds with other sugar molecules. Therefore, sucrose becomes a non-reducing sugar due to lack of free ketone or aldehyde group. Sucrose is considered an active lyoprotectant for the lyophilization of therapeutic proteins. During the lyophilization process, therapeutic proteins can denature as water is expelled unless a replacement molecule is offered to support the protein structure. Sucrose fills the vacancies left by the dehydration of water molecules, and therefore, prevents protein denaturation [13, 226, 227].



Excipient Name	Molecular formula	Molecular weight	Melting point	Boiling point	Tg
Mannitol	C ₆ H ₁₄ O ₆	182.17 g/mol	167 °C	295 °C	~ 85 °C
Sucrose	C ₁₂ H ₂₂ O ₁₁	342.20 g/mol	186 °C	Decomposes	~ 70 °C

Table 5.1 The chemical structures presented above are of: the excipients used in this study; [A] Mannitol and [B] Sucrose. Summarized in the table are their corresponding physical property values [224, 227].

5.2 Aims and objectives

Little work has been performed to date probing the effect of lyoprotectant on the stabilization/prevention of aggregation of IgG during multiple cycles of lyophilization. The main objective of this study was to scrutinize a polyclonal IgG antibody lyophilized with sucrose and mannitol (alone and in combination in

various molar ratios) in response to the influence of multiple cycles of lyophilization. This exploration of the latent impact of lyoprotectants on the aggregation of IgG is another advancing step towards the development of a novel standard screening method that would enable us to improve an overall therapeutic efficiency of IgG and other such proteins.

5.3 Materials

All other materials which were employed were same as described in the section 4.2 of Chapter 4.

5.4 Sample preparation methodology

5.4.1 Reconstitution of lyophilized protein (IgG powder)

This has been already described in section 2.1.1.2 of Chapter 2.

5.4.2 Lyophilization of reconstituted IgG

Lyophilization of IgG has been discussed in section 2.1.4.2 of Chapter 2.

5.4.3 Preparation of IgG formulations

IgG was lyophilised on its own, with sucrose and mannitol alone, and in combination with both. Dry sucrose and mannitol powders were dissolved in filtered deionized water containing 0.01 mM PBS to the desired

concentration. The concentrated IgG solutions were directly mixed with appropriate amount of sugar from stock solutions to achieve the desired protein and sugar concentrations. Samples of IgG exposed to 1, 2, 3, 4, 5, 6, and 7 cycles of lyophilization were prepared. Formulations were prepared in the form of liquids and dry powders.

5.4.3.1 Liquid formulations

IgG (6.67 μ M) liquid formulations which were prepared with sucrose and mannitol alone, and in combination are presented in Table 5.2.

<u>Serial</u> <u>No.</u>	<u>Formulation</u> <u>Type</u>	<u>Number of</u> <u>Cycles</u>
(i)	IgG	(0 – 3)
(ii)	IgG + Sucrose (1.8 mM, 3.6 mM, 5.8 mM)	(0 – 3)
(iii)	IgG + Mannitol (1.8 mM, 3.6mM, 5.8 mM)	(0 – 3)
(iv)	IgG + Sucrose (1.8 mM) + Mannitol (1.8 mM)	(0 – 3)
(v)	IgG + Sucrose (1.8 mM) + Mannitol (3.6 mM)	(0 – 3)
(vi)	IgG + Sucrose (3.6 mM) + Mannitol (1.8 mM)	(0 – 3)
(vii)	IgG + Sucrose (3.6 mM) + Mannitol (3.6 mM)	(0 – 3)

Table 5.2 Break down of the liquid formulations of IgG lyophilized with sucrose and mannitol in different molar ratios.

5.4.3.2 Powdered formulations

IgG (1.2 mM) powdered formulations which were prepared with sucrose and mannitol alone, and in combination are presented in Table 5.3.

<u>Serial</u> <u>No.</u>	<u>Formulation</u> <u>Type</u>	<u>Number of</u> <u>Cycles</u>
(i)	IgG (1.2 mM)	(0 – 7)
(ii)	IgG (1.2 mM) + 20 mM Sucrose	(1)
(iii)	IgG (1.2 mM) + 40 mM Sucrose	(1)
(iv)	IgG (1.2 mM) + 20 mM Mannitol	(1)
(v)	IgG (1.2 mM) + 40 mM Mannitol	(1)
(vi)	IgG (1.2 mM) + 20 mM Sucrose + 40 mM Mannitol	(1)
(vii)	IgG (1.2 mM) + 40 mM Sucrose + 20 mM Mannitol	(1)

Table 5.3 Break down of the powdered formulations of IgG lyophilize with sucrose and mannitol in different molar ratios.

5.5 Methods of analysis

5.5.1 Dynamic light scattering

The characterization of particle size was conducted using a Viskotek DLS (Malvern Instruments Ltd, Worcestershire, UK) equipped with a 630 nm laser. Approximately 80 µl of sample solution was injected into the cuvette to

determine particle size. Each sample was first equilibrated for 30 minutes at 25 °C prior to the first measurement. Data collection was performed by taking 40 acquisitions for each measurement.

5.5.2 Atomic force microscopy

AFM tapping mode imaging was employed to study the different components in the powdered lyophilized formulations of IgG. Imaging (topography and phase) was performed with a D – 3000 AFM and a Multimode II AFM (Bruker Nano, Coventry, UK) equipped with an E-scanner. All images were taken at a scan rate between 1 – 2 Hz, with a 512 x 512 pixel resolution.

5.5.3 Differential scanning calorimetry (DSC)

A Q-2000, differential scanning calorimeter (TA Instruments Ltd, Fleming Centre, Manor, Crawley, West Sussex, UK) with purged nitrogen gas was used. Dry powdered samples (2 – 5 mg) were analyzed in crimped hermetically sealed aluminum pans. Samples were heated from 0 °C – 200 °C at a scan rate of 10 °C/min. The melting point of the IgG antibody lyophilized multiple times on its own and T_g /melting point of the sugar-containing antibody formulations were obtained as the midpoint of the corresponding transition by integrating the slope of the DSC curve.

5.5.4 ATR-FTIR spectrometry

A Nicolet FT-IR-spectrometer was employed to record spectra for the determination of changes in the secondary structure of lyophilized IgG. Sample powder (2 – 3 mg) was placed on a clean glass slide and then mounted on the sample stage. The spectra for each sample were recorded from 4000 to 650 cm^{-1} in ATR mode at room temperature. Each measurement was an average of 200 scans, at a scan speed of 0.15 sec^{-1} and a resolution of 2 cm^{-1} . The optical bench was purged with dry nitrogen to avoid interference from water vapour infrared absorption. Each spectrum was background corrected for the glass slide. The amide I (1720 – 1600 cm^{-1}) and amide II (1575 – 1480 cm^{-1}) regions were used to analyse changes in the secondary structure of protein.

5.6 Results and Discussion

5.6.1 DLS analysis

The effect of sucrose and mannitol on the aggregation of IgG was studied both individually and in combination in two subsequent sets of experiments.

5.6.1.1 Individual effect of sucrose and mannitol

The separate effect of the concentration of sucrose and mannitol on the aggregation of IgG was investigated using DLS for three cycles of lyophilization (Figure 5.1).

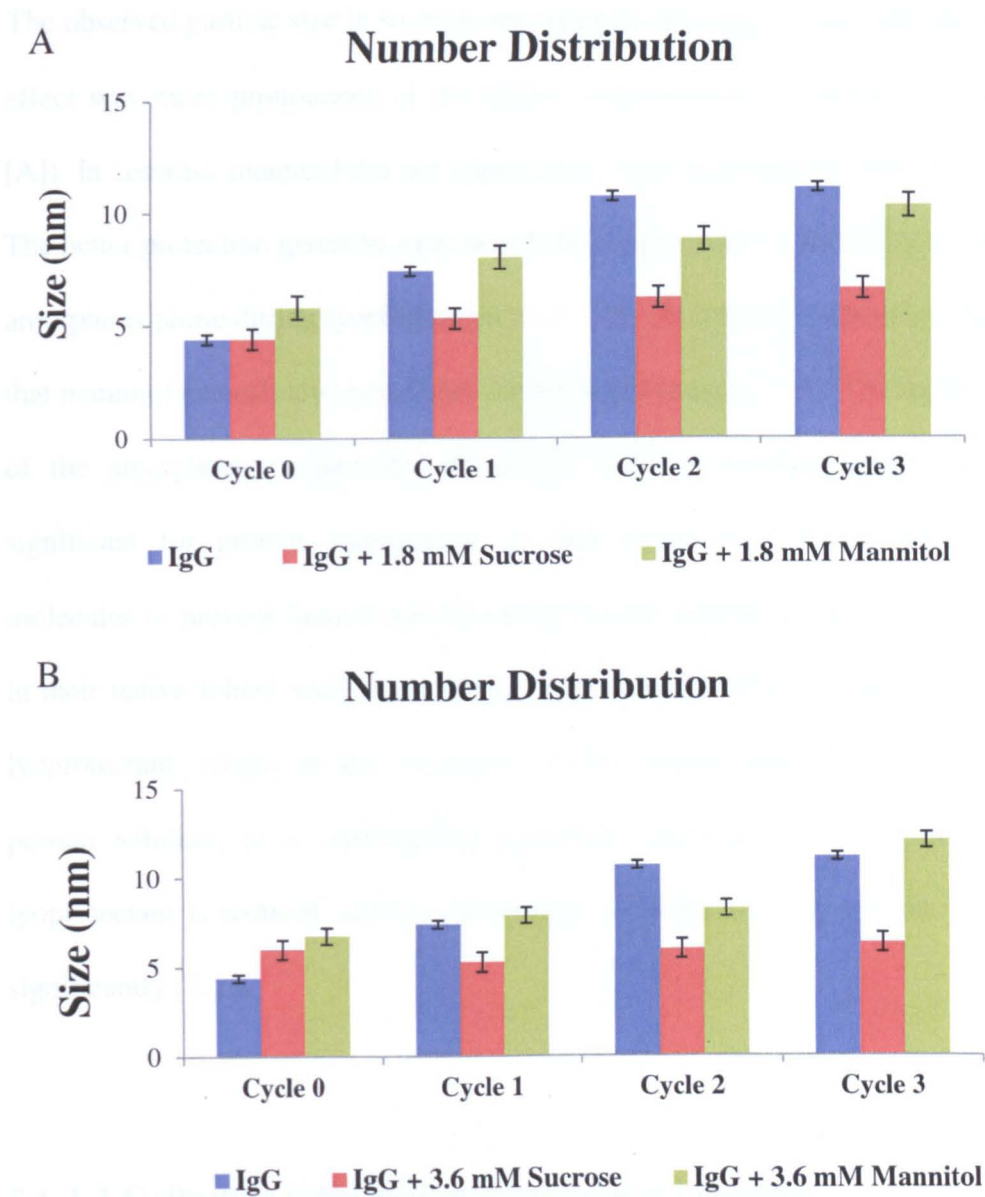


Figure 5.1 The comparison of an influence of sucrose (red bars) and mannitol (green bars) during successive cycles of lyophilization: on the aggregation of IgG lyophilized on its own (blue bars). [A] and [B] represent data obtained when IgG (1 mg/ml) was lyophilized with Sucrose/Mannitol at molar concentration of 1.8 mM, and 3.6 mM respectively. (Mean size \pm SD). Sucrose appears to have an inhibitive effect on aggregation and this effect is more pronounced at higher concentration. This is in contrast to that of mannitol which significantly promotes aggregation even at higher concentration.

The observed particle size in sucrose was reduced compared to the IgG alone. This effect was more pronounced at the higher concentration of sucrose (Figure 5.1 [A]). In contrast, mannitol did not appreciably effect aggregation (Figure 5.1 [B]). The better protection given by sucrose is believed to be due to its ability to form an amorphous phase during lyophilization [228, 229]. In contrast, it has been reported that mannitol extensively crystallizes during lyophilization [230]. The maintenance of the amorphous or partially amorphous state of a lyoprotectant is highly significant for protein stabilization, as this phase can interact with protein molecules to prevent them from denaturing i.e; the protein molecules are trapped in their native folded state in the glassy sucrose matrix. The crystallisation of the lyoprotectant, results in the expulsion of the solutes from the heterogeneous protein solution, as a consequence molecular interaction of the protein with lyoprotectant is reduced and the probability of denaturation of protein increases significantly [228].

5.6.1.2 Collective influence of sucrose and mannitol

To further evaluate the potential stabilizing effect of sucrose and mannitol, the combined effect of sucrose and mannitol on the aggregation of IgG during multiple cycles of lyophilization was investigated. Again, it was observed that the increased presence of sucrose decreased particle size and by inference aggregation (Figure 5.2). The improved effect of combining sucrose and mannitol is possibly due to the known inhibitory effect of sucrose on the crystallization of mannitol

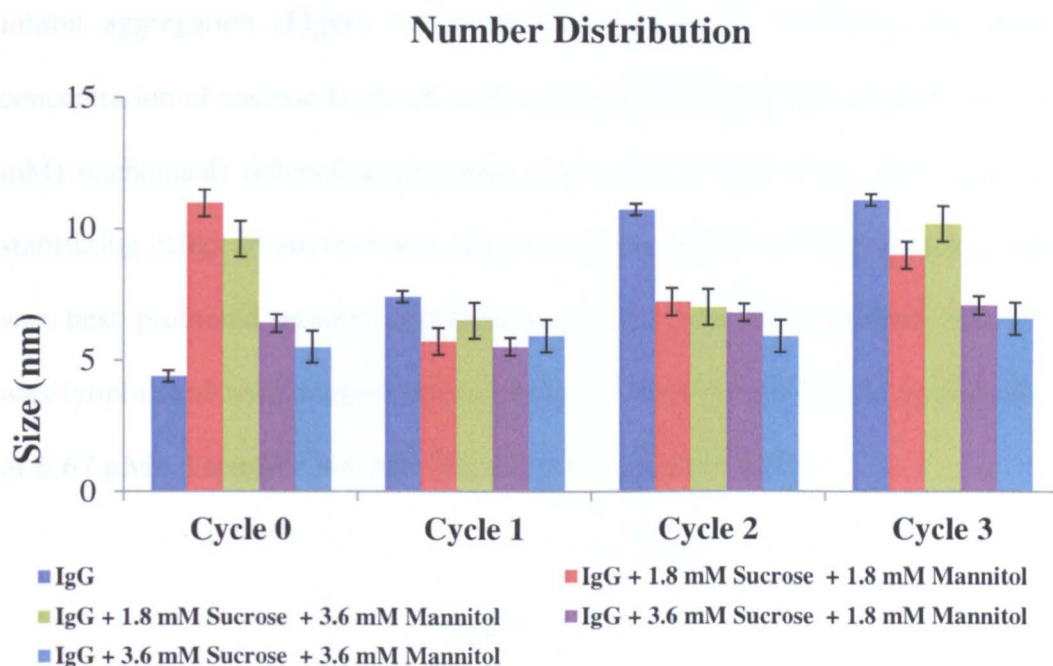


Figure 5.2 The comparison of an influence of the effect of increase in the concentration of sucrose/and mannitol during successive cycles of lyophilization: on the size of IgG formulated with mannitol and sucrose in combination. (Mean size \pm SD). The presence of sucrose within the combined formulations appears to decrease the observed aggregation enhancing effects of mannitol (when used on its own). The data indicate an increase in the molar concentration of sucrose provides better protection than mannitol in the combined formulations. However, in combination with mannitol, IgG, formulated with sucrose at equal and optimum concentration shows enhanced protection.

during lyophilization [228, 230]. Unlike, sucrose, the increased presence of mannitol within the combined formulations appears to have no significant protective effect on IgG aggregation (Figure 5.2 purple bars). It was observed in combined formulations, at fixed molar concentration of sucrose (1.8mM) that doubling the molar concentration of mannitol from 1.8 mM to 3.6 mM does not

inhibit aggregation (Figure 5.2 green bars). However, switching the molar concentration of sucrose from 1.8 mM to 3.6 mM (keeping that of mannitol (1.8 mM) unchanged) reduced aggregation (Figure 5.2 Purple bars). The superior stabilizing effect of sucrose was reflected in the combined formulations. IgG was best protected against aggregation for the conditions studied, when it was lyophilized with sucrose and mannitol in combination in the molar ratio of 6.67 μ M : 3.6 mM : 3.6 mM Mannitol, (1 mg/ml of IgG).

5.6.2 AFM analysis of the lyophilized formulations (powders)

The AFM topographic and phase imaging data of the lyophilized powders of IgG, formulated with sucrose and mannitol (alone and combination) was collected as described in Methods (Chapter 2).

5.6.2.1 Controls for lyophilized powders of sucrose and mannitol

Before investigating the effect of sugar lyoprotectants (sucrose and mannitol) on the stability of IgG (anti-glucose – 6 – phosphate dehydrogenase antibody) during lyophilization, sucrose and mannitol were separately formulated in 0.01 M PBS prior to lyophilization. Figure 5.3 shows representative imaging data from TM-AFM control experiments for one time lyophilized powders of mannitol and sucrose. The AFM topography was exploited to investigate the

pattern of projections of lyophilized sugars, which demonstrated a non-identical behaviour of both sugars on the surfaces at nano – scale. Lyophilized powder of mannitol (Figure 5.3-A) and sucrose (Figure 5.3 – C) indicate heterogeneous and uneven surfaces. In Figure 5.3 (A and C), the regions of the substrate darker in colour exemplify that they lower in height or larger in phase lag. On the other hand, patches lighter in colour are relatively higher in topography (small phase lag) [231]. The corresponding phase imaging data of mannitol (Figure 5.3 – B) and sucrose (Figure 5.3 – D), illustrate a multiple component surface (light yellow, dark yellow and white particulates) with significant phase contrast. The phase image which is produced as a result of phase change between the cantilever oscillation and the driving amplitude (signal applied to the piezo) during tip-sample interaction, reveal information about the nature of probe – sample interactions and the properties of the material imaged [231, 232]. The dark yellow components in colour are an indicative of high probe-sample adhesion (viscoelasticity), which results in the dissipation of more energy in from the oscillating AFM probe, and have been known to occur as a consequence of negative phase shift (phase lag) or holding up of AFM tip in these regions compared to the rest of imaged surface. This kind of tip-sample interaction produces deformation in a sample and has been proposed (reported) for amorphous materials [232, 233]. In contrast, light yellow components illustrate a relatively less probe-sample adhesion, less energy lost into the material during probe-sample interaction, as a result of positive phase shift and a characteristic for hard materials [232, 233]. Therefore, a possible reason of significant phase

contrast observed in Figure 5.3 (B and D) is related to the formation of crystalline (light yellow) and amorphous (dark yellow) structures during lyophilization. In addition, it would be expected that a flatter and harder surface that would be presented by a crystalline state will lead to a lower contact area with the AFM tip and hence a lower energy loss in comparison to the same material in amorphous form. One would also expect the amorphous form to have a higher surface energy and hence more adhesion to the probe, again leading to greater energy loss. The white particulates are likely the crystals of NaCl. TM – AFM phase images clearly demonstrate that mannitol has a larger propensity to form crystalline structures than sucrose during lyophilization. It has been reported that mannitol has a high propensity toward crystallization, however, the formation of an amorphous phase by mannitol in these studies (Figure 5.3 – B) could be due to the inhibition of crystallization by NaCl [234]. It can also be deduced from phase imaging (Figure 5.3 – D) that sucrose forms distinct amorphous and crystalline structures almost in equal proportion at the surface during lyophilization.

Furthermore, if the white particulates are likely to be crystals of NaCl, it can be said that the tendency of NaCl to crystallize in mannitol is larger than in sucrose. Therefore, our findings suggest that mannitol is more prone to crystallization than sucrose during lyophilization. These findings lie in agreement with literature [230]. Using an AFM to detect crystallinity in these studies stems from the fact,

that the crystalline and amorphous morphologies of other materials have been previously analyzed by atomic force microscopy such as those of polyamide nanofilms adsorbed on grafted gold [231].

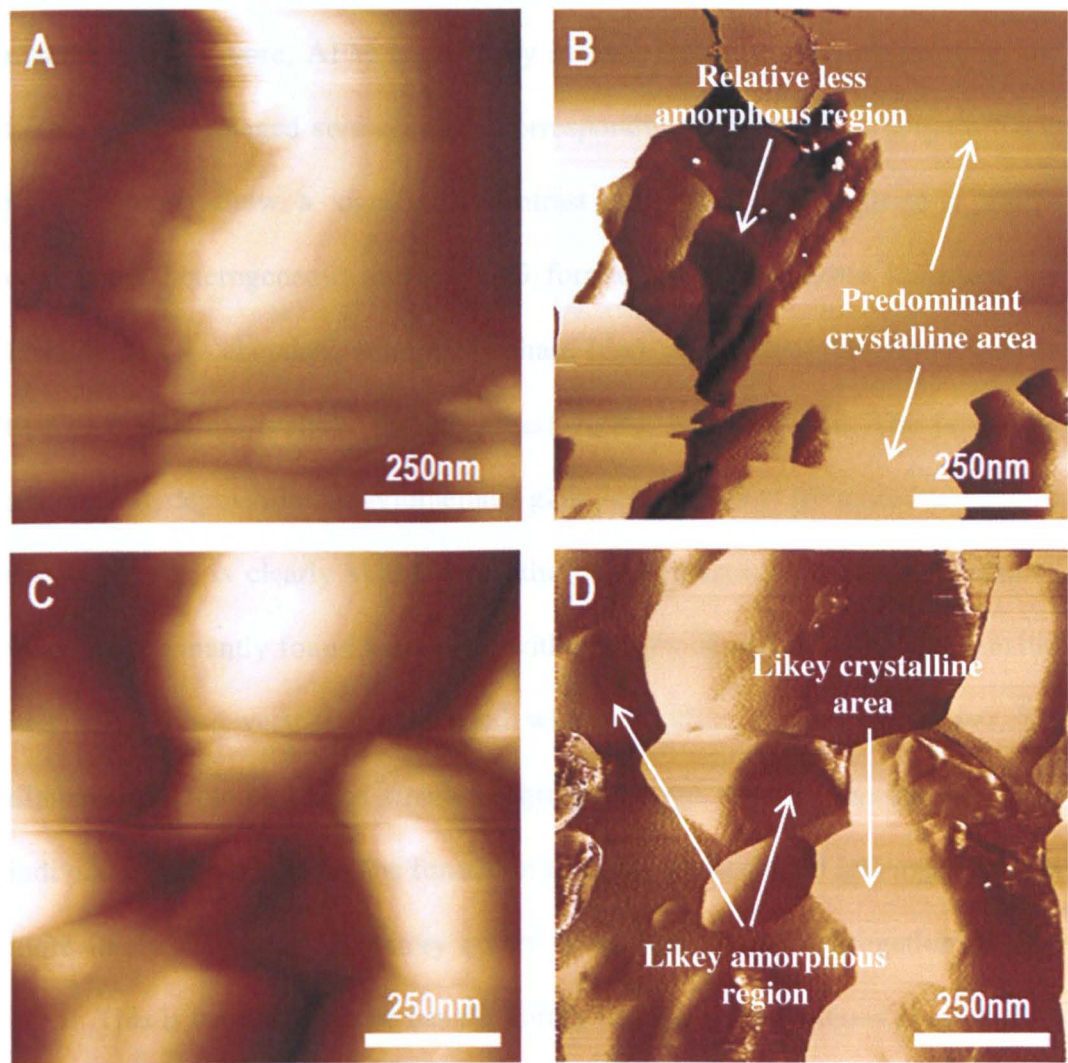


Figure 5.3 [A – B] and [C – D] respectively represent the AFM images (topography and phase) of lyophilized mannitol and sucrose powders. Each scan is one micron. All images have height (Z – scale) of 100 nm and a phase angle of 160°. For more images see Appendix 5.5

5.6.2.2 IgG lyophilized with sucrose (powder)

Taping mode AFM data of an IgG lyophilised with sucrose is shown in Figure 5.4. The topography images of 1.2 mM IgG lyophilised with 20 mM sucrose reveal that the deposited material is highly aggregated on the surface in a non-uniform manner. Furthermore, AFM topography images indicate non-uniformity in the flatness of the imaged surfaces. The corresponding phase images (Figure 5.4 – right column) show a significant contrast and therefore, illustrate a multi-component heterogeneous surface. IgG formulated with sucrose indicated the formation of an abundant amorphous phase (dark rough areas) in comparison to that of crystalline (yellow smooth areas) during lyophilization. The formation and random deposition of agglomerated globular features of (proposed to be IgG) dissimilar size is clearly visible from the phase images. The globular features were predominantly found associated with amorphous regions and were smaller in size to those very few associated with crystalline regions. Moreover, the dimensions of some of the smaller aggregates were close to that expected for individual IgG molecules. The formation of more smaller sized IgG aggregates is more likely due to an inhibitory effect of sucrose on the aggregation of IgG [235]. This is because sucrose has the ability to form an amorphous phase during lyophilization.

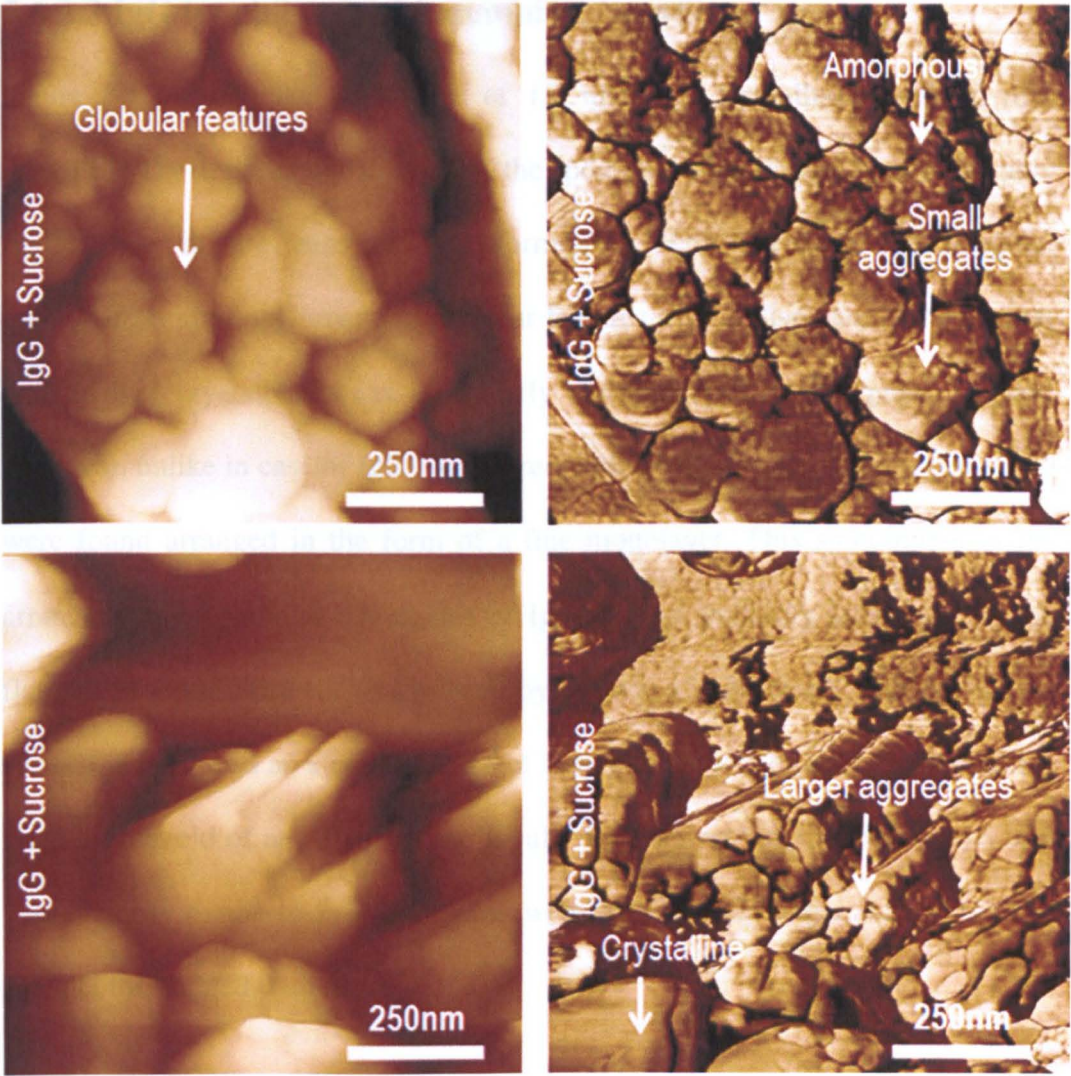


Figure 5.4 AFM topography (left) and phase (right) images of 1.2 mM IgG lyophilised with 20 mM sucrose. Each scan is one micron. The Z – scale of for both topography images were 120 nm whereas phase images were collected at an angle of 100°.

5.6.2.3 IgG lyophilized with mannitol (powder)

Figure 5.5 displays the AFM data of 1.2 mM IgG lyophilised with 20 mM mannitol. The topography images of the indicated sample appear considerably flatter than in the case of IgG formulated with sucrose. The irregular immobilization of agglomerated globular features of IgG disparate in dimension, and distinct crystalline areas are clearly demonstrated by the phase images. However, unlike in case of IgG lyophilized with sucrose, most of the aggregates were found arranged in the form of a fine monolayer. This smoothness in the arrangement of globular aggregates of IgG is most probably facilitated by the flatness of crystalline surface offered by mannitol underneath. The crystalline surface is produced as a consequence of lyophilization. Some of the crystalline areas are devoid of any aggregates globular IgG. Moreover, the dimensions of a vast majority of the visible aggregates were significantly larger than in case of the IgG formulated with sucrose.

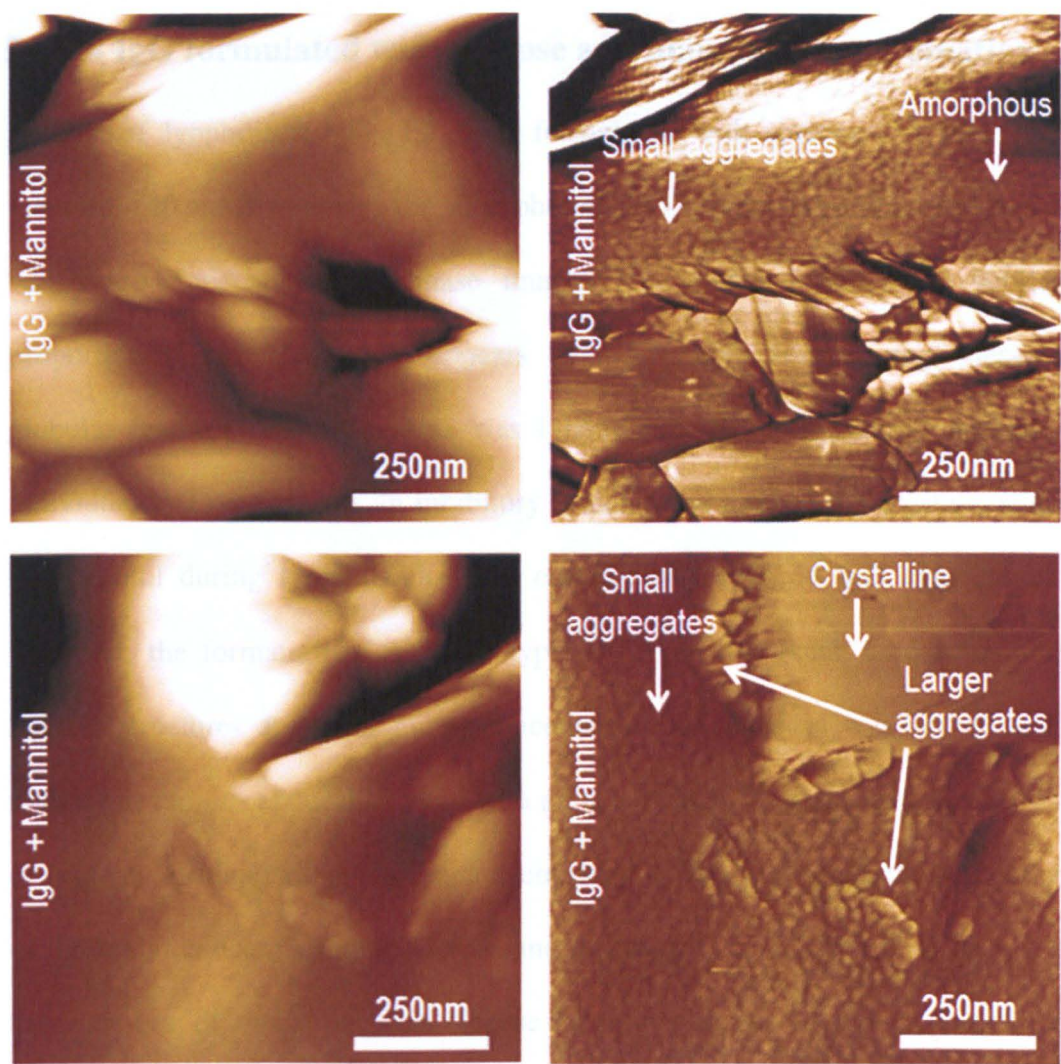


Figure 5.5 AFM topography (left) and phase (right) images of 1.2 mM IgG lyophilised with 20 mM mannitol. Each scan is one micron. The Z – scale of for topography images were 120 nm whereas phase images were collected at an angle of 100°.

5.6.2.4 IgG formulated with sucrose and mannitol in combination

In case of lyophilised IgG (1.2 mM) formulated with sucrose (20 mM) and mannitol (40 mM) together, the amorphous and different crystalline structures which are noticeable from phase images are produced almost in similar proportion (Figure 5.6). IgG appears to form much smaller agglomerated globular features than when IgG was lyophilized with sucrose and mannitol individually. This suggests an inhibitory effect of sucrose on the crystallization of mannitol during lyophilization and consequently reduced IgG aggregation. However, the formation of different types of crystalline (such as needles and stripes) structures at higher molar concentration of mannitol was noted, as it makes one curious about the impact of a particular kind of crystal on aggregation of protein. Without changing the concentration of IgG (1.2 mM), the switching of the molar concentration of sucrose and mannitol from 1 : 2 to 2 : 1 removes the formation of crystalline areas (Figure 5.7 right pannel). Moreover, this effect enhanced the ability of IgG to oppose aggregation as a significant reduction in the size of the globular features of IgG was observed. Most of the globular IgG features displayed in phase images are closer to individual molecules/molecules (Figure 5.7). Therefore, suggesting an inhibitory effect of sucrose on the crystallization of mannitol during lyophilization and this effect pronounced at higher molar concentration of sucrose [235]. This suggests the superior protective ability or stabilizing effect of sucrose than mannitol on IgG during lyophilization [235, 236] as shown in Figure 5.6. The maintenance of the amorphous or partially amorphous state of lyoprotectants is important for protein

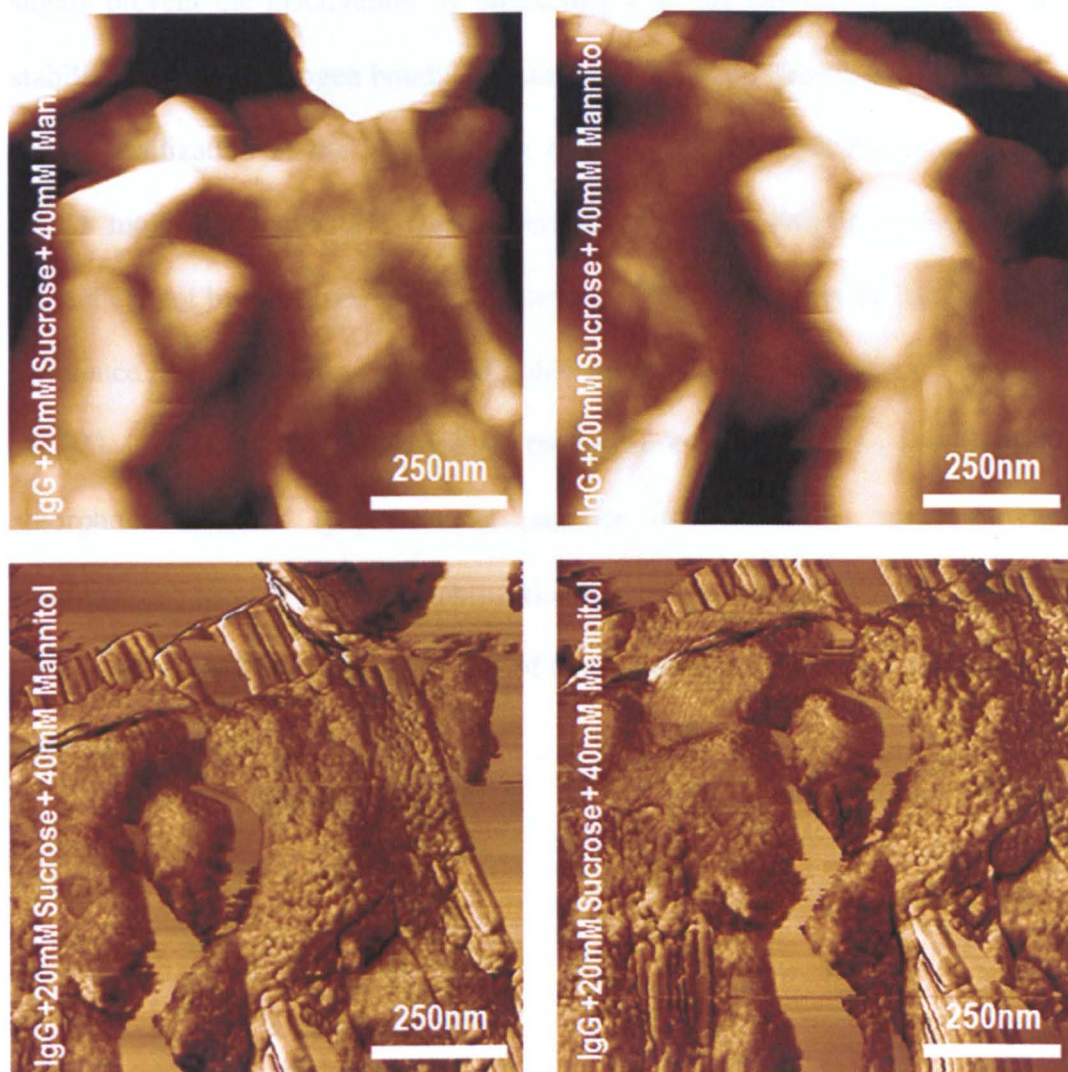


Figure 5.6 AFM topography [top]: and phase [bottom] images of powders of 1.2 mM IgG lyophilized sucrose and mannitol in the molar ratio of 1 : 2. Each scan is one micron. The Z – scale of for topography images were 120 nm whereas phase images were collected at an angle of 12°.

stabilisation, because it is then only that the lyoprotectant can interfere/interact with protein molecules to prevent them from denaturation/crystallization because

sugars prevent the inactivation by interacting with the surface of proteins, and stabilize them by hydrogen bonding against heat and cold denaturation [13, 237]. The crystallization of the lyoprotectant removes solutes from the solution and blocks molecular interaction with protein during freeze lyophilization. Hence, protein cannot be protected from denaturation. Therefore, it can be said, that the difference in the proportion of polymorphic structures in the lyophilized powders of IgG is due to the difference in the amount of amorphous or partially amorphous state of lyoprotectants (sucrose and mannitol, alone and in combination) formed during lyophilization [237, 238]. Another factor could be the nature of the molecular interaction of the sugar with protein in solution phase during lyophilization [13, 237, 238].

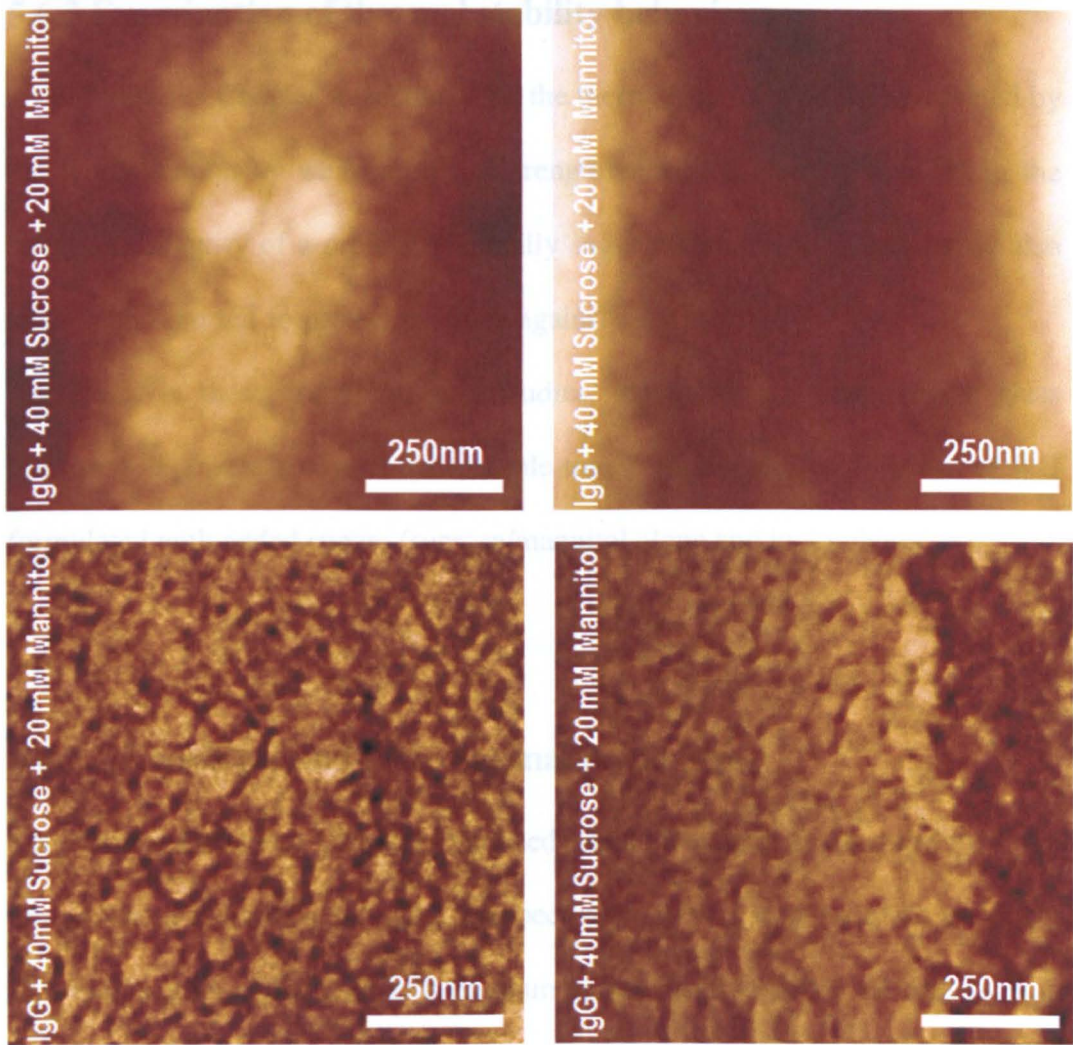


Figure 5.7 AFM topography [top] and phase [bottom] images of powders of 1.2 mM IgG lyophilized sucrose and mannitol in the molar ratio of 2 : 1. Each scan is one micron. The Z – scale of for topography images were 120 nm whereas phase images were collected at an angle of 12°. IgG likely seems to have a crystalline surface underneath more probably formed by the partial or complete crystallization of mannitol, allowing IgG molecules to land flat on the surface in an organized manner. The crystallization of mannitol can be claimed from the control experiments, which was later on also proved during SEM imaging of mannitol.

5.6.3 Examination of thermal stability behaviour

As described in Chapter 4 (section 4.8), the thermal stability could be affected by the lyophilization by weakening the strength of various bonds involved in the structural integrity of a protein. Generally sugar molecules such as sucrose also have been reported to protect proteins against such stresses [10, 223, 229, 237]. Therefore, in these complementary studies, the melting points and the glass transition (T_g) were analysed for multiple times lyophilized formulations of IgG formulated with added sugars (sucrose/mannitol alone and in combination).

5.6.3.1 Excipients and their thermal behaviour

The thermal behaviour of non-lyophilized and lyophilized sucrose and mannitol are presented in Figures 5.8 and 5.9 respectively. Table 5.4 summarizes the effect of lyophilization and formulation medium on the melting points of both sucrose and mannitol. The melting points of sugars were reduced, when exposed to lyophilization. In both sugars, there was no significant shift in melting points when samples were formulated in deionized prior to their lyophilization. In contrast, a significant decrease in the melting points was observed, when sugars were lyophilized in a medium containing dissolved buffer. This suggested that the presence of buffer in the formulation promoted the effect of lyophilization to reduce the strength of bonds in the sugar molecules. This also supports the idea that addition of an impurity (which in this case is buffer) decreases the melting point of bulk substance in the mixture. The melting-point depression as a result of

modifications (disorder) to bulk solid structure due to solid (bulk) – solid (impurity) transitions of has been reported [239]. Furthermore, T_g around $\sim 90^\circ\text{C}$ was observed only in case of sucrose samples which were formulated in buffer (Figure 5.10) suggesting the potential influence of buffer in the initiation of glass transition which is obvious due to the interaction of salt molecules with the bulk molecules.

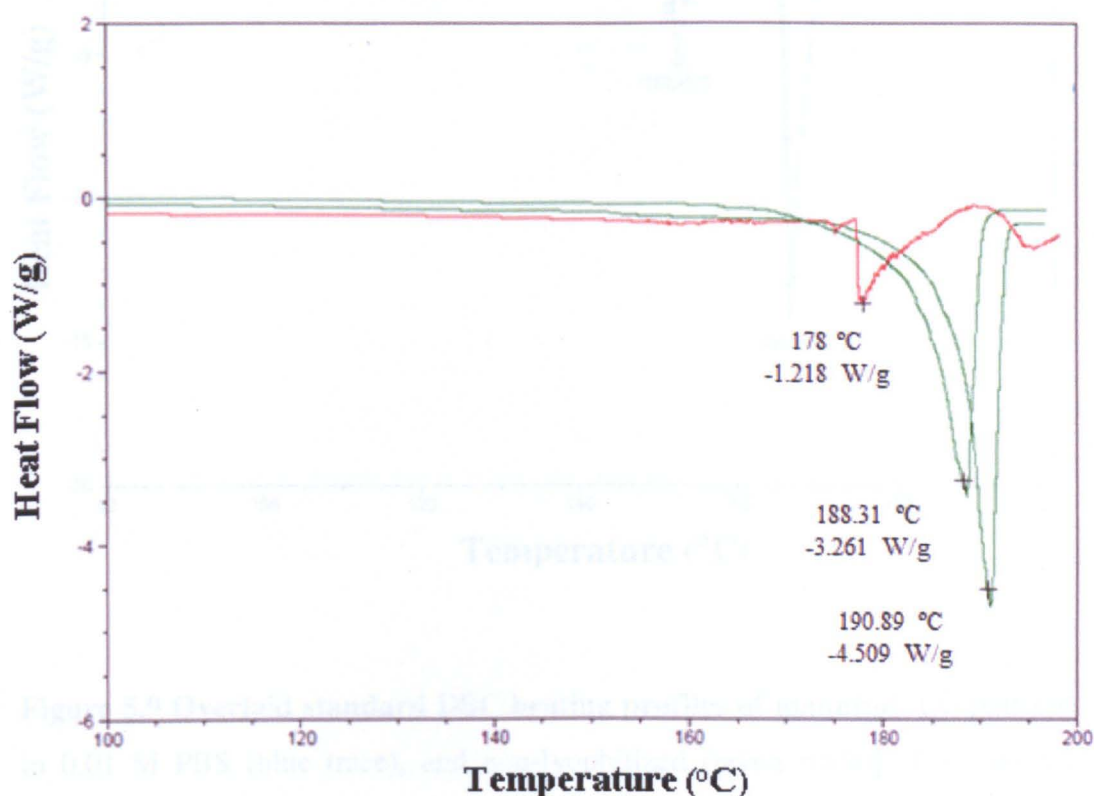


Figure 5.8 Overlaid standard DSC heating profiles of sucrose: G1 – green trace (non – lyophilized sucrose); G2 – green trace (sucrose lyophilized in deionized water) and red trace (sucrose lyophilized in 0.01 M PBS). The samples were heated up to 220°C at the rate of 10°C per minute. The endothermic peak towards the extreme right of the each trace is an indicative of the melting point of sugar in the respective traces.

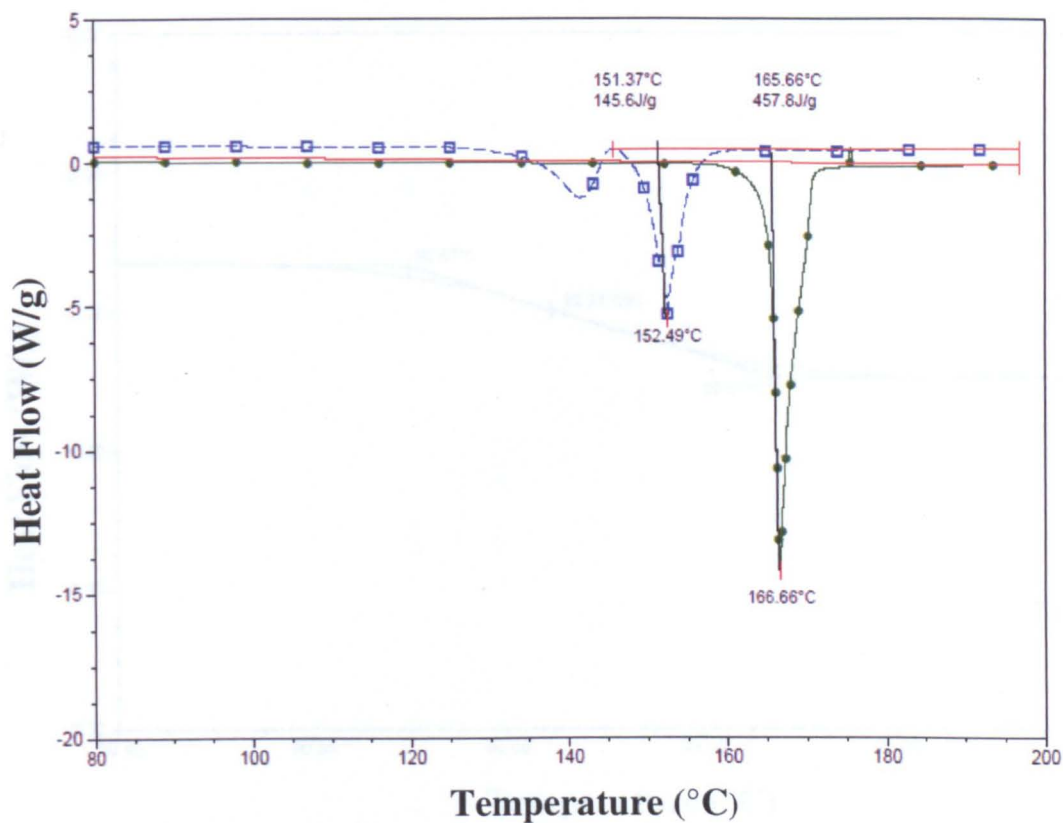


Figure 5.9 Overlaid standard DSC heating profiles of mannitol: Lyophilized in 0.01 M PBS (blue trace), and non-lyophilized (green trace)]. The samples were heated up to 220 °C at the rate of 10 °C per minute. The endothermic peak towards the extreme right of the each trace is an indicative of the melting point of sugar in the respective traces.

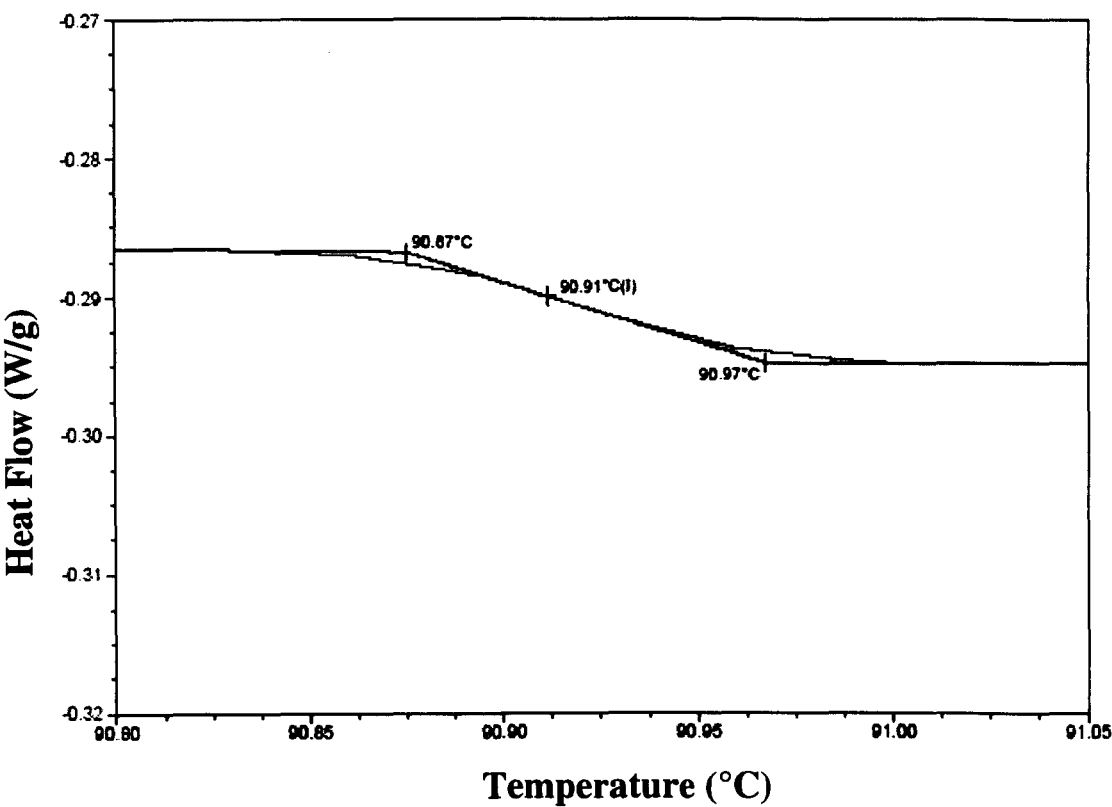


Figure 5.10 Part of the DSC profile (red trace, Figure 5.8) of sucrose: Lyophilized in 0.01 M PBS displays a typical glass transition event ~ 90 °C.

Table 5.4 Effect of lyophilization on the melting points and Tg of excipients

No. of Cycles	Formulation	Protein:Excipient	Melting Point (°C)	Tg (°C)
	(Powdered)	Concentration (mM)	of Excipient	
0	Sucrose (original powder)	00 : 20	~ 190.89	---
1	Sucrose (in deionized water)	00 : 20	~ 188.31	---
1	Sucrose (in 0.01 M PBS)	00 : 20	~ 178.00	~ 92 ± 0.34
0	Mannitol (original powder)	00 : 20	~ 166.66	---
1	Mannitol (in deionized water)	00 : 20	~ 162.36	---
1	Mannitol (in 0.01 M PBS)	00 : 20	~ 152.49	---

* Tg indicates glass transition temperature

5.6.3.2 Impact of sucrose and mannitol when used separately

The representative melting curves of IgG (1.2 mM) lyophilized with sucrose and mannitol at two different molar concentrations (20 mM and 40 mM), are shown in Figure (5.11).

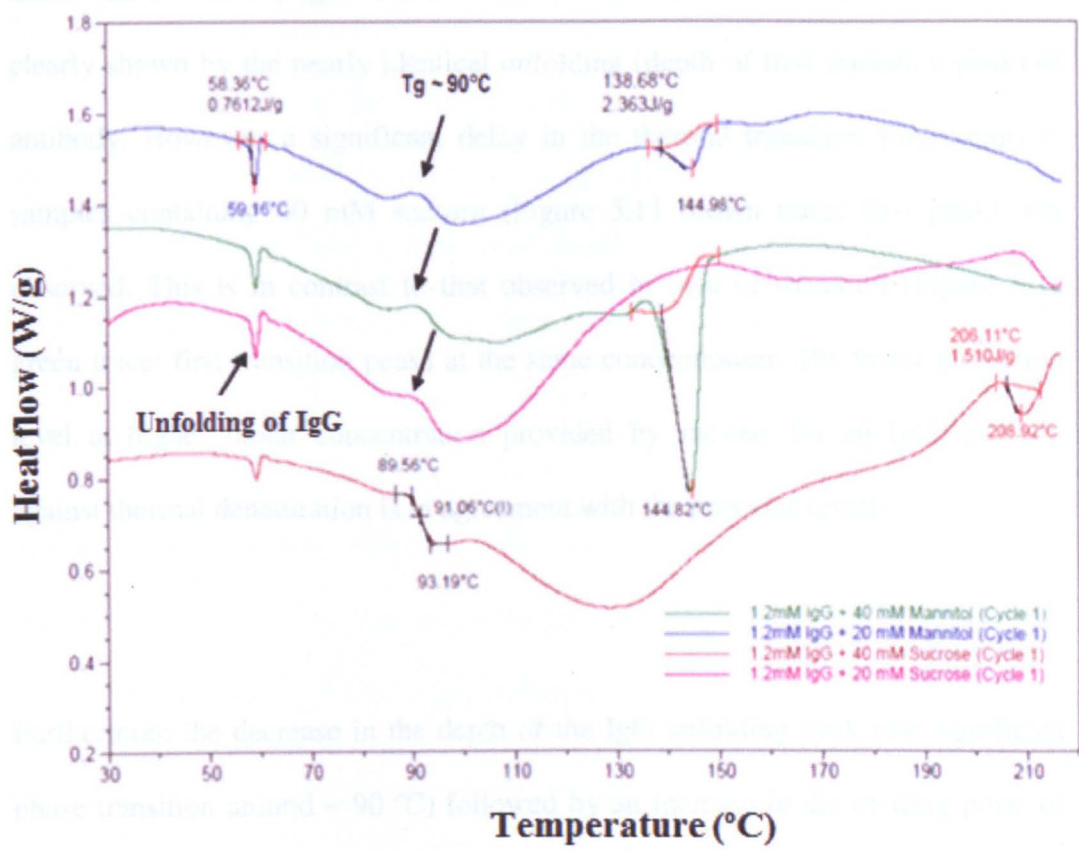


Figure 5.11 Overlaid standard DSC heating profiles of: 1.2 mM IgG lyophilized with mannitol [20 mM (blue trace), 40 mM (green trace)] and sucrose [20 mM (pink trace), 40 mM (brown trace)]. The formulations were heated up to 220 °C at the rate of 10 °C per minute. The inverted peak followed by the slope in the beginning of each trace correspond to the melting (Tm) of IgG and phase transition (Tg) around ~ 90 °C. The endothermic peak towards the extreme right of the each trace is an indicative of the melting point of sucrose/mannitol in the respective traces.

There was no significant shift in the melting temperature of IgG (changed from 58 °C to 59 °C) without any obvious unfolding of Fc fragment. The measured T_g and melting points of sucrose and mannitol on their own and with IgG (both alone and in combination) are shown in Table 5.5. The effect of sucrose (Figure 5.8 pink trace) and mannitol (Figure 5.8 blue trace) at 20 mM concentration is similar, as clearly shown by the nearly identical unfolding (depth of first transition peak) of antibody. However, a significant delay in the thermal transition (unfolding) in samples containing 40 mM sucrose (Figure 5.11 brown trace: first peak) was observed. This is in contrast to that observed in case of mannitol (Figure 5.11 green trace: first transition peak) at the same concentration. The better protection level at higher molar concentration provided by sucrose for an IgG antibody against thermal denaturation is in agreement with the previous results.

Furthermore the decrease in the depth of the IgG unfolding peak (the significant phase transition around ~ 90 °C) followed by an increase in the melting point of sucrose in the presence of high molecular weight IgG (150 kDa) is indicative of an enhanced protection given to IgG during lyophilization (Figure 5.11). The observed T_g for sucrose seems higher than that generally reported in literature (~ 58 – 70 °C) [240]. However, a T_g of sucrose around ~ 85 °C has been previously reported [240]. The increased T_g of sucrose could be probably attributed to the very fast initial freezing of the solution [13]. Secondly, some of the sucrose molecules held in between protein molecules immobilized in the viscous sucrose

matrix could lead to high activation energies prerequisite for any transition to occur completely [241 – 244].

Mannitol lyophilized with IgG, observed a significant decrease ($\sim 23\text{ }^{\circ}\text{C}$) in its melting point and surprisingly was also able to produce glass transition effect almost similar to that produced by sucrose. However, it is necessary to mention, that without any significant decrease in the melting point, mannitol failed to produce any transition phase when lyophilized on its own (Figure 5.9). This more likely demonstrates a kind of molecular interaction/configuration between the sugar (mannitol) and the potential influence of antibody on the ability of a sugar to produce a glass transition effect coupled with decrease in its melting point. The trapping of antibody within the amorphous medium (sucrose/mannitol) stops inter-protein interactions and also prevents antibody from getting exposed to stresses and therefore, does provide enhanced protection against denaturation.

5.6.3.3 Impact of sucrose and mannitol in combination

The representative melting curves of IgG (1.2 mM) lyophilized with sucrose and mannitol in combination, are shown in Figure 5.12. There was no significant change in the unfolding temperature of IgG in the combined formulations ($\sim 1\text{ }^{\circ}\text{C}$). It was also observed that by switching the molar concentrations of sucrose and mannitol from 1 : 2 to 2 : 1 in the combined formulation significantly improves the glass transition (T_g) from $\sim 90\text{ }^{\circ}\text{C}$ to $\sim 124\text{ }^{\circ}\text{C}$). Sucrose and mannitol (molar ratio

of 1 : 2) in combination provided a protective effect on the unfolding (first transition peak: blue trace) of IgG (1.2 mM) similar to that produced by sucrose or mannitol alone. In contrast, the protective effect in combination on the unfolding of IgG (first transition peak :green trace) significantly improved on switching the

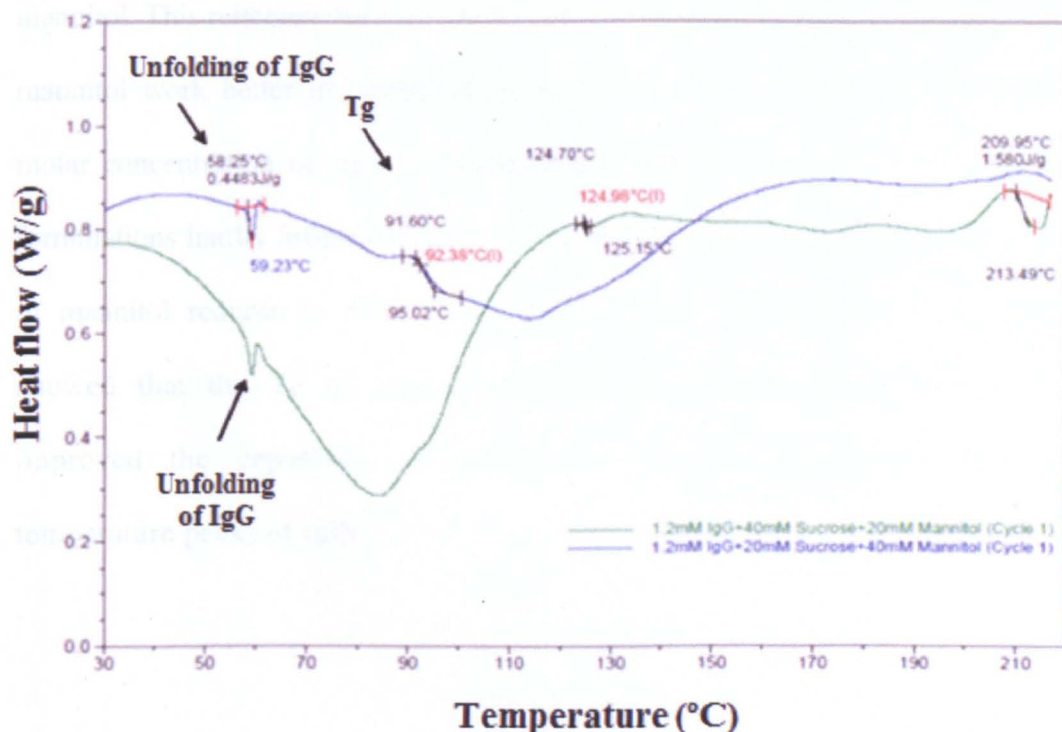


Figure 5.12 Overlaid standard DSC heating profiles of: 1.2 mM IgG lyophilized with sucrose and mannitol in combination. (i) 1.2 mM IgG + 20 mM sucrose + 40 mM Mannitol (blue trace) and (ii) 1.2 mM IgG + 40 mM sucrose + 20 mM mannitol (green trace) sucrose. The formulations were heated up to 220 °C at the rate of 10 °C per minute. The inverted peak in the beginning of each trace correspond to the melting (T_m) of IgG. Higher molar concentration of sucrose increases T_g in the combined formulation ~124 °C (green trace), whereas at higher molar concentration of mannitol T_g event takes place around ~90 °C. The melting point of sucrose increases even in the combined formulations, whereas melting point of mannitol reduces in combination as described in section (5.6).

molar concentrations of sucrose and mannitol from 1 : 2 to 2 : 1. This suggests, that even in the combined formulations, sucrose (40 mM) demonstrates the better protective ability. However, in the molar ratio of 2 : 1, it appears, that the glass forming propensity of sucrose (green trace) enhances in combination with mannitol. This reiterates the fact, earlier described by DLS results, that sucrose and mannitol work better in combination than sucrose alone. The exchange of the molar concentration of sucrose and mannitol from 1 : 2 to 2 : 1 in combined formulations hardly influences the melting point of sucrose, but the melting point of mannitol reduces ($\sim 50\text{ }^{\circ}\text{C}$) significantly (blue trace) [Figure 5.12]. DSC showed that the T_g of sucrose enhanced in combination with mannitol improved the capability of sucrose to suppress aggregation (melting temperature peak) of IgG.

Table 5.5 T_g and melting points of multiple times (1 – 7) lyophilized powdered IgG (AG – 6 – PDH) antibody formulations

No. of Cycles	Formulation	Protein:Excipient	Melting Point ($^{\circ}\text{C}$)	Melting Point ($^{\circ}\text{C}$)	T_g ($^{\circ}\text{C}$)
	(Powdered)	Concentration (mM)	First transition	of Excipient	
1	IgG	1.2 : 0	$\sim 58 \pm 0.15$	---	---
1	IgG + Sucrose (I)	1.2 : 20	$\sim 59 \pm 0.18$	$\sim 206 \pm 0.45$	$\sim 90 \pm 0.50$
1	IgG + Sucrose (II)	1.2 : 40	$\sim 59 \pm 0.15$	$\sim 207 \pm 0.87$	$\sim 91 \pm 0.20$
1	IgG + Mannitol (I)	1.2 : 20	$\sim 59 \pm 0.17$	$\sim 208 \pm 0.61$	$\sim 90 \pm 0.10$
1	IgG + Mannitol (II)	1.2 : 40	$\sim 59 \pm 0.12$	$\sim 209 \pm 0.56$	$\sim 90 \pm 0.30$
1	IgG + Sucrose + Mannitol (I)	1.2 : 20 : 40	$\sim 59 \pm 0.13$	$\sim 210, 120 \pm 0.29$	$\sim 92 \pm 0.34$
1	IgG + Sucrose + Mannitol (II)	1.2 : 40 : 20	$\sim 59 \pm 0.21$	$\sim 206 \pm 0.50$	$\sim 124 \pm 0.15$

* T_g indicates glass transition temperature,

(AG – 6 – PDH): antiglucose – 6 – phosphate dehydrogenase antibody

5.7 Conclusions

The present study provides a comprehensive analysis of the effect of repeated lyophilization on the aggregation, stability and protection of a polyclonal IgG antibody in combination with sugars, sucrose and mannitol. The tendency of IgG to aggregate increased during multiple cycles of lyophilization. The increase in the mean size of the globular IgG related features and their association with amorphous regions in the powdered formulations shown by AFM complements the DLS and DSC findings. The inhibitive effect of sucrose on the aggregation of IgG both alone as well as in combination with mannitol shown by DLS and AFM is consistent with literature. However, DSC disagrees with DLS in indicating failure of mannitol to reduce aggregation. The reason for this difference remains a topic for future research. This work could form the basis of a broad spectrum strategy to characterize, minimize and prevent aggregation in protein therapeutics through the screening of potential excipients.

Chapter 6

The effect of sucrose and mannitol on the secondary structure and morphology of polyclonal IgG during cycles of lyophilization

6.1 Introduction

Protein products lyophilized with a suitable lyoprotectants generally have fewer stability-related concerns and resist alterations to their structure than proteins lyophilized alone [12, 24, 32, 242]. The probable mechanisms of prevention and stabilization of lyoprotectants has been described in chapter 1. However, lyophilization poses challenges such as low temperature (cooling); freeze-concentration, ice-formation; and dehydration (expulsion of water molecules), from the abrupt alteration into the physical environment and the intensification in solute concentration, phase separation, and redistribution of solutes [13, 24, 242]. Moreover, lyophilization stresses can also enhance crystallization of the buffer and an initially amorphous excipient [238, 242]. The crystallization of an amorphous excipient can damage protein secondary structure and the desired physical property (cake and porous nature for better solubility and quicker

reconstitution) of the formulation. All these factors can contribute significantly to the biological inactivity of a protein [12, 238, 242].

In view of the above discussed significance of structural and physical properties required of a protein formulation, a study was conducted into the effect of sucrose and mannitol (alone and in combination) on the structural and morphological behaviour of a polyclonal IgG (antiglucose – 6 – phosphate dehydrogenase) antibody during multiple cycles of lyophilization. The dry formulations were stored at – 4 °C for several months, prior to their structural and morphological analysis. FT-IR in ATR mode was employed for the determination of any changes in the secondary structure [130, 200, 202]. SEM was introduced to provide physical insights into the multiple times lyophilized formulations of IgG [91, 111, 187].

6.2 Aims and objectives

The objectives of this study were to analyse the effect of sucrose and mannitol (alone and in combination in various molar ratios) on the structural and physical characteristics of a polyclonal IgG antibody during multiple cycles of lyophilization (MCL). These strategies would provide further insight for optimizing the effect of the indicated sugars on the intrinsic proficiency of IgG to resist possible structural and physical alterations. The achievement of

optimization to yield desired structural and physical attributes in the studied protein formulation would, therefore, be another contributory step towards the development of screening scheme that would enable to improve an overall therapeutic efficiency of IgG and other such proteins.

6.3 Materials

D – Sucrose (99 %); D – mannitol (98 %); were obtained from Sigma Aldrich. All other materials which were employed were as described in the section 4.3 of Chapter 4.

6.4 Sample preparation methodology

Move to Methods [Chapter 4]

6.4.1 Preparation of IgG formulations

IgG was lyophilized on its own, with sucrose and mannitol alone, and in combination with both exactly in the same manner as described in section 5.4.4.

6.4.2 Powdered formulations

IgG (1.2 mM) powdered formulations of IgG were prepared with sucrose and mannitol exactly in the manner described in the section (5.4.5.2)

6.5 Methods of analysis

6.5.1 Infra-red ATR-FTIR inspection

The structural studies were carried out using a Nicolet FT-IR-spectrometer in an identical manner as in the previous chapter 4.

6.5.2 Scanning electron microscopic examination

The morphological characteristics of the powdered formulations of IgG (lyophilized with sucrose and mannitol alone and in combination) were studied by SEM. The different parameters which were used in these experiments have been already described in Chapters 3 and 4.

6.6 Results and Discussion

6.6.1 Effect of sugars on secondary structure of powdered IgG

The influence of sucrose and mannitol on the structural stability of IgG was probed both in their individual capacity as well as in combination. Prior to start of these experiments, control experiments for both sugars were performed.

6.6.1.1 Sugar controls for Infra-red ATR – analysis

Secondary structures in the non-lyophilized and lyophilized powders of sucrose and mannitol were analysed by ATR. Sucrose and mannitol displayed molecular

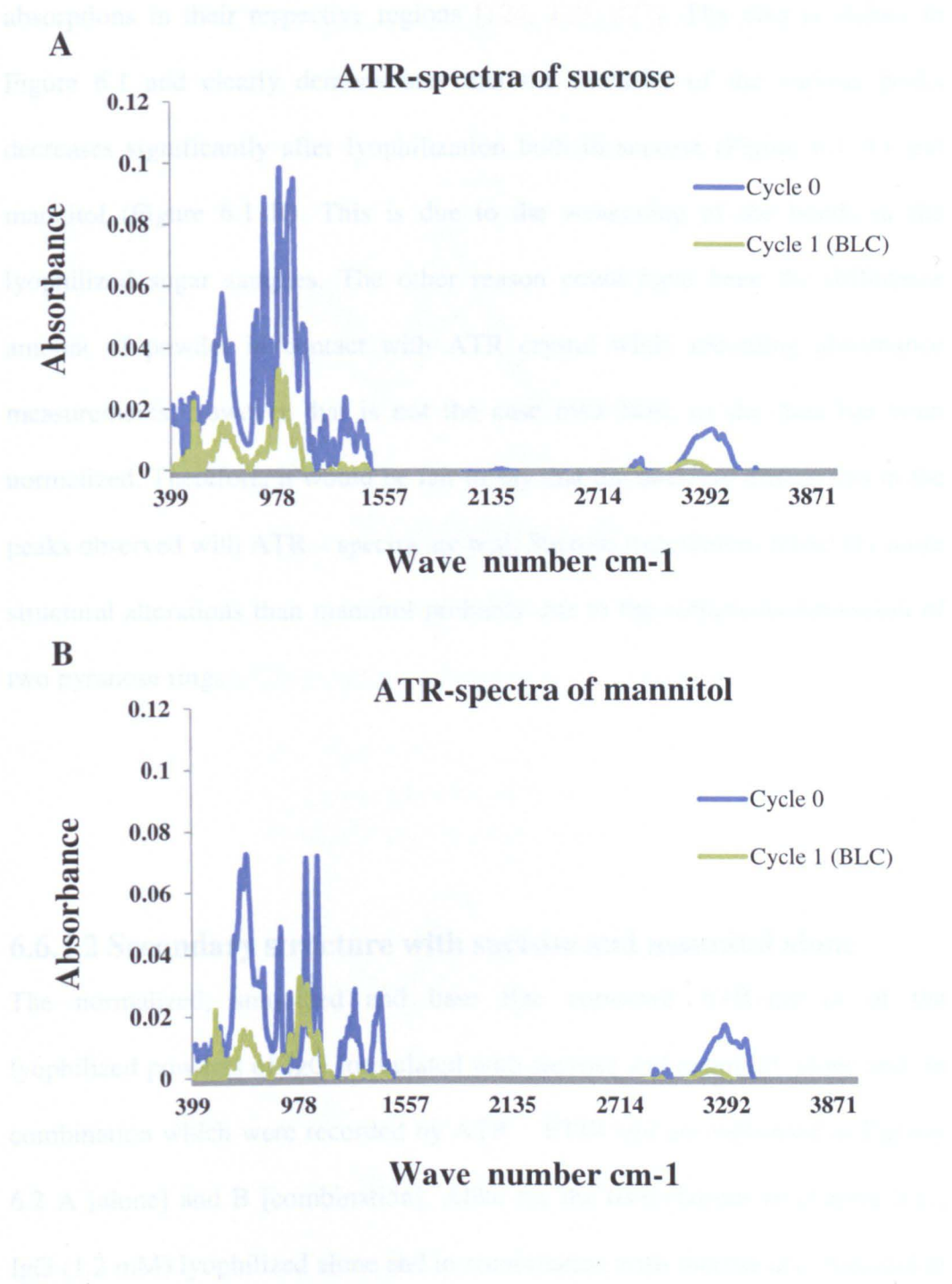


Figure 6.1 Overlaid, base line corrected ATR spectra of: non – lyophilized (blue trace) and lyophilized (green trace) sugars deposited on the clean surface of a glass slide using a diamond crystal. **[A]** Sucrose: **[B]** mannitol. Spectra were recorded between 4000 cm⁻¹ and 300 cm⁻¹. The peaks are bigger prior to lyophilization in both sugars.

absorptions in their respective regions [124, 129, 227]. The data is shown in Figure 6.1 and clearly demonstrates that the intensity of the various peaks decreases significantly after lyophilization both in sucrose (Figure 6.1 A) and mannitol (Figure 6.1 B). This is due to the weakening of the bonds in the lyophilized sugar samples. The other reason could have been the difference amount of powder in contact with ATR crystal while recording absorbance measurements; however that is not the case over here, as the data has been normalized. Therefore, it would be fair to say that the intensity differences in the peaks observed with ATR – spectra are real. Sucrose experiences relatively more structural alterations than mannitol probably due to the collapse/compression of two pyranose rings.

6.6.1.2 Secondary structure with sucrose and mannitol alone

The normalized, smoothed and base line corrected ATR-spectra of the lyophilized powders of IgG formulated with sucrose and mannitol alone and in combination which were recorded by ATR – FTIR and are presented in Figures 6.2 A [alone] and B [combination]. Alike for the formulations in chapter four, IgG (1.2 mM) lyophilized alone and in combination with sucrose and mannitol at both concentrations (20 mM and 40 mM) displayed two characteristic molecular absorptions in the regions from (1690 – 1638 cm^{-1}) and (1568 – 1517 cm^{-1}) which respectively correspond to amide bands I and II [124,129, 187, 200, 205].

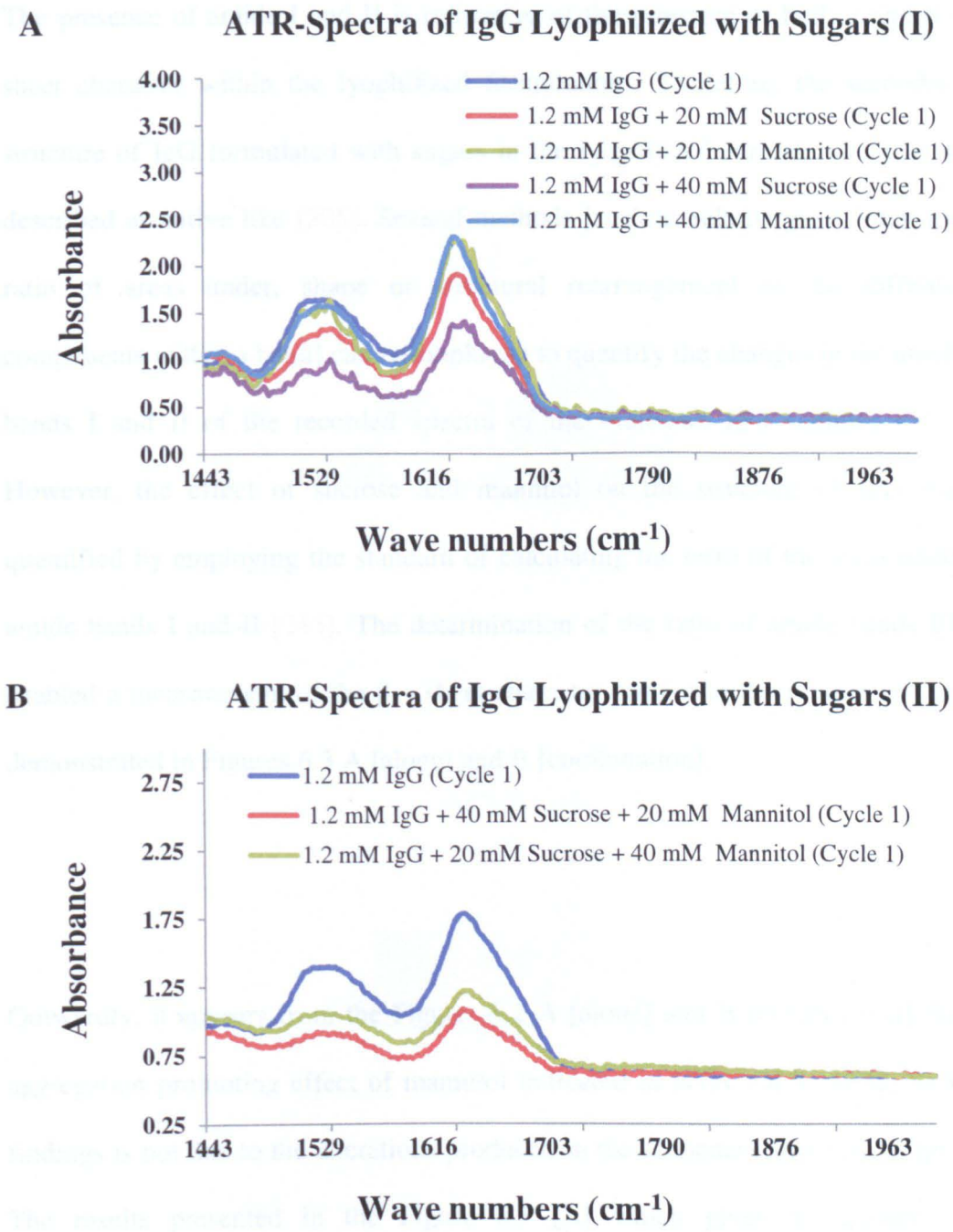


Figure 6.2 Overlaid, base line corrected and normalized FTIR-ATR spectra of: lyophilized IgG [formulated with sucrose and mannitol] deposited on the clean surface of a glass slide. [I]:- when used separately and [II] when introduced in combination [II]. Spectra were recorded between 1300 and 2000 cm⁻¹. The two main peaks towards right under each curve correspond to amide bands I and II.

The presence of amide I and II is indicative of the presence of both α and β – sheet character within the lyophilized formulations. Therefore, the secondary structure of IgG formulated with sugars in the lyophilized formulations can be described as native like [205]. Several methods [such as relative peak intensity, ratio of areas under, shape or structural rearrangement of the different components within a band] can be employed to quantify the changes in the amide bands I and II of the recorded spectra of the indicated IgG samples [225]. However, the effect of sucrose and mannitol on the structure of IgG was quantified by employing the standard of calculating the ratio of the areas under amide bands I and II [244]. The determination of the ratio of amide bands I/II enabled a measurement of the β – sheet character present in the protein and are demonstrated in Figures 6.3 A [alone] and B [combination].

Outwardly, it appears from the Figures 6.2 A [alone] and B [combination] that aggregation promoting effect of mannitol indicated in NTA, DLS, AFM, SEM findings is not due to the alterations produced in the secondary structure of IgG. The results presented in the Figure 6.3 [A] which gives an account of individual effect, suggested no significant change in the amide I/II ratio for IgG lyophilized with mannitol [green bars (20 mM); light blue bars (40 mM)]. However, in case of IgG lyophilized with sucrose (20 mM and 40 mM), an increase in the ratio of amide bands (I/II) suggest of the ability of sucrose to

maintain IgG secondary structure. However, results from the Figure 6.3 [B], which give an account of the combined effect, indicate some change in the amide

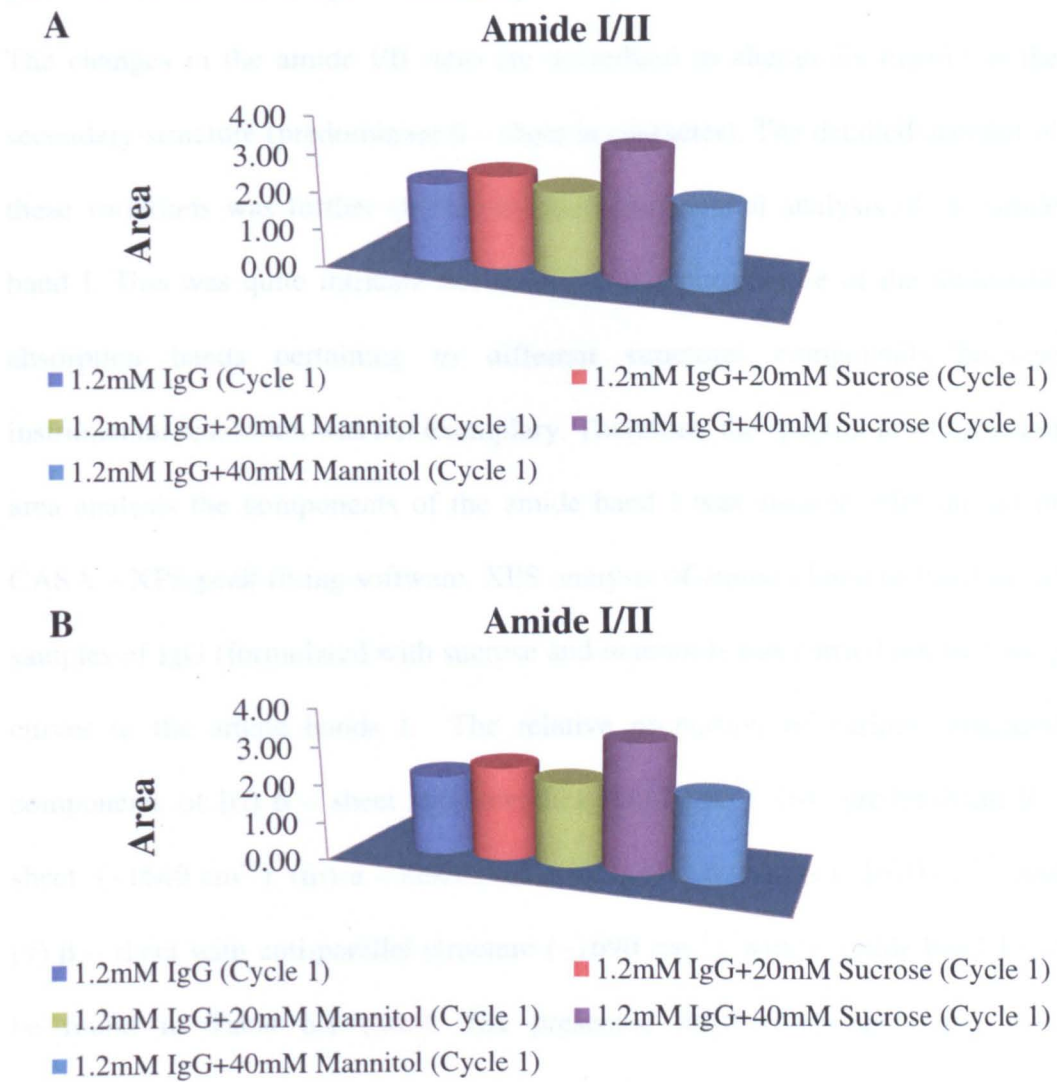


Figure 6.3 Ratio of areas under bands I and II of : lyophilized IgG formulated with sucrose and mannitol : - [A] Separate; and [B] in combination. The standard deviation of (SD ~ 0.07) recorded for three sets of measurements recorded for each sample. Influence of sucrose (40mM) has a significant impact on the amide I/II ratio both alone and in combination.

I/II ratio for IgG lyophilized with 20 mM sucrose and 40 mM mannitol [red bar] and this effect became more significant when molar concentration of sucrose and mannitol were switched from 1 : 2 to 2 : 1. Consequently demonstrating enhanced protection to IgG's secondary structure when more sucrose was used. The changes in the amide I/II ratio are accredited to alterations mainly in the secondary structure (predominant β – sheet in character). The detailed account of these variations was further studied by the componential analysis of an amide band I. This was quite intricate due to the overlapping nature of the molecular absorption bands pertaining to different structural components because instrumental resolution was not exemplary. Therefore, the spectral resolution and area analysis the components of the amide band I was ensured with an aid of CASA – XPS peak fitting software. XPS-analysis of amide I band of lyophilized samples of IgG (formulated with sucrose and mannitol) was carried out by fitting curves to the amide bands I. The relative proportion of various structural components of [(i) β – sheet side stretches (1617 cm^{-1}), (ii) predominant β – sheet ($\sim 1640\text{ cm}^{-1}$), (iii) α – helix (1652 cm^{-1}), (iv) β – turns ($\sim 1670\text{ cm}^{-1}$) and (v) β – sheet with anti-parallel structure ($\sim 1690\text{ cm}^{-1}$), within amide band I can be found in Table 6.1 [206]. The presented band components and their corresponding areas serve as a method for the determination of alterations in the secondary structure within the amide band. I, which otherwise appear insignificant when only the amide I/II ratio is taken into account. From the Table 6.1, it is clear that IgG lyophilized with both sucrose and mannitol shows considerable change in structural rearrangement happening amongst the

individual components within the amide band I. In response to this effect of structural rearrangement as a consequence of lyophilization, the ability of sucrose to resist alteration in each individual structural component was significantly higher than mannitol both alone and in combination.

It can be found from the Table 6.1, that the concentration of the main β – sheet structural component in IgG reduced by about 27.5 % (at 20 mM) and 10.7 % (at 40 mM) in the case of mannitol. In contrast, such reduction was only 12 % in IgG formulated with 20 mM sucrose. Furthermore, doubling the molar concentration of sucrose from 20 mM to 40 mM yielded a 7 % increase in the main β – sheet structural component. Similar effects can be found for the concentration of amino acid side chains, β – turns and β – sheet with antiparallel structure. The α – helical content disappeared in IgG lyophilized with sucrose (20 mM) and mannitol 40 mM). For a sugar alone, the least altered structural rearrangement of all the indicated individual components (α and β) was observed in IgG lyophilized with sucrose (40 mM), whereas the best protection against overall alteration of structural components was achieved in case of IgG lyophilized with sucrose and mannitol in a combination in their molar ratio of 40 mM and 20 mM respectively [Table 6.1, Part II]. This minimization of the extent of structural variation within the amide band I is indicative of a decrease in the propensity of aggregation.

Table 6.1 Analysis the effect of sucrose and mannitol on different structural components stationed within amide band I, based on percentage and area

Part I. Individual effect

Amide band I (~1690-1600 cm ⁻¹)	Component 1 β – sheet <i>Amino-acid Side chains</i> (~1615 -1620 cm ⁻¹) (~ 1617 cm ⁻¹)	Component 2 β – sheet <i>Main in the Middle Amide I</i> (~1628 -1645 cm ⁻¹) (~ 1639 cm ⁻¹)	Component 3 α – helix (~1650 -1658 cm ⁻¹) (~ 1652 cm ⁻¹)	Component 4 β – turns (~1660 -1677 cm ⁻¹) (~ 1670 cm ⁻¹)	Component 5 β – sheet <i>Anti-parallel structure</i> (~1686 -1697 cm ⁻¹) (~ 1690 cm ⁻¹)
Range					
Peak position					
IgG (% : area)	2 : 4.1	55.37 : 110.7	10.5 : 20.1	2.02 : 4	30.5 : 6.1
IgG + 20 mM Sucrose	1.87 : 2.4	43.41 : 55.7	0 : 0	52.6 : 64.9	4.14 : 5.3
IgG + 40 mM Sucrose	1.65 : 3	62.52 : 64.40	4.3 : 7	1.97 : 2.3	29.7 : 30
IgG + 20 mM Mannitol	12.48 : 20.4	26.64 : 943.6	16.15 : 26.4	30.28 : 49.6	14.45 : 23.6
IgG + 40 mM Mannitol	0 : 0	44.63 : 61.6	0 : 0	33.6 : 46.4	21.73 : 30

Table 6.1 Part II. Effect in Combination					
Amide band I (~1690-1600 cm ⁻¹)	Component 1 β – sheet <i>Amino-acid Side chains</i>	Component 2 β – sheet <i>Main in the Middle Amide I</i>	Component 3 α – sheet	Component 4 β – turns	Component 5 β – sheet <i>Anti-parallel structure</i>
Range	(~1615 -1620 cm ⁻¹)	(~1628 -1645 cm ⁻¹)	(~1650 -1658 cm ⁻¹)	(~1660 -1677 cm ⁻¹)	(~1686 -1697 cm ⁻¹)
Peak position	(~ 1617 cm ⁻¹)	(~ 1639 cm ⁻¹)	(~ 1652 cm ⁻¹)	(~ 1670 cm ⁻¹)	(~ 1690 cm ⁻¹)
IgG (% : area)	2 : 4.1	55.37 : 110.7	10.5 : 20.1	2.02 : 4	30.5 : 61.1
IgG + S + M (20 mM + 40 mM)	0 : 0	48.7 : 25.0	0 : 0	30.8 : 15.9	20.6 : 10.5
IgG + S + M (40 mM + 20 mM)	1 : 3.6	57.8 : 37.8	4 : 6.7	6.2 : 7.6	29 : 20

However, irrespective of the ability of sucrose to prevent aggregation at an optimum concentration alone and in combination with mannitol, aggregation still occurs to some extent due to structural alterations such as rearrangement in the β – sheet structural components especially side chains, which may potentially weaken the protein structure. More importantly sliding of side chains can aggravate both intra and inter-protein interactions by enhancing attractive electrostatic interactions between oppositely charged hydrophilic residues, which otherwise remain distant from each other. Therefore, these reasons could probably also explain the unfolding of Fabs or exothermic aggregation peak (depth of the first transition peak) for DSC analysis of IgG presented in Chapters 4 and 5. The proportion of completely or partially unfolded molecules within the aggregates depends on the intensity of structural rearrangement (proportion of β – sheet). The presence of sucrose in lyophilized formulations in IgG both alone and in combination induced the least alteration in the concentration of β – sheet structural components. Subsequently, the degree of aggregation would be correspondingly reduced in the sample that has been lyophilized with an optimum amount of sucrose as we observed in IgG lyophilized with higher molar concentration of sucrose both alone and in combination.

6.6.2 Morphological examination

6.6.2.1 SEM controls sucrose and mannitol

SEM control experiments for lyophilised mannitol and sucrose are presented in Figure 6.4. Both sucrose and mannitol were formulated in 0.01 M PBS prior to lyophilization. SEM images of non-lyophilized sucrose showed the expected well defined cuboidal morphology. The incubation, for a period of three to four hours following lyophilization transforms amorphous sucrose to crystalline state under certain conditions (33 % relative humidity at 25 °C) has been discovered in the previous studies [245]. In the similar studies here, micrographs obtained with lyophilized sucrose powder indicate the formation predominant amorphous like structures with less significant growth of likely crystalline structures (Figure 6.4 middle panel). This is in contrast to that observed in mannitol, which exhibited a strong tendency to crystallize during lyophilization (Figure 6.4 Bottom Panel).

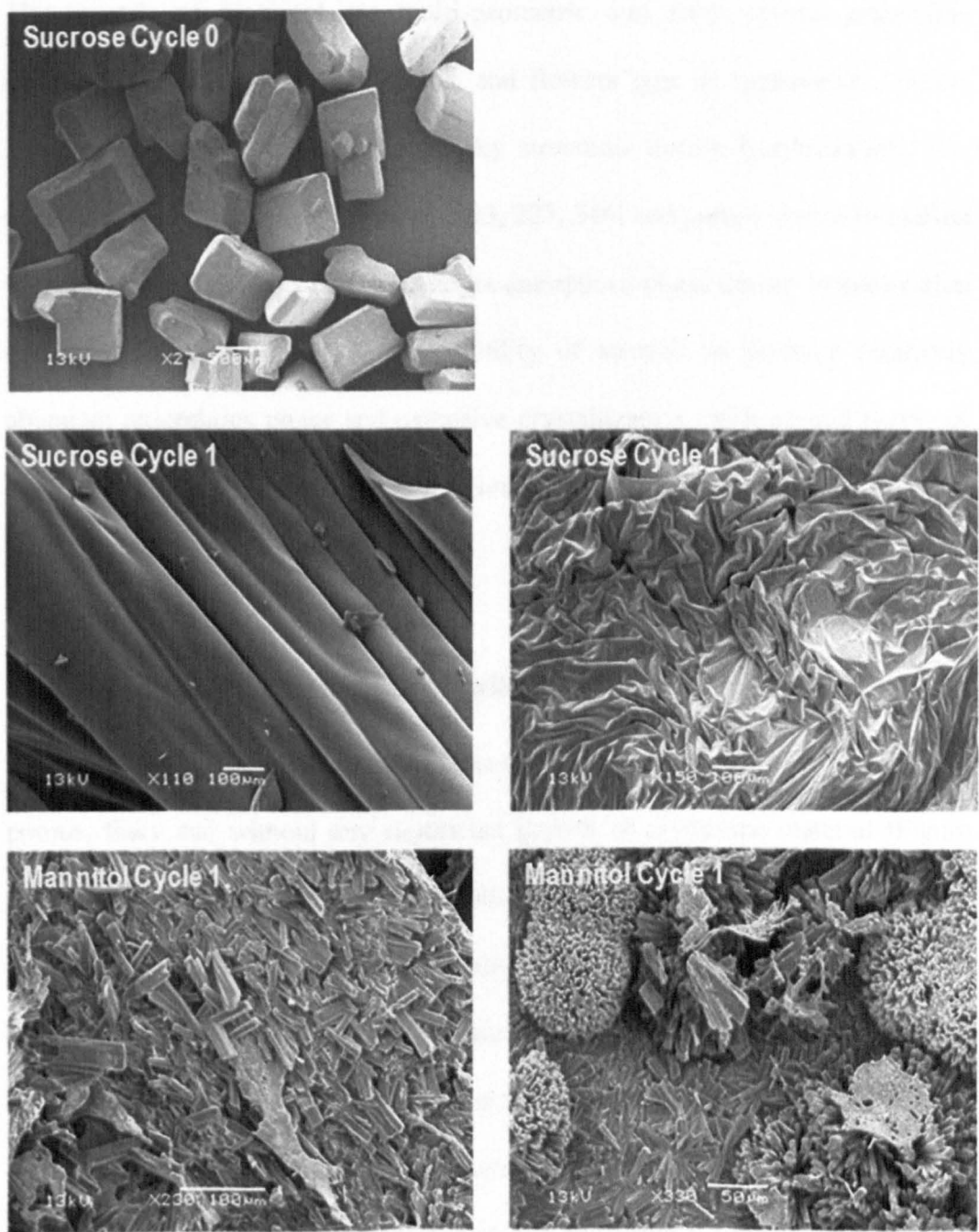


Figure 6.4 SEM images of lyophilized sucrose and mannitol controls: Except the top one, both scans in each panel represent two different locations of the same sample. Different scan sizes obtained at a magnification of 13 kV.

The crystals of mannitol are multi-geometric and form several crystalline architectures such as needles, stripes, and flowers type in appearance. Unlike, sucrose, mannitol appears to form flaky structures during lyophilization. The exclusive crystallization of mannitol [223, 227, 246] and partial crystal formation by sucrose from aqueous solution and its amorphous phase during lyophilization has been reported [10, 223]. This ability of sucrose to produce relatively abundant amorphous phase and extensive crystallization (with several types) of mannitol differentiated by SEM, compliments AFM results presented in Chapter 5.

6.6.2.2 Comparative behaviour with sucrose and mannitol

Visually the surfaces of the formulations of IgG lyophilized with sucrose appeared porous, flaky and without any significant growth of crystalline material [Figure 6.5]. Without changing the molar concentration of protein, an increase in the molar concentration of sucrose enhanced porosity and flakiness of the powdered formulation. In contrast, the effect of mannitol was quite different to that observed for sucrose [Figure 6.6]. The porosity and flakiness was significantly reduced with the abundant growth of crystalline structures in IgG lyophilized with mannitol. With increase in the concentration of mannitol, the visual growth in the crystalline material, denseness and consistent decline in the porosity is an indicative of the poor capability of mannitol to interact with IgG due to its susceptibility to crystallize.

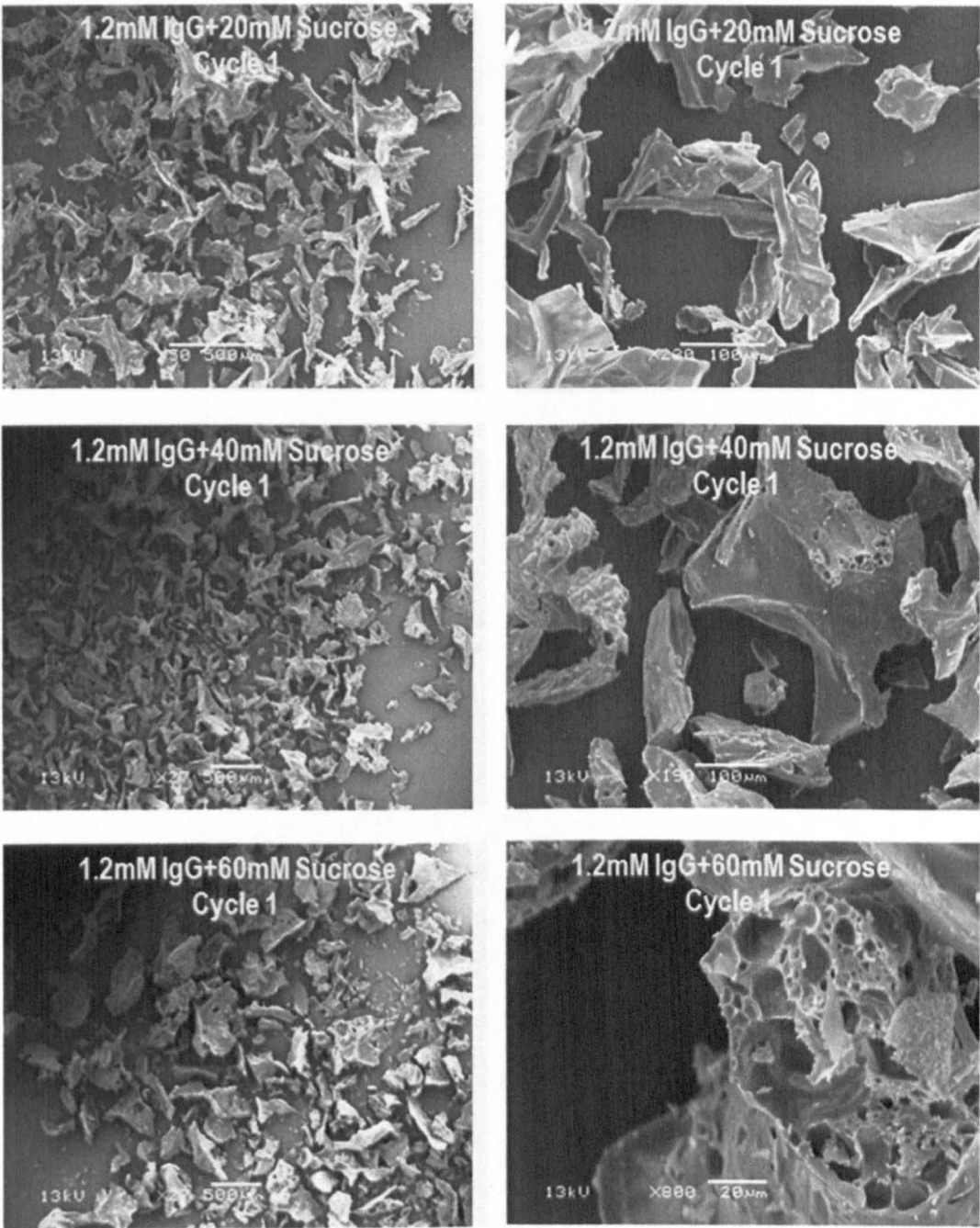


Figure 6.5 SEM images of 1.2 mM IgG lyophilized with sucrose: 1 : 20 [Top panel], 1 : 40 [Middle panel] 1 : 60 [Bottom panel]; both scans in each panel represent two different locations of the same sample. Different scan sizes obtained at a magnification of 13 kV.

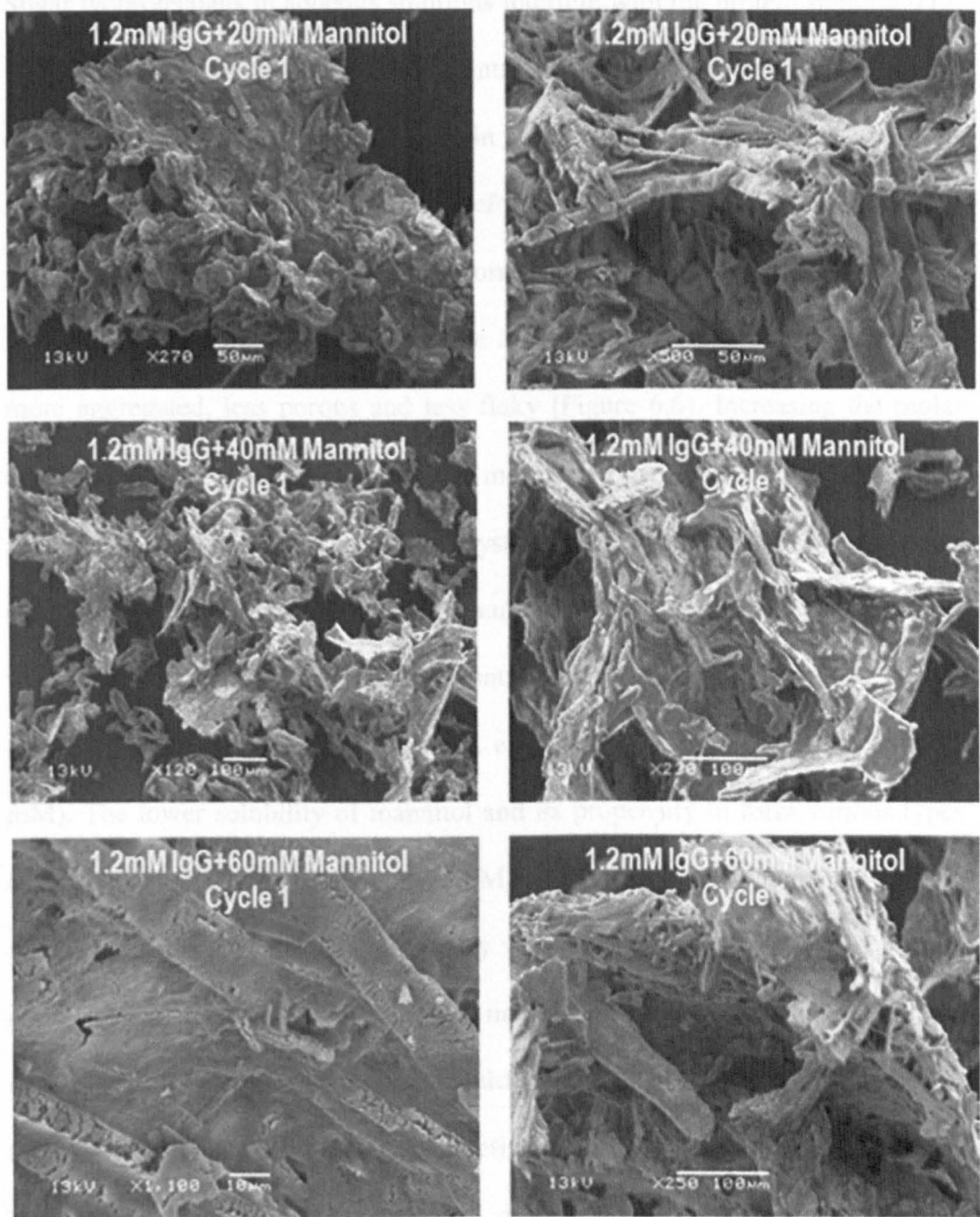


Figure 6.6 SEM images of 1.2 mM IgG lyophilized with mannitol: 1 : 20 [Top panel], 1 : 40 [Middle panel] 1 : 60 [Bottom panel]; both scans in each panel represent two different locations of the same sample. 50 – 100 micron scans obtained at a magnification of 13 kV.

Sugar lyoprotectants in aqueous solutions interfere with the protein stability, [12, 131,134, 221]. Generally lyoprotectants are often employed in a higher concentration than the therapeutic protein itself; their precipitation traits (such as solubility and crystallization) will therefore govern the precipitation dynamics and the morphology of the final dried formulation. Mannitol due to its tendency to crystallize (Figure 6.4) resulted in the appearance of particle families that are more aggregated, less porous and less flaky [Figure 6.6). Increasing the molar concentration of mannitol resulted in more agglomeration of the amorphous particles and promoted the growth of crystalline strip like features. Formulations containing sucrose resulted in a large number of homogenous smaller particles with porous surfaces (Figure 6.5). In contrast, mannitol-containing formulations resulted in less homogeneous particles, even at lower molar concentration (20 mM). The lower solubility of mannitol and its propensity to form various types of crystal structures [as shown by AFM in Chapter 5 and Figure 6.4-bottom panel], probably denature the secondary structure of the IgG molecules, which could lead to increase in inter-protein interaction and hence aggregation. The diversity in the particle morphology could also be attributed to the difference in the extent of denaturation of the interacting protein molecules, how do they interact and their orientation/alignment during their interaction, which in-turn could be influenced by the type of crystal formed by mannitol during lyophilization. On the other hand, in comparison to mannitol, the formation of predominantly less crystals with relatively insignificant structural diversity them, therefore, would serve as the likely explanation for sucrose being able to

potentiate the formation of relatively porous, flaky and much smaller aggregates of IgG. These indicated characteristics are important in order to achieve desired therapeutic standard.

6.2.2.3 Influence of sucrose and mannitol in combination

The surfaces of the formulations of IgG lyophilized with sugars in combination visibly demonstrate increased porosity, flakiness and smaller sized agglomerates without any significant growth of crystalline material [Figure 6.7]. IgG with both sugars gives the impression of producing much smaller agglomerated flaky features than when IgG was lyophilised with sucrose and mannitol individually. Formulations containing sucrose and mannitol in equal molar concentration appeared more homogeneous [Figure 6.7 top panel]. Switching of the molar concentration ratio of sucrose and mannitol from 1 : 2 – 2 : 1 produces an effect that is completely the best in terms of porosity, flakiness, and reduced crystallinity, when it comes to optimization [Figure 6.7 middle panel; right image]. In contrast, increasing the molar concentration of mannitol decreased porosity and promoted the growth of flaky agglomerates even in the combined formulations [Figure 6.7 middle panel, left image]. This indicates an inhibitory effect of sucrose on the crystallization of mannitol during lyophilization and this influence becomes clearer at higher molar concentration of sucrose [Figure 6.7 bottom pannel]. SEM images confirmed that the extensive crystallization propensity of mannitol (on its own) is reduced with IgG. However, sucrose once

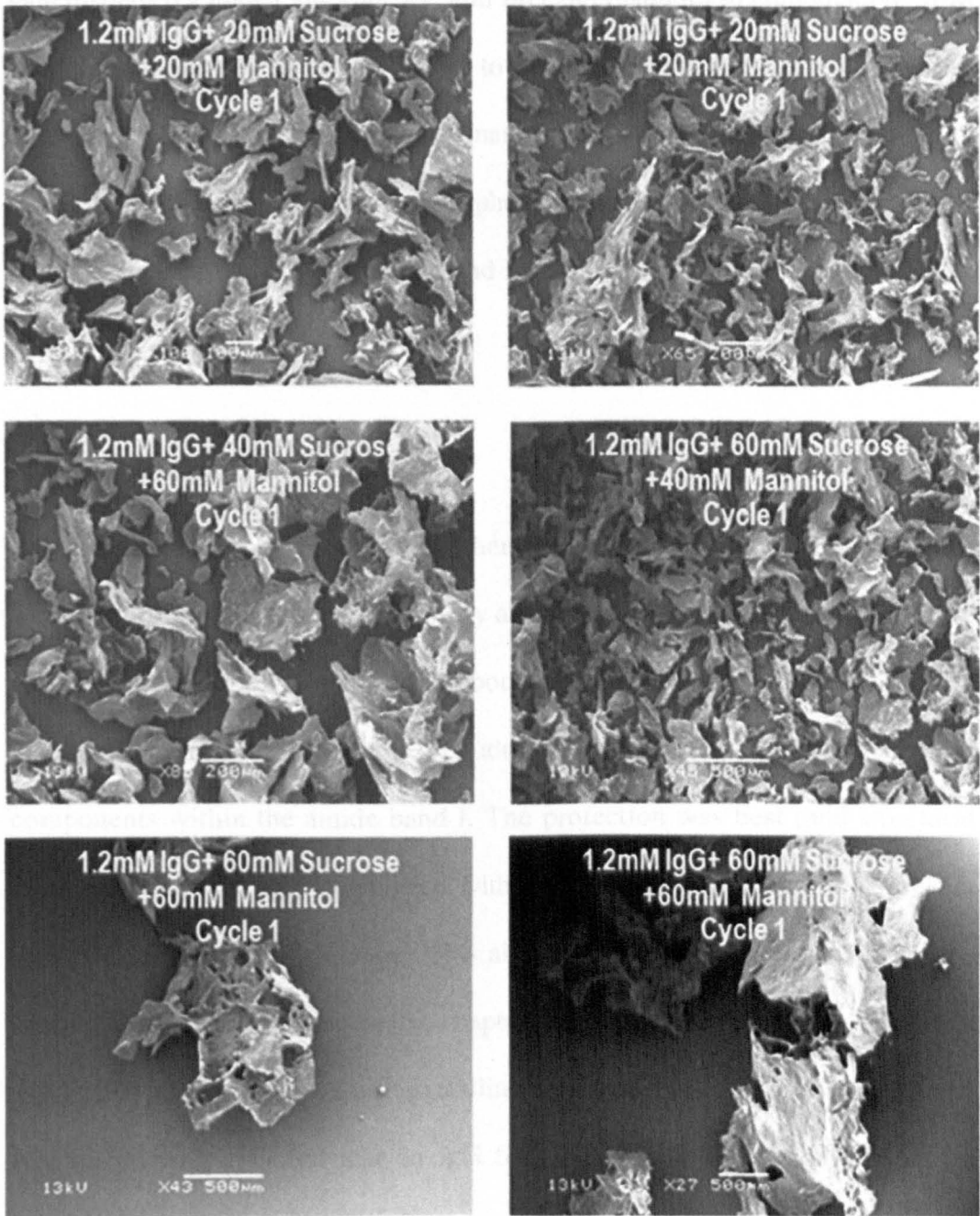


Figure 6.7 SEM images of 1.2mM IgG lyophilized with sucrose and mannitol in combination: 100 – 500 micron scans obtained at magnification between 13 kV. 1 : 20 : 20 [Top panel – both scans, two different locations of the same sample]; 1 : 40 : 60 [Middle panel – left scan]; 1 : 60 : 40 [Middle panel right scan]; 1 : 60 : 40 [Bottom panel – both scans, two different locations of the same sample].

gain displayed a higher amorphicity with IgG and mannitol in combination. SEM results demonstrated an effect similar to AFM findings, and suggested greater defensive propensity of sucrose than mannitol on IgG during lyophilization on the basis of its ability to form an amorphous material with IgG, indicative of an intimate association between sucrose and IgG.

6.7 Conclusions

The present study provides a comprehensive analysis of the effect of sucrose and mannitol on the structural stability and morphological traits of IgG during lyophilization on polyclonal IgG antibody. Sucrose showed a superior ability compared to mannitol in opposing alterations in the secondary structural components within the amide band I. The protection was best (and structural alterations least) in IgG lyophilized with sucrose at 40 mM. This is consistent with our AFM and DLS findings. This also lies in agreement with AFM results in chapter 5 and SEM results in this chapter, where relative increase in the size of aggregates and proportion of crystalline material was much larger in IgG lyophilized with mannitol than in IgG formulated with sucrose. Moreover, an increase in the magnitude of unfolding peak (depth of the first transition peak) during lyophilization with mannitol revealed by DSC results in Chapter 5 complements the fact that secondary structural alterations within the components shown by FT-IR destabilized the intra-protein bonded complex, and consequently, reduced the thermal stability of IgG. SEM findings demonstrated

an increase in the propensity of IgG with mannitol, to form crystalline and tightly packed formulation and this effect was enhanced with an increase in the concentration of mannitol. On the other hand, IgG formulated with sucrose displayed better porosity and flakiness and less crystallinity than with mannitol. The desired morphological characteristics enhanced in IgG when formulated with sucrose (40 mM) and in combination with mannitol (60 mM).

Chapter 7

An examination of the effect of multiple cycles of lyophilization on antigen-binding activity of IgG (Polyclonal) alone and with sugars

7.1 Introduction

With the introduction of hybridoma technology by Kohler and Milstein [247], and the subsequent development of monoclonal antibodies with highly specific interactions with antigens of interest, the target specific destruction of a disease became an evident reality. The antibodies have also been used as carriers for drugs to the site of the infection [248]. In the modern day, antibody – therapeutics represent an important class of medicines for a number of diseases such as autoimmune, cardiovascular, infectious diseases, cancer and inflammation [249, 250]. With significant advances made in antibody based therapy for malignancies such as breast cancer, colorectal cancer and lymphoma [249, 250], there has been a growing demand to develop new and modified antibody therapeutics. For this reason and the potential immunogenicity caused by the murine antibodies when used on their own, the original murine antibody

(of mouse origin) has been engineered into a chimeric or humanized antibody. The fusing of murine variable domains (antigen binding) with constant domains of human antibody results into the creation of a chimeric antibody (70 % human and equipped with full human Fc), which has been reportedly less immunogenic [251]. Using CDR- grafting methods, a humanized antibody is produced when the hyper-variable loops in the murine antibody are completely replaced by those in the human antibody. Humanized antibodies have been reported to be less immunogenic and 85 – 90 % human [252]. Humanization means the conversion of non-human antibody to a human-like antibody in order to circumvent the human immune system. It involves either the replacement of constant regions of murine mAbs with those of a human mAb or modification of the protein sequences in the constant regions and variable framework regions of non-humanized antibody to increase their resemblance to antibody variants occurring naturally in humans. This is achieved by grafting the non-humanized complementarity-determining regions (CDRs) onto a human antibody framework, resulting in more human like antibodies with reduced immunogenicity. Table 7.1 shows some of the mAbs under the final stages of clinical approval, whereas Table 7.2 presents a list of murine, chimeric and humanized monoclonal antibodies already approved by FDA for therapeutic use [249, 250, 253].

Table 7.1 Monoclonal antibodies in late stages of clinical trials [249]

Description	Target	Indication	Sponsor
Ch14.18. chimeric mAb	GD2	Neuroblastoma. Used in combination with chemotherapy radiotherapy and colony-stimulating factors	NCI
Rencarex (WX-9250; cG250) chimeric mAb	G250 antigen	Nonmetastatic kidney cancer. Used after surgery	Wilex
MDX-010 humanized mAb	CTLA-4	Melanoma. Used alone and in combination with gp100 peptide vaccine	Medarex
Panitumumab (ABX-EGF) human mAb	EGFR	Non-small cell lung cancer	Abgenix/ Immunex
Remitogen (Hu1D10) humanized mAb	MHC class II	Non-Hodgkin lymphoma	Protein Design Labs

Table 7.2 Therapeutic Monoclonal Antibodies Approved For Therapeutic Use [250]

Generic name	Trade name	Antibody format	Antigen	Approved indication	¹³ FDA approval	¹³ EMA approval
Muromonab	Orthoclone	Murine, IgG2a	CD3	Allograft rejection in allogeneic renal transplantation	86/06/19	NA
Abciximab ¹	ReoPro	Chimeric, IgG1	GP1Ib/IIIa r	Maintenance of coronary patency	94/12/22	NA
Rituximab ²	Mabthera	Chimeric, IgG1	CD20	CD20-positive B-cell non-Hodgkin's lymphoma	97/11/26	98/06/02
Dacizumab	Zenapax	Humanized, IgG1	CD25 (IL2r)	Allograft rejection	97/12/10	99/02/26
Basiliximab	Simulect	Chimeric, IgG1	CD25 (IL2r)	Allograft rejection	98/05/12	98/10/09
Palivizumab	Synagis	Humanized, IgG1	Protein F	Respiratory syncytial virus (RSV inhibitor) in children	98/06/19	99/08/13
Infliximab	Remicade	Chimeric, IgG1	TNF α	Crohn's disease and rheumatoid arthritis	98/08/24	99/08/13
Trastuzumab	Herceptin	Humanized, IgG1	HER2/Neu	Metastatic breast cancer	98/09/25	00/08/28
Etanercept ³	Enbrel	huFc γ 1/TNFr	TNF α and β	Autoimmune diseases such as ankylosing spondylitis	98/11/02	00/02/03
Gemtuzumab ⁴	Mylotarg	Humanized, IgG4	CD33	CD33-positive acute myeloid leukemia	00/05/17	NA
Alemtuzumab ⁵	Mabcampath	Humanized, IgG1	CD52	B-cell chronic lymphocytic leukemia	01/05/07	01/07/06
Ibritumomab ⁶	Zevalin ⁹⁰ Y	Mouse, IgG1	CD20	B-cell non-Hodgkin's lymphoma	02/02/19	04/01/16
Adalimumab ⁷	Trudexa	Human, IgG1 (PD)	TNF α	Crohn's disease and rheumatoid arthritis	02/12/31	03/09/01
Alefacept ³	Amevive	huFc γ 1/LFA-3	CD2	Chronic plaque psoriasis	03/01/30	NA
Omalizumab	Xolair	Humanized, IgG1	IgE	Treatment of asthma	03/06/20	05/10/25
Tositumomab ^{6,8}	Bexxar ¹³¹ I	Murine, IgG2a	CD20	CD20-positive B-cell non-Hodgkin's lymphoma	03/06/27	NA
Efalizumab	Raptiva	Humanized, IgG1	CD11a	Moderate to severe plaque psoriasis	03/10/27	04/09/20
Cetuximab	Erbix	Chimeric, IgG1	EGFR	Metastatic colorectal and head and neck carcinoma	04/02/12	04/06/29
Bevacizumab	Avastin	Humanized, IgG1	VEGF-A	Metastatic colorectal and non-small cell lung carcinoma	04/02/26	05/01/12
Natalizumab ⁹	Tysabri	Humanized, IgG4	Integrin- α 4	Multiple sclerosis	04/11/23	06/06/27
Ranibizumab	Lucentis	Humanized, IgG1	VEGF-A	Wet-type age-related macular degeneration	06/06/30	07/01/22
Panitumumab ¹⁰	Vectibis	Human, IgG2	EGFR	Metastatic colorectal carcinoma	06/09/27	07/12/19
Ecuzumab ¹¹	Soliris	Humanized, IgG2/4	C5	Paroxysmal nocturnal haemoglobinuria	07/03/16	07/06/20
Certolizumab ¹²	Cimzia	Humanized, IgG1	TNF α	Crohn's disease	08/04/18	NA

The antibodies or fragments approved for therapeutic use (Table 7.1) like other protein based formulations are generally stored in a dry form (lyophilized) owing to their propensity to aggregate in solution as discussed in Chapter 1. Therefore, from a pharmaceutical point of view, amongst the several characteristics to be examined, the capability to bind an antigen or the activity of the therapeutic antibodies after lyophilization and reconstitution is clearly a significant parameter that needs to be explored. This is because specific recognition at a molecular level is the fundamental requirement for an active therapeutic [254]. Such molecular recognition is governed by the specific interaction of multiple non-covalent bonds such as electrostatic, electro-dynamic (van der Waals), hydrogen bonds or hydrophobic interactions.

7.1.1 Mechanisms of action of therapeutic antibodies

A brief description of the five reported mechanisms (see Figure 7.1) of antibody-antigen interaction; from pathogenic point of view are provided:

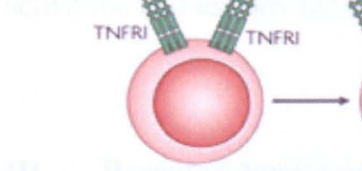
I. Ligand blockade

This mechanism involves blocking of the binding site of the ligand (antigen) and therefore prevents activation of cognate receptors of ligands. The blocking could be facilitated either by whole therapeutic antibody (IgG) molecule or by an antibody fragment or receptor immunoadhesins.

II. Receptor Modulation

1. Ligand Blockade

Antibodies can block the interaction of ligands with their receptors.



Ligand blockade

III. Receptor Blockade

Antibodies can block the interaction of ligands with their receptors.



Receptor blockade

IV. Receptor Down Regulation

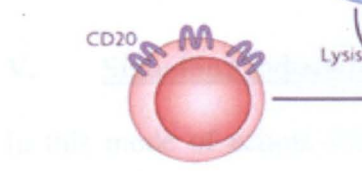
Antibodies can block the interaction of ligands with their receptors.



Receptor down regulation

V. Depletion

Antibodies can block the interaction of ligands with their receptors.



Depletion

VI. Signalling Induction

Antibodies can block the interaction of ligands with their receptors.



Signalling induction

Figure 7.1 Five reported mechanisms of therapeutic antibody-antigen interaction are illustrated schematically. TNF : - tumour necrosis factor; TNFRI : - tumour necrosis receptor I; TCR : - T cell receptor; MAC : - membrane attack complex [255].

II. Receptor blockade

Ligand receptor interaction can also be prevented by antibodies by positioning themselves into the cognate receptors which results in the inhibition of receptor activation and impairs functioning.

III. Receptor down regulation

In this mode of operation, the antibodies after binding to cellular surfaces get internalized and down regulate to inhibit the activation of cell surface receptors of the ligand.

IV. Depletion

This involves breakdown of antigen-bearing cells via complement-mediated lysis and opsonization, as well as Fc receptor for IgG (FcγR) – mediated clearance.

V. Signalling induction

In this mode of action, therapeutic antibodies induce active signals that affect cellular life.

7.1.2 Overview of methods for studying antibody-antigen binding

Over the last couple of decades, the development of various assays (such as an ELISA, RIA) [254] and several physical detection methods such as AFM [64, 132, 256], SPR [257] have been successfully employed for the measurement antigen-antibody interactions. However, each indicated method has its own complexities. ELISA has been widely employed for the measurement antibody-antigen interactions such as anti-cardiolipin antibodies [258], anti-phospholipid antibodies [259], thrombocytopenic purpura [260], thrombocytopenia, [261], and recently anti-tumor necrosis factor antibodies [262]. ELISA involves immobilization of one of the interacting partners, usually an antigen on the surface of a micro-plate, and then compounded with an antibody linked to an enzyme (direct approach) [263]. However, if the primary antibody is not linked to an enzyme, then antigen is first complexed with primary antibody (without any linked enzyme) followed by detection with a secondary antibody linked to an enzyme (indirect approach). The detection is achieved by measuring the conjugated enzyme activity via incubation with suitable substrate to produce a signal [263]. Both assays have their own merits and potential difficulties [263]. AFM involves the direct measurement of the intermolecular interaction by suitable functionalization of the interacting agencies. The utilization of AFM [64, 256, 264, 265], shows such measurements in the piconewton range under physiological conditions. However, direct force measurement of inter-molecular interactions by AFM becomes intricate due to several factors. For instance the complicated tertiary structures of both antibody and antigen require robust

attachment to the interacting surfaces (AFM tip and substrate) for accurate force measurements. Furthermore, such interactions are influenced by conformational state, environment, and steric hindrance offered by the involved molecules. The other drawback emanates from the potential non-specific interactions which may occur between the surfaces [64, 256, 264, 265].

In the 1990s, the emergence of biomolecular interaction analysis (BIA) or surface plasmon resonance (SPR) based new biosensor technology significantly improved the biophysical measurement of antigen-antibody binding interactions at an interface [266, 267, 268, 269, 270, 271, 272]. SPR enables these measurements as a function of time. The binding is marked by an increase in refractive index when one of the interacting associates, branded as the analyte (antigen or antibody), interacts to a ligand immobilized (antigen or antibody) on the surface of the bio-sensor chip [273]. Unlike ELISA, SPR does not require any labelling of the interacting partners, and therefore, eliminates binding artefacts due to the label [274].

Over the last couple of decades there has been a significant amount of increase in research concentrated on addressing the role of lyophilization induced aggregation in affecting the activity of bio-pharmaceuticals (protein therapeutic) [13, 164]. The convenience of methods to measure the activity of protein

therapeutic or markers with high sensitivity and specificity is critically significant. Among several potential methods discussed above (ELISA, AFM, SPR), this work employs ELISA.

7.1.3. ELISA, its principle and formats

ELISA is the most extensively employed and amongst the best validated methods for testing the activity of therapeutic proteins [275].

The basic general principle behind an ELISA is that it involves the immobilization of one of the interacting partners (either an antigen or an antibody) on the surface of polyvinyl chloride (PVC) micro-plate, followed by washing of the coated surface to remove any unbound molecules. The PVC surface immobilized (coated) with an antigen (for consideration) is then incubated with an antibody which is linked to an enzyme that produces fluoresces upon the addition of a suitable substrate (due to oxidation). The intensity with which the colour is produced is related to the amount of antigen/antigen with binding activity (functionality) [263].

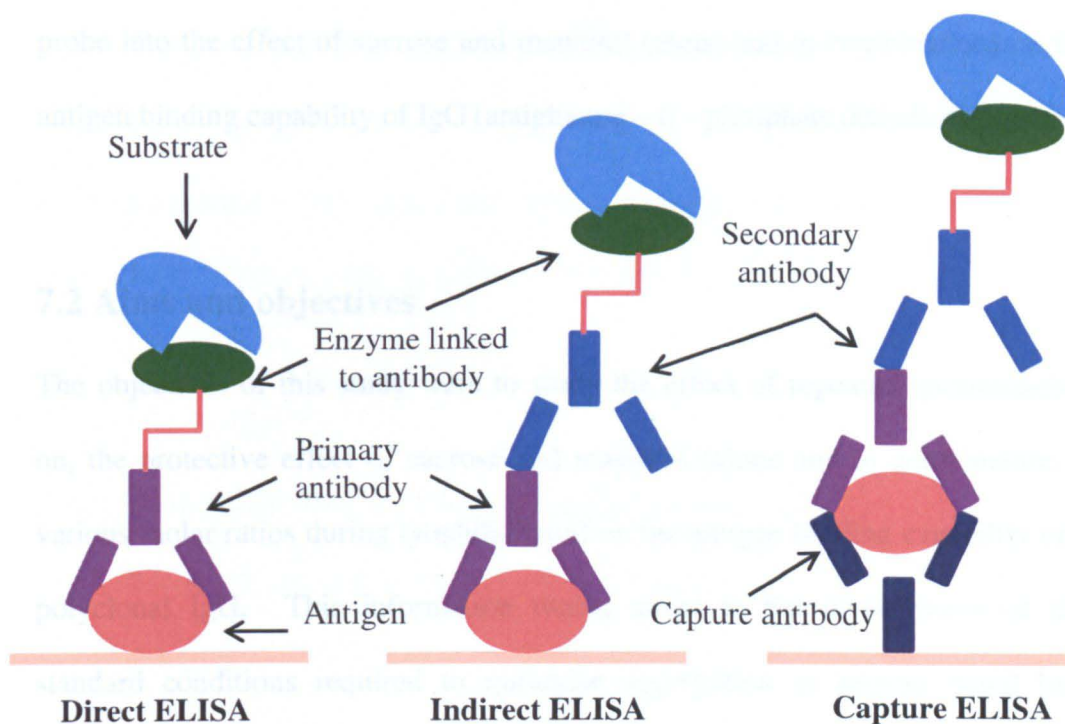


Figure 7.2 Schematic representations of the three methods for performing an ELISA experiment: There is a difference in the number and in the arrangement of interacting partners (antigen and antibodies) in all three formats. The method of choice depends on the nature of the interacting partners involved. Direct approach is considered ideal when primary antibody is linked to an enzyme or could be linked to an enzyme. Indirect involves one step more in the middle, that is the addition of secondary antibody which is enzyme linked. Capture ELISA is an indirect ELISA performed on the capture antibody which is immobilized on the PVC microwell surface first [263, 276].

ELISA can be performed in at least three well established formats highlighted in Figure 7.2 [263, 275]. In this study, we report the measurement of the antigenic binding activity of multiple times (1 – 7) lyophilized IgG antibody using an indirect ELISA approach presented in Figure 7.2. We have also attempted to

probe into the effect of sucrose and mannitol (alone and in combination) on the antigen binding capability of IgG (antiglucose – 6 – phosphate dehydrogenase).

7.2 Aims and objectives

The objectives of this study were to study the effect of repeated lyophilization on, the protective effect of sucrose and mannitol (alone and in combination in various molar ratios during lyophilization) on the antigen binding capability of a polyclonal IgG. This information would assist in the optimization of the standard conditions required to minimise aggregation in protein based biopharmaceuticals.

7.3 Materials

Primary antibody, secondary antibody, antigen, substrates, buffers, sugars which and other materials which were used in this study have been reported in the section 2.1 of Chapter 2.

7.4 Methods

7.4.1 Lyophilization of IgG alone and with sugars

This has been already described in section 2.1.1.2 of Chapter 2.

7.4.2 Preparation of primary antibody solution

The multiple times lyophilized IgG (0 – 7) and IgG lyophilized with sugars (sucrose, mannitol, trehalose, and sorbitol) alone and in combination were diluted to 1 : 1000 in blocking buffer (1 % BSA v/v in PBS).

7.4.3 Preparation of secondary antibody solution

The HRP-linked anti-rabbit IgG antibody solution was diluted to 1 : 2000 in blocking buffer.

7.4.4 Preparation of antigenic solution

The lyophilized powder of G-6-P-DH antigen was reconstituted in 5 mM sodium citrate as per manufacturer's instructions and dilutions were made to a range of concentrations 50 ng/ml, 500 ng/ml, 1 µg/ml, 5 µg/ml, 7 µg/ml, 10 µg/ml, and 15 µg/ml.

7.4.5 Preparation of buffer solutions

- Wash buffer (Tween 20)
- Blocking buffer (1 % BSA v/v in PBS)
- TMB substrate (1 tablet in 10 mL of 0.1M sodium acetate + 3 µL of H₂O₂.)
- OPD substrate (1 tablet in 10 mL of filtered deionized water)

4.6 Preparation of plates ELISA plates

The ELISA plates were prepared using an indirect ELISA approach (Figure 7.3).

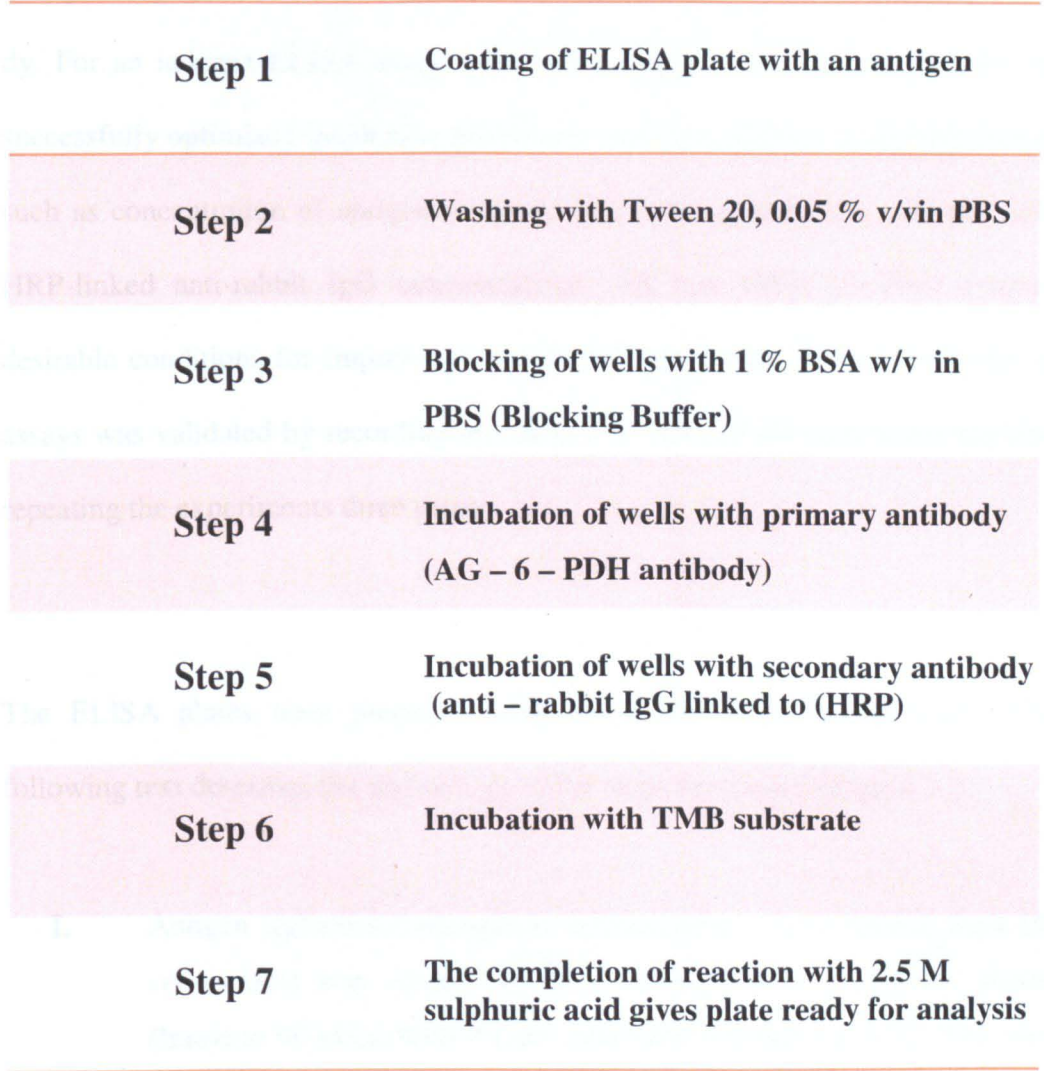


Figure 7.3 The chronology of the steps involved in the preparation of an ELISA plate via an indirect approach.

The most challenging aspect for generating robust immunoassays is the design of experiments for the optimization ligand – receptor interactions. The identification of critical factors such as right concentration of antigen, primary and secondary

antibodies, incubation periods, use of appropriate washing/blocking buffers and their impact on interactions with a minimal number of experiments is crucial for the optimization of binding interactions between an antigen and detection antibody. For an indirect ELISA assay, after conducting a series of experiments, we successfully optimized incubation periods for each step and the intra-plate factors such as concentration of antigen for plate well coating, detection antibody, and HRP-linked anti-rabbit IgG concentrations. All this effort involved ensured desirable conditions for improving specific binding events. The optimization of assays was validated by recording less than 1 % error in the measurements after repeating the experiments three times.

The ELISA plates were prepared using an indirect ELISA approach. The following text describes the chronology of the steps involved in Figure 7.2

- I. Antigen [(glucose-6-phosphate dehydrogenase from baker's yeast (*S. cerevisiae*)] was coated on 96 – well polystyrene ELISA plates (Immuno 96 MicroWell™) and incubated overnight at 4 °C. This was executed in order to ensure that antigen covered the surfaces of the multiwell plate.

- II. In the subsequent day, the indicated sample solution was removed and the plate was washed three times with the wash buffer composed of Tween 20, 0.05 % v/v in PBS.

- III.** The next step involved the blocking of wells by putting in 250 μ l of 1 % BSA w/v in PBS (blocking buffer) for an hour at room temperature. The removal of blocking buffer was ensured by washing the wells three times as described earlier.
- IV.** The individual wells of the plate were mounted with 125 μ l of IgG [lyophilized alone (1 – 7) and with sugars (sucrose/mannitol or both, cycle 1) diluted 1 : 2000] in blocking buffer. The plate was subjected to incubation for couple of hours at room temperature. The removal of IgG solution from the plate wells was once again ensured by washing the wells three times with washing buffer as before.
- V.** The individual wells of the plate were mounted with 125 μ l of anti-rabbit IgG linked to horseradish peroxidase (HRP); diluted 1 : 2000 in blocking buffer. The plate was subjected to incubation for couple of hours at room temperature. The removal of anti – rabbit IgG – HRP solution from the plate wells was once again ensured by washing the wells three times with washing buffer as before.
- VI.** The next stage of the reaction involved the addition of TMB substrate (100 μ l) into each well for an approximate incubation period of 10 minutes.
-

VII. Finally the addition of 20 μl of 2.5 M sulphuric acid enabled the completion of the reaction process for the preparation of required plates, which were readily introduced into the Dynex microplate reader for measurement of absorbance (measured at 450 nm).

I.	1	2	3	4	5	6	7	8	9	10	11	12
A	0.5µg/ml	0.5µg/ml	1µg/ml	1µg/ml	5µg/ml	5µg/ml	7µg/ml	7µg/ml	10µg/ml	10µg/ml	15µg/ml	15µg/ml
B	0.5µg/ml	0.5µg/ml	1µg/ml	1µg/ml	5µg/ml	5µg/ml	7µg/ml	7µg/ml	10µg/ml	10µg/ml	15µg/ml	15µg/ml
C	0.5µg/ml	0.5µg/ml	1µg/ml	1µg/ml	5µg/ml	5µg/ml	7µg/ml	7µg/ml	10µg/ml	10µg/ml	15µg/ml	15µg/ml
D	0.5µg/ml	0.5µg/ml	1µg/ml	1µg/ml	5µg/ml	5µg/ml	7µg/ml	7µg/ml	10µg/ml	10µg/ml	15µg/ml	15µg/ml
E	0.5µg/ml	0.5µg/ml	1µg/ml	1µg/ml	5µg/ml	5µg/ml	7µg/ml	7µg/ml	10µg/ml	10µg/ml	15µg/ml	15µg/ml
F	0.5µg/ml	0.5µg/ml	1µg/ml	1µg/ml	5µg/ml	5µg/ml	7µg/ml	7µg/ml	10µg/ml	10µg/ml	15µg/ml	15µg/ml
G	0.5µg/ml	0.5µg/ml	1µg/ml	1µg/ml	5µg/ml	5µg/ml	7µg/ml	7µg/ml	10µg/ml	10µg/ml	15µg/ml	15µg/ml
H	0.5µg/ml	0.5µg/ml	1µg/ml	1µg/ml	5µg/ml	5µg/ml	7µg/ml	7µg/ml	10µg/ml	10µg/ml	15µg/ml	15µg/ml
II.	1	2	3	4	5	6	7	8	9	10	11	12
A	Cycle 0	0.5µg/ml	Cycle 0	1µg/ml	Cycle 0	5µg/ml	Cycle 0	7µg/ml	Cycle 0	10µg/ml	Cycle 0	15µg/ml
B	Cycle 1	20mM S	Cycle 1	20mM S	Cycle 1	20mM S	Cycle 1	20mM S	Cycle 1	20mM S	Cycle 1	20mM S
C	Cycle 2	40mM S	Cycle 2	40mM S	Cycle 2	40mM S	Cycle 2	40mM S	Cycle 2	40mM S	Cycle 2	40mM S
D	Cycle 3	60mM S	Cycle 3	60mM S	Cycle 3	60mM S	Cycle 3	60mM S	Cycle 3	60mM S	Cycle 3	60mM S
E	Cycle 4	20mM M	Cycle 4	20mM M	Cycle 4	20mM M	Cycle 4	20mM M	Cycle 4	20mM M	Cycle 4	20mM M
F	Cycle 5	40mM M	Cycle 5	40mM M	Cycle 5	40mM M	Cycle 5	40mM M	Cycle 5	40mM M	Cycle 5	40mM M
G	Cycle 6	60mM M	Cycle 6	60mM M	Cycle 6	60mM M	Cycle 6	60mM M	Cycle 6	60mM M	Cycle 6	60mM M
H	Cycle 7	S+M(1:1)	Cycle 7	S+M(1:1)	Cycle 7	S+M(1:1)	Cycle 7	S+M(1:1)	Cycle 7	S+M(1:1)	Cycle 7	S+M(1:1)

Figure 7.4 Plate layout for an indirect ELISA testing of samples. Each sample of IgG, was tested against at least six antigenic concentrations simultaneously within a plate. **I.** Plate maps for wells coated with relative antigenic concentrations from (0.5 µg/ml to 15 µg/ml) for testing different samples of IgG. **II.** Shows scheme of testing multiple times (0 – 7) lyophilized IgG samples, and one cycled IgG containing sucrose and mannitol (alone and in combination).

III.	1	2	3	4	5	6	7	8	9	10	11	12
A	HRP-IgG	HRP-IgG	HRP-IgG	HRP-IgG	HRP-IgG	HRP-IgG	HRP-IgG	HRP-IgG	HRP-IgG	HRP-IgG	HRP-IgG	HRP-IgG
B	HRP-IgG	HRP-IgG	HRP-IgG	HRP-IgG	HRP-IgG	HRP-IgG	HRP-IgG	HRP-IgG	HRP-IgG	HRP-IgG	HRP-IgG	HRP-IgG
C	HRP-IgG	HRP-IgG	HRP-IgG	HRP-IgG	HRP-IgG	HRP-IgG	HRP-IgG	HRP-IgG	HRP-IgG	HRP-IgG	HRP-IgG	HRP-IgG
D	HRP-IgG	HRP-IgG	HRP-IgG	HRP-IgG	HRP-IgG	HRP-IgG	HRP-IgG	HRP-IgG	HRP-IgG	HRP-IgG	HRP-IgG	HRP-IgG
E	HRP-IgG	HRP-IgG	HRP-IgG	HRP-IgG	HRP-IgG	HRP-IgG	HRP-IgG	HRP-IgG	HRP-IgG	HRP-IgG	HRP-IgG	HRP-IgG
F	HRP-IgG	HRP-IgG	HRP-IgG	HRP-IgG	HRP-IgG	HRP-IgG	HRP-IgG	HRP-IgG	HRP-IgG	HRP-IgG	HRP-IgG	HRP-IgG
G	HRP-IgG	HRP-IgG	HRP-IgG	HRP-IgG	HRP-IgG	HRP-IgG	HRP-IgG	HRP-IgG	HRP-IgG	HRP-IgG	HRP-IgG	HRP-IgG
H	HRP-IgG	HRP-IgG	HRP-IgG	HRP-IgG	HRP-IgG	HRP-IgG	HRP-IgG	HRP-IgG	HRP-IgG	HRP-IgG	HRP-IgG	HRP-IgG
IV.	1	2	3	4	5	6	7	8	9	10	11	12
A	TMB/OPD	TMB/OPD	TMB/OPD	TMB/OPD	TMB/OPD	TMB/OPD	TMB/OPD	TMB/OPD	TMB/OPD	TMB/OPD	TMB/OPD	TMB/OPD
B	TMB/OPD	TMB/OPD	TMB/OPD	TMB/OPD	TMB/OPD	TMB/OPD	TMB/OPD	TMB/OPD	TMB/OPD	TMB/OPD	TMB/OPD	TMB/OPD
C	TMB/OPD	TMB/OPD	TMB/OPD	TMB/OPD	TMB/OPD	TMB/OPD	TMB/OPD	TMB/OPD	TMB/OPD	TMB/OPD	TMB/OPD	TMB/OPD
D	TMB/OPD	TMB/OPD	TMB/OPD	TMB/OPD	TMB/OPD	TMB/OPD	TMB/OPD	TMB/OPD	TMB/OPD	TMB/OPD	TMB/OPD	TMB/OPD
E	TMB/OPD	TMB/OPD	TMB/OPD	TMB/OPD	TMB/OPD	TMB/OPD	TMB/OPD	TMB/OPD	TMB/OPD	TMB/OPD	TMB/OPD	TMB/OPD
F	TMB/OPD	TMB/OPD	TMB/OPD	TMB/OPD	TMB/OPD	TMB/OPD	TMB/OPD	TMB/OPD	TMB/OPD	TMB/OPD	TMB/OPD	TMB/OPD
G	TMB/OPD	TMB/OPD	TMB/OPD	TMB/OPD	TMB/OPD	TMB/OPD	TMB/OPD	TMB/OPD	TMB/OPD	TMB/OPD	TMB/OPD	TMB/OPD
H	TMB/OPD	TMB/OPD	TMB/OPD	TMB/OPD	TMB/OPD	TMB/OPD	TMB/OPD	TMB/OPD	TMB/OPD	TMB/OPD	TMB/OPD	TMB/OPD

Figure 7.4 Part III. Shows scheme of adding of 125 μ L of (1 in 2000) HRP-linked secondary antibody to each antibody. **IV.** Displays addition of substrate 120 μ L to each well of the plate.

V.	1	2	3	4	5	6	7	8	9	10	11	12
A	2.5 M H ₂ SO ₄	2.5 M H ₂ SO ₄	2.5 M H ₂ SO ₄	2.5 M H ₂ SO ₄	2.5 M H ₂ SO ₄	2.5 M H ₂ SO ₄	2.5 M H ₂ SO ₄	2.5 M H ₂ SO ₄	2.5 M H ₂ SO ₄	2.5 M H ₂ SO ₄	2.5 M H ₂ SO ₄	2.5 M H ₂ SO ₄
B	2.5 M H ₂ SO ₄	2.5 M H ₂ SO ₄	2.5 M H ₂ SO ₄	2.5 M H ₂ SO ₄	2.5 M H ₂ SO ₄	2.5 M H ₂ SO ₄	2.5 M H ₂ SO ₄	2.5 M H ₂ SO ₄	2.5 M H ₂ SO ₄	2.5 M H ₂ SO ₄	2.5 M H ₂ SO ₄	2.5 M H ₂ SO ₄
C	2.5 M H ₂ SO ₄	2.5 M H ₂ SO ₄	2.5 M H ₂ SO ₄	2.5 M H ₂ SO ₄	2.5 M H ₂ SO ₄	2.5 M H ₂ SO ₄	2.5 M H ₂ SO ₄	2.5 M H ₂ SO ₄	2.5 M H ₂ SO ₄	2.5 M H ₂ SO ₄	2.5 M H ₂ SO ₄	2.5 M H ₂ SO ₄
D	2.5 M H ₂ SO ₄	2.5 M H ₂ SO ₄	2.5 M H ₂ SO ₄	2.5 M H ₂ SO ₄	2.5 M H ₂ SO ₄	2.5 M H ₂ SO ₄	2.5 M H ₂ SO ₄	2.5 M H ₂ SO ₄	2.5 M H ₂ SO ₄	2.5 M H ₂ SO ₄	2.5 M H ₂ SO ₄	2.5 M H ₂ SO ₄
E	2.5 M H ₂ SO ₄	2.5 M H ₂ SO ₄	2.5 M H ₂ SO ₄	2.5 M H ₂ SO ₄	2.5 M H ₂ SO ₄	2.5 M H ₂ SO ₄	2.5 M H ₂ SO ₄	2.5 M H ₂ SO ₄	2.5 M H ₂ SO ₄	2.5 M H ₂ SO ₄	2.5 M H ₂ SO ₄	2.5 M H ₂ SO ₄
F	2.5 M H ₂ SO ₄	2.5 M H ₂ SO ₄	2.5 M H ₂ SO ₄	2.5 M H ₂ SO ₄	2.5 M H ₂ SO ₄	2.5 M H ₂ SO ₄	2.5 M H ₂ SO ₄	2.5 M H ₂ SO ₄	2.5 M H ₂ SO ₄	2.5 M H ₂ SO ₄	2.5 M H ₂ SO ₄	2.5 M H ₂ SO ₄
G	2.5 M H ₂ SO ₄	2.5 M H ₂ SO ₄	2.5 M H ₂ SO ₄	2.5 M H ₂ SO ₄	2.5 M H ₂ SO ₄	2.5 M H ₂ SO ₄	2.5 M H ₂ SO ₄	2.5 M H ₂ SO ₄	2.5 M H ₂ SO ₄	2.5 M H ₂ SO ₄	2.5 M H ₂ SO ₄	2.5 M H ₂ SO ₄
H	2.5 M H ₂ SO ₄	2.5 M H ₂ SO ₄	2.5 M H ₂ SO ₄	2.5 M H ₂ SO ₄	2.5 M H ₂ SO ₄	2.5 M H ₂ SO ₄	2.5 M H ₂ SO ₄	2.5 M H ₂ SO ₄	2.5 M H ₂ SO ₄	2.5 M H ₂ SO ₄	2.5 M H ₂ SO ₄	2.5 M H ₂ SO ₄

Figure 7.4 Part V. Demonstrates liberation of yellow colour upon the addition 20 µL of 2.5 M H₂SO₄ to each well of the plate. The more intense the colour indicates more strong binding to an antigen.

7.5 Measurements

The recorded absorbance measurements using Dynex plate reader were plotted against concentrations for each sample type of IgG. The activity of IgG in a given sample was determined by plotting the absorbance readings against antigenic concentrations. A series of ELISA experiments were conducted on successively increasingly diluted solutions of each individual IgG sample at known concentrations. Same procedure was adopted for each sample of IgG lyophilized multiple times (0 – 7), IgG with sucrose and mannitol separately and in combination. The only change that was to be made was at step 4 by changing the IgG sample formulated under specific conditions such as number of cycles that the primary antibody has been exposed to and the type /quantity of sugar/s that was used during lyophilization.

The same procedure was adopted for each sample of IgG lyophilized multiple times (0 – 7), IgG with sucrose and mannitol separately and in combination. The only change that was made was at step 4 by changing the IgG sample formulated under specific conditions such as number of cycles that the primary antibody has been exposed to and the type of sugar/s that was used during lyophilization.

7.6 Results and Discussion

7.6.1 Antigen binding propensity of multiple times lyophilized IgG

Indirect ELISA approach (Figures 7.2, 7.3) was employed to detect antigen binding propensity of a range of IgG samples which were subsequently exposed to multiple times lyophilization (0 – 7) on its own (Figure 2.2 Chapter 2).

The data for antigen-binding propensity for multiple times lyophilized IgG samples against six different antigenic concentrations are summarized in Figure 7.5. There occurred a significant decrease in the binding strength of IgG (~ 60 %) after cycle one onwards up to cycle seven. For one and two times lyophilized IgGs, among these six antigenic concentrations used, the binding activity displayed by IgG was the highest, (~ 80 %) at 15 µg/ml and lowest (~ 62 %) at 0.5 µg/ml. However, over all the lowest activity (~ 7 %) was exhibited by IgG exposed to seven consecutive cycles of lyophilization. In all samples, the higher-antigen concentration (15 µg/ml) ELISA results were superior to any lower antigen concentration used. This was confirmed by a (~ 43 %) increase in the activity response in IgG exposed to two cycles of lyophilization when antigen concentration was lifted from 0.5 – 15 µg/ml. All other IgG samples from cycle two onwards were poorly active and showed no response to an increase in the antigen concentration.

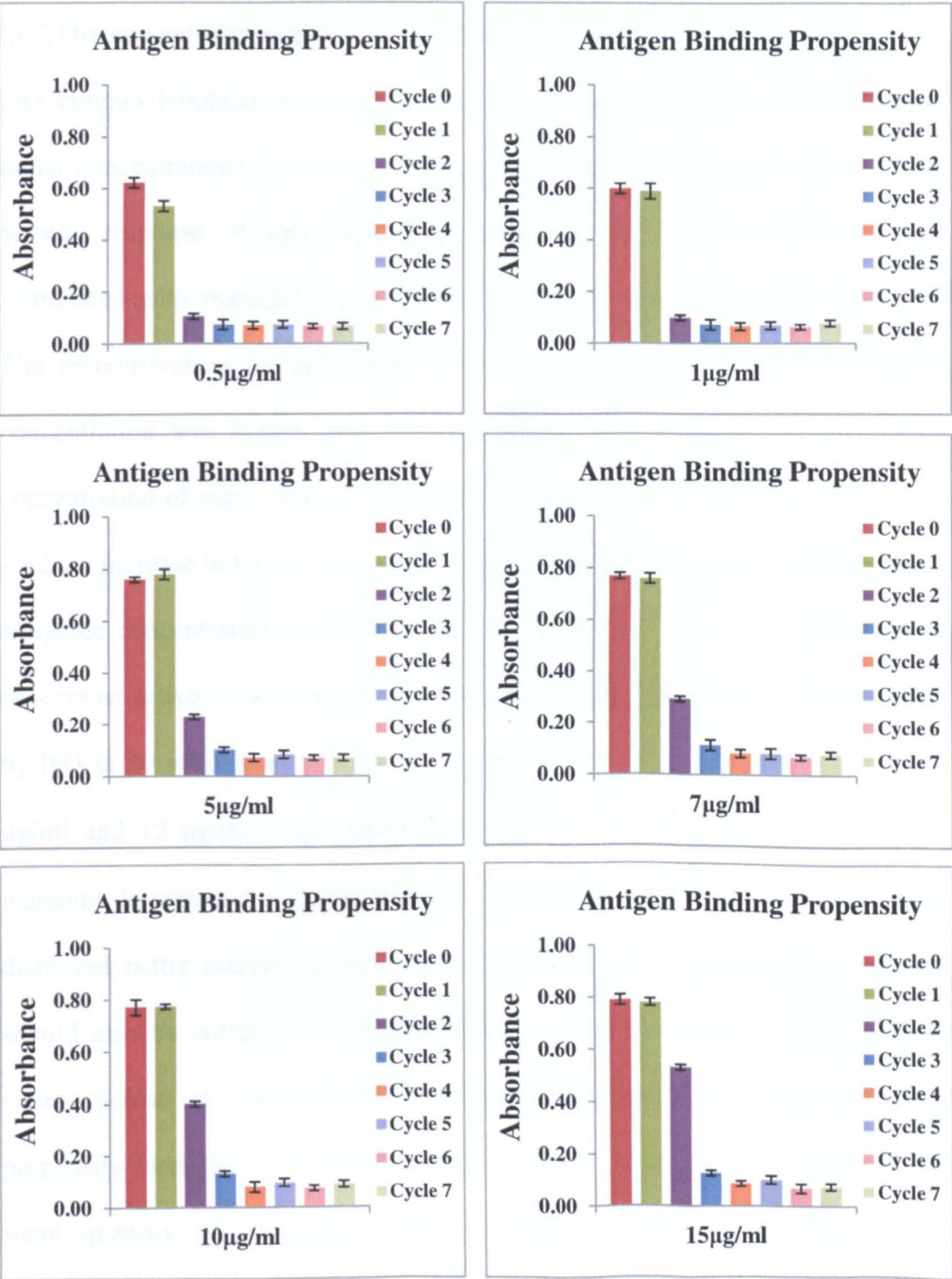


Figure 7.5 Indirect ELISA assay of multiple times lyophilized IgG antibody obtained at six different antigenic (G – 6 – PDH) concentrations indicated. IgG showed significant decrease in the antigen binding propensity with multiple cycles of lyophilization after cycle 2. The binding activity lifted with antigenic concentration in Cycle 2.

7.6.2 Diverse activity response of IgG lyophilized with individual sugars

IgG samples lyophilized separately with sucrose and mannitol at three different molar concentrations (20 mM, 40 mM and 60 mM) were ELISA tested and the activity response of IgG lyophilized with sucrose were compared to IgG formulated with mannitol at six different antigenic concentrations (Figure 7.5). The responsiveness of IgG lyophilized with sucrose against each antigenic concentration was higher than IgG lyophilized with mannitol at each molar concentration of sugar (Figure 7.5). IgG containing sucrose demonstrated a (~ 5 – 12 %) increase in the activity response in comparison to mannitol against all six antigenic concentrations (Figure 7.5 A and B). However, it was interesting to observe an activity response of IgG in 40 mM mannitol identical to that displayed by IgG in 20 mM sucrose. With the exception two antigenic concentrations (10 µg/ml and 15 µg/ml), the behaviour of IgG in 60 mM sucrose and 60 mM mannitol demonstrated a similar response. IgG lyophilized with sucrose (20 mM) displayed better activity against most of the antigenic concentrations used. It should also be noted that doubling (Figure 7.6 B) the molar concentration of either sucrose or mannitol did not significantly alter their antigen binding propensity from those displayed in (Figure 7.6 A). The reason probably is the same quantity of monomeric protein being available for binding in the formulations with higher molar concentration of sucrose. However, decrease in the IgG activity was observed after the molar concentration of sugars was tripled (Figure 7.6 C), especially at the 15 µg/ml, the activity of the IgG formulated in 60mM sucrose was reduced by 10 % when compared to 20 mM sucrose.

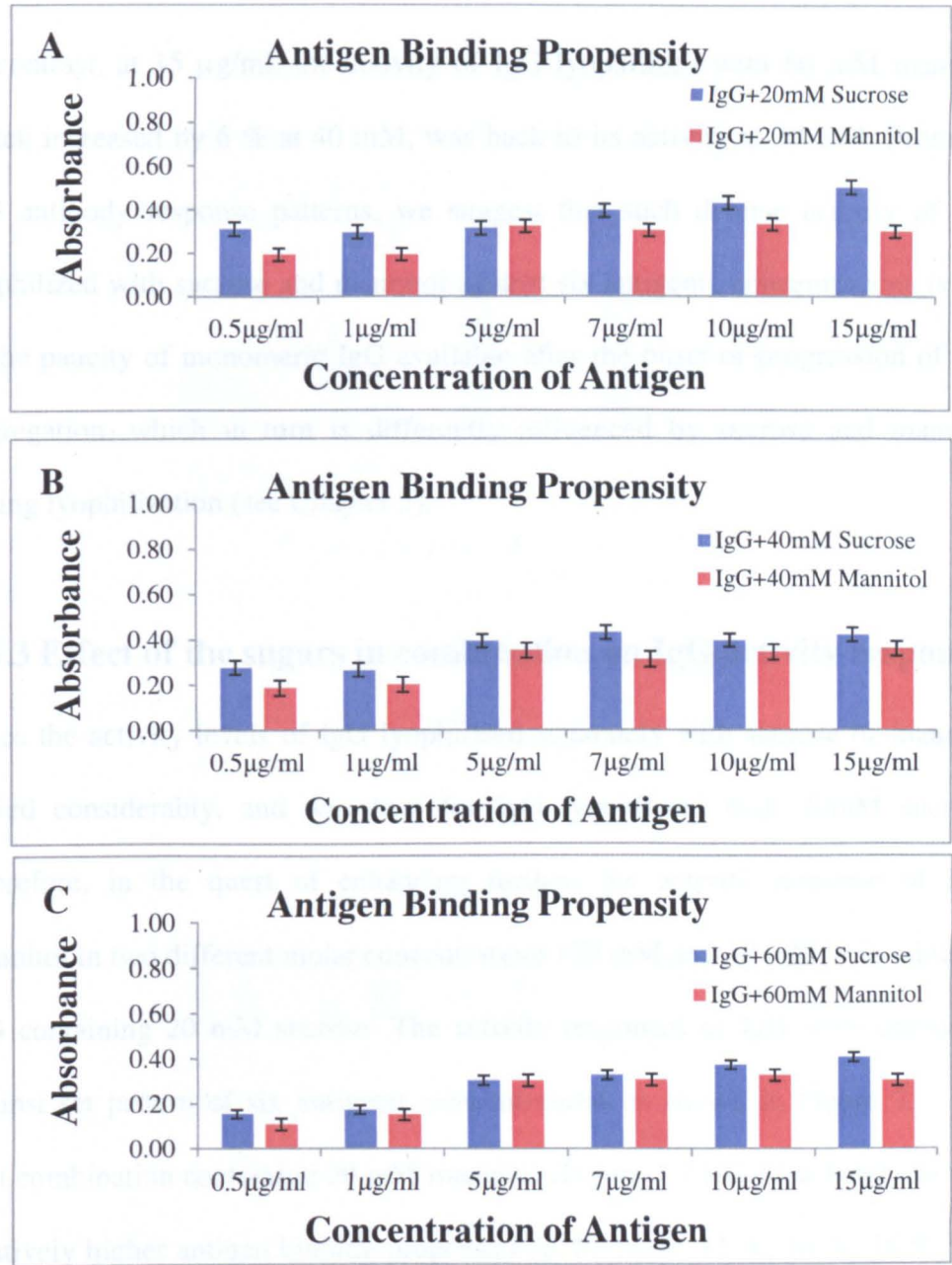


Figure 7.6 Indirect ELISA testing of IgG lyophilized with sucrose and mannitol separately at six different antigenic concentrations indicated an increase in the antigen binding activity (ABA) with the concentration of antigen used. The effect of the sugars presented in [A], [B], and [C], showed that IgG formulated in sucrose [Blue bars] displayed relatively better antigen binding activity than IgG containing mannitol [Red bars]. Using fairly large concentration of the both sugar excipients brought a dip in the activity of IgG [A ~ B > C] and this dip in the activity was more pronounced in IgG lyophilized with mannitol [C-Red bars]. 1.2mM IgG lyophilized in 20mM sucrose [A-Blue Bars] exhibited best antigen binding activity among IgG lyophilized with sugars.

In contrast, at 15 $\mu\text{g/ml}$, the activity of IgG lyophilized with 60 mM mannitol which increased by 6 % at 40 mM, was back to its activity at 20 mM. From the IgG antibody response patterns, we suggest that such diverse activity of IgG lyophilized with sucrose and mannitol against six antigenic concentrations is due to the paucity of monomeric IgG available after the onset or progression of IgG aggregation, which in turn is differently influenced by sucrose and mannitol during lyophilization (see Chapter 5).

7.6.3 Effect of the sugars in combination on IgG activity response

Since the activity levels of IgG lyophilized separately with sucrose or mannitol varied considerably, and was best for IgG lyophilized with 20mM sucrose. Therefore, in the quest of enhancing further, the activity response of IgG, mannitol in two different molar concentrations (20 mM and 40 mM) was added to IgG containing 20 mM sucrose. The activity responses of IgG were compared against set pattern of six antigenic concentrations as shown in Figure 7.7. The first combination containing 20 mM mannitol (Figure 7.7 [A]-Blue bars), showed relatively higher antigen binding propensity (6 %, 11 %, 11 %, 16 %, 16 %, and 32 %) against all six antigenic concentrations (0.5 $\mu\text{g/ml}$, 1 $\mu\text{g/ml}$, 5 $\mu\text{g/ml}$, 7 $\mu\text{g/ml}$, 10 $\mu\text{g/ml}$ and 15 $\mu\text{g/ml}$) used, than the corresponding formulation containing 40 mM mannitol (Figure 7.7 [A] - Red bars). The antigen binding propensity increased with antigenic concentration. However, unexpectedly, the activity response of IgG containing 40 mM Mannitol showed no improvement in antigenic concentration from 5 – 15 $\mu\text{g/ml}$ (Figure 7.7 [A]-Red-bars).

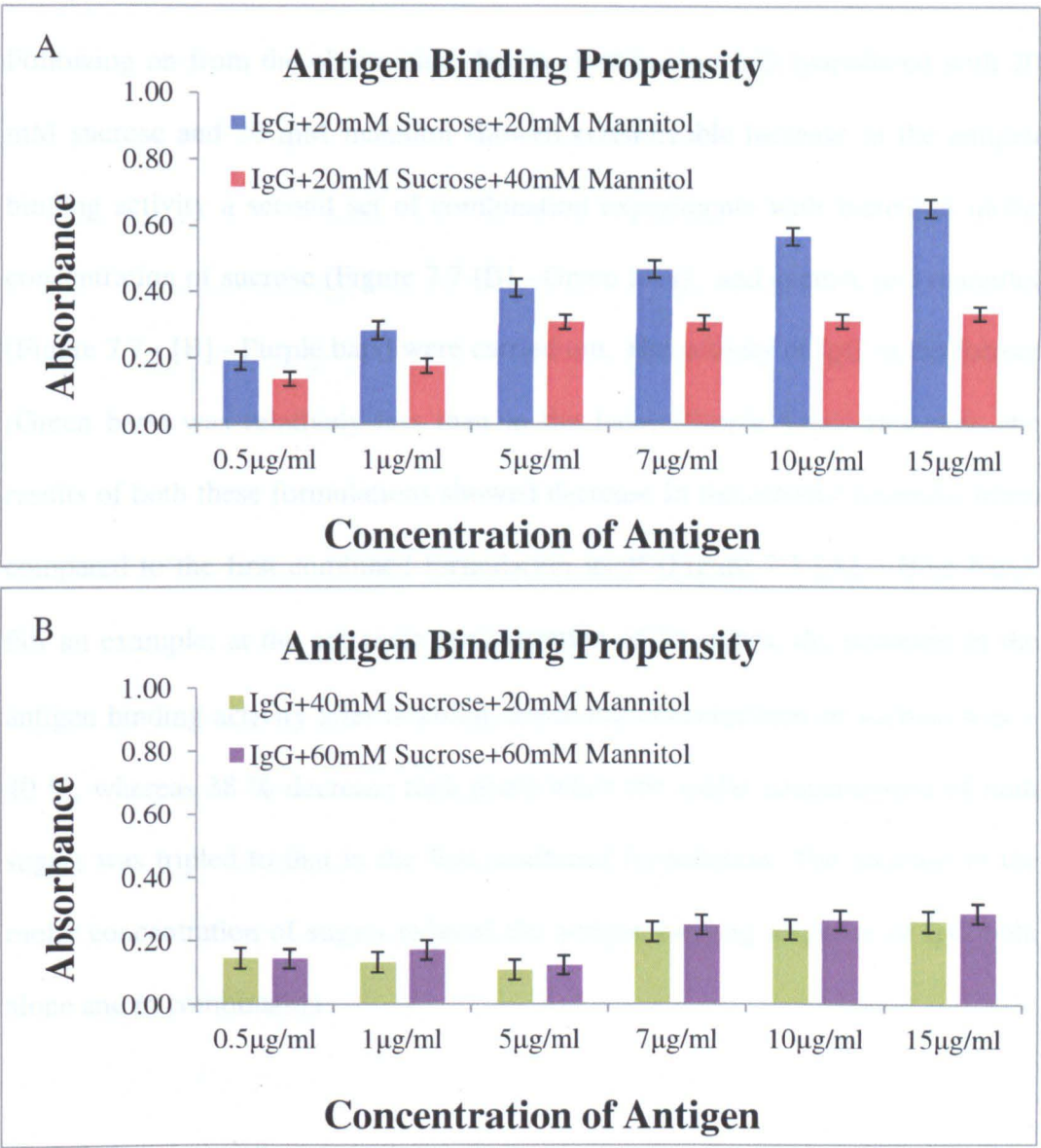


Figure 7.7 Indirect ELISA testing of IgG lyophilized with sucrose and mannitol in combination indicated increase in the antigen binding activity (ABA) with the increase in the concentration of the antigen used. The presence of 20mM mannitol in 1.2 mM IgG containing 20 mM sucrose (Blue bars), demonstrated a significant increase in the antigen binding activity than the corresponding IgG formulation with 40 mM mannitol (Red bars). The doubling of the molar concentration of sucrose from 20 mM to 40 mM in the first combined formulation caused a decrease in the antigen binding activity of IgG (Green bars). The data obtained for IgG with threefold increase in the molar concentration of both sucrose and mannitol showed no strong influence in enhancing the antigen binding activity of IgG (Purple bars) when compared to other examined formulations of IgG containing single or two excipients together.

Following on from the observation that in combination IgG lyophilized with 20 mM sucrose and 20 mM mannitol showed considerable increase in the antigen binding activity a second set of combination experiments with increased molar concentration of sucrose (Figure 7.7 [B] - Green bars), and sucrose and mannitol (Figure 7.7 - [B] - Purple bars) were carried out. The activity of IgG in the former (Green bars) was relatively less than in the latter (Purple bars). However, the results of both these formulations showed decrease in the activity response when compared to the first combined formulation itself (Figure 7.7 [A] – Blue bars). For an example: at the antigenic concentration of 15 $\mu\text{g/ml}$, the decrease in the antigen binding activity after doubling the molar concentration of sucrose was ~ 40 %, whereas 38 % decrease took place when the molar concentration of both sugars was tripled to that in the first combined formulation. The increase in the molar concentration of sugars reduced the antigen binding response of IgG both alone and in combination.

7.7 Discussion

Lyophilization has been reported to cause inactivity of proteins [277]. With the understanding that therapeutic proteins have a critical role in antigen binding during pathogenesis, the effect of multiple lyophilizations alone and in conjugation with sugars on the strength of IgG to bind to an antigen was examined.

The present results clearly demonstrated that multiple lyophilizations makes IgG highly susceptible to inactivity compared to one or two lyophilization steps. The significant decrease in the antigen binding strength could be attributed to the amount and nature of IgG monomers present in the protein solution (Primary antibody). One would expect a decrease in the antigen binding activity under following circumstances: (i) a lack of sufficient structurally unaltered monomeric IgG in a free state (non – aggregated), (ii) IgG monomers available but with altered secondary structure, (iii) IgG monomers aggregated (structurally unaltered), (iv) IgG monomers aggregated (structurally altered) and (v) fully aggregated. The stress created by lyophilization can induce all of the above indicated changes at the same point of time and therefore can reduce the activity of protein [25, 26, 29]. In case, of the (ii) factor, the decrease in the antigen binding activity reveals weakened bonded network within the antigen binding fragments (Fabs) of the antibody. This could be also established from the findings in the earlier chapter 4, where we discovered that multiple lyophilization caused decrease in the proportion of monomeric IgG, an increase in the particle size,

growth in the crystalline features, increase in the concentration of β – sheet main component coupled with alterations in other β – sheet secondary structural components within amide band I and intensification in the extent of thermal unfolding. However, one could not find any definite association or relationship amongst the indicated factors and their influence on antigen binding activity other than the β – sheet structural changes. It is because the structures of the hypervariable regions (CDRs) of the variable domains of light and heavy chains of the antibody molecule found in the loops are based on β – sheet secondary structure. These loops, infact are the portions that specifically bind the antigen. Therefore, decrease in the antigen binding affinity during multiple cycles of lyophilization could be attributed to the changes in β – sheet structure of the loops that hold hypervariable regions. The relatively increased activity response demonstrated by IgG lyophilized with sucrose suggests more structural stability in the hypervariable regions compared to that of IgG lyophilized with mannitol [278]. The finding that mannitol was less effective probably reflects its intrinsic inability to form sufficient amorphous phase and susceptibility to crystallize during lyophilization. The improvements in the antigen binding propensity noted upon the addition of mannitol to sucrose, suggests the importance of the role of mannitol in stabilizing lyophilized cake structure of the protein formulation in the medium of sucrose. In the present experiments, there was no evidence that increasing the molar concentration of sucrose both alone or in combination improved the IgG activity. This disagrees with findings in the other chapters and must be noted.

7.7 Conclusions

The identification of critical factors in maintaining the protein binding activity and their optimization is highly significant for improving the efficiency of therapeutic proteins. For the same quantity of antibody, the antigen binding propensity was shown to be highly dependent upon the concentration of antigen coated to the well. IgG activity significantly decreased with multiple lyophilization after cycle two onwards. In comparison to mannitol, the sucrose had a stronger and positive influence on the antigen binding activity of IgG when the sugars were used separately. However, in combination, the addition of mannitol significantly improved the binding strength of IgG. Individually, the activity response of IgG in 40 mM mannitol was similar to that displayed by IgG in 20mM sucrose. However, adding more sugar (more than double) to the same quantity of IgG in the formulation does not improve the antigen binding activity. The future interest, therefore, will be to investigate the possible immunological role of IgG antibodies with other sugars and other higher antigen concentrations to establish a robust relationship between the amount of sugars and antigens involved.

Chapter 8

Summary and potential for further improvement in future investigations

8.1 Framework of the investigations conducted in this project

A general approach of the investigations conducted in this project is presented in Figure 8.1. In the preliminary investigations, the effect of lyophilization on the particle size and morphology of the ferritin and IgG, both in air and liquid, were characterized. The second phase of experiments investigated the influence of multiple cycles (0-7) of lyophilization on an antiglucose-6-phosphate dehydrogenase antibody (IgG) without excipients. The penultimate set of experiments probed the impact of excipients (sucrose and mannitol alone, and in combination) on aggregation behaviour of IgG during lyophilization. The parameters examined were particle size, morphology, secondary structure, thermal stability, effect of humidity (data not included) and antigenic – binding activity. Liquid formulations were analyzed by dynamic light scattering (DLS) and atomic force microscopy.

I. Screening of the effect of lyophilization on ferritin aggregation in air and in liquid.

Particle size measurements (AFM), Morphology (SEM)

II. Screening of the effect of lyophilization on the IgG aggregation in air and in liquid.

Particle size measurements (AFM), Morphology (SEM)

III. Screening of the effect of multiple lyophilizations on the aggregation of IgG in liquid and solid state.

Particle size measurement (DLS and NTA); Morphology (SEM and AFM); Secondary structure (ATR-FT-IR); Thermal Stability (DSC);
Antigen binding activity (ELISA)

IV. Screening of the effect of multiple lyophilizations on the aggregation of IgG with excipients in liquid and solid state.

Particle size measurement (DLS); Morphology (SEM and AFM);
Secondary structure (ATR-FT-IR); Thermal Stability (DSC);
Antigen binding activity (ELISA)

Figure 8.1 Schematic overview of the experiments performed in this project.

(AFM) for particle size characterization. AFM and SEM were employed to identify and characterize different components in the powdered lyophilized formulations. Differential scanning calorimetry (DSC) and ATR -Fourier transform infrared (FTIR) spectroscopy were also used to classify any thermal and structural alterations. Antigen binding activity was investigated by an indirect ELISA method. The investigations were aimed to provide an insight in order to develop a broad spectrum novel screening standard for the detection, quantifications and control of aggregation in IgG and other such therapeutic proteins.

8.1.1 Nanoscale characterization of lyophilized ferritin and IgG

8.1.1.1 Characterization with AFM only

The nanoscale characterization of the effect of lyophilization on ferritin, both in air and liquid was scrutinized in Chapter 3 and Chapter 4 (beginning) respectively. The real time imaging of the samples was performed using AFM in tapping mode and particle size measurements were carried out by SPIP image analysis software.

In case of both Ferritin and IgG, molecules were randomly arranged onto the hydrophilic surface of mica. In air, arrangement of the deposits of ferritin and IgG molecules onto mica surface was denser than in liquid, both before and after lyophilization. IgG on exposure to air, aggregated heavily compared to ferritin.

Overall, both in air and liquid, there occurred a decrease in the proportion of monomers (for both ferritin and IgG) and smaller multimeric forms, whereas higher multimers and larger aggregates showed an increase after lyophilization. In air, however, the decrease in the proportion of monomeric features was relatively more for both ferritin and IgG. Morphologies of the lyophilized ferritin using SEM revealed aggregation with visible crystalline surfaces. SEM micrographs gave an impression of decrease in the porosity of ferritin after lyophilization.

8.1.2 Multiple times lyophilized IgG without excipients

8.1.2.1 Characterization with DLS, AFM, DSC, SEM and ATR

The influence of multiple lyophilizations on IgG without excipients was studied in Chapter 4. The reason behind not using excipients was to investigate the inherent strength of IgG to resist the effect of stress produced by multiple lyophilizations. The size distributions, morphology, structural and thermal stability were the parameters examined. IgG lyophilized on its own was able to offer certain resistance against aggregation, however, this resistance is not sufficient to overcome the stresses inflicted during multiple cycles of lyophilization. The propensity of IgG particles to aggregate (increase in size) enhanced during multiple cycles of lyophilization was shown by DLS and NTA. This was complimented by AFM which confirmed an increase in the average size of the globular features embedded in amorphous regions.

Moreover, these findings were further endorsed by the complimentary results from both ATR and DSC measurements. The former demonstrated structural alterations accompanied by significant increase in the β – sheet character (structural rearrangement), whereas latter revealed an increase in the thermal unfolding propensity of IgG. This piece of work laid an insight into the inherent ability of IgG to defy aggregation. Moreover, this strategy became essential for comparative analysis when the effect of the excipients on IgG during successive lyophilization was investigated in Chapter 5.

8.1.3 IgG lyophilized with excipients

8.1.3.1 Characterization with DLS, AFM and DSC

The influence of excipients (sucrose and mannitol) on IgG particle size with DLS, nanoscale characterization of different components and thermal stability with DSC was probed in Chapter 5. The tendency of IgG formulated with sucrose or mannitol, alone and in combination to aggregate also increased with multiple cycles of lyophilizations. However, the presence of sugars in the protein formulations lowered the temptation of aggregation. Sucrose displayed profound inhibitive effect on the aggregation of IgG both alone as well as in combination with mannitol (Chapter 5, DLS results). The best protection was achieved in combination when 1 mg/ml of IgG was formulated with 3.6 mM sucrose and 3.6 mM mannitol. AFM images of lyophilized formulations revealed globular protein-like features of variable size. However,

the mean size of the agglomerates increased significantly with successive lyophilization. The increase in the mean size of the globular IgG and their association with amorphous regions in the powdered formulations indicated by AFM complements the DLS and DSC findings. Samples of IgG formulated with mannitol showed more protein aggregation and had more crystalline features. DSC confirmed that the propensity of the unfolding of IgG increased during multiple cycles of lyophilization. However, the denaturation temperature (T_m) of IgG [Fab fragments] $\sim 58^\circ\text{C}$ remained unchanged. The unfolding of the Fc domain of IgG occurred at lower temperatures following multiple cycles of lyophilization. Sucrose at higher molar concentration provided protection against thermal denaturation, both alone and in combination with mannitol.

The inhibitive effect of sucrose on the aggregation of IgG both alone as well as in combination with mannitol shown by DLS and AFM is consistent with literature. However, DSC disagrees with DLS in indicating failure of mannitol to reduce aggregation. The reason for this difference remains a topic for future research.

8.1.3.2 Characterization with SEM and FT-IR

The Chapter 6, studies structural and morphological characteristics of a polyclonal IgG formulated with sucrose and mannitol, both alone and in combination during

successive cycles of lyophilization. IgG formulated with sucrose displayed efficient secondary structures with lesser alterations in the secondary structural components stationed within amide band I. The alterations were least in IgG lyophilized with sucrose at 40 mM, therefore, validates our AFM, DLS findings, presented in Chapter 5. Mannitol pronounced aggregation, produced several types of crystalline features, decreased porosity (solubility) when used alone was confirmed by SEM and therefore, compliments AFM results. The magnitude of unfolding (Fabs) increased with mannitol shown by DSC is complementary to ATR which indicated significant in the main β – sheet structural component. In contrast, sucrose in IgG formulations showed comparatively enhanced porosity and flakiness with few crystalline faces. This effect pronounced at higher molar concentration of sucrose in IgG formulations both alone and in combination with mannitol. This work could form the basis of a broad spectrum strategy to characterize, minimize and prevent aggregation in protein therapeutics through the screening of potential excipients.

8.1.4 Antigen-binding activity of IgG

In Chapter 7, the antigen-binding activity of polyclonal IgG lyophilized on its own multiple times and once with excipients [sucrose and mannitol, both alone and in combination] against six different antigenic (G – 6 – PDH) concentrations (from 0.5 – 15 $\mu\text{g/ml}$) was explored using an indirect ELISA approach. A HRP – linked anti-

rabbit IgG was used as secondary antibody for detection against TMB/OPD substrates.

8.1.4.1 Antigen-binding activity of lyophilized IgG (on its own)

The antigen binding propensity of IgG increased with an increase in the concentration of antigen coated to the wells, both in case of multiple times lyophilized IgG (on its own) and IgG lyophilized once with sucrose and mannitol (alone and in combination). There occurred a significant decrease (~ 60 %) in the binding activity against each antigenic concentration used in case of IgG exposed to multiple cycles of lyophilization. The antigen binding propensity was retained only upto cycle one. Although in cycle two, an increase in the activity response at higher antigenic concentration was observed. However, cycle two onwards up to cycle 7, there occurred a significant decrease in the activity of IgG against each antigenic concentration used and this decrease was identical from cycle 5 – cycle 7.

8.1.4.2 Activity of IgG with sugar excipients

The antigen binding propensity of IgG with sucrose was relatively higher than in mannitol at each molar concentration used, both alone and in combination. However, there occurred a decrease in the antigen binding activity when the molar concentration of either sugar was increased. This was confirmed by a 20 % decrease in the activity of IgG, when the molar concentration of sucrose was doubled in 1.2 mM IgG lyophilized with sucrose (20 mM) alone. Similar results were obtained

after doubling the molar concentration of mannitol in formulations containing single excipient. IgG lyophilized with 20 mM mannitol demonstrated best activity from the IgG lyophilized with single excipient. The presence of appropriate quantity of mannitol significantly enhanced activity response of IgG in formulations containing sucrose. Upon the addition of 20 mM mannitol, this was best demonstrated by observing a significant improvement in the activity (20 %) of the best formulation containing single excipient (1.2 mM IgG lyophilized with 20 mM sucrose). However, any increase (beyond 1 : 40) in the molar concentration of either sugar (sucrose or mannitol) in the formulations containing single excipient or double excipients reduced the activity of IgG. This decrease in the activity response could be attributed to the presence of too many sugar molecules occupying the linear or three-dimensional antigenic conformation of the binding site (a unique site formed by the interaction of two native protein loops or subunits). This results in the deficit of freely available epitope (binding site of an antigen). The binding site is usually one to six monosaccharides or 5 – 8 amino acid residues on the surface of the antigen. Generally, variety of binding sites is possible on the surface of antigen, with each potential binding site having its own structure designed as a consequence of covalent and non-covalent interactions such as ionic bonds, hydrophilic and hydrophobic interactions. If either the ligand or the receptor binding site is not in an ideal state due to deposition of too many sugar molecules, or through fixation, the epitope may be malformed to a certain degree and this may affect its ability to interact with an antibody. Therefore, for a competent interaction to facilitate between an antigen and the antibody, the

binding site must be fully free and not crowded with too much sugar. This suggests the necessity to optimize the molar concentration of sugar for efficient binding which we were able to achieve in case of IgG lyophilized with 20 mM sucrose in individual formulations. This suggested molar concentration of sugar excipients (no matter how good they are) only up to a certain critical limit in enable IgG during lyophilization to maintain the population of its active monomers that could readily bind to an antigen.

8.1.5 Impact of this research work

The investigations which were carried out in this project established that multiple lyophilization is not a right approach to stabilize proteins. It is not ideal to expect the maintenance of all the necessary therapeutic characteristics in a protein formulation (such as an IgG) even up to the cycle 1. Multiple lyophilizations have a negative impact on the thermal stability, antigen binding activity, porosity and amorphicity. These studies established the influence of sucrose and mannitol (alone and in combination in different molar ratios) on the proteins during lyophilization. The achievement of desired characteristic in a protein therapeutic requires several additives in combination, even if one of the additives provides most of the wanted benefits when used alone. The reduction in aggregation, resistance in the thermal unfolding, and decrease in the alterations in the secondary structural components with an increase in the molar concentration of the sugar equal or more than optimum may reduce antigen binding propensity which is very much vital from a therapeutic point of consideration. Therefore,

from the conducted studies, it is understood, that the protein must be retained not only in its native-like state, but also in a native like environment with an optimum protection provided by suitable sugars during lyophilization in order to ensure that the protein that was protected becomes fully functional to deliver therapeutically a desired performance. This study standardized characterization approaches for stabilizing IgG alone and with sucrose and mannitol (alone and in combination). The benchmark provided by this work would serve as a precursor for developing a novel screening standard for optimizing and improving the therapeutic efficiency of other proteins besides furnishing a detailed account of the disparity in correlating the data from multiple novel techniques. The findings of our work can be directly translated to biotech and biopharm industries for the enhancement of protein based therapeutics.

Appendix 1

Materials

Materials	Batch No.	Supplier
Horse spleen ferritin	F4503	Sigma Aldrich
A-G-6-PDH IgG antibody	A9521	Sigma Aldrich
G-6-PDH antigen (<i>S. cerevisiae</i>)	G6378	Sigma Aldrich
HRP-linked anti-rabbit IgG	ABE2047	Bioscience UK Ltd
D-sucrose (99%)		Sigma Aldrich
D-mannitol (98%)	037K0208	Sigma Aldrich
D-sorbitol (98%)	047K0025	Sigma Aldrich
D-(+)-trehalose dehydrate (95%)	90208	Fluka
PBS tablets	P4417	Sigma Aldrich
DNPS (K= 0.06-0.6N/m; TM in Liquid, CM in air) SNL (K=); RTESPA (20-80N/m)		Veeco CA
Mica 1, (3"x 1")	G250 – 1	Agar Scientific
TWEEN 20 washing solution	167008	Thermo Scientific
Polypropylene plates (Immuno 96 MicroWell™)	167008	Thermo Scientific
12.5-mm aluminum pin stubs	G301	Agar Scientific
DSC Lids and Pans	T110404 (lid) T110516 (pan)	TA hermetic
Tetramethyl benzidine (TMB) substrate	T5525	Sigma Aldrich
Tween 20		Sigma Aldrich
Bovine serum albumin (BSA)		Sigma Aldrich
Sterile 0.2 µm Ministart filters	16532	Anachem

Sodium citrate-dihydrate (99%)	6132 – 04 – 03	Sigma Adrich
Silica Gel	S/0761/53	Fischer Chemical
Lens Cleaning Tissue	2105841	Whatman
OPD substrate	P9187	Sigma Aldrich
ELISA plates (Nunc)	167008	ThermoScientific

A. 1.1 List of materials used in this project.

Appendix 2

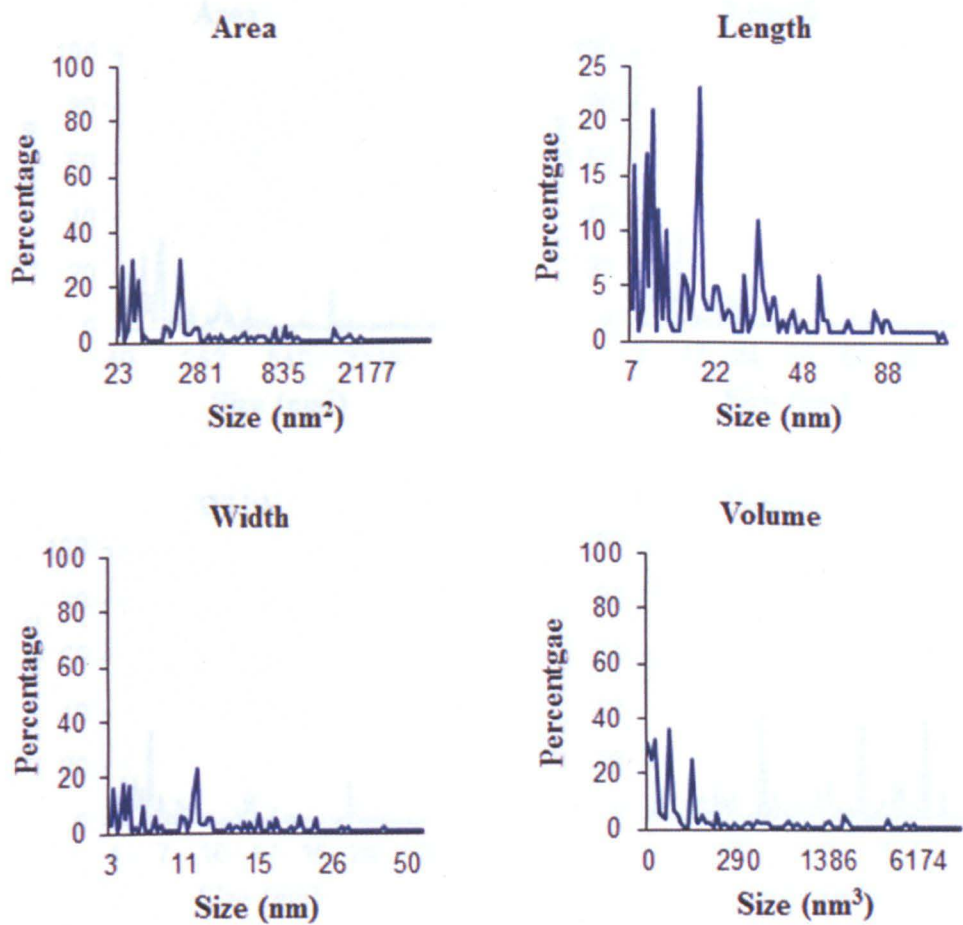
Novel Techniques

Name of the Techniques
Atomic Force Microscopy (AFM)
Dynamic Light Scattering (DLS)
Nanoparticle Tracking by Nanosight (NTA)
Differential Scanning Calorimetry (DSC)
Fourier-transform Infra-red Spectroscopy (FT-IR)
Scanning Electron Microscopy (SEM)
Polarization Microscopy (PM)
Surface Plasmon Resonance (SPR)
Enzyme Linked Immunosorbant Assay (ELISA)
Analytical Ultra-Centrifugation (AUC)
Size Exclusion Chromatography (SEC)
Ultra-Violet Absorption Spectrometry (UV)
Lyophilization

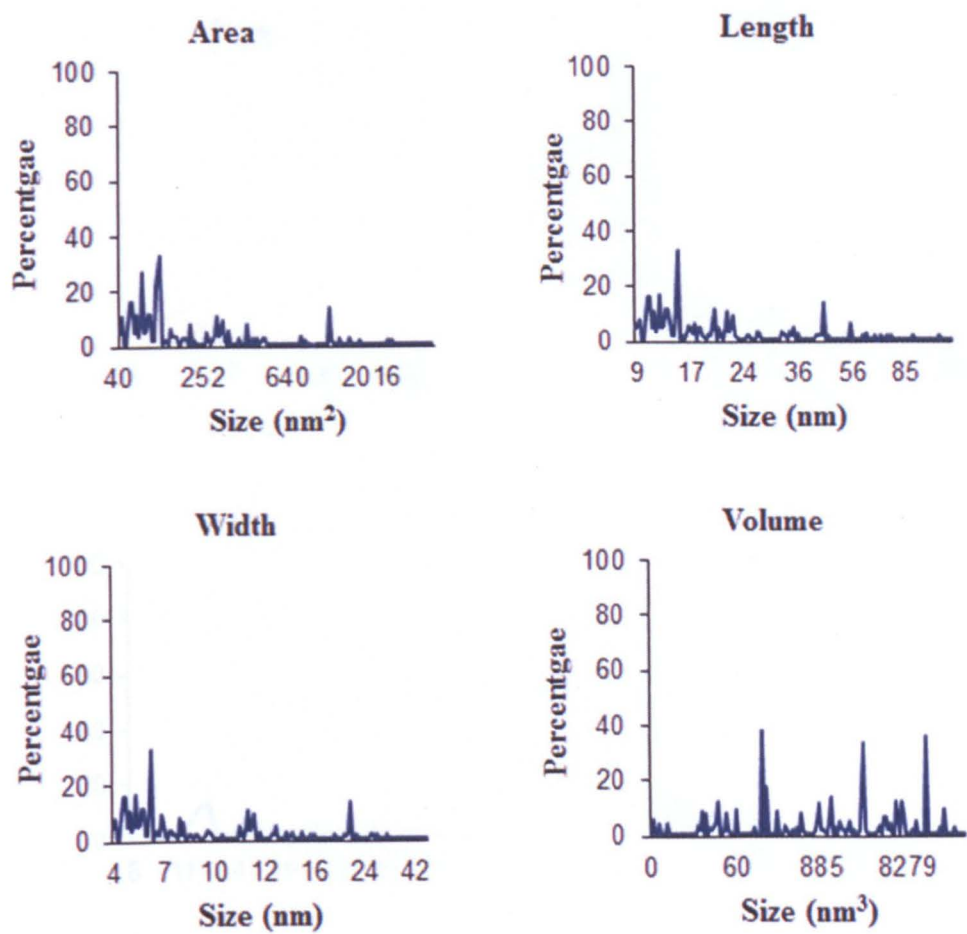
A.2.1 List of novel techniques.

Appendix 3

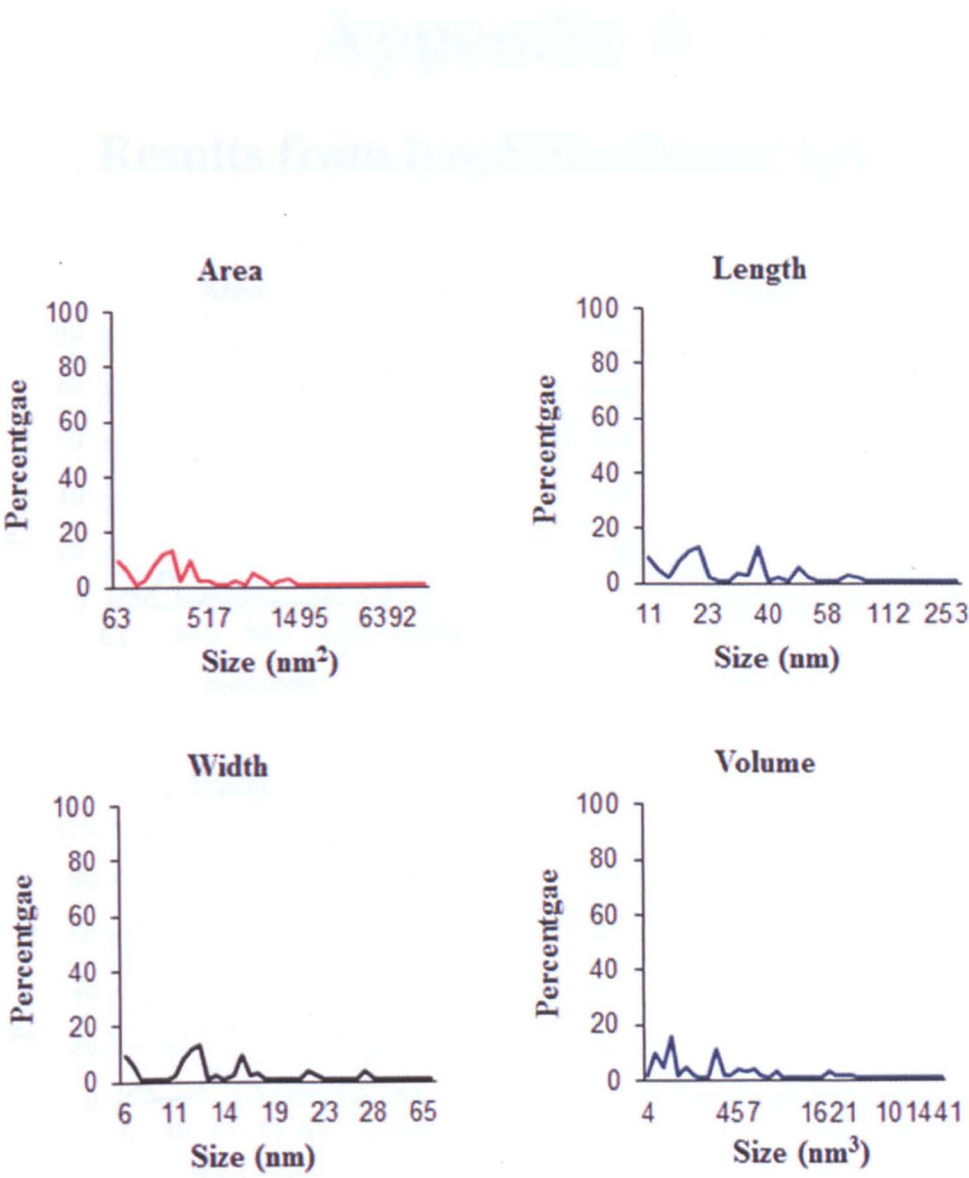
AFM size measurements of ferritin aggregates



A.3.1 AFM measured aggregation profiles of ferritin in air (Cycle 0)



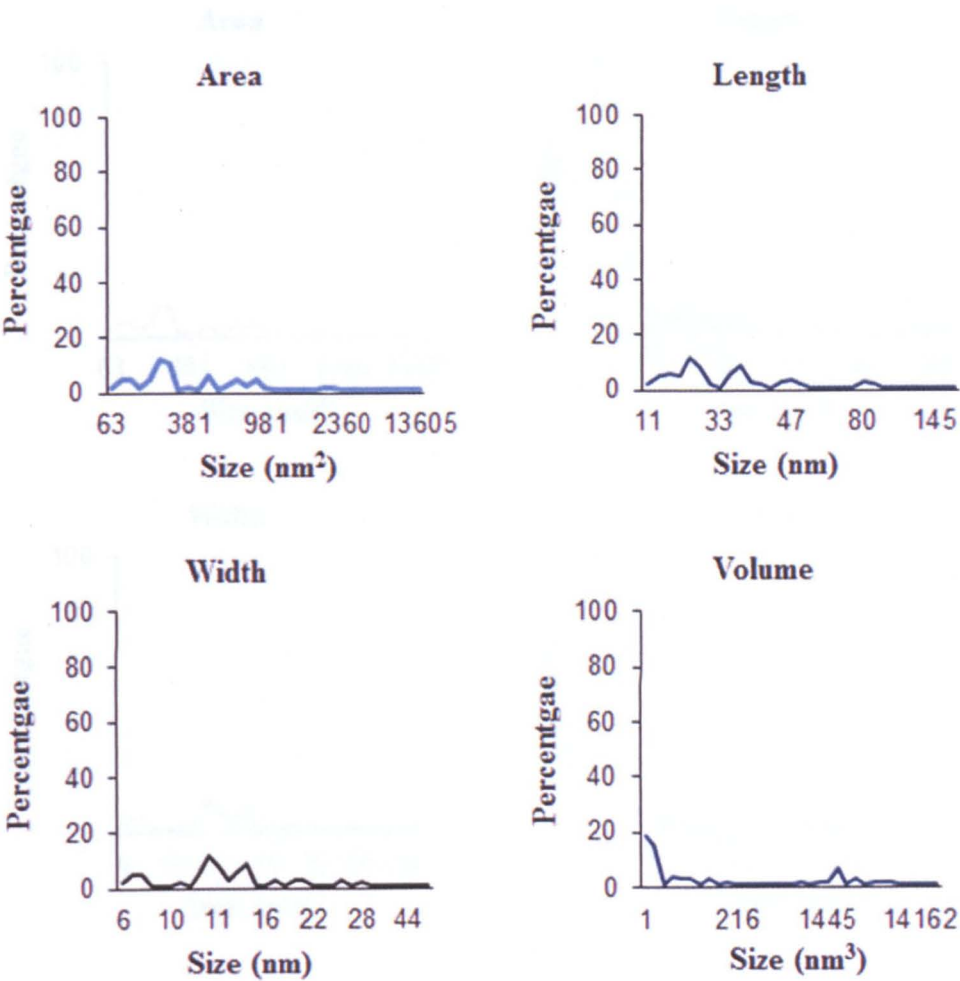
A.3.2 AFM measured aggregation profiles of ferritin in liquid (Cycle 0)



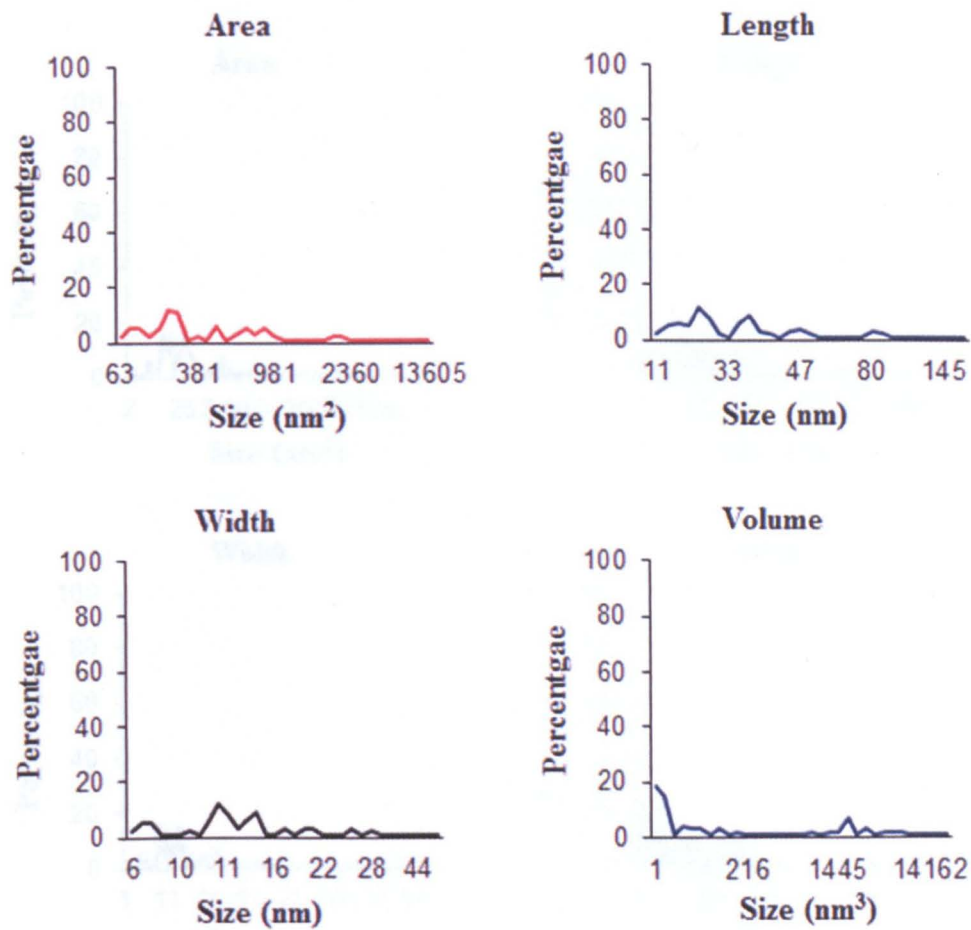
A.3.3 AFM measured aggregation profiles of ferritin in liquid (Cycle 1)

Appendix 4

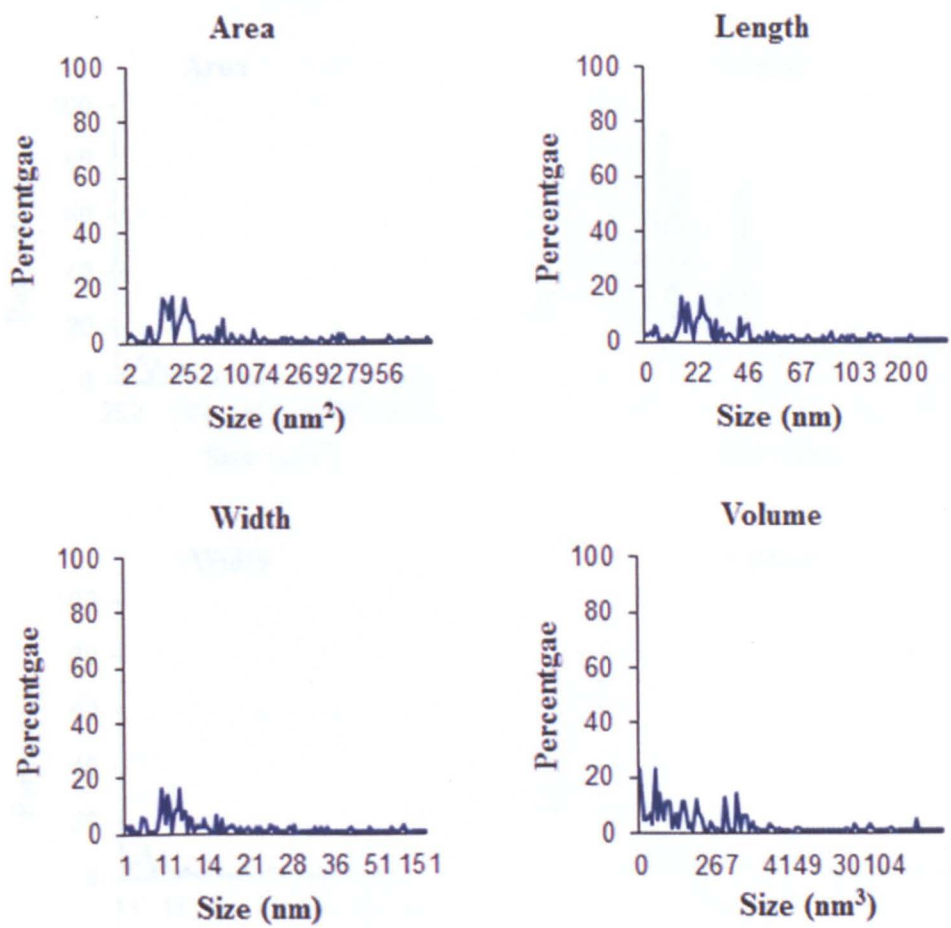
Results from lyophilization of IgG



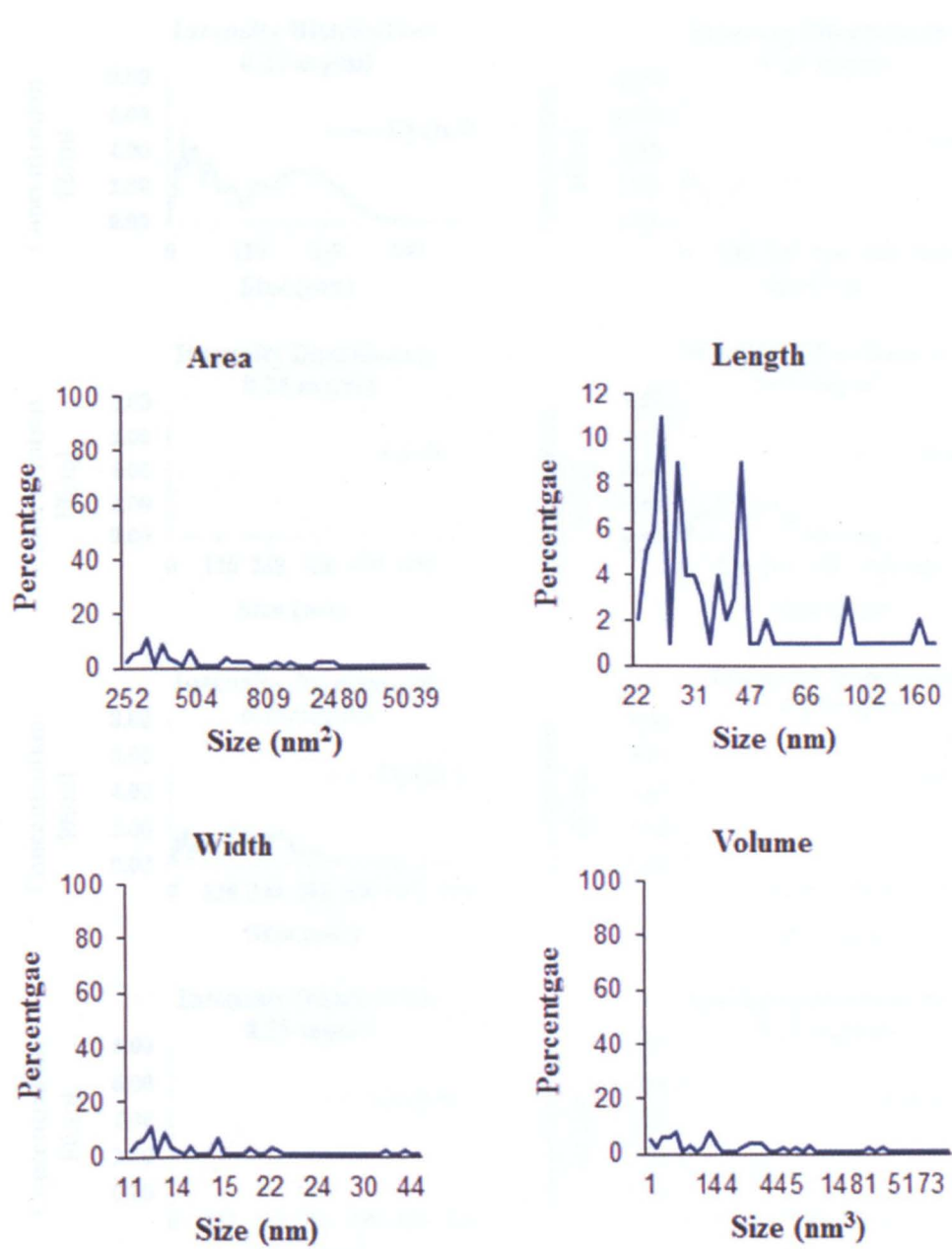
A.4.1 AFM measured aggregation profiles of IgG (0.75 µg/ml, Cycle 0)



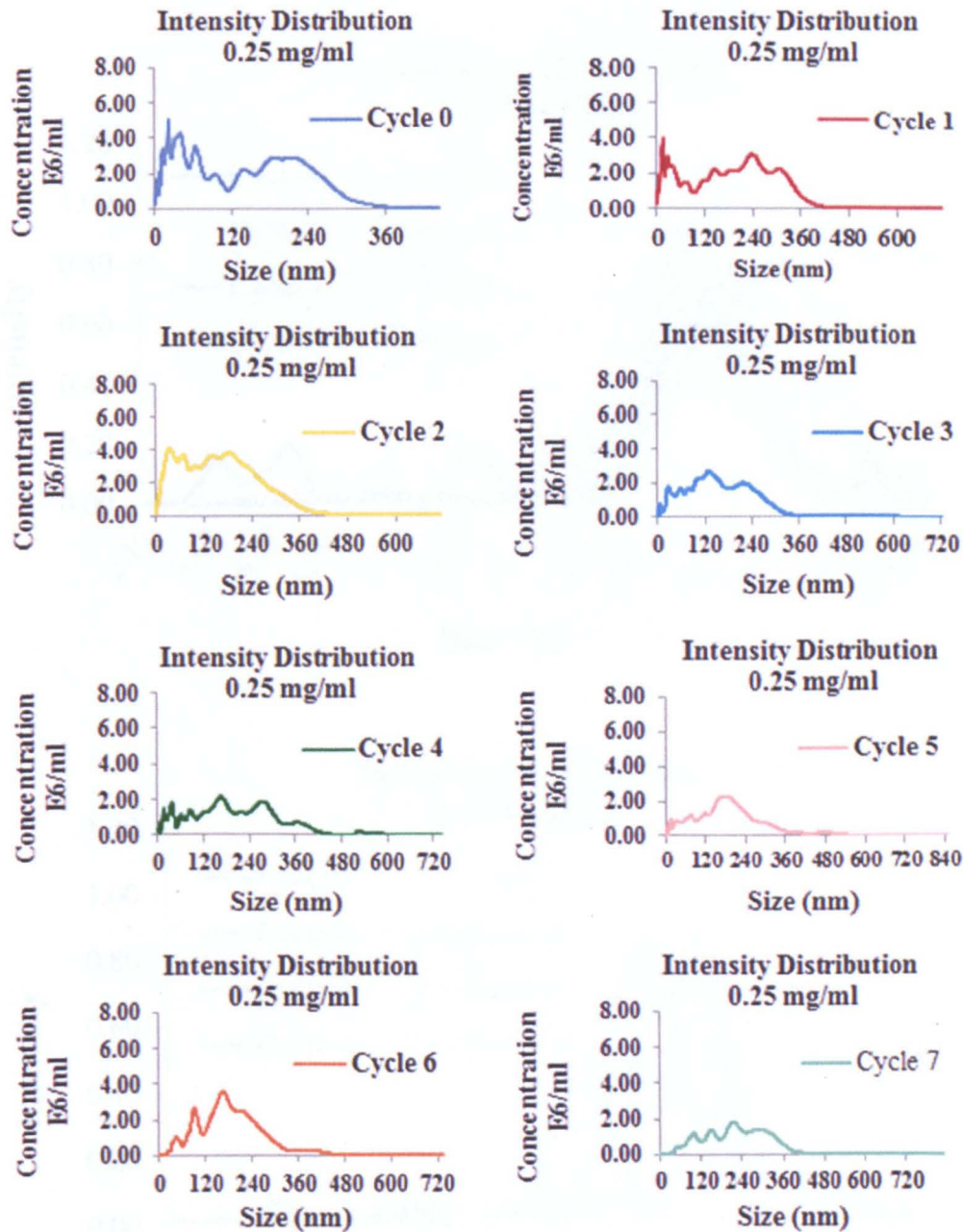
A. 4.2 AFM measured aggregation profiles of IgG (0.75 $\mu\text{g/ml}$, Cycle 1)



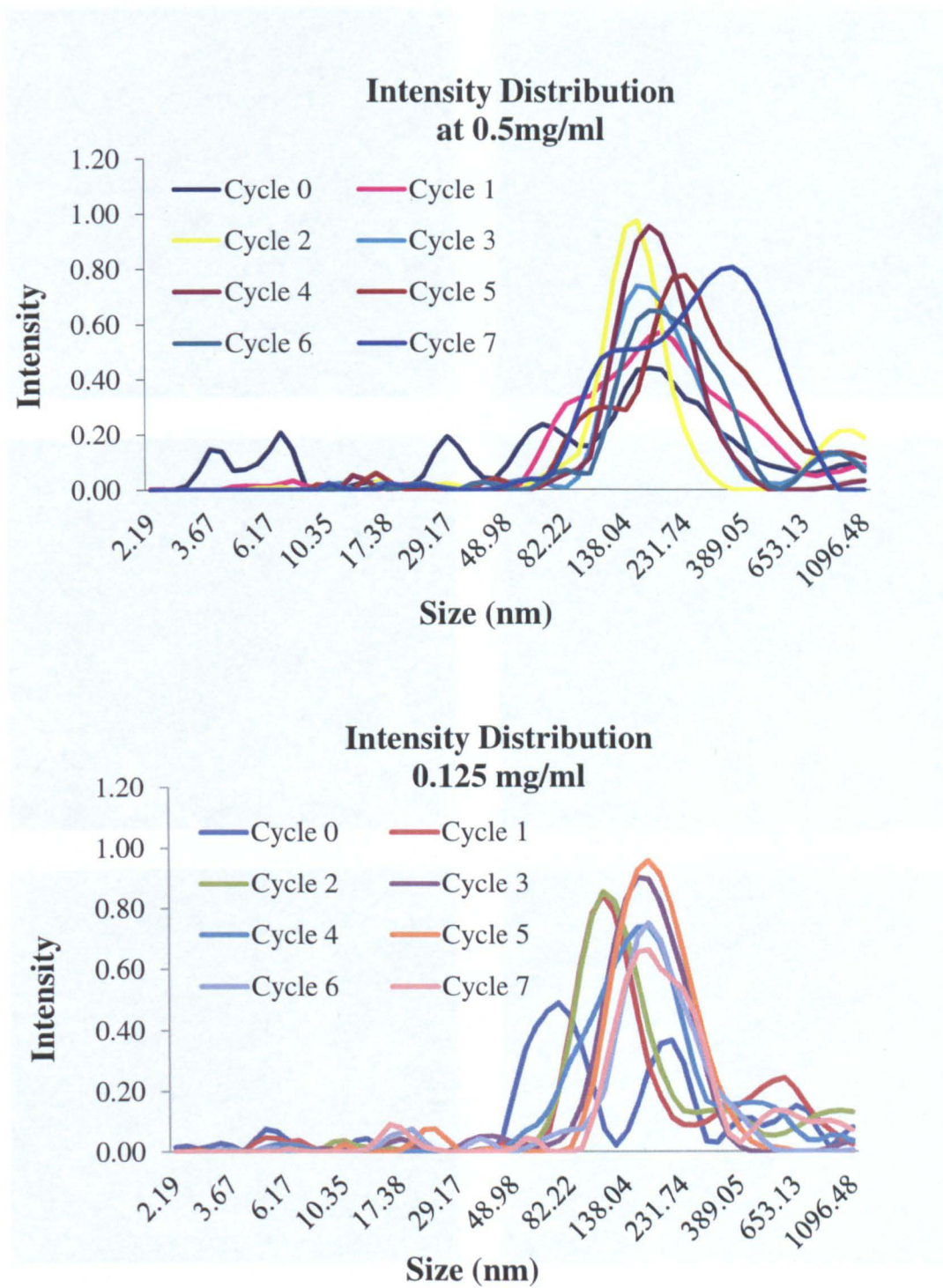
A.4.3 AFM measured aggregation profiles of IgG (1 µg/ml, Cycle 0).



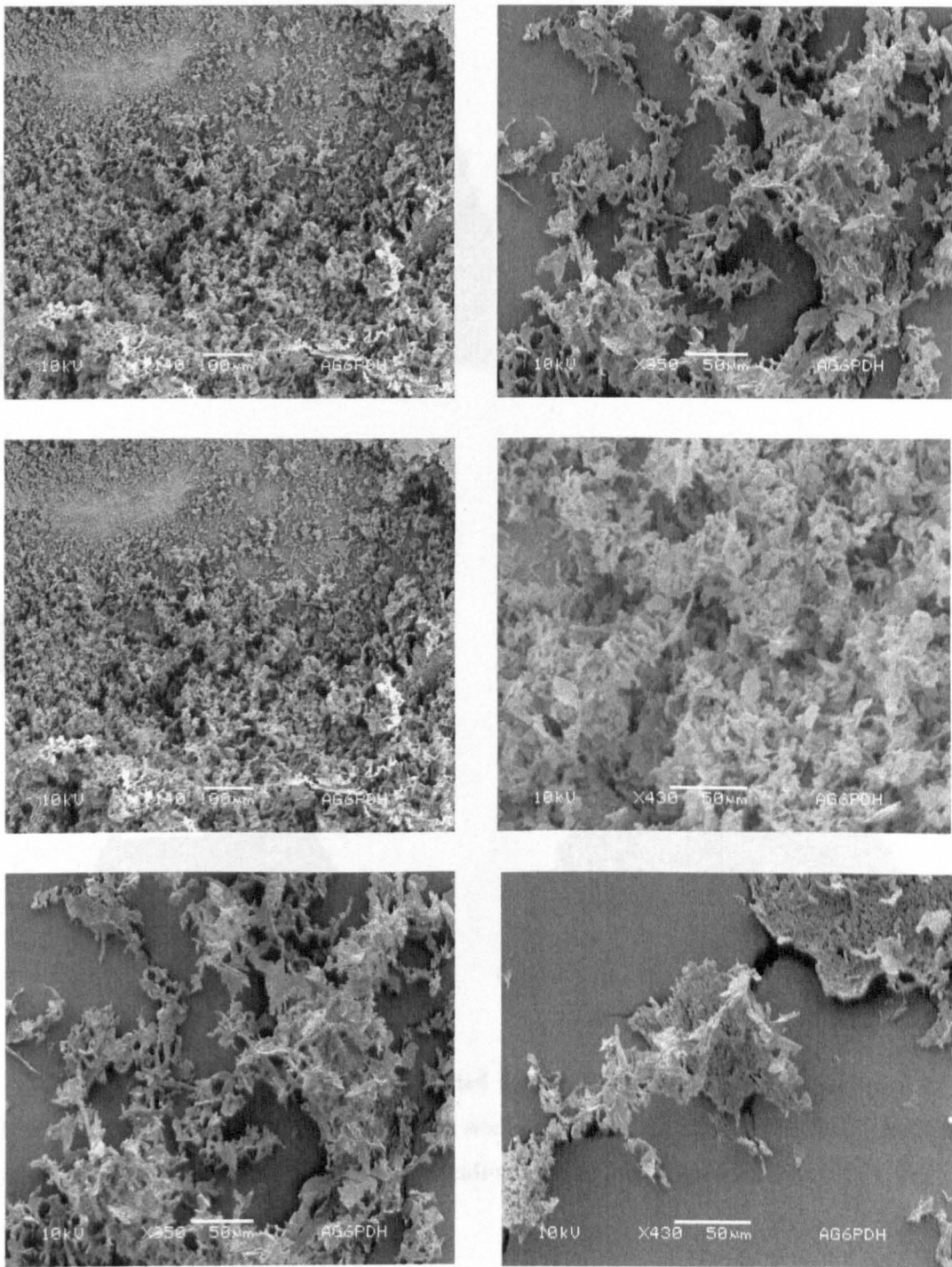
A.4.4 AFM measured aggregation profiles of IgG (1 µg/ml, Cycle 1)



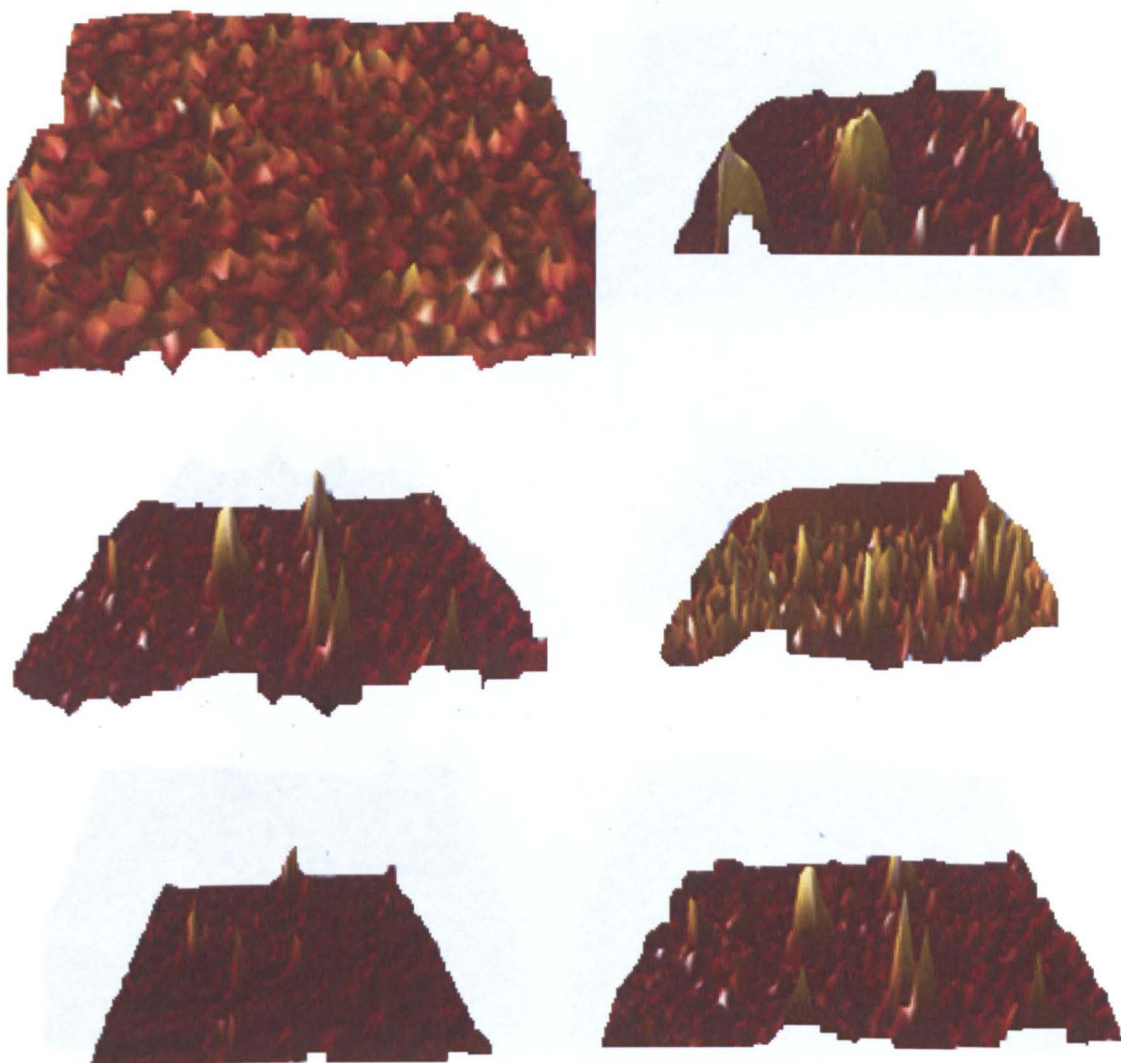
A.4.5 Aggregation profiles of multiple times (0 – 7) lyophilized IgG formulations obtained by NTA at room temperature after doubling the concentration of the suspended protein from 0.25 – 0.5 mg/ml.



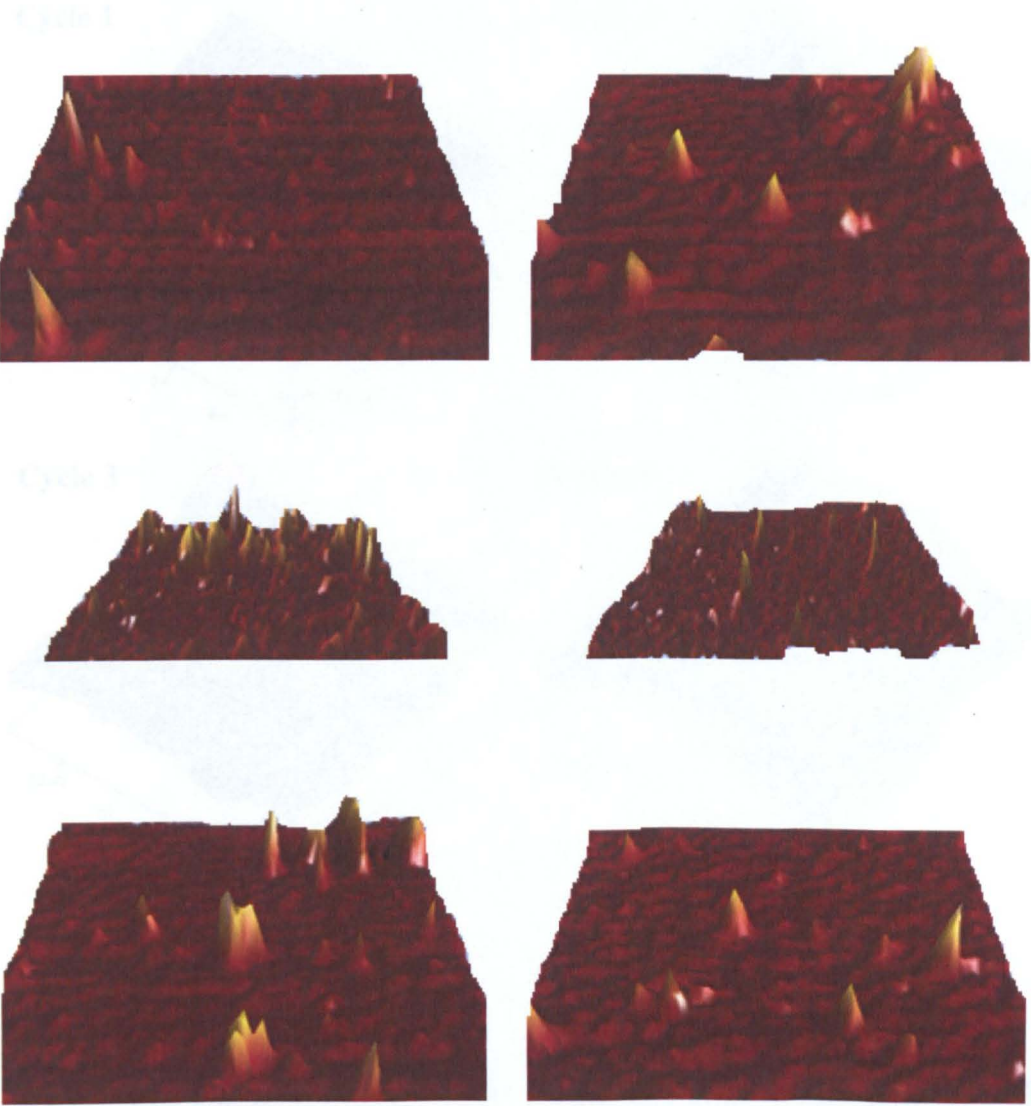
A.4.6 Overlaid aggregation profiles of multiple times (0 – 7) lyophilized IgG formulations obtained by DLS at room temperature at two different concentrations (0.125 and 0.5 mg/ml) of the protein solution.



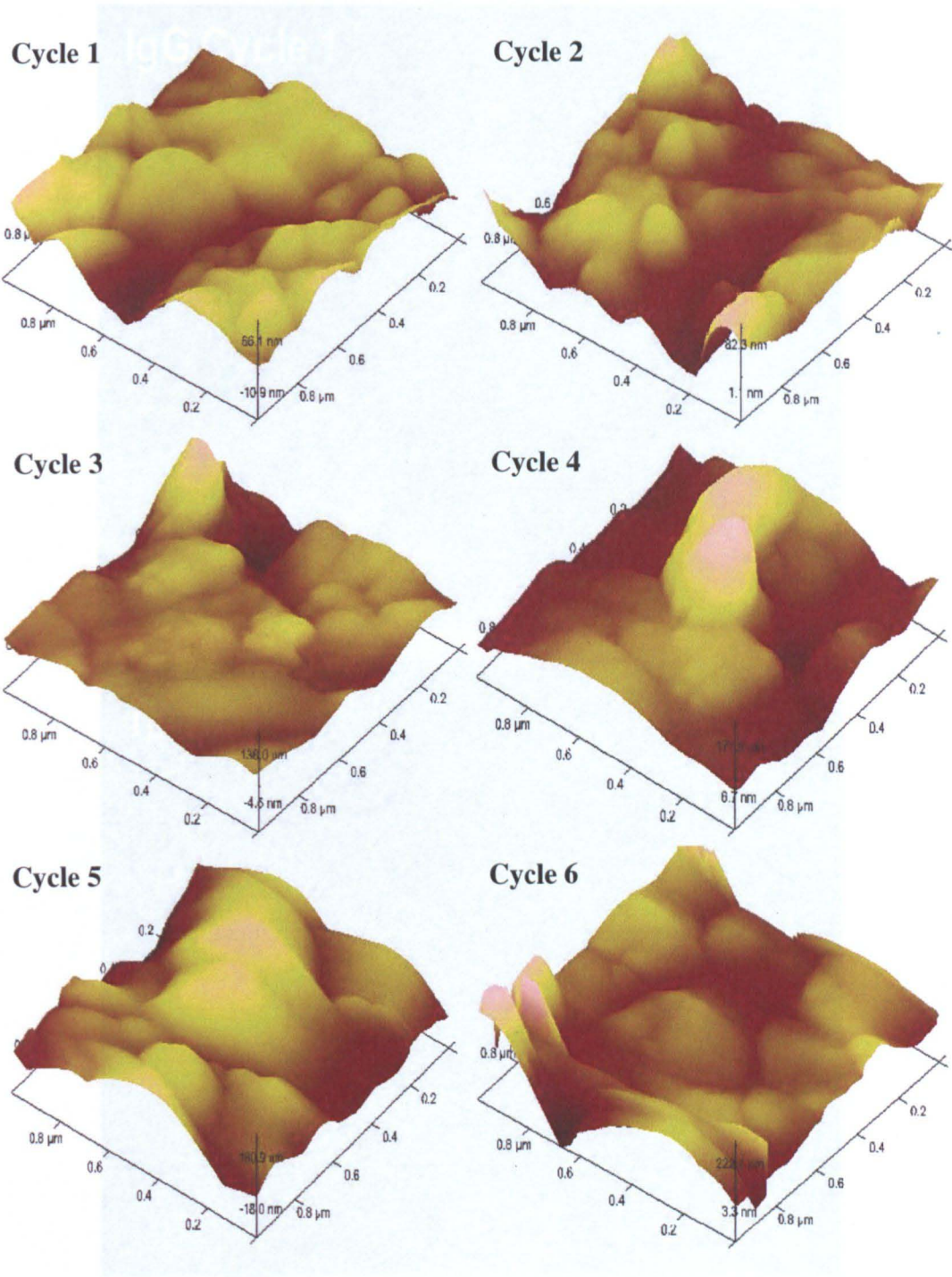
A.4.7 SEM images of IgG (zero – cycled) indicating porous and flaky nature of the antibody formulation which are important for quick solubility. Each scan is 50 micron obtained at low magnification (10 kV).



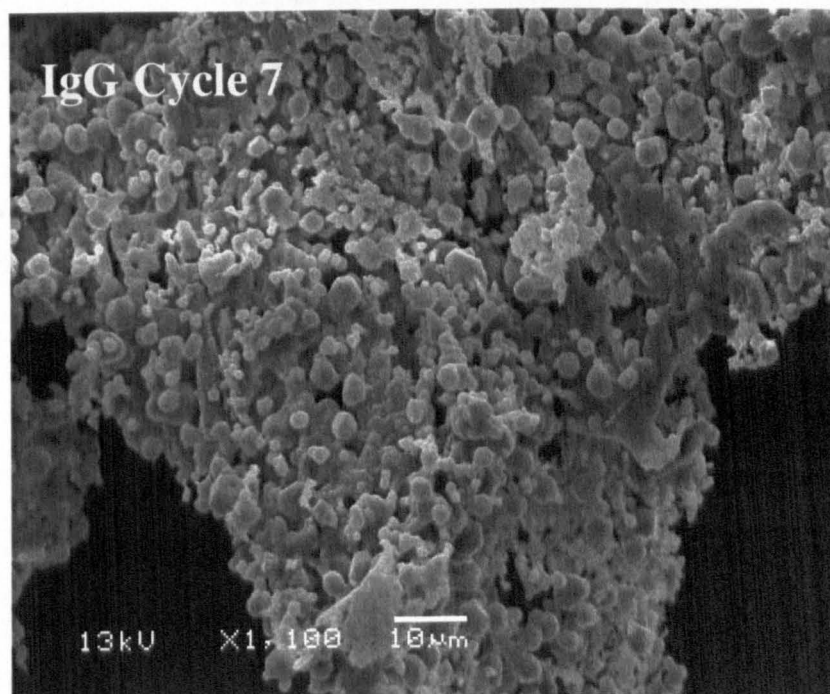
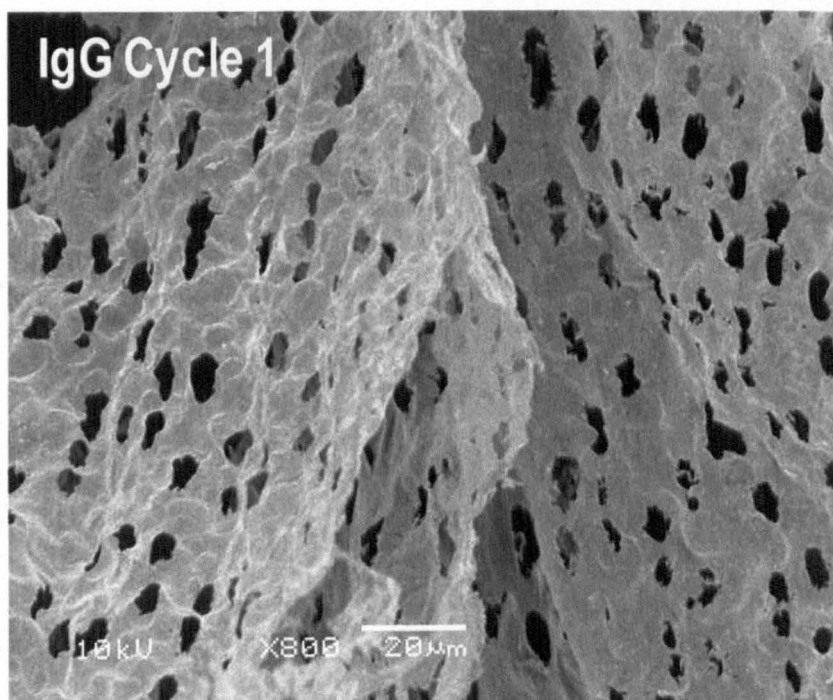
A.4.8 3 – D AFM images of zero – cycled IgG in PBS (0.01 M PBS), indicating formation of a range of aggregates. Each scan is one micron obtained at scan speed of 2 Hz. Images taken from different locations of the same sample. Z – scales are 3.9 nm – 12 nm.



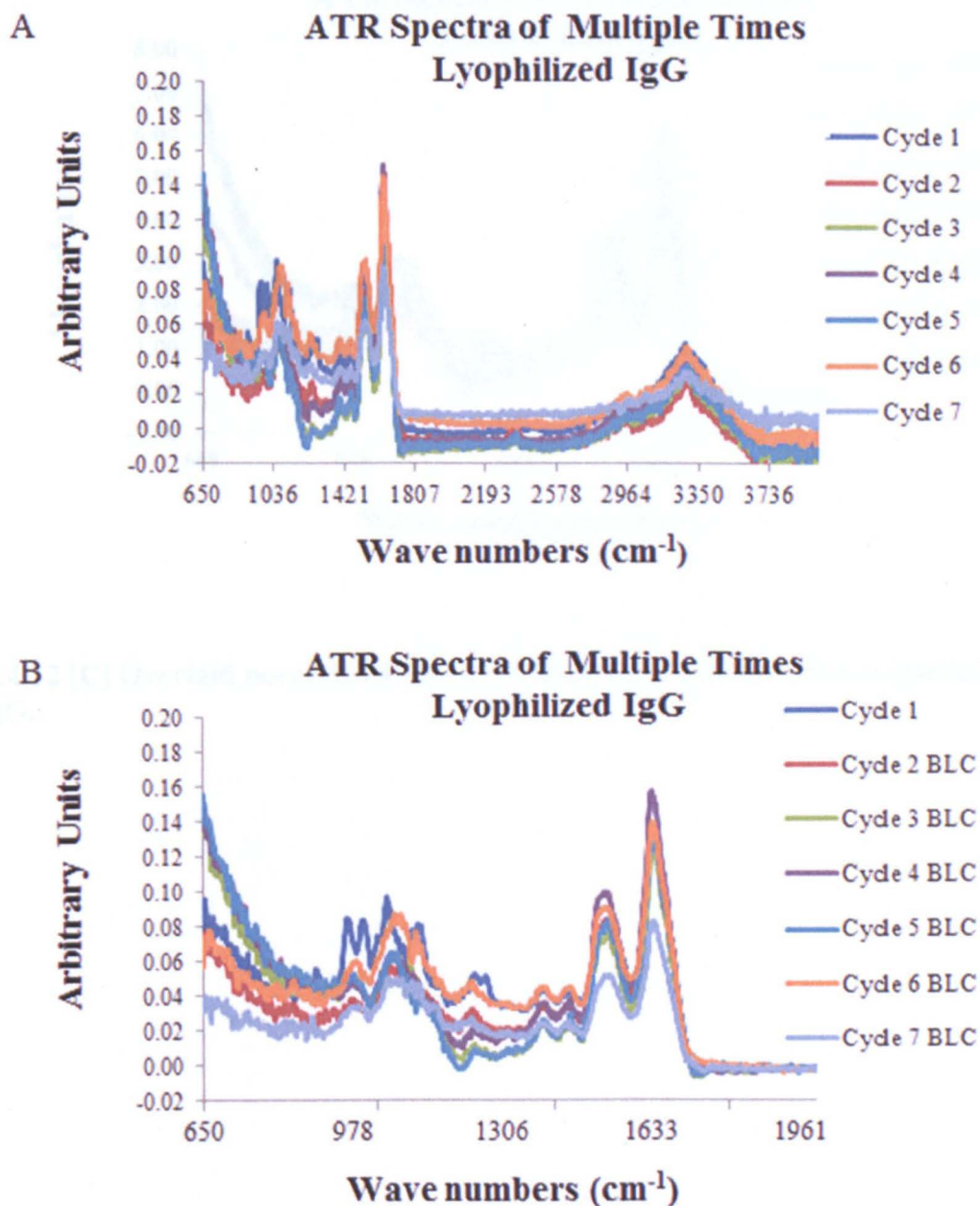
A.4.9 3-D AFM images of one cycled IgG PBS (0.01 M PBS), indicating formation of a range of aggregates. Each scan is one micron obtained at scan speed of 2 Hz from different locations of the same sample. Z – scales are 4 – 12 nm.



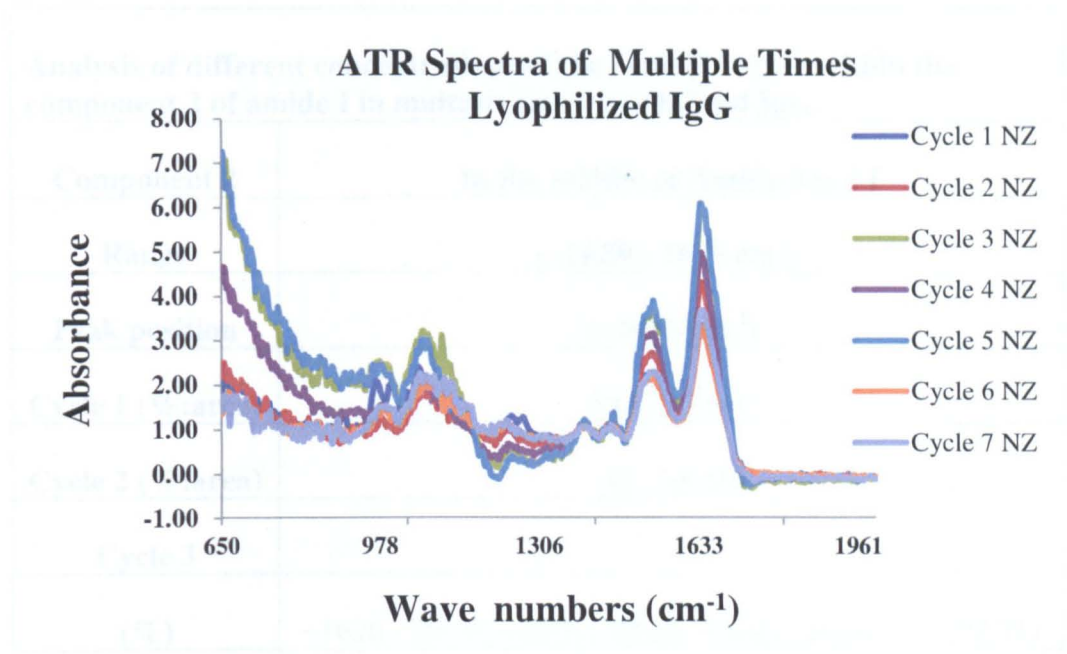
A.4.10 3 – D AFM images of multiple times lyophilized IgG indicating formation of a range of aggregates. Size of aggregates appears to increase after multiple lyophilization. Each scan is one micron obtained at scan speed of 2 Hz. Z – scales are 66 nm, 82 nm, 138 nm, 171 nm, 180 nm and 222 nm for 1, 2, 3, 4, 5 and 6 times lyophilized IgG respectively.



A.4.11 Second set: - SEM images of multiple times lyophilized IgG indicating formation of a range of aggregates. Size of aggregates and crystalline content appears to increase, whereas porosity and flakiness decreased after multiple lyophilization.



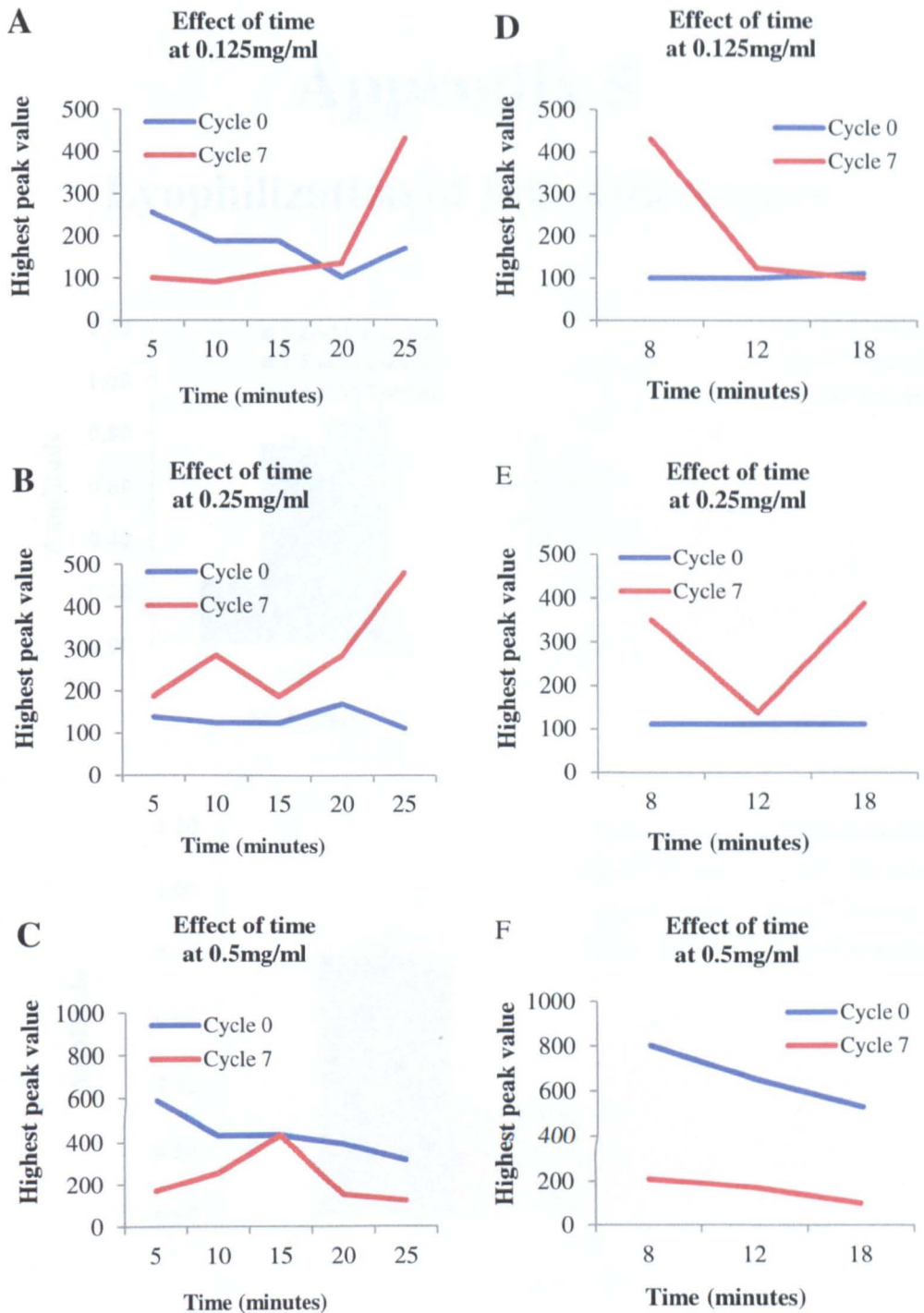
A.4.12 Overlaid ATR-IR spectra of multiple times lyophilized IgG:- Raw data[A]: Baseline corrected data [B]. Amide I and II appear in all samples; indicating secondary structure does not completely collapse during multiple lyophilization.



A.4.12 [C] Overlaid normalized ATR – IR spectra of multiple time lyophilized IgG.

Analysis of different concentrations of the main β – sheet within the component 2 of amide I in multiple times lyophilized IgG.	
Component 2	In the middle of Amide band I
Range	(~1628 – 1645 cm^{-1})
Peak position	(~1639 cm^{-1})
Cycle 1 (%:area)	55.37 : 110.7
Cycle 2 (%:area)	52 : 90.07
Cycle 3	
(%)	~1626 : 20.10; ~1636 : 10.24; ~1649 : 26.20 ----- (52.71)
Area	~1626 : 62.40; ~1636 : 32.10; ~1649 : 80.00 ----- (175.5)
Cycle 4	
(%)	~1633 : 26.25; ~1641 : 26.45, ----- (52.70)
Area	~1633 : 63.60; ~1641 : 64.00, ----- (127.4)
Cycle 5	
(%)	~1625 : 18.03; ~1636 : 10.56; ~1649 : 31.08 ----- (59.57)
Area	~1625 : 56.50; ~1636 : 33.10; ~1649 : 97.30 ----- (177.5)
Cycle 6 (%:area)	46.95 ; 69.1
Cycle 7	
(%)	~1637 : 2.25; ~1638 : 36.50 ----- (38.75)
Area	~1637 : 4.01; ~1638 : 69.40 ----- (73.40)

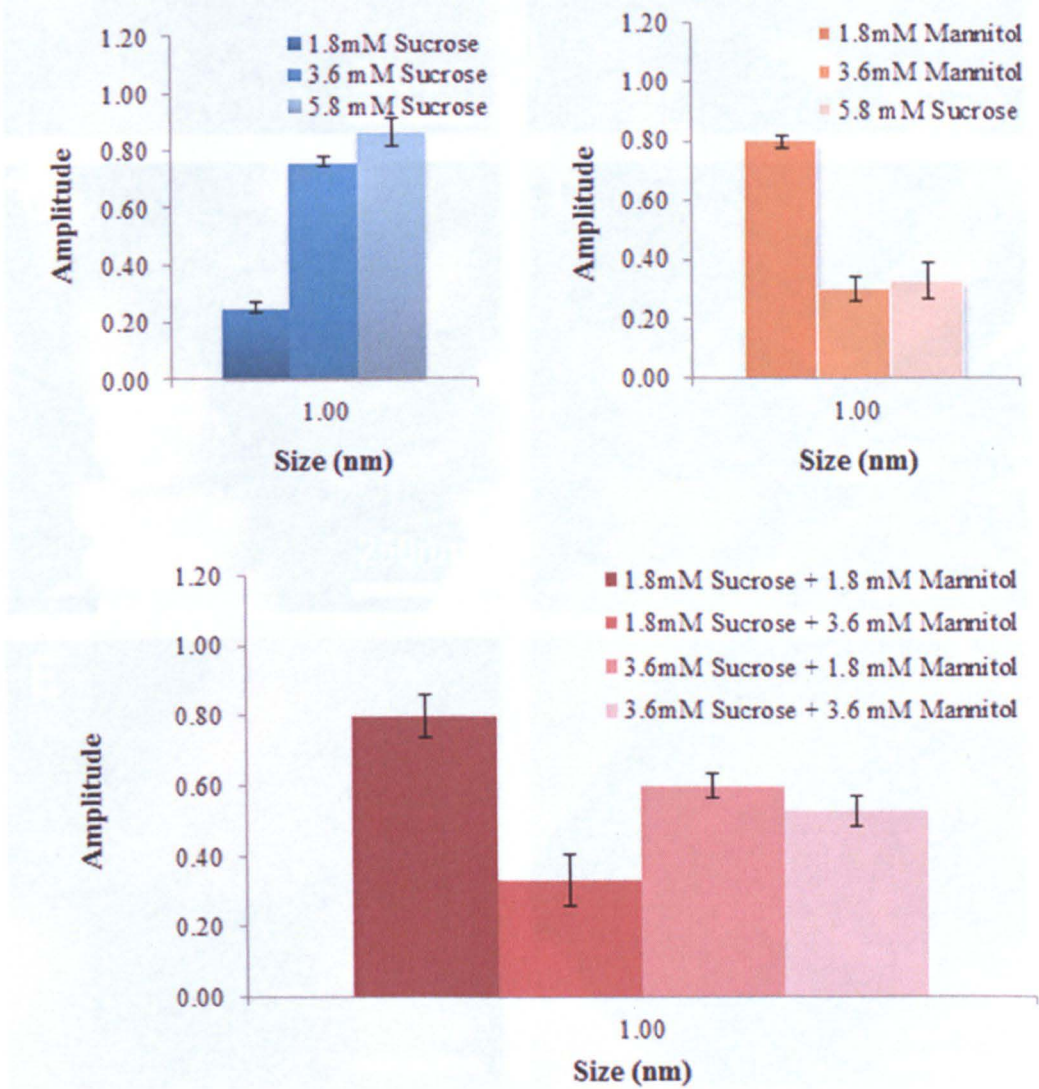
A.4.13 The different concentrations within main β – sheet component realized by IgG, under the influence of multiple cycles of lyophilization.



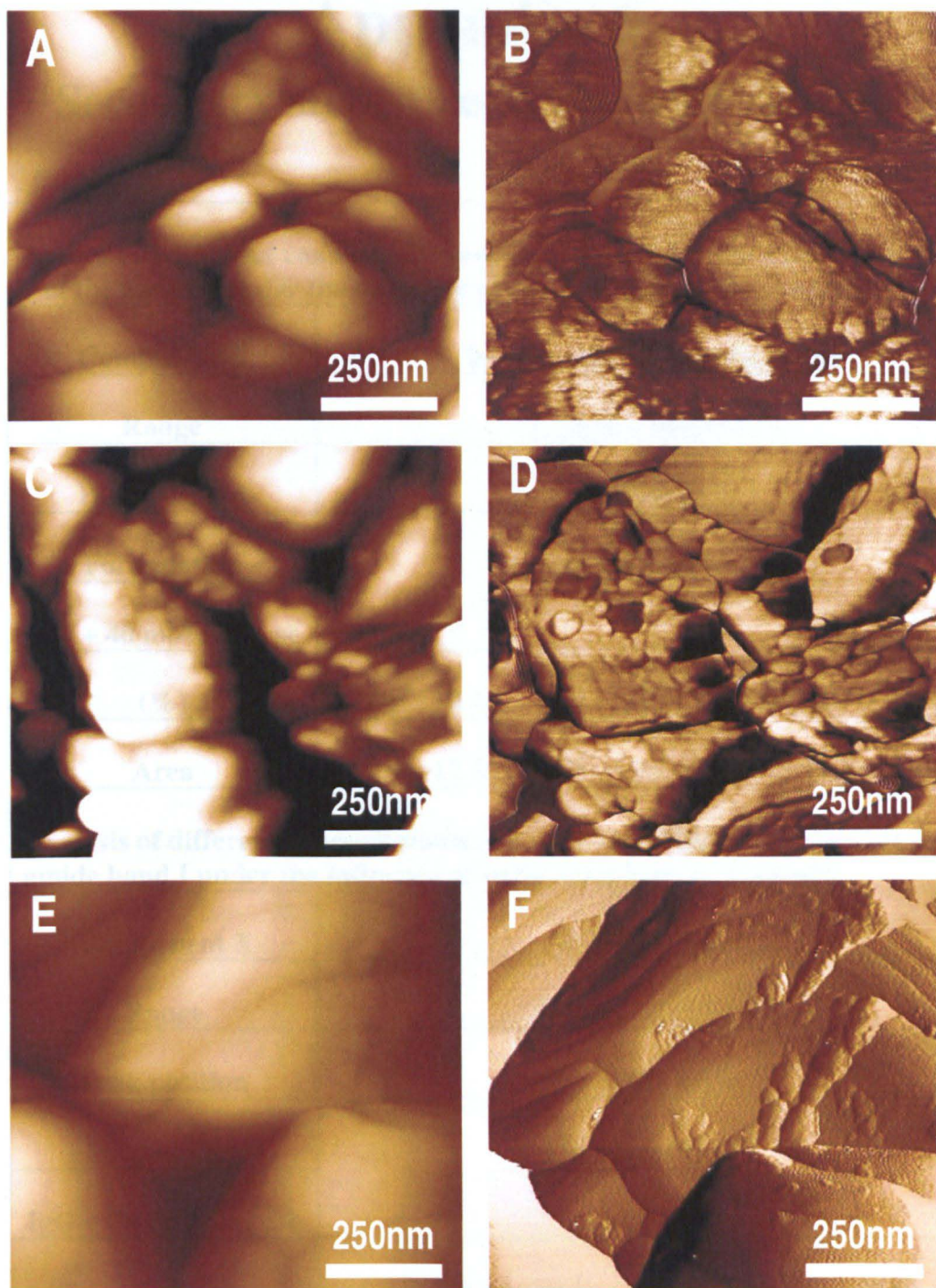
A.4.14 Aggregation behaviour of zero and seven times lyophilized IgG over time at three different concentrations. [A, B, C] and [C, D, E] respectively represents average of the data from ten and thirty DLS acquisitions. Aggregation decreases with time at higher concentration, whereas at lower concentrations, significant change after multiple lyophilizations.

Appendix 5

Lyophilization of IgG with Sugars



A.5.1 DLS control experiments for sugars alone and in combination. Size of sucrose equivalent to 1 nm was detected by DLS; however, no aggregation was detected irrespective of increase in the molar concentration of sugars.



A.5.2 [A – B], [C – D], and [E – F] respectively represent the AFM images (topography and phase) of once lyophilized: IgG + Sucrose (1 : 2, w/w), IgG + Mannitol (1 : 2, w/w), IgG + Sucrose + Mannitol (1 : 2 : 2, w/w/w). Each scan is one micron. All images have height (Z – scale) of 100 nm and a phase angle of 160°.

Appendix 6

Secondary structure of IgG with Sugars

Analysis of different concentrations of main β – sheet within the component 2 of the amide I under the influence of sugar excipients individually.	
Component 2	In the middle of Amide band I
Range	(~1628 – 1645 cm^{-1})
Peak position	(~1639 cm^{-1})
Formulation	Concentrations
IgG + 40 mM Sucrose	
(%)	
Area	~1624 : 10.42; ~1636 : 1.5; ~1646 : 50.52 ----- (62.52)
	~1624 : 12.30; ~1636 : 1.7; ~1646 : 50.40 ----- (64.40)
Analysis of different concentrations of β – turns within the component 3 of amide band I under the influence of sugar excipients individually.	
Component 3	in Amide band I
Range	(~1660 – 1677 cm^{-1})
Peak position	(~ 1670 cm^{-1})
Formulation	Concentrations
IgG + 20 mM Sucrose	
(%)	
Area	~1665.97 : 29.4 ; ~1665.49 : 21.2 ---- (52.6)
	~1665.97 : 37.7 ; ~1665.49 : 27.2 ---- (64.9)

A.6.1 Influence of sucrose on the different β – sheet concentrations in components 2 and 3 within the amide band I.

Analysis of different concentrations of main β – sheet within component 2 of the amide I under the influence of sugar excipients in combination	
Component 2	In the middle of Amide band I
Range	(~1628 – 1645 cm^{-1})
Peak position	(~1639 cm^{-1})
Formulation (I)	Concentrations
IgG + 20 mM Sucrose + 40 mM Mannitol	
(%)	~1624 : 11.09; ~1642 : 37.6 ----- (48.7)
Area	~1624 : 5.70; ~1642 : 19.3 ----- (25.0)
IgG + 40 mM Sucrose + 20 mM Mannitol	Concentrations
(%)	~1633 : 25.56; ~1643 : 32.24 ----- (57.8)
Area	~1633 : 16.80; ~1643 : 21.1 ----- (37.9)
Analysis of different concentrations of β-turns within the component 3 of amide band I under the influence of sugar excipients in combination	
Component 3	within amide band I
Range	(~1660 – 1677 cm^{-1})
Peak position	(~ 1670 cm^{-1})
IgG + 20 mM Sucrose + 40 mM Mannitol	Concentrations
(%)	~1673.66 : 11.5 ; ~1660.40 : 19.3 ---- (30.8)
Area	~1673.66 : 5.9 ; ~1660.40 : 9.9 ---- (15.9)

A.6.2. Influence of sucrose and mannitol together on β -sheet concentrations in components 2 and 3 of the amide band I.

References

- [1] W. Wang, C.J. Roberts (2010) *Aggregation of Therapeutic Proteins*, Wiley and Sons.
- [2] S. Zolls, R. Tantipolphan, M. Wiggenhorn, G. Winter, W. Jiskoot, W. Friess, A. Hawe (2011), Particles in therapeutic protein formulations, Part 1: Overview of analytical methods, *Journal of Pharmaceutical Sciences*, 101:914-935
- [3] Gary Walsh, (1998) *Biopharmaceuticals: Biochemistry and Biotechnology*, Wiley and Sons.
- [4]http://medlibrary.org/medwiki/Monoclonal_antibody_therapy#FDA_approved_therapeutic_antibodies
- [5] www.phrma.org/research/new-medicines
- [6] D. J. A. Crommelin and R. D. Sindelar (2002) An introduction for pharmacists and pharmaceutical scientists, *Pharmaceutical biotechnology*
- [7] H. Almeida, M.H. Amaral, P. Lobao, (2011), Drugs obtained by biotechnology processing, *Brazilian Journal of Pharmaceutical Sciences*, 47:199-205
- [8] U. Hansson, (1968) Aggregation of human IgG upon freezing, *Acta Chemica Scandiva*, 22:483-489
- [9] Sochava (1997) Heat capacity and thermodynamic characteristics of denaturation and glass transition of hydrated and anhydrous proteins, *Biophysical Chemistry*, 69:34 – 41
- [10] Y. H. Liao, M. B. Brown, T. Nazir, A. Quaquer, G. P. Martin (2002) Effects of sucrose and trehalose on the preservation of the native structure of spray-dried lysozyme, *Pharmaceutical Research*, 19:1847–1853
- [11] M. J. Pikal, K. Dellerman, M. L. Roy (1991) Formulation and stability of freeze-dried proteins: Effects of moisture and oxygen on the stability of freeze-dried formulations of human growth hormone. *Developmental Biology Stand*, 74:21–38
- [12] L. Chang, D. Shepherd, J. Sun, D. Ouellette, X. Grant, X. Tang, M. J. Pikal (2005) Mechanism of protein stabilization by sugars during freeze drying and storage: Native structure preservation, specific interaction and/or immobilization in a glassy matrix. *Journal of Pharmaceutical Sciences*, 94:1427–1444
- [13] W. Wang, (2000) Lyophilization and development of solid protein, 203; 1-60
-

-
- [14] S. Kiese, A. Pappenberger, W. Fries, and M. Hans-Christain, (2009) Equilibrium studies of protein aggregates and homogeneous nucleation in protein formulation, *Journal of Pharmaceutical Sciences*, 6-12
- [15] S. Jaing and S.L. Nail, (1998) Effect of process conditions on recovery of protein activity after freezing and freeze-drying, *European Journal of Pharmaceutics and Biopharmaceutics*, 45:249-257
- [16] V. S. Purohit, C.R. Middaugh, S.V. Balasubramanian, (2006) Influence of aggregation on immunogenicity of recombinant human Factor VIII in hemophilia A mice, *Journal of Pharmaceutical Sciences*, 95:358-371
- [17] Y. J. Wang, M.A. Hanson, (1988), Parental formulations of proteins and peptides: stability and stabilisers, *Journal of Parenter Science and Technology*, 42: 2-26
- [18] A. M. Morris, M.A. Watzky, and R.G. Finke, (2009) Protein aggregation kinetics, mechanism and curve fitting, *Proteins and Proteomics*, 1794:375-397
- [19] K. L. yielding, G.M. Tomkins, (1962) Inhibition of glutamic dehydrogenase by O-phenanthroline and its analogs, *Biochemica et Biophysica Acta*, 62:327-331
- [20] D. Burdick, B. Soreghan, M. Kown, (1992) Assembly and aggregation properties of synthetic Alzheimer's A4/ β amyloid peptide analogs, *The Journal of Biological Chemistry*, 267: 546-554
- [21] R. M Murphy, (2002) Peptide aggregation in neurodegenerative disease, *Annual Review of Biomedical Engineering*, 4: 155-174
- [22] A. P. Pawar, K.F. Dubay, C.M. Dobson, Murphy, (2005) Prediction of aggregation-prone and aggregation susceptible regions in proteins associated with neurodegenerative diseases, *Journal of Molecular Biology*, 350: 379-392
- [23] B. S. Shastry, (2005) Neurodegenerative disorders of protein aggregation, *Neurochemistry International*, 43: 1-7
- [24] E. Y. Chi, S. Krishnan, T. W. Randolph, J. F. Carpenter, (2003) Physical stability of proteins in aqueous solution: Mechanism and driving forces in non-native protein aggregation, *Pharmaceutical Research*, 1325: 1336
- [25] C. J. Roberts, (2007) Non-native aggregation kinetics, *Biotechnology and Bioengineering*, 98-927-937
- [26] A. L. Fink (1998) Protein aggregation: folding aggregates, inclusion bodies and amyloid, *Folding and Design*, 3:R9-R23
- [27] G. W. Platt, S.E. Radford (2009) Glimpses of the molecular mechanisms of β_2 -microglobulin fibril formation in vitro: Aggregation on a complex energy landscape, *FEBS Letters*, 583: 2623-2629
-

-
- [28] J. London, C. Skrzynia, M. E. Goldberg, (1974) Renaturation of *Escherichia coli* Tryptophanase after Exposure to 8 M urea, *European Journal of Biochemistry*, 47:409 – 415
- [29] C. A. Haasse - Pettingell, and J. King, (1988) Formation of aggregates from a thermolabile in vivo folding intermediate in P22 tailspike maturation; A model for inclusion body formation, *The Journal of Biological Chemistry*, 263: 4977-4983
- [30] R. Wetzel (1994) Mutation and off-pathway aggregation of proteins, *Trends in Biotechnology*, 12:193-198
- [31] T. J. Ahern, M. C. Manning, (1992) Stability of protein pharmaceuticals, Part B; In vivo pathways of degradation and strategies for protein stabilization, *Plenum Press, New York*, 3: 43–88
- [32] J. S. Philo and T. Arakawa, (2009) Mechanisms of Protein Aggregation, *Current Pharmaceutical Biotechnology*, 10:348 -351
- [33] J. J. Balbach, A. T. Petkova, N. A. Oyler, O. N. Antzutkin, D. J. Gordon, S. C. Meredith, and R. Tycko, (2002) Supramolecular structure in full length Alzheimer's beta-amyloid fibrils: Evidence for a parallel beta-sheet organization from solid-state nuclear magnetic resonance, *Biophysical Journal*, 83:1205-1216
- [34] www.mun.ca/biology/scarr/MGA2_03-18b.html
- [35] images.flatworldknowledge.com/ballgob/ballgob-fig18_004.jpg
- [36] P. M. Harrison, H. S. Chan, S. B. Prusiner, F. E. Chen, (2008) Conformational propagation with prion-like characteristics in a simple model of protein folding, *Protein Science*, 10:819-835
- [37] V. S. Purohit, C.R. Middaugh, S.V. Balasubramanian , (2006) Influence of aggregation on immunogenicity of recombinant human Factor VIII in hemophilia A mice, *Journal of Pharmaceutical Sciences*, 95:358–371
- [38] A. M. Morris, M.A. Watzky, and R. G. Finke, (2009) Protein aggregation kinetics, mechanism and curve fitting, *Proteins and Proteomics*, 1794:375-397
- [39] S. Kiese, A. Pappenberger, W. Fries, and M. Hans-Christain, (2009) Equilibrium studies of protein aggregates and homogeneous nucleation in protein formulation, *Journal of Pharmaceutical Sciences*, 6-12
- [40] D. N. Brems, S.M. Plastied. W.W. Kauffmann, H.A. Havel, (1986), Characterization of an associated equilibrium folding intermediate of bovine growth hormone, *Biochemistry*, 25:6539-654
- [41] K. Ahrer, A. Buchacher, G. Iberer, A. Jungbauer, (2006) Effect of ultra-/diafiltration conditions on present aggregates in human immunoglobulin G preparations, *Journal of Membrane Science*, 274:108-115
-

- [42] A. S. Rebecca, E. A. Lutz, G. Imola, (2008), α -synuclein conformation affects its tyrosine-dependent oxidative aggregation, *Biochemistry*, 47: 13604-13609
- [43] T. Arakawa, S. J. Prestrelski, W. C. Kenny, J. F. Carpenter, (2001), Factors affecting short-term and long-term stabilities of proteins, *Advanced Drug Delivery*, 46:307-326
- [44] Z. Z. Hua, B.G. Li, Z. J. Liu, D. W. Sun, (2003) Freeze-drying of liposomes with cryoprotectants and its effect on retention rate of encapsulated Ftorafur and Vitamin A, *Drying Technology: An International Journal*, 21:1491-1505
- [45] W. Abdelwahed, G. Degobert, S. Stainmesse, H. Fessi (2006) Freeze-drying of nanoparticles: Formulation, process and storage considerations, *Advanced Drug Delivery Reviews*, 58:1688-1713
- [46] F. Carpenter, S.J. Prestrelski and T. Arakawa, (1993) Separation of freezing- and drying-induced denaturation of lyophilized proteins using stress-specific stabilization, *Archives of Biochemistry and Biophysics*, 456-464
- [47] L. Bongini, D. Fanelli, F. Piazza, S. Sandin, and U. Skoglund, (2004) Freezing immunoglobulins to see them move, *Proceedings of the National Academy of Sciences*, 101: 6467-6471
- [48] M. Paborji, N.L. Pochopin, W.P. Coppola, J.B. Bogardus, (1994), Chemical and physical stability of chimeric L6, a mouse human monoclonal antibody, *Pharmaceutical Research*, 11:764-771
- [49] J. M. Sarciaux, S. Mansour, Micheal, J. Hagemane and S.L. Nail, (1999), Effects of buffer composition and processing conditions on aggregation of bovine IgG during freeze-drying, *Journal of Pharmaceutical Sciences*, 88:1344-1359
- [50] C. C. Hsu, H.M. Nguyen, D.A. Yeung, and D.A. Brooks, (1995), Surface denaturation at solid-void interface: A possible pathway by which opalescent particulates form during the storage of lyophilised tissue-type plasminogen activator at high temperatures, *Pharmaceutical Research*, 12:69-77
- [51] B. S. Chang, B. S. Kendrick, and J. F. Carpenter, (1996) Surface induced denaturation of proteins during freeze drying and its inhibition by surfactants, *Journal of Pharmaceutical Research*, 85:1325-1330
- [52] L. F. Pease, J. T. Elliot, D. H. Tsai, M. R. Zachariah, (2008), Determination of protein aggregation with differential mobility analysis: Application to IgG antibody, *Biotechnology and Bioengineering*, 101:1214-1222
- [53] B. M. Eckhardt, J. Q. Oeswein, and T. A. Bewley, (1991), Effect of freezing of aggregation of human growth hormone, *Pharmaceutical Research*, 8:1360-136
- [54] S. Yoshioka, Y. Aso, K. Itzutsu and T. Terao, (1993) Aggregates formed during storage of β -galactosidase in solution and in the freeze-dried state, *Pharmaceutical Research*, 687-690

-
- [55] W. Wang, (2005) Protein aggregation and its inhibition in bio-pharmaceutics, *International Journal of Pharmaceutics*, 289:1-30
- [56] K. D. Caldwell, Y.S. Gao, (1993) Electrical field flow fractionation in particle separation, *Analytical chemistry*, 65:1764-1772
- [57] W. Abdelwahed, G. Degobert, S. Stainmesse, H. Fessi, (2006), Freeze-drying of nanoparticles: formulation, process and storage considerations, *Advanced Drug Delivery Review*, 58:1688–1713
- [58] T. J. Anchordoquy, T.W. Randolph, J.F. Carpenter, (2001) Maintenance of quaternary structure in the frozen state stabilizes lactate dehydrogenase during freeze drying, *Archives of Biochemistry and Biophysics*, 390:35- 41
- [59] K. Izutsu, S. Yoshioka and S. Kojima, (1994), Physical stability and protein stability of freeze-dried cakes during storage at elevated temperatures, *Pharmaceutical Research*, 994-999
- [60] T. Cochran, and S. L. Nail, (2009) Ice nucleation temperature influences recovery of activity of a model protein after freeze drying, *Journal of Pharmaceutical Sciences*, 9:3495-8
- [61] U. Hansson, (1968) Aggregation of human IgG upon freezing, *Acta Chemica Scandinavica*, 22:483-489
- [62] Ramos *et al*, (1997) Stabilization of enzymes against thermal stress and freeze-drying by mannosyl-glycerate, *Applied and Environmental Microbiology*, 63:4020-4025
- [63] A. Hawe, J. C. Kasper, W. Friess, W. Jiskoot (2009) Structural properties of monoclonal antibody aggregates induced by freeze–thawing and thermal stress, *European Journal of Pharmaceutical Sciences*, 38: 79-87
- [64] S. Allen, X. Y. Chen, J. Davies, M. C. Davies, A. C. Dawkes, J. C. Edwards, C. J. Roberts, J. Sefton, S. J. B. Tendler, and P. M. Williams, (1997) Detection of antigen-antibody events with atomic force microscope, *Biochemistry*, 36:7457-7463
- [65] L. Li, S. Chen, S. Oh, and S. Jiang (2002) In situ single-molecule detection of antibody-antigen binding by tapping-mode atomic force microscopy, *Analytical Chemistry*, 74:6017-6022
- [66] A. S. Paulo and R. Garcia, (2000) High-resolution imaging of antibodies by tapping-mode atomic force microscopy: Attractive and repulsive tip-sample interaction regimes, *Biophysical Journal*, 78:1599-1605
- [67] N. H. Thomson, (2005) The substructure resolution of IgG resolved to 25 kDa using amplitude modulation AFM in air, *Ultramicroscopy*, 105: 103-110
- [68] C. Moller, M. Allen, V. Ellings, A. Engel, and D. J. Muller, (1999) Tapping mode atomic force microscopy produces faithful high resolution images of protein surfaces, *Biophysical Journal*, 77:1150-1158
-

- [69] J. M. Andrews, and C. J. Roberts, (2007) Non-native aggregation of a-chymotrypsinogen occurs through nucleation and growth with competing nucleus sizes and negative activation energies. *Biochemistry* 46: 7558–7571
- [70] K. Aher, A. Buchacher, G. Iberer, D. Josic, and A. Jungbauer, (2003) Analysis of aggregates of IgG using size-exclusion chromatography, static and dynamic light scattering, *Journal of Chromatography*, 1009:89-96
- [71] P. Chames, M.V. Regenmortel, E. Weiss and D. Baty, (2009) Therapeutic antibodies: successes, limitations and hopes for the future, *British Journal of Pharmacology*, 157:220-233
- [72] A. S. Trevani, G. Andonegui, C. Kempfer, E. Malchiodi, and J.R. Jeffner, (1996) Activation of human neutrophils induced by immune complexes prepared with cationic and anionic fractions of normal IgG antibodies, *Journal of Immunology*, 43:341-344
- [73] C. Prin, M.C. Bene, B. Gobert, P. Montagne, and G.C. Faure, (1995) Isoelectric restriction of human immunoglobulin isotypes, *Biochemica and Biophysica Acta*, 287-290
- [74] L. M. Amzal, and R.J. Poljak, (1979) Three - dimensional structure of immunoglobulins, *Annual Review in Biochemistry*, 48:961-97
- [75] J. Yang, C. Ng, H. Lowman, R. Chestnut, G. Bennett, V. Quarmby, (2008) Quantitative determination of humanized monoclonal antibody rhuMAb2H7 in cynomolgus monkey serum using a Generic Immunoglobulin Pharmacokinetic (GRIP) assay, *Journal of Immunological Methods*, 335:8-20
- [76] www.piercenet.com/files/TR0006-Extinction-coefficients
- [77] J. S. Hamada, (1997) Characterisations of protein fractions of rice bran to devise effective methods for protein solubilisation, *Cereal Chemistry*, 75:662-668.
- [78] K. D. Caldwell, Y.S. Gao, (1993) Electrical field flow fractionation in particle separation, *Analytical chemistry*, 65:1764-1772
- [79] U. Galili, E. A. Rachmilewitz, A. Peleg, and I. Flechner, (1984) A unique natural human IgG antibody with anti-alpha-galactosyl specificity, *Journal of Experimental Medicine*, 160:1519-1531
- [80] F. He, D. H. Phan, S. Hogan, R. Bailey, G.W. Becker, L.O. Narhi, Razinkov (2010) Detection of IgG aggregation by a high throughput method based on extrinsic fluorescence, *Journal of Pharmaceutical Sciences*, 99:2598-2608
- [81] N. G. Khlebtsov, V. A. Bogatyrev, B. N. Khlebtsov, L. A. Dykman, P. Englebienne, (2004), A multilayer model for gold nanoparticle bioconjugates: Application to study gelatin and human IgG adsorption using extinction and light spectra and dynamic light scattering method, *Colloidal Journal*, 622-635

-
- [82] T. Shimzu, K. Yoshimune, T. Komoriya, T. Akiyama, X. Ye, H. Kohno, (2013) Monoclonal antibodies against large oval aggregates of A β ₁₋₄₂, *Journal of Bioscience and Bioengineering*, 115:216-220
- [83] V. Ostapchenko, M. Gasset, L.V. Baskakov, (2012) Atomic Force Fluorescence Microscopy in the Characterization of Amyloid Fibril Assembly and Oligomeric Intermediates, *Methods in Molecular Biology*, 849:157-167
- [84] C. Preininger, H. Clausen-Schaumann, A. Ahluwalia, D. D. Rossi, (2000) Characterization of IgG Langmuir–Blodgett films immobilized on functionalized polymers, *Talanta*, 52:921-930
- [85] D. J. Scott, P. Hucuk, A brief introduction to the analytical ultracentrifugation of proteins for beginners
- [86] J. S. Philo (2009), A critical review of methods for size characterization of non-particulate protein aggregates, *Current Pharmaceutical Biotechnology*, 10:359–372.
- [87] L. Bongini, D. Fanelli, F. Piazza, S. Sandin, and U. Skoglund, (2004) Freezing immunoglobulins to see them move, *Proceedings of the National Academy of Sciences*, 101: 6467-6471
- [88] C. Dolmann and R. Thorpe, Analysis and purification of IgG using size-exclusion high performance liquid chromatography
- [89] L. C. Santora, Z. Kaymakcalan, P. Sakorafas, I.S. Krull, (2001) Human monoclonal antibody and antigen using cation exchange, size exclusion chromatography and BIA core, *Analytical Bio-chemistry*, 299:119-129
- [90] V. Filipe, R. Poole, O. Oladunjoye, K. Braeckman's, W. Jiskoot, (2012) Detection and Characterization of Subvisible Aggregates of Monoclonal IgG in Serum, *Pharmaceutical Research*, 29:2202-2212
- [91] T. G. Rochow, E.G. Rochow, (1995) Scanning Electron Microscopy, *An Introduction to Microscopy by Means of Light, Electrons, X-Rays, or Ultrasound*, 273-278
- [92] A. J. McQuillan, (2001) Probing solid–solution interfacial chemistry with ATR-IR spectroscopy of particle films, *Pharmaceutical Research*, 13:1034-1038
- [93] A. H. Ghassemi, M. J. Steenbergen, H. Talsma, C. F. Nostrum, W. Jiskoot, D. J. A. Crommelin, W. E. Hennink, (2009) Preparation and characterization of protein loaded microspheres based on a hydroxylated aliphatic polyester, poly(lactic-co-hydroxymethyl glycolic acid), *Journal of Controlled Release*, 138:57-63
- [94] A. Voller, D. E. Bidwell, A. Bartlett (1979), The enzyme linked immunosorbent assay (ELISA), A guide with abstracts of microplate applications, 1979-2125
-

-
- [95] O. Sahin, S. Magonov, C. Su, C.F. Quate, O. Solgaard (2007) An atomic force microscope tip designed to measure time-varying nanomechanical forces, *Nature Nanotechnology*, 2:507-514
- [96] C. Gerber, H. P. Lang, (2006) How the doors to the nanoworld were opened, *Nature Nanotechnology*, 1:3-5
- [97] D. J. Muller, Y. F. Dufrene, (2008) Atomic force microscopy as a multifunctional molecular toolbox in nanobiotechnology, *Nature Nanotechnology*, 3:261-269
- [98] www.research.ibm.com/nanoscience/local_oxidation
- [99] A. Raman, S. Trigueros, A. Cartagena, A.P.Z. Stevenson, M. Susilo, E. Numan, and S. A. Contera (2011) Mapping nanomechanical properties of live cells using multi-harmonic atomic force microscopy, *Nature Nanotechnology*, 6:809-814
- [100] O. Sahin, S. Maganov, C. Su, C.F. Quate, O. Solgaard, (2007) An atomic force microscope tip designed to measure time-varying nanomechanical forces, *Nature Nanotechnology*, 2:507-514
- [101] N. R. Wilson, J. V. Macpherson, (2009) Carbon nanotube tips for atomic force microscopy, *Nature Nanotechnology*, 4:483-491
- [102] V. Kilson, J. J. Kuna, S. A. Contera, E. Tossati, S. Francesco, (2010) Direct mapping of the solid-liquid adhesion energy with subnanometre resolution, *Nature Nanotechnology*, 5:41- 405
- [103] G. B. Irvine, O. M. El-Agnaf, G. M. Shankar and D. M. Walsh, (2008) Protein aggregation in the brain: The molecular basis for Alzheimer's and Parkinson's Diseases, *Molecular Medicine*, 14:451-464
- [104] L. Tetard, A. Passian, T. Thundat, (2010) New modes for sub-surface atomic force microscopy through nanomechanical coupling, *Nature Nanotechnology*, 5:105-109
- [105] N. Jalili, K. Laxminarayana, (2004) A review of atomic force microscopy imaging systems: application to molecular metrology and biological sciences, *Mechatronics*, 14:907-945
- [106] R. Garcia, E.T. Herruza, (2012), The emergence of multifrequency force microscopy, *Nature Nanotechnology*, 7:217-226
- [107] A. S. Paulo, R. Garcia, (2000) High-Resolution imaging of antibodies by tapping-mode atomic force microscopy: attractive and repulsive tip-sample interaction regimes, *Biophysical Journal*, 78:1599-1605
- [108] R. X. Xiuo, W. Li, (2002) Preparation and characterization of macroporous poly (*N*-isopropylacrylamide) hydrogels for the controlled release of proteins, *Journal of Polymer Science*, 41:152-159
-

-
- [109] D. J. Stokes, (2003) Recent advances in electron imaging, image interpretation and applications: environmental scanning electron microscopy, *Philosophical Transactions of The Royal Society*, 361:2771-2787
- [110] H. M. Wyss, M. Hutter, M. Muller, L. P. Meier, L. J. Gaukler, (2003) Quantification of microstructures in stable and gelated suspensions from cryo-SEM, *Journal of Colloid and Interface Science*, 248:340-346
- [111] M. A. Hayat, V.N. Reinhold, (1974), Principles and techniques of scanning electron microscopy: *Biological applications*, 2:17 and 171.
- [112] W. K. Kan, A. Nanci, (2003) Backscattered electron imaging of lectin binding sites in tissues following freeze-fracture cytochemistry, *Journal of Electron Microscopy Technique*, 8:363-370
- [113] K. Kataoka, A. Harada, Y. Nagasaki (2012) Block copolymer micelles for drug delivery: Design, characterization and biological significance, *Advanced Drug Delivery Reviews*, 64:37-48
- [114] C. M. Hoo, N. Starostin, P. West, M. L. Mecartney (2008) A comparison of atomic force microscopy (AFM) and dynamic light scattering (DLS) methods to characterize nanoparticle size distributions, *Journal of Nanoparticle Research*, 10:89-96
- [115] M. Kaszuba, D. McKnight, M.T. Connah, F. K. McNeil-Watson, U. Nobbmann, (2008) Measuring sub nanometre sizes using dynamic light scattering, *Journal of Nanoparticle Research*, 10:823-829
- [116] www.malvern.com/labeng/technology/dynamic_light_scattering
- [117] K. L. Kelly, E Coronado, L. L. Zhao, G. C. Schatz, (2003) The Optical Properties of Metal Nanoparticles: The Influence of Size, Shape, and Dielectric Environment, *Journal of Physical Chemistry*, 107:668-677
- [118] X. Renliang, (2001) Particle Characterization: Light Scattering Methods, *Kluwer Academic Publishers*, Ch.2:56-82
- [119] S. K. Singh, N. Afonina, M. Awwad, K. Bechtold-Peters, J. T. Blue, D. Chou, (2010), An industry perspective on the monitoring of subvisible particles as a quality attribute for protein therapeutics, *Journal of Pharmaceutical Sciences*, 99:3302-21
- [120] V. Filipe, A. Hawe, W. Jiskoot, (2010), Critical evaluation of Nanoparticle Tracking Analysis (NTA) by NanoSight for the measurement of nanoparticles and protein aggregates, *Pharmaceutical Research*, 27:796-810.
- [121] Nanoparticle tracking analysis (NTA) and Dynamic light scattering (DLS) - a comparison, *Nanosight.com, Application Note*, 1-5
- [122] P. Gill (2010), Differential scanning calorimetry techniques: Applications in biology and nanoscience, *Journal of Biomolecular Techniques*, 21:167-193.
-

-
- [123] M. R. Renick, W. R. Brantley, F. M. Beck, C. S. Webb, (2004) Studies of orthodontic elastomeric modules. Part 1: Glass transition temperatures for representative pigmented products in the asreceived condition and after orthodontic use, *American Journal of Orthodontics and Dentofacial Orthopedics*, 126:337-343
- [124] D. Naumann, D. Helm, H. Labischinski, (1991) Microbiological characterizations by FT-IR spectroscopy, *Nature*, 351:81-82
- [125] P. Yu, G. Waldo, (2010) Relationship of protein molecular structure to metabolisable proteins in different types of dried distillers grains with solubles: a novel approach, *British Journal of Nutrition*, 104:1429-1437
- [126] X. Zhang, P. Yu, (2012) Using ATR-FT/IR molecular spectroscopy to detect effects of blend DDGS inclusion level on the molecular structure spectral and metabolic characteristics of the proteins in hullless barley, *Molecular and Biomolecular Spectroscopy*, 95:53-63
- [127] J. Grdadlnik, (2003) Saturation effects in FT-IR spectroscopy: Intensity of amide I and amide II bands in protein spectra, *Acta Chim Slov*, 50:777-778
- [128] N. Oulahal, C. Mariani, E. Notz, P. Degraeve, (2009) Examination of wooden shelves used in the ripening of a raw milk smear cheese by FTIR spectroscopy, *Food control*, 20:658-663
- [129] C. Jones, B. Mulloy, A.H. Thomas, (1993) Microscopy, Optical Microscopy and macroscopic techniques ,Ch. 14:183
- [130] J. Kong, S. Yu, (2007) Fourier Transform Infrared spectroscopic analysis of protein secondary structures, *Acta Biochimica et Biophysica Sinica*, 39:549 -559
- [131] I. Yamashita, (2001) Fabrication of a two-dimensional array of nano-particles using ferritin molecule, *Thin Solid Films*, 393:12-18
- [132] S. Allen, J. Davies, M. C. Davies, A. C. Dawkes, C. J. Roberts, S. J. B. Tendler, (1999) The influence of epitope availability on atomic-force microscope studies of antigen-antibody interactions, *Biochemistry Journal*, 342:173-178
- [133] R. H. Ho, Y. H. Chen, C. M. Wang, (2012) Surface differentiation of ferritin and apoferritin with atomic force microscopic techniques, *Colloids and Surfaces B: Biointerfaces*, 94:231-235
- [134] N. Rathore, R. S. Rajan, (2008) Current perspectives on stability of protein drug products during formulation, fill and finish operations, *Biotechnology Progress*, 24:504-514
- [135] T. W. Randolph, F. J. Carpenter, (2007) Engineering challenges of protein formulations, *AIChE Journal*, 53:1902-1907
- [136] A. Treffry, S.H. Banyard, R. J. Hoare, and P. M. Harrison, (1986) Proteins of iron metabolism: Proteins at interfaces, *Advances in Colloid and Interface Science*, 25: 267
-

-
- [137] C. A. Johnson, Y. Yuan, A. M. Lenhoff, (2000) Adsorbed Layers of Ferritin at Solid and Fluid Interfaces Studied by Atomic Force Microscopy, *Journal of Colloid and Interface Science*, 223: 261-273
- [138] H. Ai, M. Fang, S.A. Jones, and Y.M. Lvov, (2002) Electrostatic layer by layer nanoassembly on biological microtemplates: platelets, *Biomacromolecules*, 3:560-564
- [139] M. Mir, I. Bogachan, J. J. Valle-Delgado, X. Fernandez-Busquets, J. Samitier (2012) In vitro study of magnetite-amyloid β complex formation, *Nanomedicine: Nanotechnology, Biology, and Medicine*, 8:974-980
- [140] P. D. Sole, C. Rossi, M. Chiarpotto, G. Ciasca, B. Bocca, A. Almonti, A. Bizzarro, C. Masullo (2013) Possible relationship between Al/ferritin complex and Alzheimer's disease, *Clinical Biochemistry*, 46:86-93
- [141] N. Galvez, B. Fernandez, J. J. Calvino, O. Stephan, J. M. Dominguez-Vera, (2008) Comparative structural and chemical studies of ferritin cores with gradual removal of their Iron contents, *Journal of American Chemical Society*, 130:8062-8068
- [142] S. Ohnishi, M. Hara, T. Furuno, and H. Sasabe, (1992) Imaging ordered arrays of water-soluble protein ferritin with atomic force microscope, *Biophysics Journal*, 63:1425-1431
- [143] M. Tominaga, A. Ohira, Y. Yamaguchi, M. Kunitake, (2004) Electrochemical, AFM and QCM studies on ferritin immobilized onto a self-assembled monolayer-modified gold electrode, *Journal of Electroanalytical Chemistry*, 566:323-329
- [144] T. Miwa, M. Yamaki, H. Yoshimura, S. Ebina, and K. Nagayama, (1995) Adsorbed layers of ferritin at solid and liquid interfaces, *Langmuir*, 11:1711
- [145] F. A. Fischbach, J.W. Anderegg, (1965) An X-ray scattering study of ferritin and apo-ferritin, *Journal of Molecular Biology*, 14:458:473
- [146] F. Caruso, D.N. Furlong, and P. Kingshott, (1997) Characterisation of ferritin adsorption onto gold, *Journal of Colloid and Interface Science*, 186:129-140
- [147] J. M. Dominguez-Veral, L. Welte2, G. Natividad, Alvezl, B. F. Andezl, J. Gomez and F. Zomara, (2007) Covalent deposition of ferritin nanoparticles on to gold surfaces, *Nanotechnology*, 19:25302-24303
- [148] A. Milliquet-Fureby, M. Malmsten, and B. Bergenstahl, (1999) Surface characterisation of freeze dried protein/carbohydrate mixtures, *International Journal of Pharmaceutics*, 191:103-114
- [149] A. T. Almeida, M. C. Salvadori, and, D. F. S. Petri, (2002) Enolase adsorption onto hydrophobic and hydrophilic solid substrates, *Langmuir*, 18:6914-6920
- [150] M. J. Waner, M. Ghilchrist, M. Schindler, and M. Dantus, (1998) Imaging the molecular dimensions and oligomerisation of proteins at solid/liquid interfaces, *Journal of Physical Chemistry*, 102:1649-1657
-

-
- [151] H. Elwing, A. Askenda, B. Ivarsson, U. Nilsson, and S. Welin, (1987) In proteins at interfaces, physicochemical and biochemical studies, *American Chemical Society*, 468-478
- [152] J. M. Cowley, D. E. Janney, R. C. Gerkin and P. R. Buseck, (2000) The structure of ferritin cores determined by electron nanodiffraction, *Journal of Structural. Biology*, 131:210-216
- [153] S. W. Kim, H. Y. Seo, Y. B. Lee, Y. S. Park, and K. S. Kim, (2008) Crystal structure of ferrihydrite nanoparticles synthesized in ferritin, *Bull. Korean Chemical Society*, 29:1969-1972
- [154] B. Wolozin (2012) Regulated protein aggregation: stress granules and neurodegeneration, *Molecular Neurodegeneration*, 7:56
- [155] Y. Liu, L. K. Wolf, M. C. Messmer (2001), A Study of Alkyl Chain Conformational Changes in self-assembled n-octadecyltrichlorosilane monolayers on fused silica surfaces, *Langmuir*, 17:4329-4335
- [156] nanonet.rice.edu/manuals/afm
- [157] D. Klinov, B. Dwir, E. Kapon, N. Borovok, T. Molotsky, A. Kotlyar, (2007) High-resolution atomic force microscopy of duplex and triplex DNA molecules, *Nanotechnology*, 18:225102
- [158] S. Kashanian, R. Rafipour, F. A. Tarighat, H. Ravan (2012) Immobilisation of cobaltferritin onto gold electrode based on self-assembled monolayers, *IET Nanobiotechnology*, 6:102-109
- [159] D. Kim, N. Chung, S. Allen, S. J. B. Tendler (2012) Ferritin-based new magnetic force microscopic probe detecting 10 nm sized magnetic nanoparticles, *ACS Nano*, 6:241-248
- [160] B. Dani, R. Platz, S. T. Tzannis, (2007), High concentration formulation feasibility of human immunoglobulin G for subcutaneous administration, *Journal of Pharmaceutical Sciences*, 96:1504-1517
- [161] M. K. Joubert, Q. Luo, Y. N. Samuel, J. Wypych, L. O. Narhi (2012) Classification and characterization of therapeutic antibody aggregates, *Journal of Biological Chemistry*, 286:25118-25133
- [162] M. C. Heller, J. F. Carpenter, T. W. Randolph (2008) Manipulation of lyophilization-induced phase separation: implications for pharmaceutical proteins, *Biotechnology Progress*, 13:590-596
- [163] J. J. Schwegman, L. M. Hardwick, M. J. Akers (2005), Practical formulation and process development of freeze-dried products, *Pharmaceutical Development and Technology*, 1:151-173
-

-
- [164] A. Bahambani, J. T. Blue (2010), Lyophilization Strategies for development of a high-concentration monoclonal antibody formulation: benefits and pitfalls, *The Review of American Pharmaceutical Business and Technology*,
- [165] A. S. Rosenberg (2006), Effects of protein aggregates: An immunologic perspective, *AAPS Journal*, 8:501-507
- [166] D. K. Sharma, D. King, P. Oma, C. Merchant, (2010), Micro-flow imaging: Flow Microscopy applied to sub-visible particulate analysis in protein formulations, *AAPS Journal*, 12:455-464
- [167] D. K. Sharma, D. King, P. Oma, C. Merchant, (2006), Aggregation analysis of therapeutic proteins, Part 1, *Bioprocess International*, 1:32-42
- [168] J. M. Ruso, Angel Peniero, (2013), Investigating protein interactions at solid surfaces-in situ, Non-labelling techniques, *Proteins In Solution and At Interfaces: Methods and Applications in Biotechnology and Material Science*. Ch.6:113-134, Wiley and Sons.
- [169] A. Kamyshny, S. Lagerge, S. Partyka, P. Relkin, and S. Magdass, (2000) Adsorption of native and hydrophobized human IgG onto silica: Isotherms, calorimetry, and biological activity. *Langmuir*, 17:8242-8248
- [170] R. G. Couston, D. A. Lamprou, Shahiduddin, C. F. Van der walle, (2012) Interaction and destabilization of a monoclonal antibody and albumin to surfaces of varying functionality and hydrophobicity, *International Journal of Pharmaceutics*, 438:71-80
- [171] L. Yu, Z. Lu, Y. Gan, Y. Liu, and C. M.g Li, (2009) AFM study of adsorption of protein A on a poly(dimethylsiloxane) surface, *Nanotechnology*, 20:285101
- [172] M. C. Williams (1984), Endocytosis in alveolar type II cells: effect of charge and size tracers, *Proceedings of the National Academy of Sciences*, 81:6054-6058
- [173] B. Walivaara, P. Warkentin, I. Lundstrom, and P. Tengvall, (1995) Aggregation of IgG on methylated surfaces studied by Tapping mode AFM, *Journal of Colloid and Interface Science*, 173:54-60
- [174] J. L. Ortega-Vineusa, P. Tengvall, and I. Lundstorm, (1998) Aggregation of HAS, IgG and fibrinogen on methylated silicon surfaces, *Journal of Colloid and Interface Science*, 207:228-239
- [175] H. X. You, C. R. Lowe, (1996) AFM studies of protein adsorption: Characterisation of immunoglobulin G by detergent washing, *Journal of Colloid and Interface Science*, 182:586-601
- [176] M. Lijima, M. Somiya, N. Yashimoto, T. Niimi, S. Kuroda (2012) Nano-visualization of oriented-immobilized IgGs on immunosensors by high-speed atomic force microscopy, *Nature Nanotechnology*, 970:1-4
-

- [177] A. Hawe, W. L. Hulse, W. Jiskoot, R. T. Roberts (2011) Taylor dispersion analysis compared to dynamic Light Scattering for the size analysis of therapeutic peptides and proteins and their aggregates, *Pharmaceutical Research*, 28:2302-2310
- [178] M. K. Boheom, J. M. Woof, M. A. Kerr, and S.J. Perkins, (1999) The Fab and Fc fragments of IgA₁ exhibit a different from that in IgG: a study by X-ray and neutron solution scattering and homology modelling, *Journal and Molecular Biology*, 286:1421-1447
- [179] O. Ouerghi, A. Touhami, A. Othmane and N. Jafferzic Renault, (2002) Investigating antibody-antigen binding with atomic force microscopy, *Sensors and Actuators*, 84:167-175
- [180] M. E. Browning-Kelley, K. Wadu-Mesthrige, V. Hari and G.Y. Liu, (1997) Atomic force microscopic study of specific antigen-antibody binding, *Langmuir*, 13:343-350
- [181] C. J. Roberts, P. M. Williams, J. Davies, A.C. Dawekes, J. Sefton, J.C. Edwards, A.G. Haymes, C. Beswick, M.C. Davies and S.J.B. Tendler, (1995) Real-space differentiation of IgG and IgM antibodies deposited on microtiter wells by scanning force microscopy, *Langmuir*, 11:1822-1826
- [182] D. Arzensek, (2010) Dynamic light scattering and application to proteins in solutions, 1-18
- [183] Protein characterization using static and dynamic light scattering: - Malvern instruments.
- [184] H. C. Mahler, R. Muller, W. Frieb, A. Delille, and S. Matheus, (2005) Induction and analysis of aggregates in a liquid IgG₁-antibody formulation, *European Journal of Pharmaceutics and Bio-pharmaceutics*, 59:407- 415
- [185] T. J. Anchordoquy, G. S. Koe, (2000) Physical stability of nonviral plasmid-based therapeutics, *Journal of Pharmaceutical Sciences*, 23:289-296.
- [186] J. C. Casper, D. Schaffert, N. Ogris, E. Wagner, W. Friess, (2011) Development of a lyophilized plasmid/LPEI polyplex formulation with long-term Stability - A step closer from promising technology to application, *European Journal of Controlled Release*, 151:246-255
- [187] F. Caruso, D. N. Furlong, K. Ariga, I. Ichinose, T. Kunitake (1998) Characterization of polyelectrolyte-protein multilayer films by atomic force microscopy, scanning electron microscopy, and Fourier Transform Infrared-reflection-absorption spectroscopy, *Langmuir*, 14:4559-4565
- [188] J. Zhang, M. Bunker, X. Chen, A. P. Parker, N. Patel, C. J. Roberts (2009) Nanoscale thermal analysis of pharmaceutical solid dispersions, *International Journal of Pharmaceutics*, 380:170-173
- [189] H. X. You and C. R. Lowe (1996), AFM Studies of Protein Adsorption: Characterization of Immunoglobulin G adsorption by detergent washing, *Journal of Colloid and Interface Science*, 182:586-601

-
- [190] S. O. Ugwu, S. P. Apte (2004), The effect of buffers on protein conformational stability, *Pharmaceutical Technology*, 86-113
- [191] X. M. Lam *et al.*, (1996) Replacing succinate with glycolate buffer improves the stability of lyophilized interferon, *International Journal of Pharmaceutics*, 142:85–95
- [192] S. Roy, I. Henderson, R. Nayar, T. W. Randolph, J. F. Carpenter (2008) Effect of pH on Stability of recombinant botulinum serotype A vaccine in aqueous solution and during storage of freeze-dried formulations, *Journal of Pharmaceutical Sciences*, 97:5132-5146
- [193] E. Garber, S. J. Demrest (2007) A broad range of Fab stabilities within a host of therapeutic IgGs, *Biochemical and Biophysical Communications*, 355:751-757
- [194] R. M. Lonescu, J. Vlasak, C. Price, M. Kirchmeier (2008) Contribution of variable domains to the stability of humanized IgG1 monoclonal antibodies, *Journal of Pharmaceutical Sciences*, 97:1416-1426
- [195] W. P. Arnoldus, Vermeer and W. Norde (2000), The thermal stability of Immunoglobulin: Unfolding and aggregation of a multi-domain protein, *Biophysical Journal*, 78:394-404
- [196] Sochava *et al.*; (1997) Heat capacity and thermodynamic characteristics of denaturation and glass transition of hydrated and anhydrous proteins, *Biophysical Chemistry*, 69:34 – 41
- [197] J. Weing, Y. Jiang, L. Nahri (2007) Effect of carbohydrate on thermal stability of antibodies, *American Pharmaceutical Review*, 1-5
- [198] J. D. Andya, C. C. Hsu and S. J. Shire, (2003) Mechanisms of aggregate formation and carbohydrate excipient stabilization of lyophilized humanized monoclonal antibody formulations. *AAPS PharmSci*, 5:21-31
- [199] S. A. Tatulian, (2013) Structural Characterization of membrane proteins and peptides by FTIR and ATR-FTIR spectroscopy, *AAPS PharmSci*, 5:21-31
- [200] S. Schule, W. Frieb, K. Bechtold-Peters, P. Garidel (2007) Conformational analysis of protein secondary structure during spray-drying of antibody/mannitol formulations, *European Journal of Pharmaceutics and Biopharmaceutics*, 65:1-9
- [201] Q. Lu, X. Hu, X. Wang X, J.A. Kluge, S. Lu, P. Cebe, et al (2010) Water-insoluble silk films with silk I structure, *Acta Biomater*, 6:1380-1387
- [202] A. Dong, P. Huang, W.S. Caughey (1990) Protein secondary structures in water from second-derivative amide I infrared spectra. *Biochemistry*, 29:3303-3308
- [203] A. Dong, Prestrelski, S. J. Prestrelski, S. D. Allison, J. F. Carpenter, (1995) Infrared spectroscopic studies of lyophilization- and temperature-induced protein aggregation. *Journal of Pharmaceutical Sciences* 84:415-424
-

- [204] S. Y. Vinyamenov, N. N. Kalnin, (2004) Quantitative IR spectrophotometry of peptide compounds in water (H₂O) solutions. II. Amide absorption bands of polypeptides and fibrous proteins in α -, β -, and random coil conformations, *Biopolymers*, 30:1259-1271
- [205] A. Barth, (2007), Infrared spectroscopy of proteins, *Biochimica et Biophysica Acta*, 1767:1073-1101.
- [206] E. Carla, G. E. Maria, G. Bremer, W. Norde (1999), ATR-FTIR study of IgG adsorbed on different silica surfaces, *Journal of Colloid and Interface Science*, 220:13-23
- [207] K. Griebenow, A. M. Klibanov (1995), Lyophilization-induced reversible changes in the secondary structure of proteins, *Proceedings of Natural Academy of Sciences*, 92:10969-10976
- [208] S. J. Prestrelski, N. Tedeschi, T. Arakawa, J. F. Carpenter, (1993), Dehydration-induced conformational transitions in proteins and their inhibition by stabilizers, *Biophysical Journal*, 65:661-671
- [209] Y. Kim, C. A. Rose, Y. Liu, Y. Ozaki, G. Datta, (1993), FT-IR and near-infrared FT-Raman studies of the secondary structure of insulinotropin in the solid state: α -helix to β -sheet conversion induced by phenol and/or by high shear force, *Journal of Pharmaceutical Sciences*, 83:1175-1180
- [210] W. G. Pitt, S. H. Spiegelberg, S. L. Cooper, (1987) Proteins at Interfaces, eds. Brush, J. L. & Horbett, T. A. *American Chemical Society*, 324-338.
- [211] E. J. Castillo, J. L. Koeing, J. M. Anderson, (1985), Protein adsorption on hydrogels: II. Reversible and irreversible interactions between lysozyme and soft contact lens surfaces, *Biomaterials* 6:338-345
- [212] K. G. Karassquillo, C. Sanchez, K. Gierbenow, (2000) Relationship between conformational stability and lyophilization-induced structural changes in chymotrypsin, *Biotechnology and Applied Chemistry*, 31:41-53
- [213] I. D. Kuntz, W. Kauzmann, (1974) Hydration of proteins and polypeptides, *Advanced Protein Chemistry*, 28:239-345
- [214] S. Luthra, J. P. Obert, D. S. Kalonia, M. J. Pikal, (2007), Investigation of drying stresses on proteins during lyophilization: Differentiation between primary and secondary-drying stresses on lactate dehydrogenase using a humidity controlled mini freeze-dryer, *Journal of Pharmaceutical Sciences*, 96:61-70
- [215] W. P. Arnoldous, Vermeer and W. Norde (2000) The thermal stability of immunoglobulin: unfolding and aggregation of a multidomain protein, *Biophysical Journal*, 78:394-404
- [216] X. C. Tang, M. J. Pikal (2004) Design of freeze-drying processes for pharmaceuticals: Practical advice, *Pharmaceutical Research*, 21:191-200

- [217] Y. Han, B. S. Jin, S. B. Lee, Y. Sohn, J. W. Joung, J. H. Lee (2007) Effects of sugar additives on protein stability of recombinant human serum albumin during lyophilization and storage, *Archives of Pharmaceutical Research*, 9:1124-1131
- [218] L. L. Chnag, D. Shepherd, J. Sun, X. C. Tang, M. J. Pikal, (2005) Effect of sorbitol and residual moisture on the stability of lyophilized antibodies: Implications for the mechanism of protein stabilization in the solid state, *Journal of Pharmaceutical Sciences*, 94:1445-1455
- [219] G. Xie, T. Timasheff, (1997) The thermodynamic mechanism of protein stabilization by trehalose, *Journal of Pharmaceutical Sciences*, 64:25-43
- [220] S. Ohtake, Y. Kita, T. Arakawa (2011) Interactions of formulation excipients with proteins in solution and in the dried state, *Advanced Drug Delivery Reviews*, 63:1053-1073
- [221] N. Grasmeijer, , M. Stankovic, H. de Waard, H. W. Fijnlink, W. L. J. Hinrichs, (2013) Unraveling protein stabilization mechanisms: Vitrification and water replacement in a glass transition temperature controlled system, *Biochemica et Biophysica ACTA (BBA)- Proteins and Proteomics*, In Press.
- [222] S. Passot, F. Fonseca, M. A. Rolca, D. Rolland, M. Marin, (2005) Physical characterisation of formulations for the development of two stable freeze-dried proteins during both dried and liquid storage, *European Journal of Pharmaceutics and Biopharmaceutics*, 60:335-348
- [223] A. Hawe, W. Frieb, (2006), Impact of freezing procedure and annealing on the physico-chemical properties and the formation of mannitol hydrate in mannitol–sucrose–NaCl formulations, *European Journal of Pharmaceutics and Biopharmaceutics*, 64:316-325
- [224] L. Bond, S. Allen, M. C. Davies, C. J. Roberts, A. P. Shivji, S. J.B. Tendler, P. M. Williams, J. Zhang, (2002), Differential scanning calorimetry and scanning thermal microscopy analysis of pharmaceutical materials, *International Journal of Pharmaceutics*, 243:71-81
- [225] B. M. Smith, L. Oswald, S. Franzan, (2002) Single-Pass Attenuated Total Reflection Fourier Transform infrared spectroscopy for the prediction of protein secondary structure, *Analytical Chemistry*, 74:3386-3391
- [226] L. Remmelle, S. Krishnan, Richard, J. Callahan, William, (2012) Development of stable lyophilized protein drug products, *Current Pharmaceutical Biotechnology*, 13:471-496
- [227] A. I. Kim, M. J. Akers, S. L. Nail, (1998) The physical state of mannitol after freeze-drying: Effects of mannitol concentration, freezing rate, and a noncrystallizing cosolute, *Journal of Pharmaceutical Sciences*, 87:931-985
- [228] L. Yu (2001) Amorphous pharmaceutical solids: preparation, characterization and stabilization, *Advanced Drug Delivery*, 48:27– 42

-
- [229] A. Simperler, A. Kornherr, R. Chopra, A. Bonnet, W. Jones, W. D. Samuel Motherwell, G. Zifferer (2006) Glass transition temperature of glucose, sucrose, and trehalose: An Experimental and in Silico Study, *Journal of Physical Chemistry*, 110:19678-19684
- [230] T. Yoshinari, R. T. Forbes, P. York, Y. Kawashim (2003) Crystallisation of amorphous mannitol is retarded using boric acid, *International Journal of Pharmaceutics*, 258:109–120
- [231] X. Chen, C. J. Roberts, J. Zhang, S. J. B. Tendler (2002), Phase contrast and attraction–repulsion transition in tapping mode atomic force microscopy, *Surface Science Letters*, 519:593-598
- [232] S. Allen, S. D. A. Connell, X. Chen, J. Davies, M. C. Davies, A. C. Dawkes, C. J. Roberts, S. J. B. Tendler, P. M. Williams (2001), Mapping the surface characteristics of polystyrene microtiter wells by a multimode scanning force microscopy Approach, *Journal of Colloid and Interface Science*, 242:470-476
- [233] N. A. Burnham, O. P. Behrend, F. Oulevey, G. Gremaud, P. J. Gallo, D. Gourdon, E. Dupas, A. J. Kulik, H. M. Pollock, G. A. D. Briggs (1997), How does a tip tap ? *Nanotechnology*, 8:67-75
- [234] H. Hawe, W. Frieb (2006) Physico-chemical lyophilization behaviour of mannitol, human serum albumin formulations, *European Journal of Pharmaceutical Sciences*, 28:224–232
- [235] T. Yoshinari, R. T. Forbes, P. York, Y. Kawashim (2002) Moisture induced polymorphic transition of mannitol and its morphological transformation, *International Journal of Pharmaceutics* 247: 69 -77
- [236] M. J. Pikal, D. Rigsbe, M.L. Roy, D. Galreath, K.J. Kovach, B. S. Wang, J. F. Carpenter, M. T. Cicerone (2008) Solid state chemistry of proteins: II. The correlation of storage stability of freeze-dried human growth hormone (hGH) with structure and dynamics in the glassy solid, *Journal of Pharmaceutical Sciences*, 97:5106-5121
- [237] L. Yu (2001) Amorphous pharmaceutical solids: - preparation, characterization and stabilization, *Advanced Drug Delivery*, 48:27– 42
- [238] B. S. Wang, M. J. Pikal, (2012) Stabilization of lyophilized pharmaceuticals by process optimization: Challenges and opportunities, *American Pharmaceutical Review*, 48:27– 42
- [239] H. K. Christenson, (2001) Confinement effects on freezing and melting, *Journal of Physics Condensed Matter*, 13:95
- [240] A. Hawe, W. Frieb (2006) Impact of freezing procedure and annealing on the physic-chemical properties and the formation of mannitol hydrate in mannitol-sucrose-NaCl formulations, *European Journal of Pharmaceutics and Biopharmaceutics*, 64:316-325
-

-
- [241] K.A. Pikal, J. F. Carpenter (1998) pH Changes during freezing in sodium and potassium phosphate buffer systems in the presence of glycine: Effect on protein stability, *Pharmaceutical Sciences*, 1:1544
- [242] J. F. Carpenter, T. Arakawa, J. H. Crowe (1991), Interactions of stabilizing additives with proteins during freeze-thawing and freeze drying, *Developmental Biology*, 74:225-232
- [243] J. H. Crowe, J. F. Carpenter, L. M. Crowe, T. J. Anchordoguy, (1990), Are freezing and dehydration similar stress vectors? A comparison of modes of interaction of stabilizing solutes with biomolecules, *Cryobiology*, 27:219-231
- [244] A. P. Inshida, P. R. Griffiths, (1993), Comparison of the amide I/II intensity ratio of solution and solid-state proteins sampled by Transmission, Attenuated total reflectance, and Diffuse reflectance spectrometry, *Applied Spectroscopy*, 47:584-589
- [245] V. Scoik, K. G. J.T. Carstensen (1990), Nucleation phenomena in amorphous sucrose systems, *International Journal of Pharmaceutics*, 58:185-96.
- [246] M. Siniti, *et al*, (1993), The thermal behavior of hexitols, Part 1 Vittrification and crystallization of iditol, mannitol, sorbitol, and dulcitol, *Thermochimica Acta*, 224:97-104.
- [246] M. Siniti, *et al*, (1993), The thermal behavior of hexitols, Part 1 Vittrification and crystallization of iditol, mannitol, sorbitol, and dulcitol, *Thermochimica Acta*, 224:97-104.
- [247] G. Kohler, C. Milstein, (1975) Continuous cultures of fused cells secreting antibody of predefined specificity, *Nature*, 256:495-497
- [248] B. Witkop (1999) Paul Ehrlich and his magic bullet -Revisited, *Proceedings of The American Philosophical Society*, 43:540-557
- [249] G. P. Adama, L. M. Weiner (2005) Monoclonal antibody therapy of cancer, *Nature Biotechnology*, 23:1148-1156
- [250] P. Chames, M. V. Regenmortel, E. Wiess, D. Baty (2009), Therapeutic antibodies: successes, limitations and hopes for the future, *British Journal of Pharmacology*, 157:220-233
- [251] M. S. Neuberger, G. T. Williams, E. B. Mitchell, S. S. Jouhal, J. G. Flangann, T. H. Rabbits, (1985), A hapten-specific chimaeric IgE antibody with human physiological effector function, *Nature*, 314:268-370
- [252] G. Winter, C. Milstein, (1991), Manmade antibodies, *Nature*, 349: 293-299
- [253] R. Pasqualini, W. Arap, (2004), Hybridoma-free generation of monoclonal antibodies, *Proceedings of the National Academy of Sciences*, 101: 257-259
-

-
- [254] K. Koren, L. A. Zuckermann, A. R. Mire. Sluis (2002), Immune responses to therapeutic proteins in humans - Clinical significance, Assessment and prediction, *Current Pharmaceutical Biotechnology*, 3:349-360
- [255] A. C. Chan, P. A. Carter (2010), Therapeutic antibodies for autoimmunity and inflammation, *Nature Reviews Immunology*, 10:301-316
- [256] P. Hinterdorfer, W. Baumgartner, H. J. Gruber, K. Schilcher, H. Schindler (1996), Detection and localization of individual antibody-antigen recognition events by atomic force microscopy, *Proceedings of the National Academy of Sciences*, 93:3477-3481
- [257] O. A. Saleh, L. L. Sohn (2004), Direct detection of antibody-antigen binding using an on-chip artificial pore, *Proceedings of the National Academy of Sciences*, 4:820-824
- [258] S. Loizou, J. D. McCrea, A. C. Rudge, R. Reynolds, C. C. Boyle, E. N. Harris, (1985) Measurement of anti-cardiolipin antibodies by an enzyme-linked immunosorbent assay (ELISA): standardization and quantitation of results, *Clinical & Experimental Immunology*, 62-738-745
- [259] H. Ogawa, D. Zhao, J. S. Dlott, G. S. Cameron, M. Yamazaki, T. Hata, D. A. Triplett, (2000) Elevated anti-Annexin V antibody levels in antiphospholipid syndrome and their involvement in antiphospholipid antibody specificities, *American Journal of Clinical Pathology*, 114:619-628
- [259] M. A. Refaai, M. Laposata, M. Elizabeth, V. Cott, (2003) Clinical significance of a borderline titer in a negative ELISA test for Heparin-induced Thrombocytopenia, *American Journal of Clinical Pathology*, 119:61-65
- [260] M. B. Marques, C. A. Mayfield, D. P. Blackall (2004) Thrombotic thrombocytopenic purpura from platelet aggregates to plasma, *American Journal of Clinical Pathology*, 121:S89-S96
- [261] M. A. Refaai, M. Laposata, M. Elizabeth, V. Cott, (2003) Clinical significance of a borderline titer in a negative ELISA test for Heparin-induced Thrombocytopenia, *American Journal of Clinical Pathology*, 119:61-65
- [262] L. Aarden, S. R. Ruuls, G. Wobink (2008), Immunogenicity of anti-tumor necrosis factor antibodies-toward improved methods of anti-antibody measurement, *Current Opinion in Immunology*, 20:431- 435
- [263] J. R. Crowther, The ELISA Guide Book, *Methods in Molecular Biology*, 149:11-31
- [264] P. Hinterdorfer, Y. F. Duferene (2006), Detection and localization of individual antibody-antigen recognition events by atomic force microscopy, *Nature Methods*, 3:347-355
-

-
- [265] U. Dammer, M. Hegner, D. Anselmetti, P. Wagner, M. Dreier, W. Huber, H. J. Guntherodt (1996) Specific Antigen/Antibody Interactions Measured by Force Microscopy, *Biophysical Journal*, 70:2437-2441
- [266] B. Liedberg, C. Nylander, I. Lundstrom (1995) Biosensing with surface plasmon resonance - how it all started, *Biosensors and Bioelectronics*, 10:1-9
- [267] B. Johne, M. Gadnell, K. Hansen, (1993) Epitope mapping and binding kinetics of monoclonal antibodies studied by real time biospecific interaction analysis using surface plasmon resonance, *Journal of Immunological Methods*, 160:191-198
- [268] R. Green, R. A. Frazer, K. M. Shakesheff, M. C. Davis, C. J. Roberts, S. J. B. Tendler (2000) Surface plasmon resonance analysis of dynamic biological interactions with biomaterials, *Biomaterials*, 18:1823-183
- [269] A. Malborg, A. Michaelsson, M. Ohlin, B. Jansson, C. A. K. Borrebaeck (1992) Real Time Analysis of Antibody-Antigen Reaction Kinetics, *Scandinavian Journal of Immunology*, 35:643-650
- [270] C. Boozera, Q. Yua, S. Chena, C. Y. Leea, Homolac, S. S. Yeec, S. Jianga, (2003) Surface functionalization for self-referencing surface plasmon resonance (SPR) biosensors by multi-step self-assembly, *Sensors and Actuators*, 90:22-30
- [271] P. Gomes, D. Andreu (2002) Direct kinetic assay of interactions between small peptides and immobilized antibodies using a surface plasmon resonance biosensor, *Journal of Immunological Methods*, 259-217-230
- [272] J. E. Dyr, J. Homola, E. Brynda, M. Houska, J. Suttar, (1998) Molecular arrangement of adsorbed fibrinogen molecules characterized by specific monoclonal antibodies and a surface plasmon resonance sensor, *Sensors and Actuators*, 51:268-272
- [273] J. Homola, (2008) Surface plasmon resonance sensors for detection of chemical and biological species, *Chemical Reviews*, 108:462-493
- [274] D. G. Myszk, X. He, M. Dembo, T. A. Morton, B. Goldstein (1998) Extending the Range of Rate Constants Available from BIACORE: Interpreting Mass Transport-Influenced Binding Data, *Biophysical Journal*, 75:583-594
- [275] C. A. Ray, V. Patel, J. Shih, C. Macaraeg, Y. Wu, T. Thway, M. Ma, J. W. Lee, B. DeSilva (2009) Application of multi-factorial design of experiments to successfully optimize immunoassays for robust measurements of therapeutic proteins, *Journal of Pharmaceutical and Biomedical Analysis*, 49:311-318
- [276] www.abdserotec.com/resources/elisa-technical-resources-and-troubleshooting/an-introduction-to-elisa.htm
-

-
- [277] Ressing *et al.*, (1992) The influence of sucrose, dextran, and hydroxypropyl- β -cyclodextrin as lyoprotectants for a freeze-dried mouse IgG₂ monoclonal antibody (MN12), *Pharmaceutical Research*, 9:266-270
- [278] L. S. Jones *et al.*, (2001) The effects of Tween 20 and sucrose on the stability of anti-L-selectin during lyophilization and reconstitution, *Journal of Pharmaceutical Sciences*, 90:1466-1477
- [279] A. Marchetti *et al.*, (2009) Ferritin is used for iron storage in bloom-forming marine pennate diatoms, *Nature Letters*, 457:467- 470
- [280] K. C. Brown *et al.*, (1998) Determining protein-protein interactions by oxidative cross-linking of a glycine-glycine-histidine fusion protein, *Biochemistry*, 37:4397- 4406